Technical University of Munich
TUM School of Engineering and Design

Distributed and Centralized Integration of Fluctuating Renewable Power: The Case of Brazil

Dipl.-Wirt.-Ing. Simon Herzog

Vollständiger Abdruck der von der TUM School of Engineering and Design
der Technischen Universität München zur Erlangung des akademischen Grades eines

Doktors der Ingenieurwissenschaften (Dr.-Ing.)

genehmigten Dissertation.

Vorsitzender: Prof. Dr. sc. Marcelo Lobo Heldwein

Prüfer der Dissertation:

1. Prof. Dr. rer. nat. Thomas Hamacher
2. Prof. Gilberto de Martino Jannuzzi, Ph.D.

Die Dissertation wurde am 05.04.2022 bei der Technischen Universität München eingereicht
und durch die TUM School of Engineering and Design am 29.11.2022 angenommen.

Contents

List of Figures

List of Tables

Abstract

This work investigates possibilities for the Brazilian electricity system to integrate a growing intermittent power production of wind and photovoltaic. The main research question is how the Brazilian energy system will evolve depending on different scenarios for prices and demand. A mathematical approach is presented to develop load profiles for Brazilian households for distributed generation and storage economic assessment. For the case of centralized integration using Brazil's large hydropower reservoirs, the work shows the region-specific results of a linear optimization model. Several scenarios cover a wide range of possible demand, fuel, and battery prices. One important outcome is that space requirements for wind farms and photovoltaic arrays are even for extreme scenarios lower compared to the sugarcane acreage of 2015 for domestic biofuel production.

Chapter 1

Introduction

In the context of growing electricity demand, falling prices for photovoltaic, and wind power generation, this work investigates, for the case of Brazil, several possibilities for the integration of fluctuating renewable power. The main research question is, how the Brazilian energy system can cope a significant growth in intermittent power production. The visualized results are presented mainly in spatial resolution for the five Brazilian macroregions North, Northeast, Central-West and Southeast, South.

Chapter 2 provides an overview about the most important facts and historic developments in geography, demography and economy. Since these dimensions are determinants of energy demand and supply, they are used to justify later assumptions.

An overview of key figures, specific developments, and unique characteristics of the Brazilian energy sector is the main topic of chapter 3. Besides economic and population growth, the main driver of future electricity demand might be replacing fossil fuels as a final energy carrier. Therefore, the whole energy sector is discussed in this chapter, focusing on transportation, where sugarcane-based ethanol plays a vital role in Brazil.

Chapter 4 delivers an approach to quantify potentials for distributed generation in Brazil, focusing on photovoltaic generation in the residential sector. This chapter includes a mathematical approach for developing residential load profiles in hourly resolution based on Brazilian statistics and regional specific meteorological conditions. Both batteries and thermal storage are discussed as options for distributed integration. The chapter ends with an economic assessment of distributed integration of photovoltaic generation.

The focus of chapter 5 is the centralized integration of intermittent renewable power. Since the Brazilian energy system relies predominantly on hydropower generation, including enormous storage capacities provided by reservoir lakes, the assessment of hydropower is one important part of this chapter. Sources, approaches, and ideas are presented on how to derive the most important figures for assessing hydropower stations' storage capacity and flexibility. The chapter includes a detailed description of the Brazilian electricity system of 2017/2018. Based on this state, a four-region, linear optimization model is developed to conduct a model-based outlook. The calculated scenarios assume a significant growth in electricity demand and

assess the impact of varying battery and fuel prices to cover possible market developments. The base scenario is meant as an extrapolation of previously described development, whereas further scenarios assume a tremendous growth in electricity demand for the production of hydrogen to produce hydrogen-based fuels. For all scenarios, power production by source, the installed capacities for generation, storage, and transmission are presented in regional resolution and an activity profile for hydropower. A common result of all scenarios is a large expansion of wind and photovoltaic power generation capacity. The spatial requirements for solar arrays and wind farms are compared for selected scenarios.

The appendix offers additional sources, results, and auxiliary calculations.

Chapter 2

Brazil country profile

This chapter delivers an overview about the most important facts and figures about Brazil in geography, demography and economy. As energy demand and supply, but also possibilities for economic activities are determined by these three dimensions, it is necessary to describe the development over recent decades and the present situation.

2.1 Geography

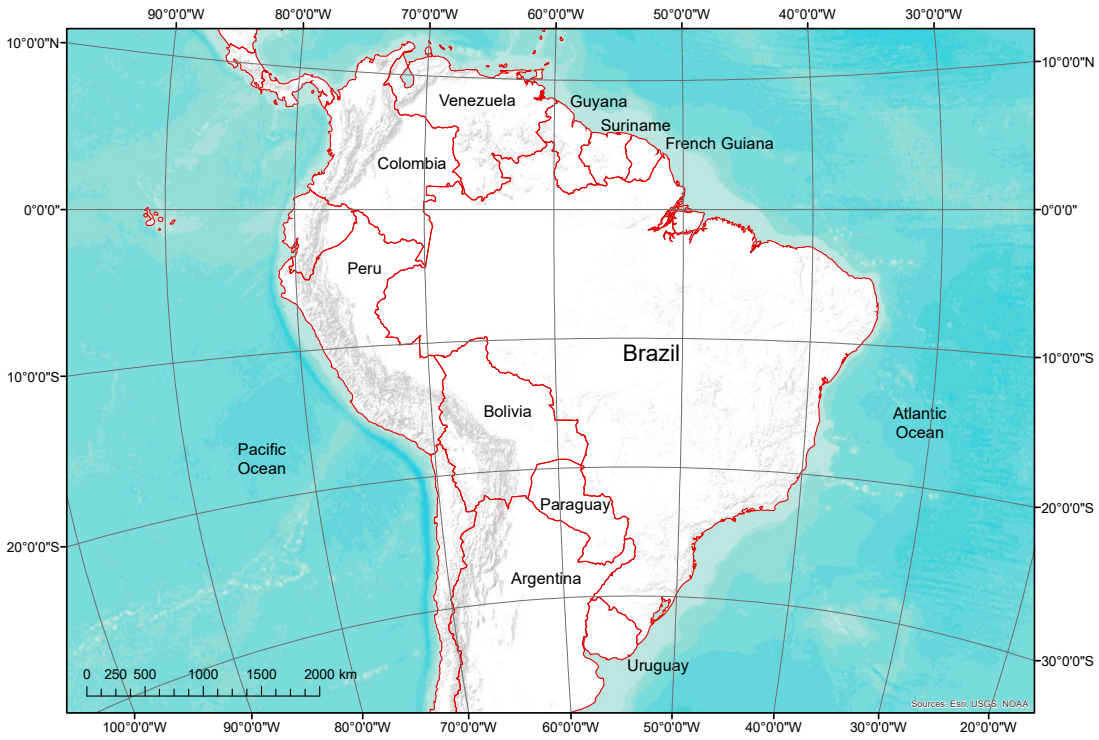

Figure 2.1: Brazil and its neighboring countries [Own representation]

Brazil is the largest country in South America by size and population. With an area of more than 8.5 million km^2 it is on rank six in the world and with its 208 million inhabitants in

2017 on rank five by population. [3, 22] The equator crosses Brazil in the very north above the cities Manaus and Belém, so that most of the countries territory is located on the southern hemisphere. Its widest extension from east to west is more than 4,300 km, from north to south slightly more than 4,000 km. Brazil has a border with all South American states except Chile and Ecuador, see figure 2.1. In the east, Brazil has a coast of more than 7,000 km to the Atlantic Ocean. Beginning in the south, its neighboring countries in clockwise direction are Uruguay, Argentina, Paraguay, Bolivia, Peru, Colombia, Venezuela, Guyana, Suriname and French Guiana.
The Federative Republic of Brazil consists of 27 federal units *(Unidades Federativas, UF)*: 26 states and one federal district *(Distrito Federal)*, which hosts the national capital Brasilia. In publications of the Brazilian Institute of Geography and Statistics *(Instituto Brasileiro de Geografia e Estatística, IBGE)*, three or more states form one of five macro-regions. [3, 23–25] The North Region is composed of the states Acre, Amapá, Amazonas, Pará, Rondônia, Roraima and Tocantins. The states Alagoas, Bahia, Ceará, Maranhão, Paraíba, Pernambuco, Rio Grande do Norte, and Sergipe form the Northeast Region. The Central-West Region consists of the Distrito Federal surrounded by the state of Goiás. The Mato Grosso and Mato Grosso do Sul are also parts of the Central-West. The Southeast Region includes the states Espírito Santo, Minas Gerais, São Paulo and Rio de Janeiro. The South Region has only the three states Paraná, Rio Grande do Sul and Santa Catarina. States and regions are annotated in figure 2.2. The colors for the regions are used throughout this work.

Figure 2.2: Federal states and macro-regions (underlined) [Own representation]

In [26] the Brazilian climate is described with the Köppen's climate classification [27]. Three different climate zones occur in Brazil: Tropical, subtropical and arid, see figure 2.3 on the left. Over two thirds of the countries territory have tropical climate (blue). The subtropical area (green) covers the whole South Region and ranges into parts of the Southeast and the Central-West. The driest places are located in the Northeast with a climate from semiarid (orange) to arid (red). The annual rainfall varies location-dependent between less than 700 mm in the north of Northeast up to 4,000 mm in the Amazonas state.

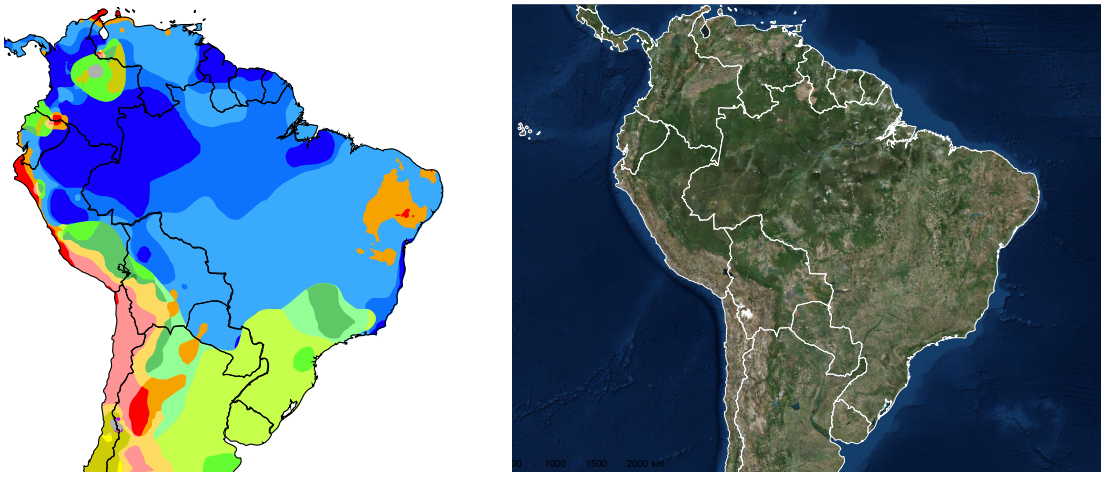

Figure 2.3: Köppen-Geiger climate type map [1] and satellite image [2]

Large contiguous areas of tropical rain forest remained as the natural and dominating vegetation in the Amazon basin. This can be recognized as the dark green area in the North, see satellite image in figure 2.3 on the right. It spreads over the boarders to Peru, Colombia and Venezuela. Despite ongoing threat of deforestation, still around 60 % are covered with different kinds of forests. [22, 28] From the Central-West to the Northeast, Brazil is crossed by a vegetation belt starting with the Pantanal tropical wetlands, turning into a savanna ecoregion called Cerrado. Moving further in the hot and dry Northeast, the Cerrado is increasingly displaced by the Caatinga, a xeric and thorny shrubland, interfused with groves of small trees and palms. In the South of Brazil extending across the border to Uruguay and Argentina, the so-called Campo limpo or Pampa, a plain grassland pervaded of some bushes, is the typical appearance of the landscape. [29] As more than 30 % of the land are used for agriculture with growing tendency, the natural vegetation is threatened in most parts of the country. Especially the Atlantic rain forest *(Mata Atlântica)*, which is the original vegetation in huge parts of the Southeast, South and at the coast up to the state Pernambuco, disappeared predominantly for cropland, pastures [13] and settlement areas. Referring to [30], Brazil lost between 1982 and 2016 around 385,000 km^2 of net tree cover, which is an area larger than Germany. The development of recent decades can be proved for example with an analysis of satellite images on several spots. [31]

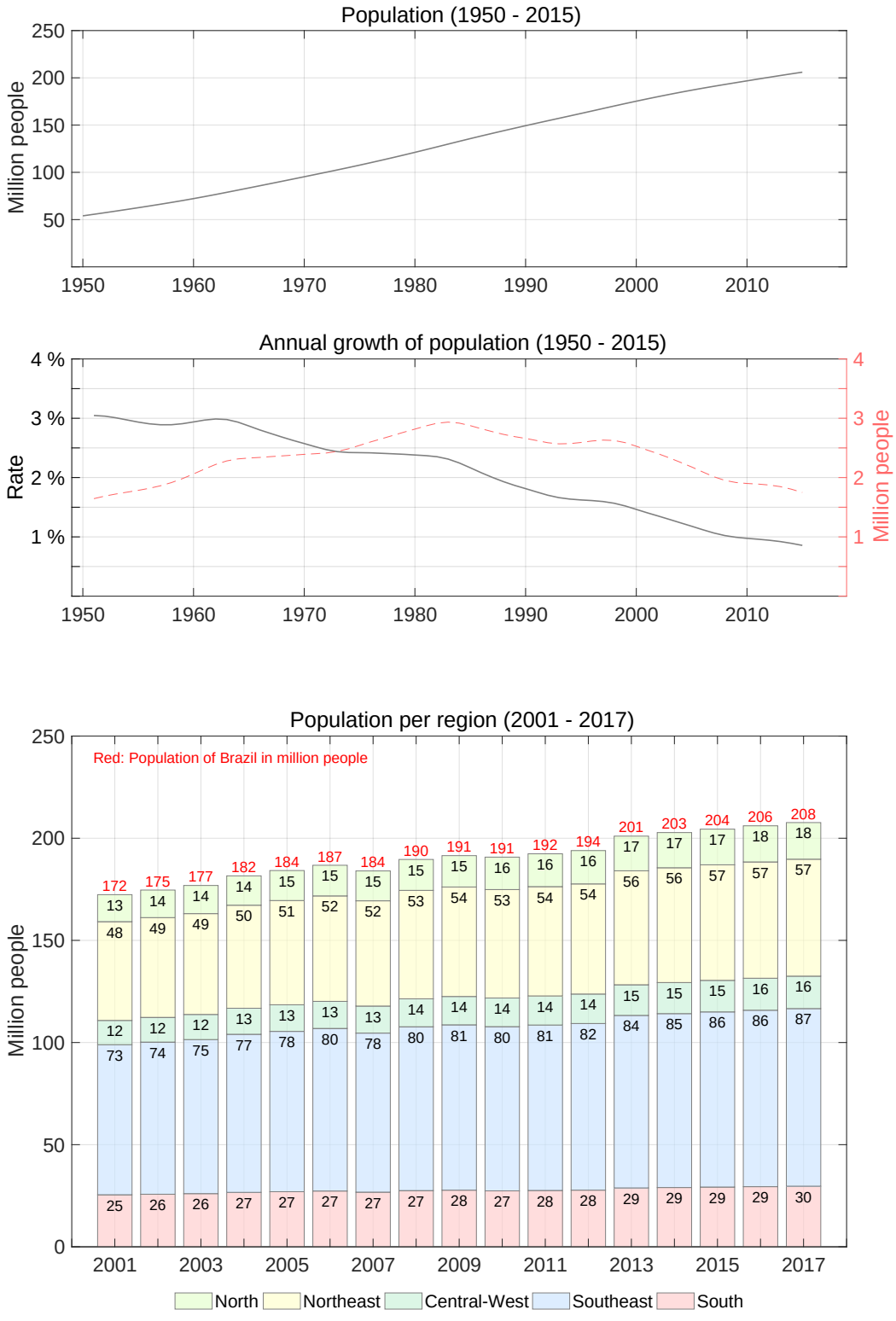

Figure 2.4: Development of population in Brazil [3]

2.2 Demography

Brazil's population showed a dynamic growth during the last decades, see figure 2.4, top. The population doubled within 25 years from 54 million people in 1950 to 108 million people in 1975. Main driver for this development were the high fertility rates of over 6 births per woman until the 1960s. Further reasons for population growth were improvements in health and medical treatment, which are indicated by rising life expectancy and falling infant mortality rate. The expected lifespan at birth was approximately 54 years in 1960 and over 75 years in 2016. In the same time, the mortality rate of children was reduced from over 64 to around 30 per 1000 births. While the population still grew from 1975 to 2015, the growth rates fell from approximately 3 % in the 1960s under 1 % in 2010. Simultaneously, the births per woman continually declined to less than 2 births per woman in the years after 2010. The slower increase resulted in a significantly longer doubling time of more than 40 years. In 2017, with 208 million inhabitants almost twice as many people lived in Brazil compared to the year 1975. Despite falling relative numbers, the Brazilian population still grew after 2010 for more than 1.5 million people per year. [4] Relative population growth rates are shown as the continuous grey line in the middle diagram of figure 2.4, whereas the red dashed line represents the absolute values.

Immigration played a subordinate role in Brazil's population growth since 1950. For instance, in the period from 1950 to 1975 the total numbers of immigrants ranged between 5,900 (1973) and 88,000 (1952), see p. 225 in [23]. According to that, immigration contributed always less than 6 % to the annual population growth. In 2017, Brazil had with -0.1 migrants per 1,000 inhabitants a negative net migration rate, meaning that slightly more people left the country than entered. [22]

The bottom diagram in figure 2.4 illustrates the development of residents in the regions from 2001 to 2017. The data was retrieved from IBGE [3]. In the 16 years before 2017, all regions grew by at least 4 million people, like the South and the Central-West. In relative values, the North (+35 %) and the Central-West (+34 %) had the highest population growth. Whereas in absolute numbers, the Southeast (+13 million) and the Northeast (+9 million) witnessed the highest increase among all regions.

Brazil's population is distributed very unequal over the country. The vast majority of people live in urbanized areas along or relatively near the Atlantic coast. Most of the largest cities in Brazil have access to the Atlantic Ocean or are located close to seaports, see figure 2.5 and [32]. In 2017, more than 85 % of the population lived in urban areas, while the trend for urbanization still continues. [22]

The top map in figure 2.6 illustrates the population in million people by state. Corresponding to that, the bottom map shows the density of population by state in people per square kilometer. The visualized data were retrieved from the Brazilian Institute of Geography and Statistics (IBGE) and represent the values for the year 2016. [3]

Although the North accounts for more than 40 % of the national territory, less than 10 % of the Brazilians live in this area. As mentioned above, tropical rain forest is the dominating appearance of the landscape, with relatively small human influence in huge parts. Amazonas, the largest state of the North region, has an area of 1.57 million km^2, which is more than the fourfold of Germany. With only around 4 million people living in the Amazonas state in 2016, its density of population of 2.5 people per km^2 belongs to the lowest of all Brazilian states. The state of Rondônia is the densest populated in the North, but with 7.4 people per km^2

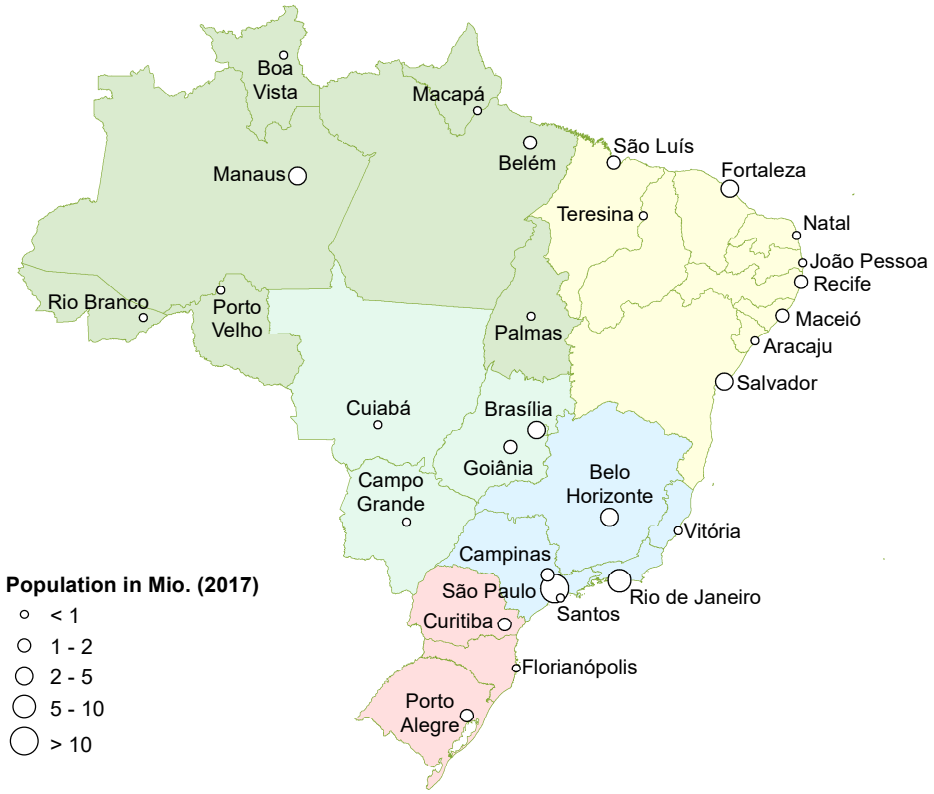

Figure 2.5: Brazil's largest cities [3]

significantly under the Brazilian average of approximately 25 people per km^2.

The Northeast region is the second largest by population and on third rank by size, with most of the people living close to the coast. Several cities between 1 and 3 million inhabitants are located directly at the Atlantic Ocean, like São Luis, Fortaleza, Recife, Maceió and Salvador, see figure 2.5. Due to difficulties for agriculture caused by the arid climate and the lack of infrastructure, the inland areas of the Northeast are sparsely populated. The states of Piauí and Maranhão have a lower population density than the Brazilian average. The other seven states are populated by more than 25 people up to 120 people per km^2.

All of the states in the Central-West are fewer populated compared to the Brazilian average, except of the Distrito Federal including the capital city Brasilia, with more than 500 people per km^2. The Central-West is the only region in Brazil without any connection to the sea.

Over 40 % of the citizens live in the Southeast, where the two largest Brazilian cities São Paulo and Rio de Janeiro are located in the states of the same names. The city São Paulo is with its more than 12 million inhabitants not only the largest city in Brazil, but also in South America. The state of São Paulo has a population over 44 million people, whereas around half of them live in the metropolitan area of the city São Paulo. In case of the state of Rio de Janeiro with close to 17 million inhabitants, around two third of the people live in metropolitan region of Rio de Janeiro and over 6.5 million people in the city itself. The states Rio de Janeiro (370 people/km^2) and São Paulo (180 people/km^2) are very densely populated, only excelled by the Distrito Federal.

The South region is the smallest of the five macro-regions, with less than 7 % of the Brazil's

territory, but on third rank by population. All states have access to the coast, whereas the major cities Florioanopolis and Porto Alegre are located directly at the sea and Curitiba relatively close to it.

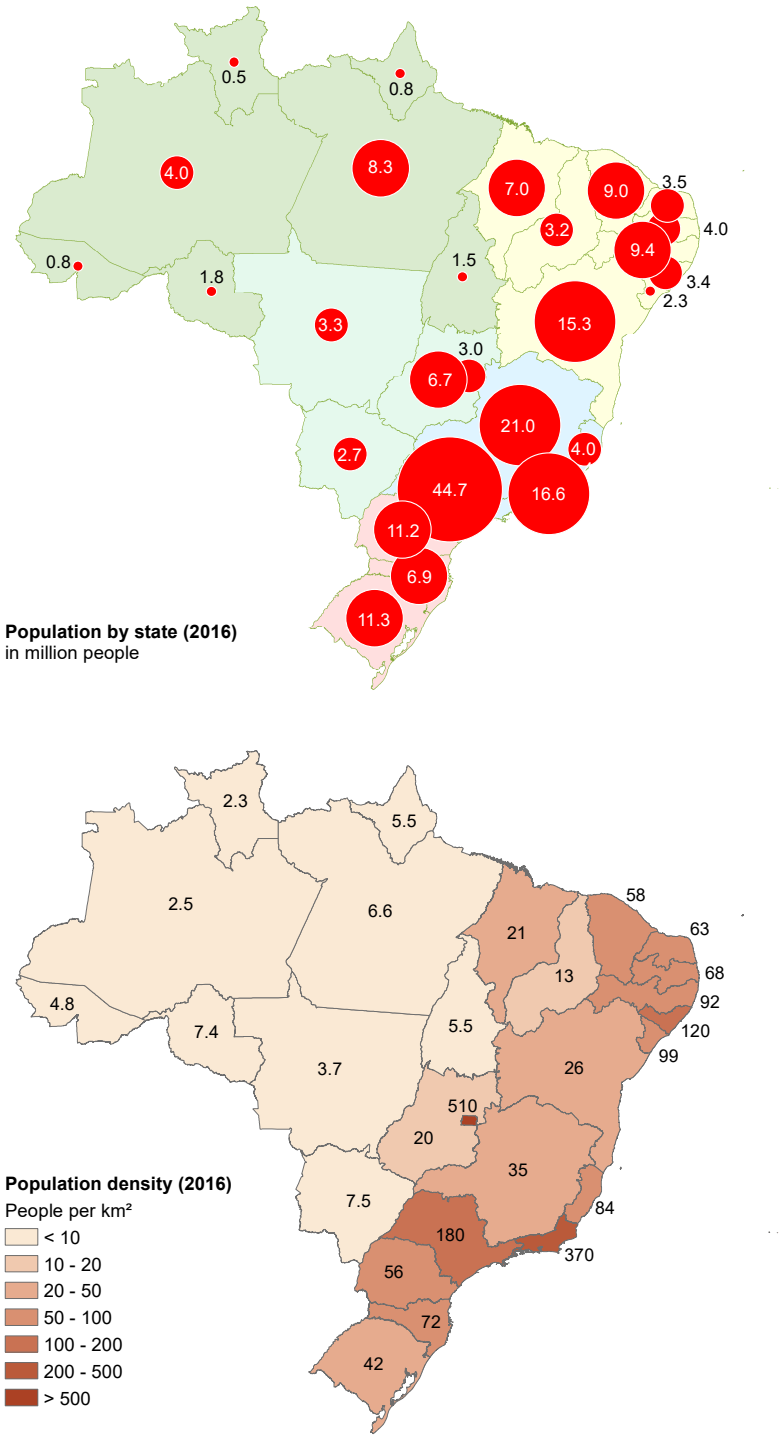

Figure 2.6: Distribution of population in Brazil [3]

2.3 Economy

Brazil has by far the largest economy in Latin America regarding the gross domestic product (GDP) in 2016, followed by Mexico and Argentina. One reason for its leading economic position in terms of total GDP is the fact, that Brazil has also the largest population of all Latin American countries. However, considering the GDP per capita, Brazil holds the seventh rank in Latin America, after Panama, Chile, Uruguay, Argentina, Mexico and Costa Rica. [33]

In 2017, the Brazilian labor force consisted of 104 million people out of the total population of 208 million, while unemployment rate almost doubled in the last three years reaching close to 13 %. [4, 34] With 69 % of the employees working in the service sector, this was in 2017 by far the most important branch in Brazil's labor market. Although Brazil is recognized to be very powerful in the agriculture sector, the share of employees working in this sector decreased from 18 % in 2007 to 10 % in 2017. In the same time, the employment in the industry sector remained relatively stable, with 22 % of the labor force employed in 2007 and 21 % in 2017. [35] The service sector not only offers most of the jobs in Brazil, it also contributed with 63 % vast majority to the national GDP in 2017. Its share increased between 2007 and 2017 from 58 % to 63 %, while in the same period, the industry employment decreased from 23 % to 18 %. The contribution of agriculture to the GDP ranged from 4 % to 5 %. [36] The development of employment and GDP in the agriculture sector show two remarkable aspects:

1. Increase in productivity, because agriculture employment almost halved whereas economic output remained on the same level
2. Lower productivity compared to the service and industry sector, as more than 10 % of the labor force generate less than 5 % of the GDP

In the top diagram of figure 2.7, several periods of steady economic growth are detectable, but also some deviations from that development. Last mentioned phases mark the economic crisis, Brazil was faced with in the last decades. The actual economic situation of citizens is not clearly recognizable, as GDP growth is driven both by recovery but also by rising population at a stagnation of income. The development of GDP per capita excludes the effect of rising population and is visualized in the bottom diagram of figure 2.7. Taking a closer look on the development of GDP per capita from 1960 to 2016, several economic phases are worth to be pointed out. A broad overview about Brazil's economic history can be found in [37], starting in the early 16th century with exports of Paubrasilia[1] and sugar.

Economic development since 1960

The economic prosperity until the early 1960s was caused in major parts by import substitution industrialization, which means that former imports were substituted by domestically produced goods. This transformation reduced the economic vulnerability from global prices for agricultural and mining products. Latter were the dominating export goods before import substitution

[1] Paubrasilia is a type of wood which was found in Brazil by first Portuguese discoverers. A similar wood was already known before in Portugal under the name *pau-brasil* and used to dye fabric in red color. The newly discovered country Brazil was named after this wood.

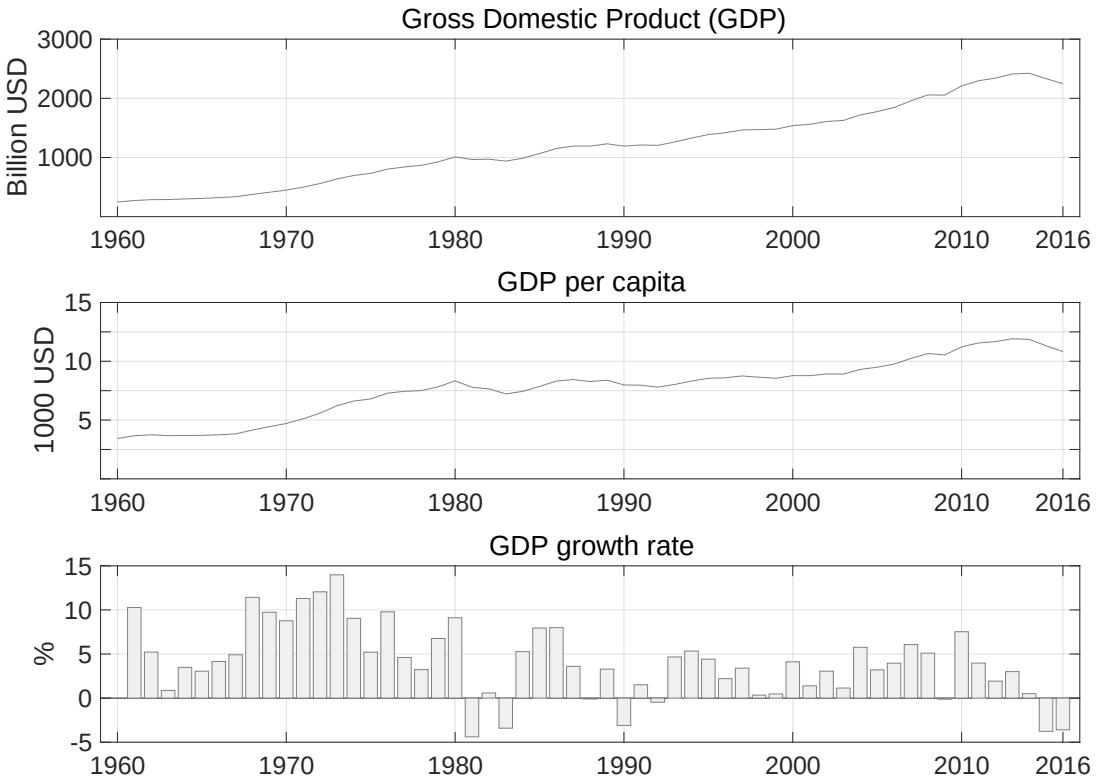

Figure 2.7: Brazil's gross domestic product in 2010 USD [4]

industrialization. Until 1964, Brazil witnessed a economic slowdown flanked by annual inflation rates over 100 % leading into a social and political crisis. Finally, the Brazilian democracy was substituted in a coup by the Brazilian military government in April 1964. [18]

The regime introduced policies and structural reforms to stabilize financial markets and support economic development. The federal government was successful in the first years after the takeover, expressed in significantly lower budget deficit, inflation rates around 20 % and in particular a historical economic boom. The bottom chart in figure 2.7 shows the enormous GDP growth rates in the late 1960s until the mid of the 1970s. Important measures for economic development were also the placement of technocrats in key economic policy-making positions to start planning and implementation of large infrastructure projects, such as expansion of transport networks, power generation and exploitation of natural resources. Most of these projects were conducted by state-owned companies, which made the government the dominant agent in Brazil's economy. Taking the top 25 firms in 1971 in terms of employment, 51 % of all employees worked for seven state-owned companies. From the 25 top firms in terms of assets, 17 were government firms having a share of 82 % of total assets. The Brazilian government became especially leading in the energy sector with dominating position in oil industry and electricity generation. In 80 % of the power generation capacity in 1971 was in state ownership compared with 36 % in 1962. In the same period, the power generation capacity approximately doubled, see table 2.1.

Table 2.1: Development of power generation capacity [18]

Year		1960	1964	1968	1972	1973
P_{inst}	GW	4.8	6.8	8.6	13.1	15.5

One further important source of economic growth was the expanded production of consumer durables. For example, the number of produced cars quadrupled from 38.000 units in 1964 to 409.000 units in 1973. The economic boom in this time was mainly driven by domestic demand. Even though exports grew also in the period from 1964 to 1972 in absolute values, their weight with less than 8 % of the GDP was too small to be a main driver. [18]

Sustained growth characterized the 1970s despite lower rates after the 1973 oil crisis. The phase of continuing economic prosperity until 1970s was later called Brazil's economic 'miracle' *(Milagre econômico brasileiro)*. [38] Several projects were conducted in this decade to reduce the import dependency, but also to mitigate the vulnerability from future oil price shocks. Concrete measures were the expansion of electricity production from hydro (for example initiation of Itaipú project), coal and nuclear power [39] besides widespread use of domestically produced ethanol from sugarcane [40] for road traffic and increased domestic crude oil production. The impacts 1979 oil crisis to the world economy affected Brazil as well as the risen world interest rates. Latter was especially a problem for the Brazilian budget, because the government inter alia borrowed billions of USD in foreign countries to finance above mentioned large-scale infrastructure projects. It got increasingly difficult for Brazil in the early 1980s paying the interests on its depts and keeping public demand on a sufficient level to prevent a recession. Brazil's economy collapsed in 1981, inducing both social tensions and dissatisfaction. [38]

This economic crisis accelerated the process of reestablishing democracy after the military dictatorship from 1964 to 1985. Compared to the preceding decade, the 1980s were characterized by low growth and investment, suffering under high interests for foreign depts. Brazil's eighties are referred as the "lost decade" *(década perdida)*, see p. 288 f. in [41]. The consensus grew in this decade, that privatization of state enterprises is one measure revitalize the economy. In the early 1990s, Brazil adopted market opening and large-scale privatization programs as key instruments to fight the economic weakness. [37] These policies showed success expressed in moderate growth until the end of the millennium, see figure 2.7.

After weak years around 2000, Luiz Inácio Lula da Silva *(Lula)*, head of Brazil's workers' party and former union leader, was elected for president in 2002, reelected in 2006 and stayed in office until 2011. [42, 43] Numerous foreign and domestic investors feared a radical shift towards left governance in contrast to liberal policies of previous years. While many of Lula early supporters were disappointed from his presidency, he became appreciated by the business community because of his moderate course. Main objectives of Lula's administration were economic development and reduction of income inequality, both in the society as a whole and in regional context. [42] One major program to fight extreme poverty was *Bolsa Família*, which was partly successful as discussed in [44, 45] and detectable in the development of the Gini index[2] shown in figure 2.8.

[2] A Gini index for income distribution of 100 indicates, that one individual receives all the population's income,

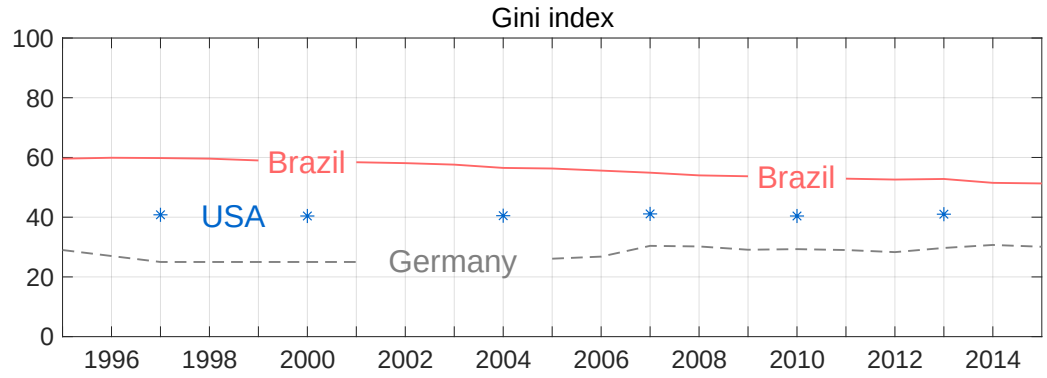

Figure 2.8: Gini index for income distribution of selected countries [4, 5]

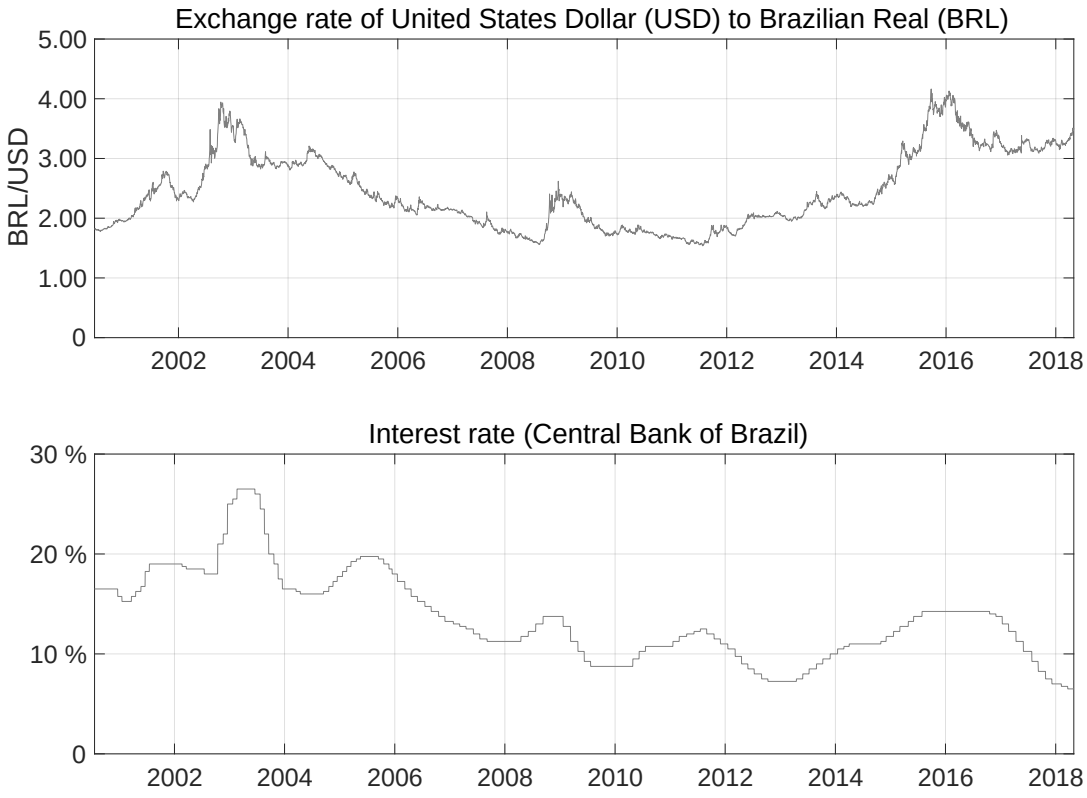

Figure 2.9: Exchange and interest rates [6, 7]

During the presidency of Lula not only the total and the per capita GDP increased, see figure 2.7, but also the Gini index decreased. Thus lower income groups participated from economic growth and were enabled to buy and apply certain products, for example passenger cars. [47] Increased production and application subsequently leads to higher energy demand, therefore economic growth and income distribution are important determinants for future energy demand. Despite these efforts for equal income distribution, the falling Gini index still proceeds

whereas 0 means everyone in the population earns the same. For further information, see chapter 6 in [46].

on a significantly higher level compared to the United States of America and Germany. Also considerable differences concerning GDP per capita remained over the country, see figure 2.10. Besides smoothing income differences and supporting economic prosperity, Lulas policies stabilized the Brazilian real (BRL) in relation to the United States Dollar (USD) and lowered interest rates, see figure 2.9.

Brazil even showed a certain resilience against the financial crisis from 2007/2008, recognizable as relatively low impact to GDP growth, exchange and interest rates in comparison to other crisis. From 2011, the economy slowed down after Dilma Rousseff succeeded Lula as president. Brazil was shocked by a corruption scandal known as "Operation Car Wash" *(Operação Lava Jato)* in 2014 affecting major parts of the political establishment including government and opposition as well as numerous Brazilian business leaders. Besides the collapse in global commodity prices, these incidents led to the recession in 2015 and 2016. One political consequence was the removal of president Dilma Rousseff from office by impeachment and Michel Temer appointed as her successor. [48, 49]

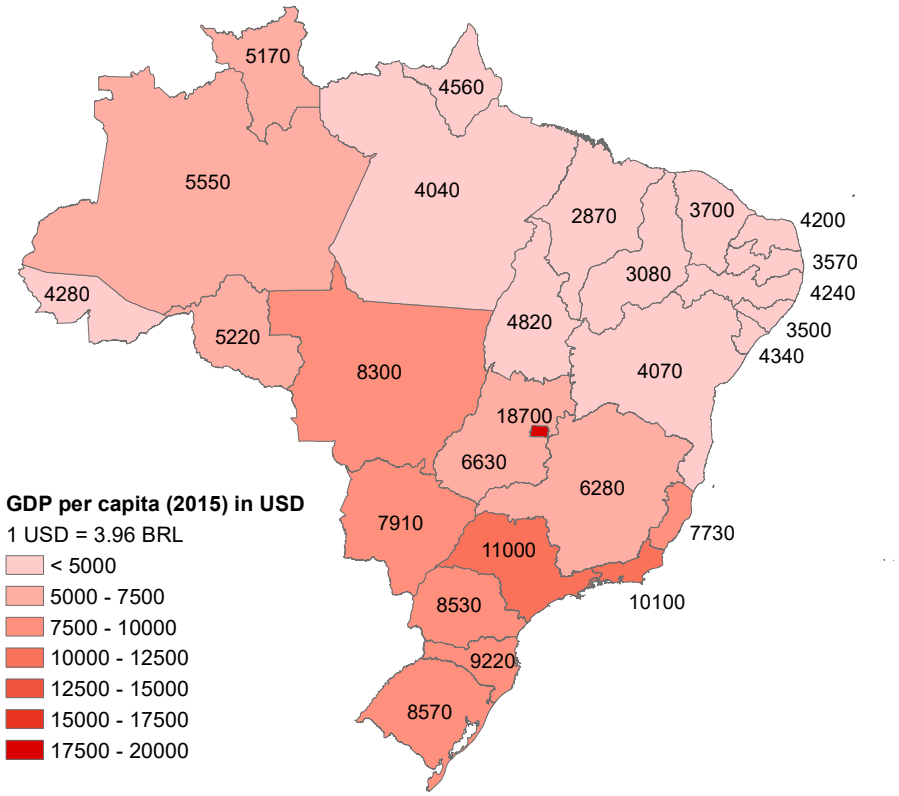

Figure 2.10: GDP per capita by Brazilian federal state [3]

Challenges for economic development

Apart from specific occurrences, Brazil held in terms of corruption[3] rank number 96 of 180 countries. Since corruption is considered to be a main factor for hindrance of economic devel-

[3]Referring to the corruption perception index for 2017 published by Transparency International. [50] In this ranking, New Zealand was the least corrupt country in the world, followed by Denmark on second rank and Finland,

opment, wealth and investment, mitigating corruption could unleash economic potentials for the future. [51] Furthermore, excessive bureaucracy as well as inefficiencies in the legal system are responsible for a significantly improvable position in the global ease of doing business ranking[4], were Brazil was in 2017 on 125th position. [52] Difficulties for foreign trade activities are also caused by high financial expenditures and time requirements for across boarder trading. [53] In the same manner exchange of goods are hindered by Brazilian import tariffs in Brazil, which are relatively high in comparison to those of other developed countries. [54] Fighting corruption and removing obstacles for doing business are necessary to exploit later discussed potentials for improvements in the energy system.

Of course, investments can also be made by locals and not only foreign investors. To enable people making investments, a sufficient income is necessary for savings and later expenditures. Taking the GDP per capita as an indicator for investment strength, obvious regional differences are remarkable within Brazil: While people in the Northeast and the North account to the poorest, the Central-West population has a mid-range income, whereas on a Brazilian scale the Southeast and South is relatively rich, see figure 2.10. Having the above mentioned inequalities of income in mind, subsequently only a minority of the citizens are able to dispose these average financial resources shown on the map. On a global scale of GDP per capita Brazil occupied in 2017 the 110th position and was therefore located in the worldwide mid-range.[5]. With a GDP per capita of 15,500 USD, Brazil was approximately 10 % under the global average of 17,300 USD. [22]

Norway and Switzerland on third position. The most corruptest countries were Syria (178th), South Sudan (179th) and Somalia (180th).

[4] Corresponding to the World Bank's *Doing Business Report* from 2018, see table 1.1. on p. 4 in [52]. The first three positions are held by New Zealand, Singapore and Denmark, the last three by Venezuela, Eritrea and Somalia.

[5] GDP/cap in 2017 USD and purchasing power parity (PPP) considering domestic price levels. The ranking includes 229 territories, not only states, for example Gibraltar is listed separately from Great Britain, the European Union besides its member states. Lichtenstein is on 1st position with 139.100 USD/cap, Burundi with 700 USD/cap on 229st. For further information, see *The World Factbook* published by the Central Intelligence Agency (CIA). [22]

Chapter 3

Energy sector in Brazil

This chapter provides an overview about key figures, specific developments and special characteristics of the Brazilian energy sector. Initially, a brief overview about the market design and the legal situation is given. Section 3.1 delivers an insight over primary energy and electricity production by source in relation to the economic and political development described in 2.3. Paragraph 3.1 also includes a description of present tariffs with focus on the residential sector. The most important components and developments of Brazil's energy demand are mentioned in section 3.2. The chapter ends with an estimation of the area for photovoltaics (PV), which could not only replace ethanol made from sugarcane in the transport sector, see subsection 3.2.2.

The national privatization programs from the 1990s also included the electricity sector. After the inauguration of Fernando Henrique Cardoso as Brazilian president, main phase of the privatization were the years from 1995 until 1998. The conversion of public electricity companies into private organizations delivered total revenues of more than 22 billion USD for Brazil. Before the sale to private investors, by market shares around 98 % of the power generation capacity were in public property, 90 % of the transmission grid and 98 % of the distribution grid. Power stations were by the majority in hands of the Brazilian state, whereas the grids where predominantly owned by the federal states. [55]

In 1996, Brazil established a regulatory agency abbreviated ANEEL *(Agência Nacional de Energia Elétrica)* based within the Ministry of Mines and Energy *(Ministério de Minas e Energia, MME)*. ANEEL has the role to provide equilibrium between the government, the consumers and investors. The ability to enforce strategic interests for national development is one main issue of the Brazilian government in terms of energy policy. In contrast to that, ANEEL has to secure fair tariffs for all consumer groups, a high reliability of power supply and transparency in many ways. For investors, ANEEL has to maintain clear and predictable rules and enable calculable remuneration. [56]

Mini and micro-generation are compensated via the net metering mechanism described in section 3.1. In contrast, new large power generation capacities are brought into the electricity market via auctions. The same method is applied to promote investments in the transmission and distribution infrastructure. The Brazilian regulator ANEEL organizes and conducts these auctions and publishes both offers, documents, and results. A further review of market mechanisms and auctions for the electricity sector in the Latin American context can be found in [57, 58].

3.1 Energy supply

Figure 3.1 shows Brazil's primary energy supply corresponding to the Brazilian Energy Balance from 2017. [8] Several aspects are remarkable concerning development and composition. First of all, the quantity of energy used slightly more than quadrupled from 1970 to 2016. The steady growth was interrupted by some phases of stagnation or even decline. The years of economic weakness mentioned in the previous chapter and illustrated in figure 2.7 are clearly visible in the development of primary energy supply. Especially noteworthy are the declines after the 1979 oil crisis, the financial crisis from 2007/2008 and the recent recession starting in 2015. Furthermore, the impacts of certain policies affecting the energy sector are recognizable. Measures taken to mitigate the dependency on mineral oil were the promotion of ethanol as car fuel made from sugarcane, the initiation of a nuclear power program, the construction of hydro dams as well as the expanded use of coal and natural gas. As a consequence, the share of these energy carriers increased, while the growth of mineral oil was disproportionately low. Nevertheless, oil was in 2016 still the most important component of primary energy supply, whereas firewood and charcoal was the main source in 1970. The relevance of wood for energy use decreased significantly since 1970. The data set also includes solar power and wind. Latter is detectable in the chart as very thin, light blue area above sugarcane. Wind power contributed 33 TWh in 2016, which was around 1 % of the total primary energy supply, while solar power made up only the 40,000th part, approximately 85 GWh from 3,350 TWh. Therefore, the share of solar power is invisible in the diagram.

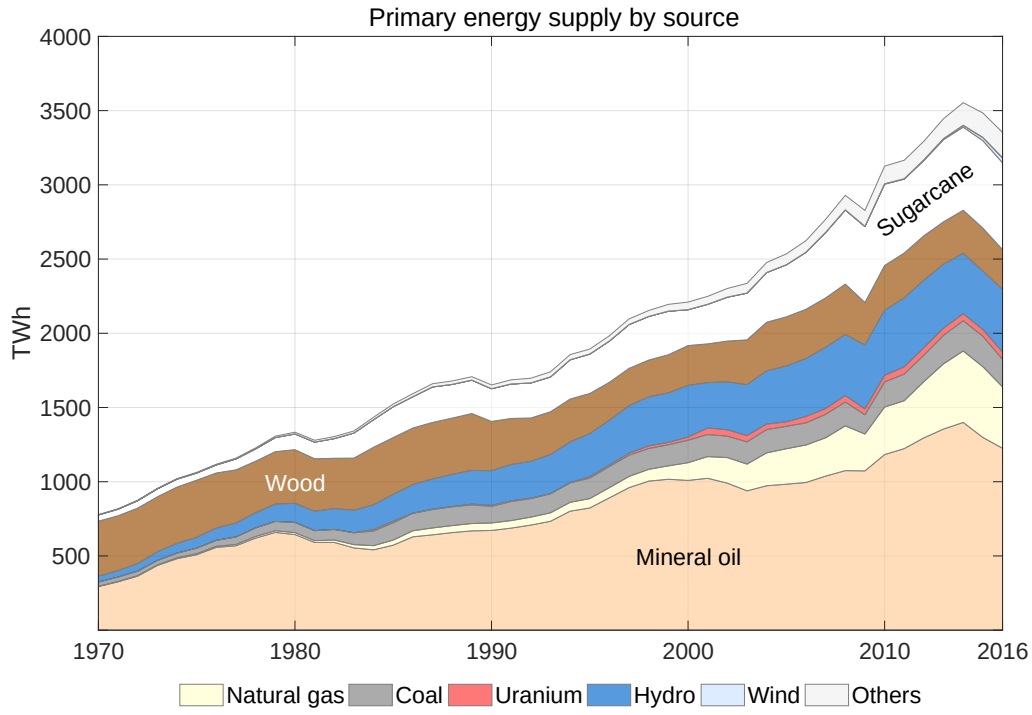

Figure 3.1: Development of Brazilian primary energy supply [8]

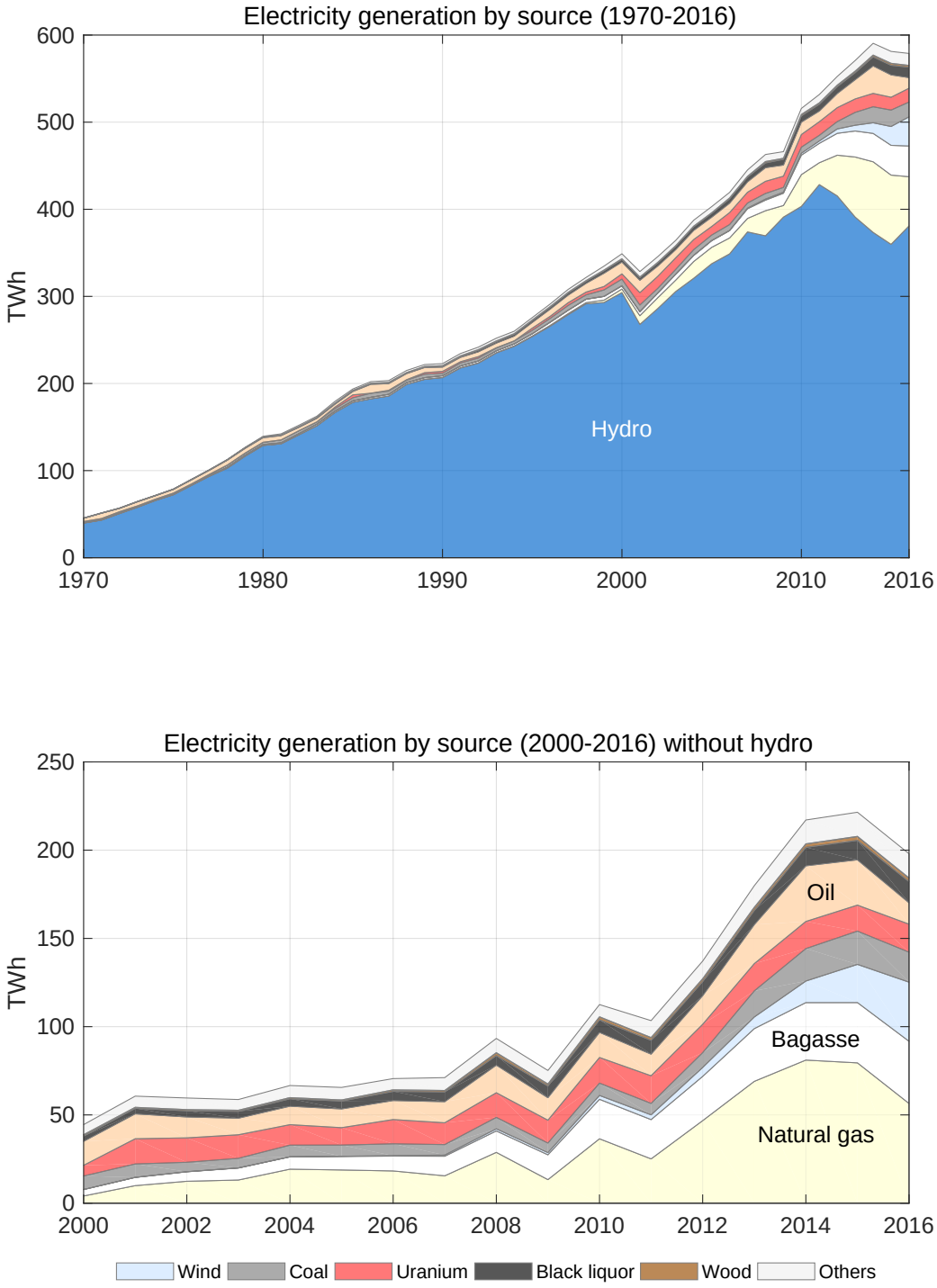

Figure 3.2: Generation of electricity by source [8]

The production of electricity increased more than tenfold from approximately 50 TWh in 1970 to just under 600 TWh in 2016, see top chart in figure 3.2. The steady growth was only interrupted by a shortage in hydroelectricity and the recent economic crisis since 2014. Hydroelectricity as the major source of renewable power has traditionally overwhelming importance for Brazil's electricity generation. The share of renewable power was persistently above 90 % from 1973 until 2000 and fell under 80 % in 2013. Reasons for this decrease were severe droughts around 2000 and 2014 [59]. Furthermore, hydropower expanded slower than the electricity demand. The bottom diagram in figure 3.2 shows in detail the power generation by source since the year 2000 excluding hydropower. This development indicates, that hydropower was complemented more and more with thermal electricity generation, mainly by natural gas and oil, but also residuals from sugar and paper industry like bagasse and black liquor. Wood and the latter two are considered both as renewable sources and thermal power. Since 2010 also wind power contributes a recognizable share. In 2016, wind energy converters produced 33 TWh or 5,8 % and overtook nuclear power, which added annually 14 TWh in the average since 2000. The share of solar power of 0.015 % in 2016 was still too low to be detectable in figure 3.2.

The development of Brazil's carbon dioxide emissions (CO_2) is illustrated in figure 3.3, excluding emissions caused by land use, land-use change and forestry (LULUCF).[1] The total emission increased fivefold from around 100 million tons in 1970 to more than 500 million tons in 2014, see diagram (a) in figure 3.3. The growth of CO_2 emissions can be mainly explained with the increased use of primary energy, not with a change in composition of sources towards fossil fuels, since specific emissions stayed in a relatively narrow range between 120 and 150 kg per MWh primary energy, see diagram (b) in figure 3.3.[2] As a result of economic weakness the demand for oil dropped, which caused the minima in specific CO_2 emissions. In comparison to the population, which doubled from 1970 to 2014, the total emissions grew disproportionately high based on the fact of almost tripled emissions per capita from 1 ton in 1970 to 2.6 tons in 2014, see diagram (c). Despite this significant increase, the Brazilian CO_2 emissions per capita were always under the global average throughout this period. The world's average was around 4 tons of CO_2 in 1970 and 5 tons of CO_2 per capita in 2014. [4] The Brazilian economy has a relatively low carbon footprint compared to other national economies. As shown in diagram (d) since 1970, around 0.2 kg CO_2 are emitted to generate 1 USD of GDP, whereas the worlds average was 0.77 kg per USD GDP in 1990 and 0.33 kg in 2014. [4]

For the above mentioned developments, significantly increased primary energy supply and electricity production per capita, see figure 3.4, were main drivers besides dynamic population growth described in section 2.2. Possible factors for mitigation of emissions are therefore efficiency and sufficiency to reduce per capita energy demand, decarbonization of processes across all sectors as well as stabilization of population.

[1] For detailed information about composition of greenhouse gas emissions in Brazil, including sources like LULUCF, industrial processes, fugitive emissions and waste disposal, see table 2.1 on p. 43 f. in [60].

[2] Primary energy supply corresponding to table 1.3.a in Brazilian Energy Balance [8] divided by total CO_2 emissions retrieved from World Bank Data [4].

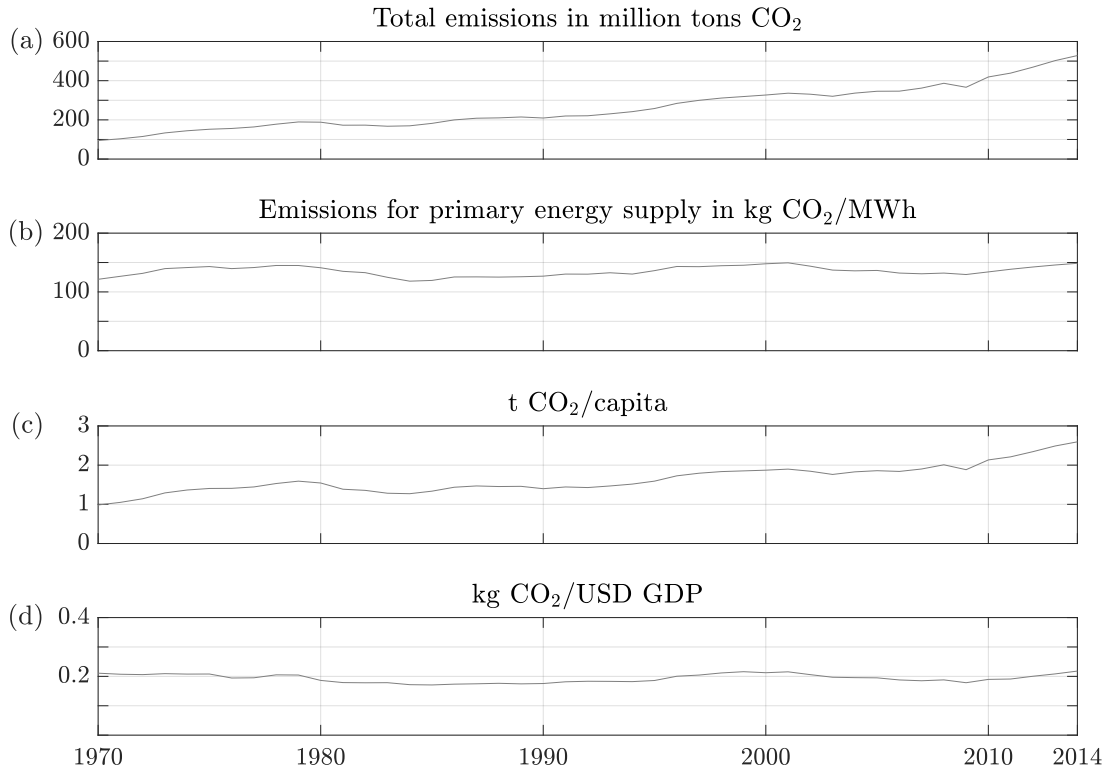

Figure 3.3: Development of total and specific emissions in Brazil [4, 8]

The Brazilian Government signed the Paris agreement and planed to reduce greenhouse gas emissions until 2030 by 43 % below the level of 2005. This reduction target in relation to 2,1 Gt (2,100 million tons) in 2005 including green house gas emissions for land-use, land-use change and forestry means a limit of 1,2 Gt in 2030. To reach this target, Brazil's government planned to measures among others like: [60]

- increasing use of biofuels
- sustainable agriculture development
- reforestation and prevention of deforestation
- higher shares of renewable energy besides hydropower
- promotion of clean technology and efficiency in the industry sector
- infrastructure and efficiency improvements in the traffic sector

A shift towards renewable energy is a main issue in this work, that includes an estimation about necessary photovoltaic installation to supply a future transport sector relying mainly on electricity. Electrification of the traffic sector has not been an explicitly mentioned target in the above cited government declaration. However, a substitution of biofuels with electricity produced by photovoltaics is in that matter important, as it could reduce the need for cropland significantly. A reduction of agricultural land for cultivating sugarcane as basis for biofuel would deliver spatial potentials for reforestation leading to a reduction of emissions, see section 3.2.2. The section about electric supply of the traffic sector derives a brief cost comparison

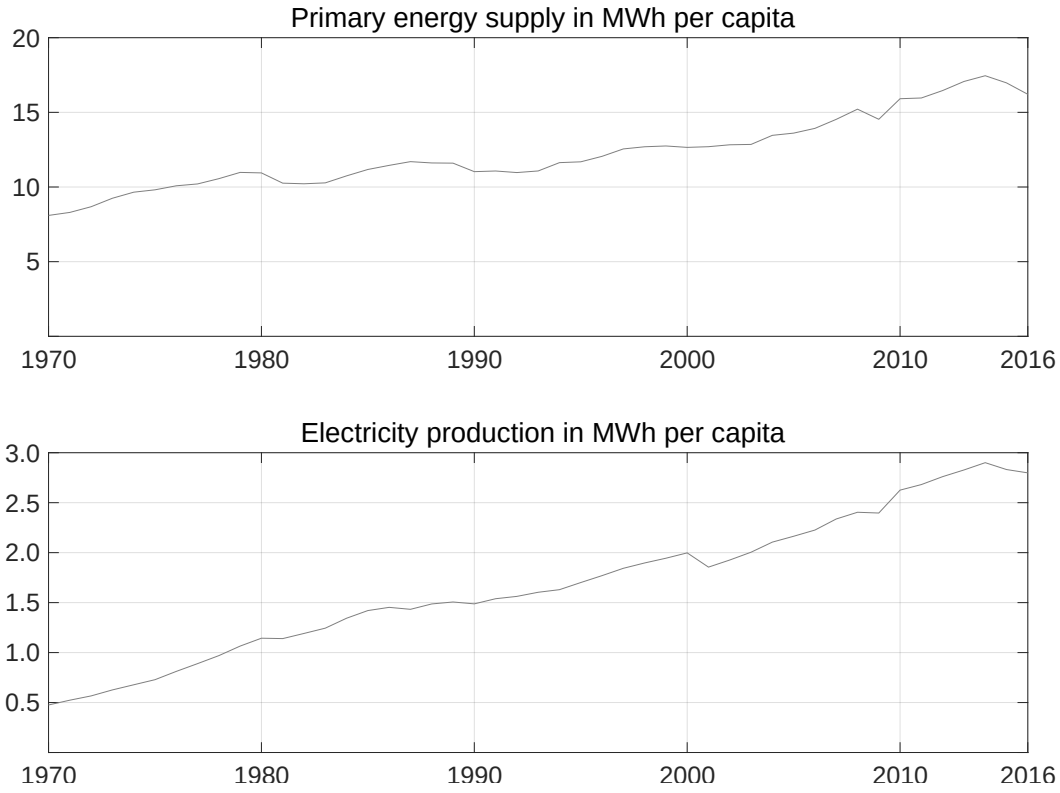

Figure 3.4: Energy per capita [4, 8]

to traditional solutions. The following paragraph delivers an overview about most important economic aspect of the present Brazilian energy sector.

Economic aspects

The following pages summarize basic economic aspects of the electricity supply in Brazil from a consumers perspective. This includes present prices and recent developments differentiated by demand sectors and regions. In section 3.1 special Brazilian tariffs and tariff components are presented, which act as incentive for both the relieving system from demand and generating distributed electricity. The final section displays the quality of supply in recent years as indicator of successful efforts towards grid stability on the one hand. On the other hand, still existing power outages can be an argument to promote distributed generation and storages such as batteries.

Electricity tariffs

Figure 3.5 displays electricity tariffs for residential consumers and highlights regional differences. Corresponding to the Brazilian tariff structure, all consumers on a voltage level less or equal than 2.3 kV belong to the so called ”group B”, the high voltage consumers greater than 2.3 kV are part of ”group A”. [61] The focus in the following paragraphs is on group B.

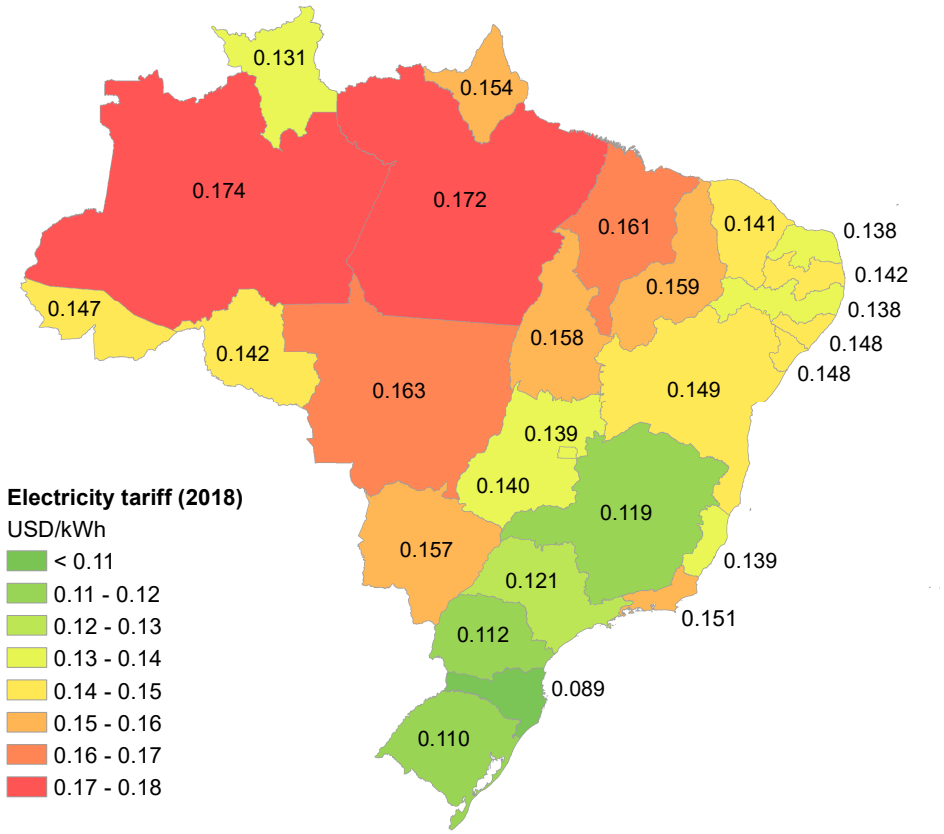

Figure 3.5: Residential tariffs by state in 2018 [9]

Expressed in USD per kWh[3], each number shows the lowest tariff per federal state retrieved in April 2018 from ANEEL *(Agência Nacional de Energia Elétrica)*, the Brazilian Electricity Regulatory Agency. [9] The minimum tariffs are relevant for later investigations as upper bound for costs of photovoltaic power supply, see section 4.5. The displayed values do not include taxes and other surcharges, such as the value-added tax ICMS and the social contributions PIS and COFINS.[4] The total share of taxes, duties and other surcharges is between 30 % and 40 % of the gross price[5], whereby this share varies from one state to another. Brazil's densely populated and wealthy South and Southeast have in national comparison the lowest electricity tariffs in contrast to the North, where the people have to pay significantly more for power supply. The tariffs range from 0.089 USD/kWh in Santa Catarina up to 0.172 USD/kWh in Pará or 0.174 USD/kWh in the state of Amazonas. Reasons for these remarkable tariff differences up to 90 % within the country can be seen in regional specific structures of electricity supply. In the sparsely populated North, the power generation relies in higher parts on costly decentralized thermal power. The South gets its electricity from large hydropower stations, which have usually sufficient water inflow throughout the whole year caused by the absence of a distinct dry season. Details about the regional distribution of electricity generation capacity are

[3] Exchange rate on April 27th 2018: 1 USD = 3,471 BRL. Tariffs do not include taxes and other surcharges.

[4] For further information about ICMS *(Imposto sobre Circulação de Mercadorias e Serviços)*, PIS *(Programa de Integração Social)* and COFIN *(Contribuição para o Financiamento da Seguridade Social)*, see [62, 63].

[5] See section *Como é composta a tarifa* in [64] and p. 9 in [65].

explained in chapter 5. Taking into account the GDP per capita as indicator for income, which was persistently under 15.000 USD, see figure 2.7, Brazilian electricity prices are perceived to be very high.

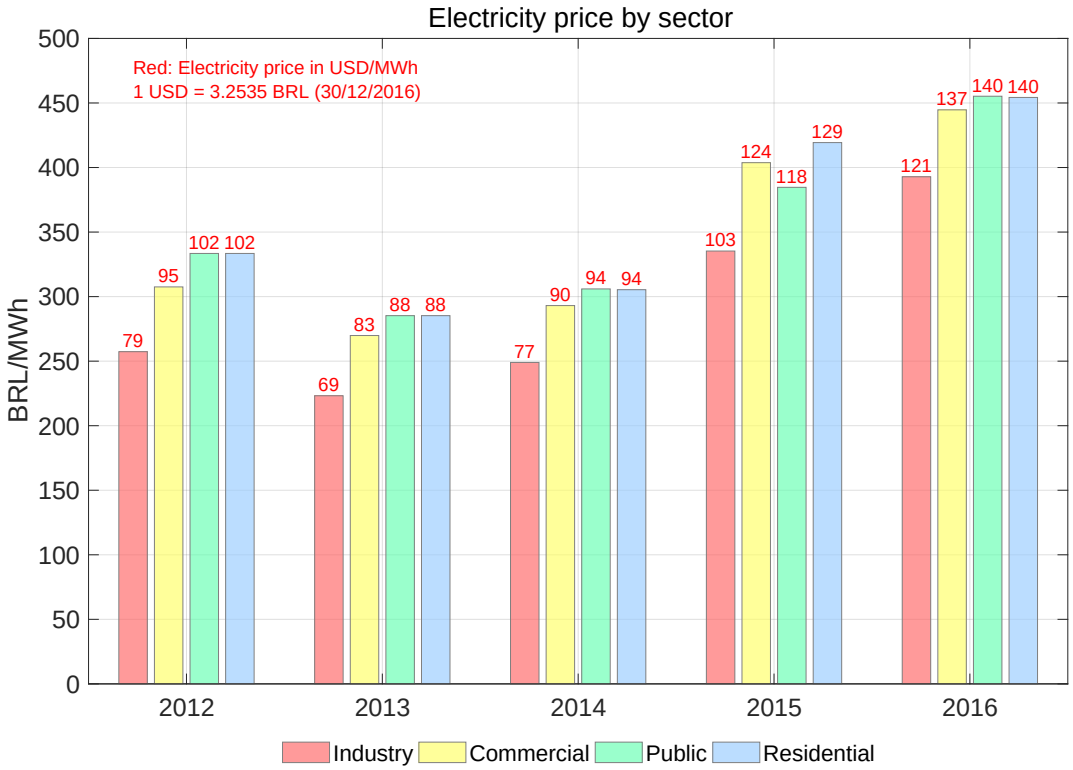

Figure 3.6: Electricity price by sector [10]

The 2017 Statistical Yearbook of electricity *(*Anuário Estatístico de Energia Elétrica) gives a further regional and sectoral insight in developments of electricity rates.[6] Figure 3.6 displays the development of electricity prices for Brazil's most import sectors by consumption. In official Brazilian statistics also the sectors rural and agriculture consumption are registered as well as public lighting, public service and own use. Due to their minor importance, see figure 3.10, and their similar price level, they are for the sake of clarity not shown here. Since 2012, the electricity prices for industry consumers have been always the lowest, despite this gap became smaller. Industry customers had to pay around 22 % less per megawatt hour than public or residential consumers in 2012. This difference melted down until 2016 to approximately 16 %. In the same time, industry consumers witnessed with almost 53 % the highest relative price increase, whereas the residential sector had with 36 % the lowest surcharge. The incline of average rates for other consumers stayed in between.
Whereas figure 3.5 provided only residential tariffs for 2018, table 3.1 lists the average rates per region over all sectors. The values displayed originate from a data query in 2018.[7] The

[6] See table 2.15 and 2.15 on p. 72 in [10]

[7] Exchange rate on April 27th, 2018: 1 USD = 3,471 BRL. Data query including months from January to September 2018, see [19].

Table 3.1: Average electricity tariff by region in 2018 [19]

	North	Northeast	Central-West	Southeast	South
BRL/MWh	513.2	421.3	458.6	446.0	417.4
USD/MWh	147.9	121.4	132.1	128.5	120.3

cross-sectoral average prices reveals the same ranking like in case of residential tariffs: The lowest price levels for electricity prevail in the South, whereas the highest in the North.

Tariff flag system

At low reservoir levels, power generation relies increasingly on thermal power causing higher costs due to fuel consumption. Therefore, the flag electricity tariff was introduced in 2015 as a seasonal price signal. Consumers participate over a surcharge partly on these additional costs. A flag in green, yellow, or red indicates visible for customers the surcharge level. The flag color can change monthly. The red flag is furthermore divided into two stages. Flag colors depend on the marginal costs of electricity generation, which represent somehow criticality of the power generation system. Based on the cost calculation conducted by the Brazilian National Grid Operator ONS *(Operador Nacional do Sistema Elétrico)*, ANEEL sets the flag color monthly determining the surcharge. As most of the electricity meters in Brazil register monthly consumption per customer, the flag tariff system works as an incentive to save electricity during shortages. The calculation method and further explanation can be found in [66]. Meaning of flag colors and surcharges corresponding to [67] are summarized in table 3.2.

Table 3.2: Meaning of flag colors

flag color	system condition	reservoir levels	surcharge in BRL/kWh
green	good	high	-
yellow	tense	medium	0.01
red (stage 1)	critical	low	0.03
red (stage 2)	very critical	very low	0.05

Net metering system

The net metering system regulates the financial compensation for grid-connected distributed generation. Resolution 482 from April 2012 acts as legal foundation for this system. [68] In this context, micro generation describes units up to 100 kW installed capacity, whereas mini generation covers the range from 100 kW to 1 MW. For net metering, these generators are connected to distribution grids on consumer side. Further technical requirements are electricity meters, which allow bidirectional metering. That can be two unidirectional meters on low voltage level: One meter measures the consumption from the grid, the other one the feed-in electricity. After one month as the typical accounting period, the invoice is calculated from the balance between generation and consumption.
The following paragraph describes the calculation of monthly costs C_{t} for a low voltage

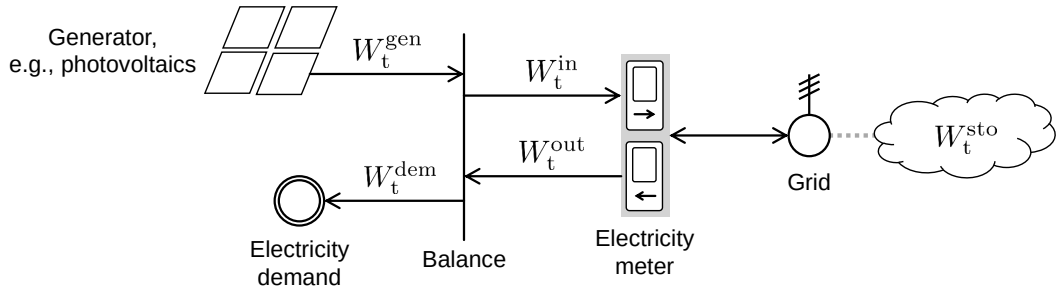

Figure 3.7: Net metering system

consumer (group A) using net metering.[8] The principle is illustrated in figure 3.7. For the sake of simplicity these calculations do not include taxes, duties and surcharges. The monthly invoice depends first of all on the energy balance between demand $W_\mathrm{t}^\mathrm{dem}$ and generation $W_\mathrm{t}^\mathrm{gen}$ during the month t. The relevant net quantity of electricity $W_\mathrm{t}^\mathrm{net}$ to calculate the invoice can be further reduced by withdrawing electricity $W_\mathrm{t}^\mathrm{out}$ from an electricity credit. Latter can be considered as a virtual storage with the energy content $W_\mathrm{t}^\mathrm{sto}$.

$$W_\mathrm{t}^\mathrm{net} = W_\mathrm{t}^\mathrm{dem} - W_\mathrm{t}^\mathrm{gen} - W_\mathrm{t}^\mathrm{out} \tag{3.1}$$

For the availability of a power connection, the customer has to pay at least a monthly basic fee $W_\mathrm{min} \cdot p_\mathrm{el}$. This basic fee is the simple product out of a minimum purchase quantity W_min and the electricity price p_el. These fixed costs are levied irrespectively of a net consumption $W_\mathrm{t}^\mathrm{net}$ less than a minimum purchase quantity W_min. Depending on the case, the monthly invoice C_t is calculated as product of net or minimum quantity and electricity price:

$$C_\mathrm{t} = \begin{cases} (W_\mathrm{t}^\mathrm{dem} - W_\mathrm{t}^\mathrm{gen} - W_\mathrm{t}^\mathrm{out}) \cdot p_\mathrm{el} & \text{if } W_\mathrm{t}^\mathrm{net} > W_\mathrm{min} \\ W_\mathrm{min} \cdot p_\mathrm{el} & \text{if } W_\mathrm{t}^\mathrm{net} \leq W_\mathrm{min} \end{cases} \tag{3.2}$$

The amount of electricity $W_\mathrm{t}^\mathrm{out}$ taken from the credit or virtual storage $W_\mathrm{t}^\mathrm{sto}$ depends first of all on the energy balance. If generation exceeds the demand within a month, no electricity is needed from the storage, see lower case in equation 3.3. The upper case describes a deficit between demand and generation. One has to distinct two further cases. If the difference between demand and generation is greater than the whole storage content, the content is used entirely. If the difference is lower than the credit, only this difference has to be withdrawn from the storage.

$$W_\mathrm{t}^\mathrm{out} = \begin{cases} \ldots & \text{if } W_\mathrm{t}^\mathrm{dem} > W_\mathrm{t}^\mathrm{gen} \quad \begin{cases} W_\mathrm{t}^\mathrm{sto} & \text{if } W_\mathrm{t}^\mathrm{dem} - W_\mathrm{t}^\mathrm{gen} > W_\mathrm{t}^\mathrm{sto} \\ W_\mathrm{t}^\mathrm{dem} - W_\mathrm{t}^\mathrm{gen} & \text{if } W_\mathrm{t}^\mathrm{dem} - W_\mathrm{t}^\mathrm{gen} \leq W_\mathrm{t}^\mathrm{sto} \end{cases} \\ 0 & \text{if } W_\mathrm{t}^\mathrm{dem} \leq W_\mathrm{t}^\mathrm{gen} \end{cases} \tag{3.3}$$

The only missing quantity in the preceding equation is the credit or virtual storage content $W_\mathrm{t}^\mathrm{sto}$. Its value is calculated with an intertemporal energy balance, which considers the content

[8] The formulas were derived from the calculation example on p. 20 ff. in [69]

W_{t-1} of the preceding month $t-1$ as well as the input W_t^{in} and the output W_t^{in} of the present month t.

$$W_t^{sto} = W_{t-1}^{sto} + W_t^{in} - W_t^{out} \tag{3.4}$$

Finally, the quantity of electricity W_t^{in} is added to the credit, when there is a surplus between generation W_t^{gen} and demand W_t^{dem}.

$$W_t^{in} = \begin{cases} W_t^{gen} - W_t^{dem} & \text{if } W_t^{gen} > W_t^{dem} \\ 0 & \text{if } W_t^{gen} \leq W_t^{dem} \end{cases} \tag{3.5}$$

According to equations 3.4 and 3.5, the storage content W_t^{sto} grows every month in case of exceeding generation over demand. Only in months of deficits, the electricity credit can be used with financial benefits. A high storage level alone does not deliver any monetary advantages. Because of the fact that electricity credits W_t^{in} expire after 60 months, see paragraph XII on p. 9 in [68], there is no incentive for a customer to produce electricity above the own consumption. Under certain circumstances, net metering is also possible if distributed generation and consumption are installed at different locations. Further explanations can be found in paragraph 5.4 in [70].
The monthly costs C_t represent the net invoice excluding taxes, duties and surcharges. The value-added tax ICMS is levied in some Brazilian states on the whole amount of energy obtained from the grid per month without considering the existence of a generator on consumer side. The state of Minas Gerais launched the initiative in 2013, that the ICMS tax has only to be payed for the positive difference between demand and supply. However, this nature of tax collection is not consistent among the Brazilian states. The legal background is further explained in paragraph 5.11 in [70]. Besides the state taxes, also the federal social contributions PIS and the COFINS have to be payed for consumed electricity. ANEEL's vision was, that these taxes to be only levied on the positive difference between consumption and feed-in, if negative, only on the value for availability. But practically, it depends on the tax regime of each state, if the taxes have to be payed only for the positive difference or for the whole amount of energy received from the grid.
Further explanations about the legal treatment as well as registration and commissioning of micro and mini power generation are given in a official publication from ANEEL, see [69]. This paper also includes a exemplary invoice calculation for the case with generation on consumer side applying net metering.

White tariff

In September 2016, resolution 733 was passed as legal foundation for the so called white tariff *(tarifa branca)*. [71] This tariff option is available for most low voltage customers (group B) with electricity prices depending on day and hour of consumption. The price per kWh is not constant during a month like in case of conventional tariffs, it varies in three steps, see figure 3.3. During off-peak hours, the electricity is offered for a reduced rate below the conventional tariff. In contrast to that, electricity consumption during peak and intermediate hours is more expensive than in other times. Therefore, the white tariff acts as incentive for consumers to

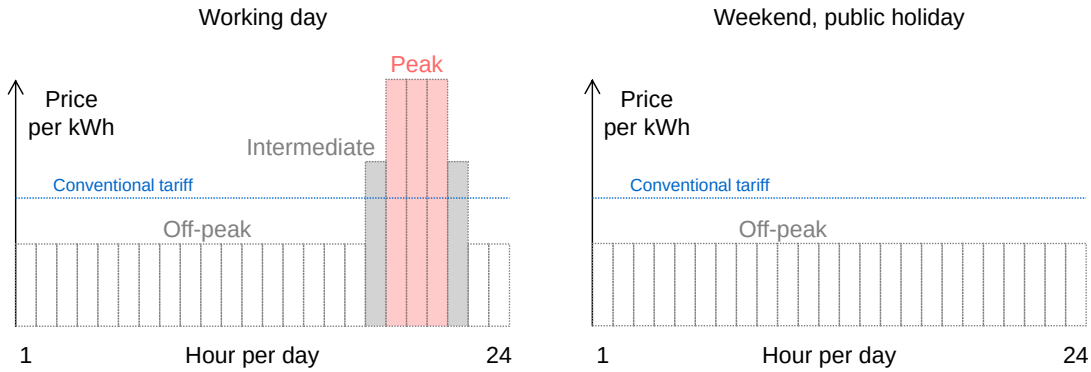

Table 3.3: White tariff in comparison to conventional tariff

shift demand from peak to off-peak hours. Subsequently, the client saves money, whereas the electricity system gets relieved and prevents shortages. Further explanations can be found in an publication from the Brazilian Association of Distribution Grid Operators, see [72]. A summary of actual rates as well as time slots for peak, intermediate and off-peak hours per distributor can be retrieved directly from the Brazilian Electricity Regulatory Agency ANEEL, see [73]. Due to the left illustration in figure 3.3, peak hours with highest rates are usually in the evening hours on working days, whereas the weekends and public holidays have off-peak prices during the whole day, as sketched in the right chart.

Quality of electricity supply

The quality of electricity supply is relevant for later investigations as outages might be a further argument to force distributed power supply and storages. In case of a grid friendly operation, distributed generators and flexible loads are able to relief the electric infrastructure and prevent shortages or even outages.
Following diagrams show the Brazilian quality of electricity supply between 2001 and 2017, see figure 3.8. In this case, nationwide average duration as well as number of outages per consumer and year are considered as indicators for quality of supply. The top chart in figure 3.8 proves achievements towards grid stability during the recent years, as the total duration per year fell in 2017 for the first time since 2001 under 15 hours per consumer in the average. Even more recognizable is the steady reduction of the number of outages: In 2001, consumers witnessed almost 15 outages per year, whereas the number declined to slightly more than 8 in 2017. In accordance to a reduction of duration and number of outages in the mentioned period, subsequently, the amount of financial compensations to be payed from distributors to customers was reduced in recent years. [11] Further indicators for quality of supply in higher spatial resolution (e.g., per municipality and distributor) can be gathered from [74].

3.2 Energy demand

This section delivers an insight in Brazil's energy demand by sector and source. For electricity, as probably the dominant energy carrier for the future, the following figures provide a state-wise

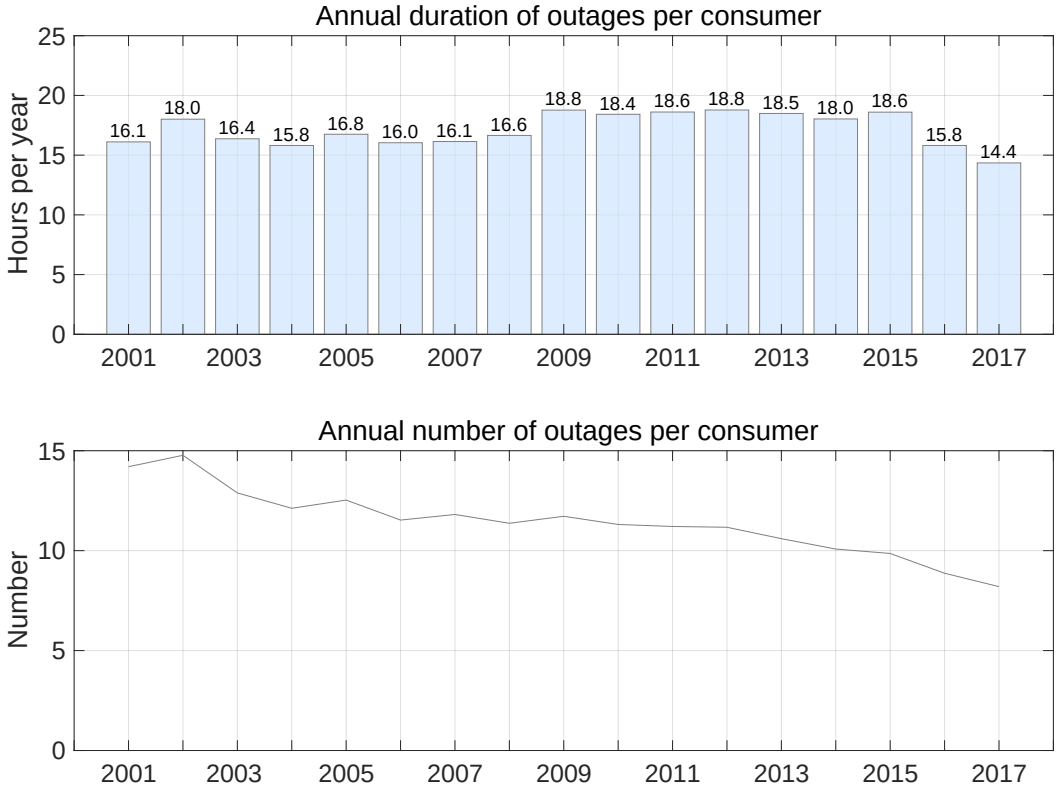

Figure 3.8: Power outages [11]

distribution of demand. Since 1970, the development was characterized for most sectors and energy carriers by a steady and significant growth, interrupted only by above mentioned phases of economic weakness. Some sources did not follow the general trend of growth, predominantly biogenic solid fuels like firewood and charcoal. In contrast to that, sugarcane products as renewable fuels witnessed an enormous growth since the 1970s, above all ethanol for combustion engines in road vehicles. Therefore, the last paragraph in this section is devoted to the energy demand of the transport sector and the importance of ethanol therein. Due to a likely growing relevance of electricity for ground transport, this chapter ends with an estimation of photovoltaic array sizes to substitute fuels. As major data sources for this paragraph, recent time series from official Brazilian institutions were used.

According to the numbers illustrated in figure 3.1, mineral oil became the most crucial source of Brazil's primary energy supply in recent decades. To reduce both carbon dioxide emissions and economic vulnerability, a reduction of crude oil consumption is one suitable way. Figure 3.9 provides a deeper insight into the use of petroleum products by sectors to identify relevant fields of activity to address previously mentioned challenges. The figures were retrieved from the Brazilian Energy Balance *(Balanço Energético Nacional)* published in 2017 by the Brazilian Ministry of Mines and Energy *(Ministério de Minas e Energia)*. [8]

Brazil's total consumption of petroleum products more than quadrupled from 1970 to 2016. For the sake of comparability to electricity, the numbers in the diagram 3.9 are expressed in terawatt hours (TWh). A more common unit for oil markets are tons of oil equivalent (toe), whereby

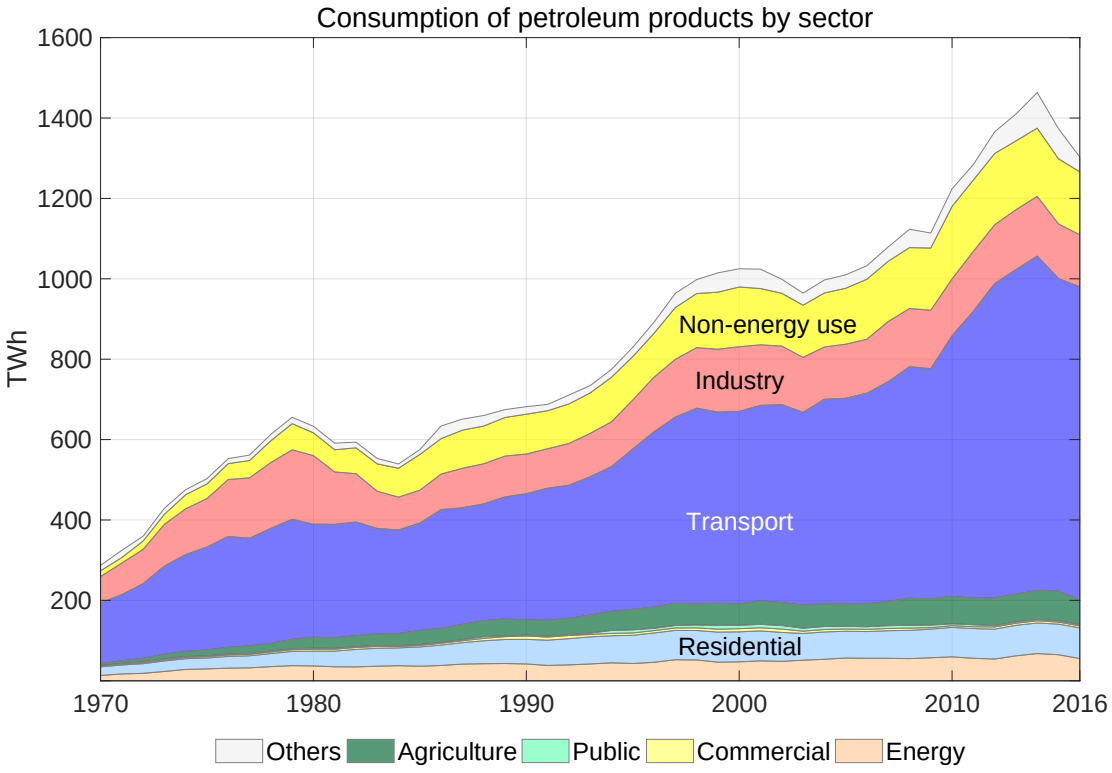

Figure 3.9: Oil consumption by sector from 1970 to 2016 [8]

1 million toe equals 11.63 TWh. Worded in tons of oil equivalent, that means an increase from around 25 million toe in the year 1970 to a peak of 126 million toe in 2014, which fell to 112 million toe due to the recent economic crises. Phases of recession have an even harder impact on oil demand than for other energy carriers. That can be recognized clearly as significant decline for the industry sector in the early 1980s as well as for the whole market since 2014. Traditionally, the Brazilian transport sector holds the highest share of oil consumption, which ranged between 44 % and 60 % in recent decades. Because of importance and likely ongoing growth of the transport sector, section 3.2.1 delivers a further insight in its composition of energy demand. The share of industry consumption declined from 23 % in 1970 to 10 % in 2016, which is slightly less than for non-energy use. Latter sector uses petrochemical products for example in road construction and the plastics industry as raw materials. Referring to the values from 2016, the remaining sectors, namely residential, agriculture, energy, public and commercial, account for almost one fifth of oil consumption. As the residential sector will be in focus of chapter 4, figure 3.13 breaks down the composition of energy use for Brazilian homes by energy carrier.

In contrast to the quadrupling consumption of petroleum products, the electricity consumption increased even more than tenfold from 1970 to 2016, what was already mentioned above in context to figure 3.2 showing the power generation by source. The sectoral composition for the use electricity since 1970 is deed in figure 3.10.

We can gather from these data, that the Brazilian industry sector was by far the biggest

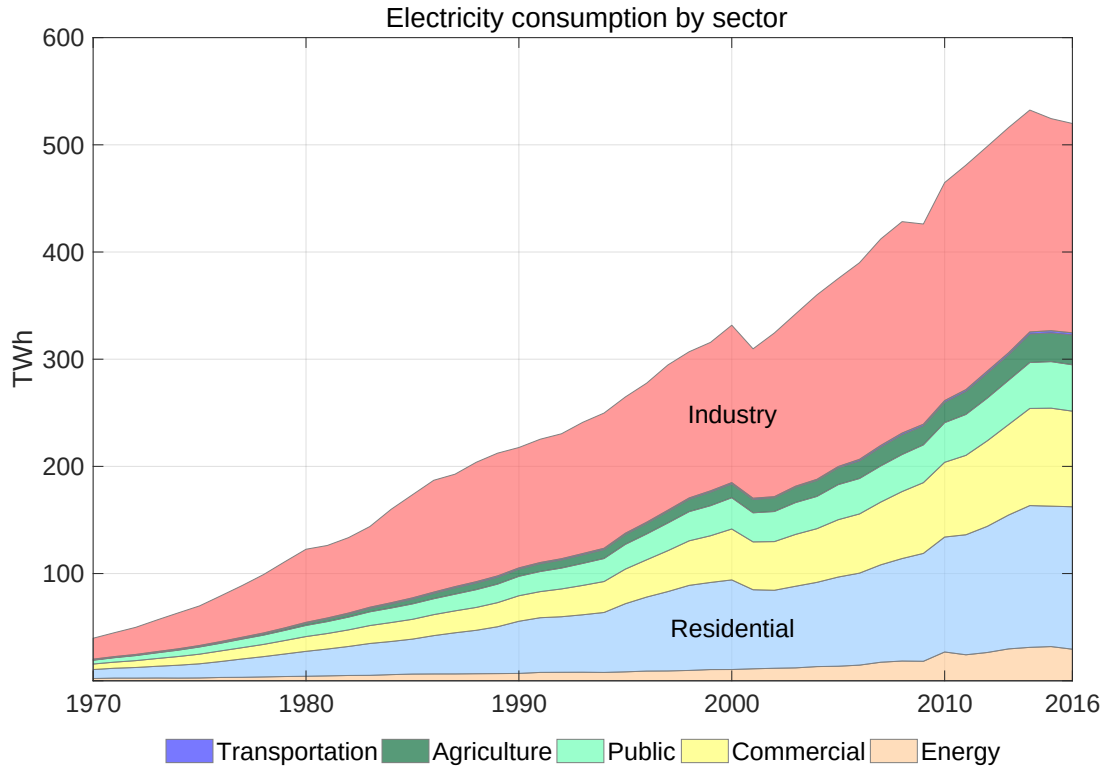

Figure 3.10: Electricity consumption by sector from 1970 to 2016 [8]

consumer of electricity, despite its share fell from around 50 % in 1970 to under 40 % in 2016. The residential sector holds the second rank, which increased its share from approximately 20 % in 1970 to 25 % in 2016. The commercial and the public sector taken together, which almost did not appear in the petroleum statistic, accounted for up to 26 % of Brazil's electricity consumption. Despite a growth by a factor of more than 80 within 46 years, the agricultural sector only had a share around 5 % in Brazil's electricity demand. The energy sector itself contributed another 5 % in 2016. With less than 1 %, the electricity consumption in the Brazilian transport sector is displayed as thin and dark blue area in figure 3.10 between industry and agriculture, which is hardly detectable. The present insignificant role of electric power for transportation can be explained by the fact, that only some electrified railways mainly for local transport in urban areas are responsible for this minor share of demand. For other modes of transport, electricity was not an issue until 2016, see figure 3.15.

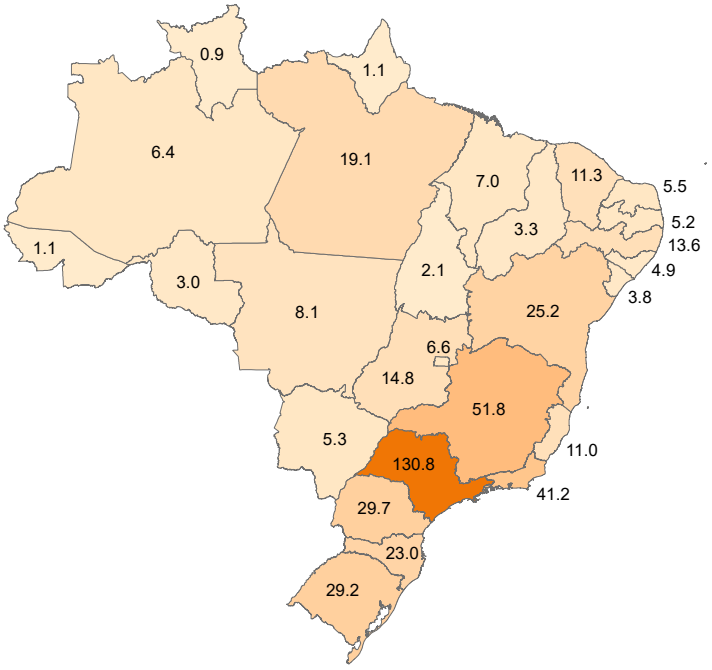

Figure 3.11: Electricity consumption by state in TWh for 2015 [12]

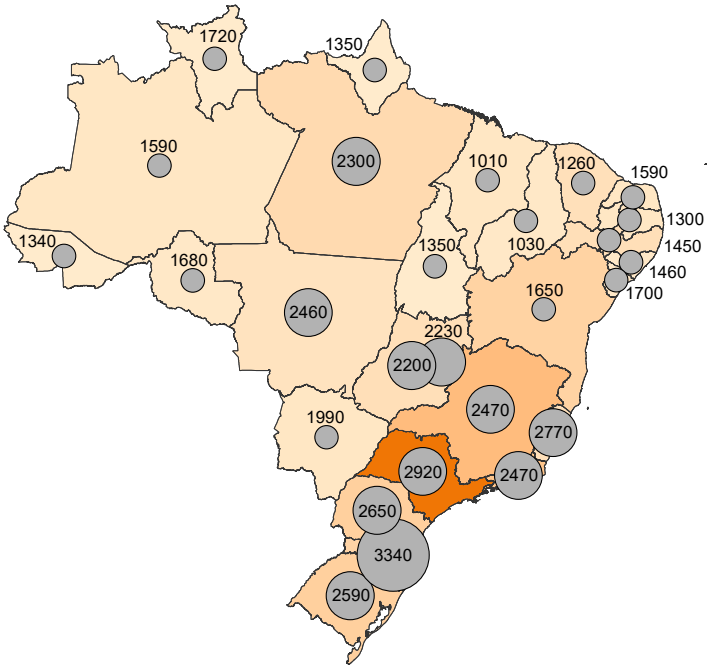

Figure 3.12: Electricity consumption per capita in kWh for 2015 [12]

The two maps in figure 3.11 and figure 3.12 deliver an idea of the regional distribution of electricity consumption. The upper map illustrates the electricity consumption over all sectors by state in absolute values (TWh) for the year 2015. Origin of the data is the statistical yearbook of electricity from 2016 *(Anuário Estatística de Energia Elétrica)* published by the Brazilian

Ministry of Mines and Energy. For later considerations, spatially differences in power demand are relevant to determine capacities enabling distributed supply. It is clearly recognizable, that the prospering, highly industrialized and densely populated state of São Paulo had by far the highest electricity consumption with more than 130 TWh. Subsequently, the sparsely populated and less wealthy regions have a low electricity consumption. The map in figure 3.12 shows the electrical power consumption per capita in 2015 in kWh. This value represents the ratio between consumption over all sectors divided by the total population per federal state, not only considering the residential sector. Taking the gross domestic product per capita into account, see figure 2.10, one can explain the illustrated per capita electricity consumption as a positive correlation between economic activity and use of electricity, but there are also some deviations remarkable. For instance, the southern state of Santa Catarina, see figure 2.2, has a higher specific consumption than the state of São Paulo, despite a lower GDP per capita. One reasons for that is Santa Catarina's large industry sector with including several energy-intensive businesses and furthermore a higher energy demand for heating due to a cooler climate. In the same way, the state of Amazonas has a comparable climate and GDP per capita like its neighboring state of Pará, but a significant lower per capita electricity consumption. The differences can be explained with a large industry and above all a large mining sector in Pará in comparison to Amazonas. [37]

As the figures 3.11 and 3.12 illustrate aggregated values for all sectors, the following passage focuses on the residential sector. A closer analysis of Brazilian household is important because of several reasons. Firstly, the private consumption increased significantly in recent years and had a share of one quarter of the total use of electricity in 2016, see figure 3.10. The electricity demand is likely to continue its growth in the future, due to a higher penetration of appliances like air conditioning systems[9] or electric vehicles (EVs). A further source of growing electricity demand is probably the substitution of fuels like firewood. Still in the 1970s and 80s, firewood was by far the most important energy carrier for Brazilian homes, being substituted more and more by liquefied petroleum gas (LPG) and electricity, see figure 3.13. Replacing firewood for cooking does not only reduce local emissions and spare forests as natural resources, it is also predominantly perceived as a gain in comfort. As population and personal standard of living grow, the electricity demand from the residential sector also grows. Therefore, it becomes increasingly important for the whole power generation sector. But the rising importance is also an issue for the customers. With electricity becoming the most relevant energy carrier in the residential sector, people suffer more from high electricity tariffs. Like figure 3.6 illustrated, private customers already had to pay in recent years the highest rates in comparison to other sectors. Therefore, solutions need to be found to both mitigate the impact of the residential sector to the gross electricity demand and to reduce the financial vulnerability of citizens from increasing electricity prices.
The development depicted in figure 3.13 not only reveals a tremendous consumption growth for petroleum gas and electricity, but also a significant increase in efficiency. Considering the final energy consumption per capita, it fell from around 2.7 MWh per person in 1970 to a minimum of 1.3 MWh in 1995. This efficiency gain has its roots mainly in the substitution of firewood by

[9] A forecast until the year 2050 of air conditioning units in the residential sector of selected countries including Brazil is given on p. 18 in [75].

gas and electricity. Since 1995, the final energy consumption per capita increased slowly and reached 1.4 MWh in 2016. One has to keep in mind that the Brazilian population more than doubled from around 96 million people in 1970 to more than 206 million in 2016, see figure 2.4. Despite the mentioned substitution of firewood, its importance resurged during the economic weakness in the first years since 2000, see bottom chart in figure 2.7. Other energy carriers used in the residential sector besides firewood, electricity and liquefied petroleum gas are charcoal, kerosene, natural gas and gasworks gas. Their contribution is recognizable in the upper area in figure 3.13. While the share of charcoal increased from 2 % in 1970 up to 5 % in the mid of the 1980s, it dropped under 2 % in 2016. Kerosene and gasworks gas almost disappeared in households, whereas natural gas reached over 1 % in 2016.

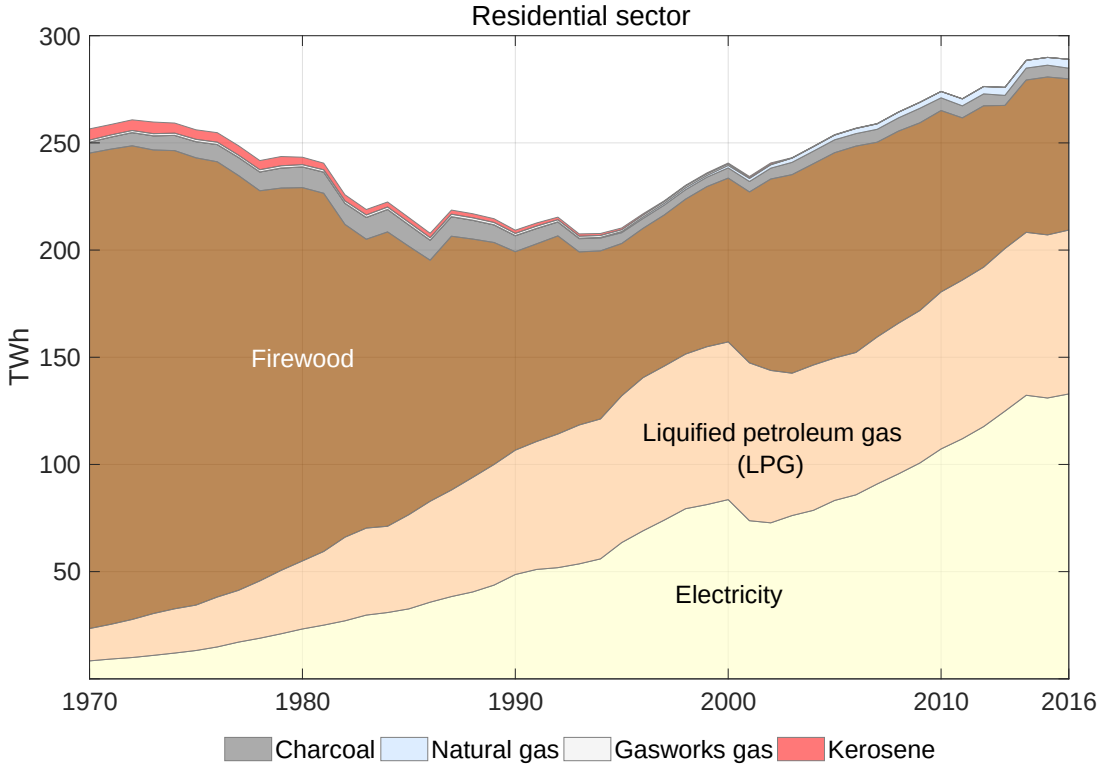

Figure 3.13: Final energy consumption of the residential sector [8]

3.2.1 Transport sector and ethanol

The vast majority of Brazilian transport relies on crude oil as the primary source of energy. The transport sector causes the essential part of Brazil's mineral oil consumption, corresponding to the data visualized in figure 3.9 and figure 3.1. The traffics share in mineral oil consumption was 51 % in the year 1970, fell to a minimum of 44 % in 1980 and grew recently to 64 % in 2016. Since mineral oil is the largest source of primary energy in Brazil, see figure 3.1, these numbers underline the importance of transport in terms of energy. Considering the final energy consumption in the traffic sector, road vehicles played by far the dominating role as it can be

recognized in figure 3.14. Cars, trucks, buses, motorcycles etc. accounted persistently for more than 80 % of the energy consumption, exceeding 90 % in 1994. In absolute values, the total consumption increased from approximately 150 TWh or 13 million toe in 1970 to more than 960 TWh or 83 million toe. As depicted in figure 3.14, this more than sixfold increase was mainly driven by road traffic. Other modes of passenger and freight transport contributed always less than 20 % since 1970 to the energy consumption, in 2016 less than 7 %. This minor share distributes further to fuel consumption of vehicles for airways, waterways and railways. Despite a fivefold growth between 1970 and 2014, aviation made up only 4 % of the final energy consumption in transport, but developed to the biggest consumer besides road traffic. These numbers only represent the energy consumption for operation of the transport sector. Expenses for infrastructure construction, vehicle production, maintenance, disposal etc. are not considered here.

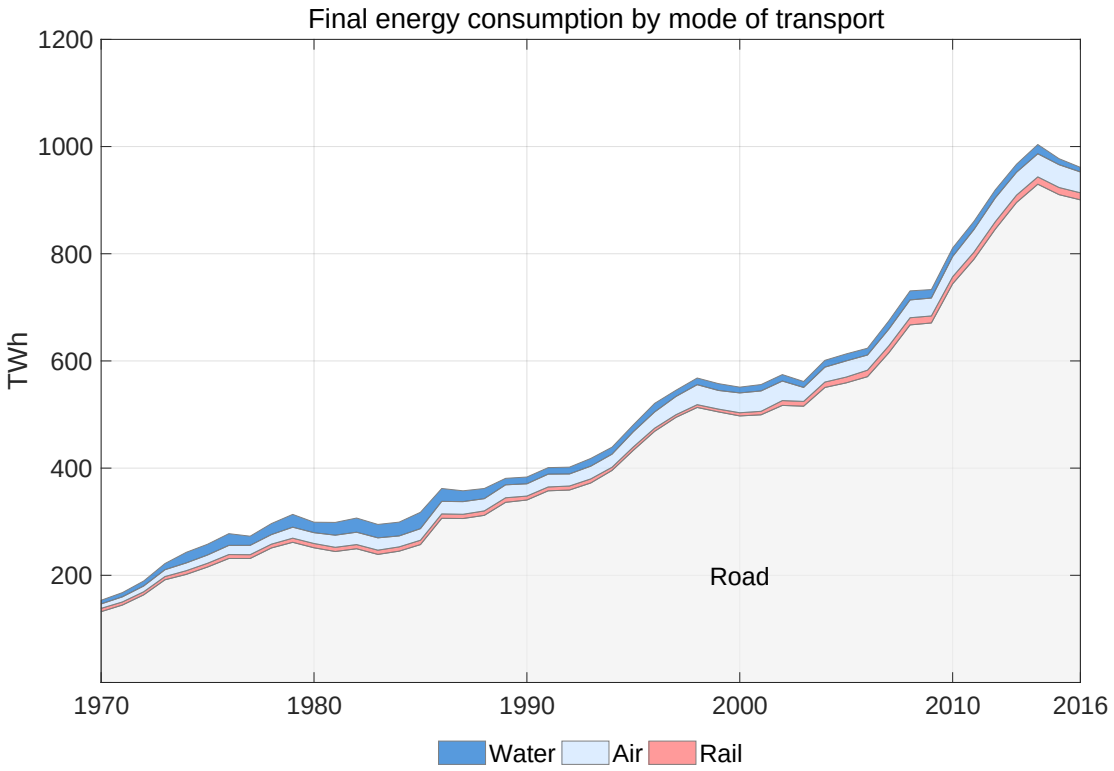

Figure 3.14: Final energy consumption in the transport sector [8]

Referring to motorized mobility, road traffic was the backbone of Brazil's transport for both passengers and freight. The data presented in table 3.4 brings together the shares of traffic performance and energy consumption to derive specific values for transport on Brazilian roads, railways, airways and waterways. Origin of the data is a report from the Brazilian Ministry of Mines and Energy, see p. 53 f. in [20]. In 2010, the total traffic performance was $1.6 \cdot 10^{12}$ passenger-kilometers (pkm), that means that every Brazilian traveled 8,000 km in the average. Road vehicles were used for 92 % of the distance, aviation for another 6 % and trains for only 1.7 %. Over 90 % of the passenger traffic on railways came from the highly urbanized states of

São Paulo and Rio de Janeiro. [20] Until 2016, the vast majority of Brazilian passenger trains were metros and commuter trains in metropolitan areas, whereas intercity train services were practically non-existent. With a share of 0.1 %, passenger transport on waterways was almost negligible, which will therefore not be discussed further. In terms of energy consumption for passenger transport, road traffic had a share of 92 % as well. With 0.4 % railroad traffic was underrepresented in energy consumption in comparison to its traffic performance, whereas air traffic was slightly overrepresented.

Table 3.4: Traffic performance and final energy consumption in 2010 [20]

	Passenger			Freight		
	pkm	TWh	kWh/pkm	tkm	TWh	kWh/tkm
	$1.6 \cdot 10^{12}$	472.0	∅ 0.30	$1.1 \cdot 10^{12}$	335.8	∅ 0.30
Road	92.2 %	92.3 %	0.30	56.8 %	91.8 %	0.49
Rail	1.7 %	0.4 %	0.06	25.0 %	2.4 %	0.03
Air	6.0 %	7.2 %	0.35	0.1 %	1.2 %	3.87
Water	0.1 %	0.2 %	0.88	18.1 %	4.5 %	0.08

In case of freight transport, around 57 % of the total traffic performance of $1.1 \cdot 10^{12}$ tonnes-kilometers (tkm) were transported on Brazilian roads, what caused almost 92 % of the freight transports energy consumption.[10] Cargo railway traffic had a share of 25 % in traffic performance, but only 2.4 % in energy consumption, which indicates a high efficiency of freight trains. In a similar way, ship transport had a share of 18 % consuming less than 5 % of the total energy used. In contrast to that, air cargo contributed only 0.1 % to the traffic performance but over 1 % to the energy consumption of the freight sector.
The values from [20] for the year 2010 were used to calculate the specific energy consumption for each transport sector. As average for the whole passenger transport in Brazil, 0.30 kWh were necessary to move a person for one kilometer. With 0.06 kWh/pkm, trains were the most energy efficient vehicles to transport people. Amounting to 0.30 kWh/pkm, journeys by car, bus, motorcycle etc. consumed considerably more energy than trains, while the specific energy consumption for air travel was 0.35 kWh/pkm. With 0.49 kWh/tkm for trucks and 0.03 kWh/tkm for cargo trains, the difference between road and rail was for freight transport even higher than for passenger transport. For cargo ships a specific consumption of 0.08 kWh/tkm was derived from the data, which presents transport on waterways significantly more efficient than on roads. Obviously, a significant higher share of ship transport is not a viable option because of several reasons, including the wide-mashed grid of existing waterways, the inaccessibility of ports for numerous freight hubs and the high expenses for making rivers navigable or for construction of new canals. In comparison to ground transport, the energy-intensive air cargo, 3.87 kWh/tkm in 2010, plays a subordinate role for freight transport.
As road traffic is the most important transport branch for both energy consumption and traffic performance, the following passage delivers an insight in development and mix of energy

[10] In 2015, pipeline transport of petroleum products accounted for 4 % of traffic performance for freight in 2015, see p. 9 in [76]. Pipelines transport is not considered in table 3.4 as [20] does not contain values for pipeline transport and corresponding energy consumption in 2010.

carriers used for moving passengers and freight on streets, see top chart in figure 3.15. The depicted date were retrieved from the Brazilian Energy Balance. [8] The bottom diagram shows also the composition of energy consumption for rail transport. In contrast to waterways, the Brazilian railway network could be improved and expanded from the present status.[11] One objective of such an infrastructure investment program would be a higher share of trains in traffic performance resulting in an increased energy efficiency of the transport sector. Therefore, railways will be considered below as alternative for road transport and as sector of potential growth.

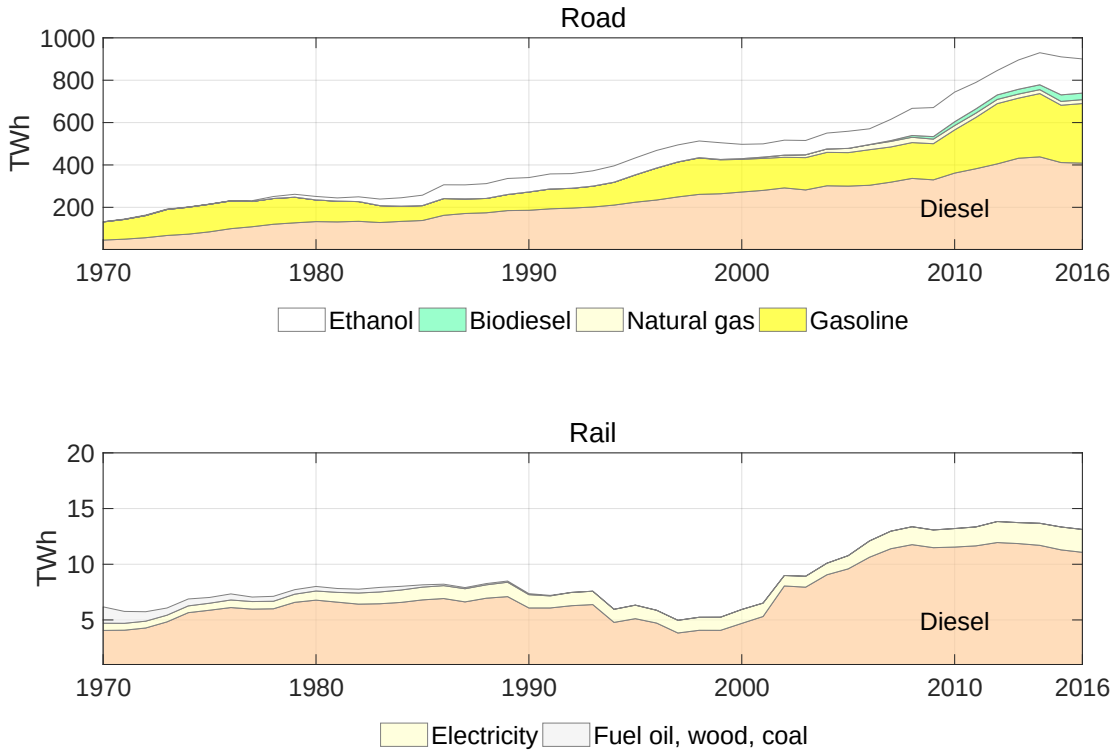

Figure 3.15: Road and rail by fuel consumption [8]

The final energy consumption for road vehicles grew from 1970 to 2016 almost sevenfold from 132 TWh (11.3 million toe) to 900 TWh (77.4 million toe). In 1970, gasoline contributed 65 % and diesel fuel 34 %. Ethanol made from sugarcane had the remaining share of 1 %. Until 2016, diesel fuel became with 45 % the most important fuel in road traffic. It is notable, that the sale of petroleum-derived diesel fuel has been banned in Brazil for cars and light-duty passenger vehicles with a payload of less than 1,000 kg. In the light of the preceding oil crisis, this diesel ban was instituted in 1976 to conserve diesel fuel for commercial vehicles. As a measure to reduce the dependency of petroleum imports, Brazil established in 1975 a national program named "PROALCOOL" to promote domestically produced ethanol as fuel. This biogenic energy source was initially blended into gasoline and later used as a complete

[11] Recent statistics about the Brazilian rail transport, which are mainly used for freight, are provided in [77]. An official map showing the recent expansion of the Brazilian railway network can be found in [78].

gasoline replacement for engines designed to run with 100 % ethanol. [79] As consequence of the alcohol program, the share of ethanol in final energy consumption of road transport grew from less than 1 % in 1975 up to 20 % in 2016. In absolute values, ethanol delivered in 2016 161.4 TWh or 13.88 million toe compared to 281.2 TWh or 24.2 million toe of gasoline. These numbers indicate that 36 % of the gasoline demand was recently substituted by ethanol. While ethanol is mainly made from sugarcane, one further biogenic fuel is biodiesel, which reached a share over 3 % in 2016. Brazilian biodiesel is mainly made from soybean oil. [14] Despite these efforts to replace petroleum-based fuels with agricultural products, gasoline still holds with around 30 % the second rank after diesel fuel. As third fossil energy resource used in road traffic is natural gas, contributing up to 4 % since 2001. Electricity for road vehicles did not play a relevant role until 2016.

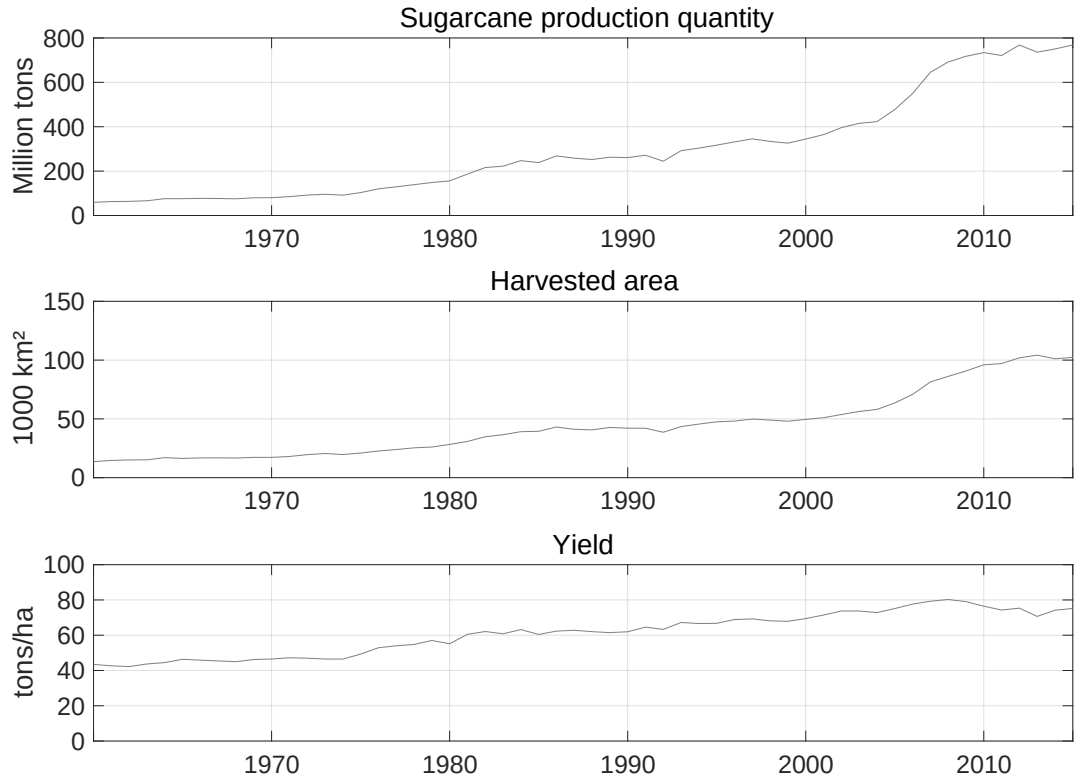

Figure 3.16: Key figures of sugarcane production (1961-2016) [13]

The bottom diagram in figure 3.15 shows the development of energy use for rolling stock on railways since 1970. First of all it is remarkable that energy consumption of rail transport is significantly lower than for road traffic. Around 5 TWh or 350,000 toe were used in 1970, consisting of 66 % diesel fuel, 10 % electricity and 24 % others, including fuel oil and solid energy carriers like firewood and coal used for steam locomotives. These fuels disappeared until the early 1990s, while electricity gathered a share of 16 % mainly because of building and expanding electrified metro lines and local train networks in Brazilian metropolises. Over the whole period of 46 years, diesel fuel remained by far the most important energy source for rail transport, having a share up to 90 %.

Referring to the unique importance of ethanol fuel in road transport, figure 3.16 delivers key figures about Brazilian sugarcane production. These data were retrieved from FAOSTAT, the database from the Food and Agriculture Organisation (FAO) from the United Nations. [13] Before establishing the national alcohol promotion program "PROALCOOL" in 1975, the countrywide sugarcane production stayed under 100 million tons per year. This quantity was harvested from 20,000 km^2 or 2 million hectares, see middle chart in figure 3.16. Before 1975, most of the sugarcane was used to produce sugar for nutrition and as basis for drinking alcohol. With ethanol gaining importance as fuel, the cropland for sugarcane doubled from 1975 until 1985. Flanked by increased yield, see bottom diagram in figure 3.16, the production quantity almost tripled during this time span. In the year 2013, more than 750 million tons of sugarcane were harvested from an area over 100,000 km^2 or 10 million hectares, which is around 14 % of the total cropland land in Brazil. [80] Due to the high land use for sugarcane, issues in context of sustainability were discussed whether this type of biogenic fuel could foster deforestation. [80–82] Since cultivating sugarcane means an energetic use of land, one could derive the efficiency of this type of land use to generate biofuel and compare it with other processes. Addressing this idea, section 3.2.2 delivers an estimation of the photovoltaic area needed to supply a hypothetical electrified Brazilian transport sector. The following passage provides further ethanol-related figures which are necessary to conduct this estimation.

The Brazilian Ministry of Agriculture, Livestock and Supply *(Ministério da Agricultura, Pecuária e Abastecimento)* published a statistical yearbook containing recent information and figures about energy crops and biogenic fuels in Brazil. [14] The data illustrated in figure 3.17 and 3.18 were retrieved from this yearbook. Figure 3.17 depicts the output per ton sugarcane, which is usually processed into sugar or ethanol as main products. Residuals like bagasse, which are partly reintegrated in the these processes, are not considered here. A brief explanation of the ethanol production process from sugarcane considering byproducts can be found in chapter 1 in [82]. Taking the ten-year average of the harvests between 2003/04 and 2013/14 in Brazil, one ton of sugarcane delivered 66.8 kg of sugar or 72.5 liter of ethanol. The later value is used as conversion ratio for the estimation below, see table 3.5. The bottom diagram in figure 3.17 shows the development of the Brazilian sugar and ethanol production per harvest from 2003/04 to 2013/14. During this relatively short period, the ethanol production almost doubled from 14.6 million m^3 to 28 million m^3. A comparable trend can be recognized in the sugar production, even though the increase within 10 years was only 52 %. No other country in the world had such a large sugarcane industry than Brazil. A worldwide comparison for the year 2012 reveals that Brazil was by far the biggest producer of sugarcane, having a share of 32 % of the global market by production quantity, followed by India (19 %) and China (7 %), see p. 20 in [14]. Despite this impressive volume of ethanol output, the Brazilian export of alcohol played a minor role. Derived from the data illustrated in figure 3.17 and 3.18, the export share was between 6 % and 21 %. A clear trend is not recognizable neither in the export share nor in the export quantity. In contrast to that, the total export revenues from ethanol show a certain growth due to risen market prices for ethanol.

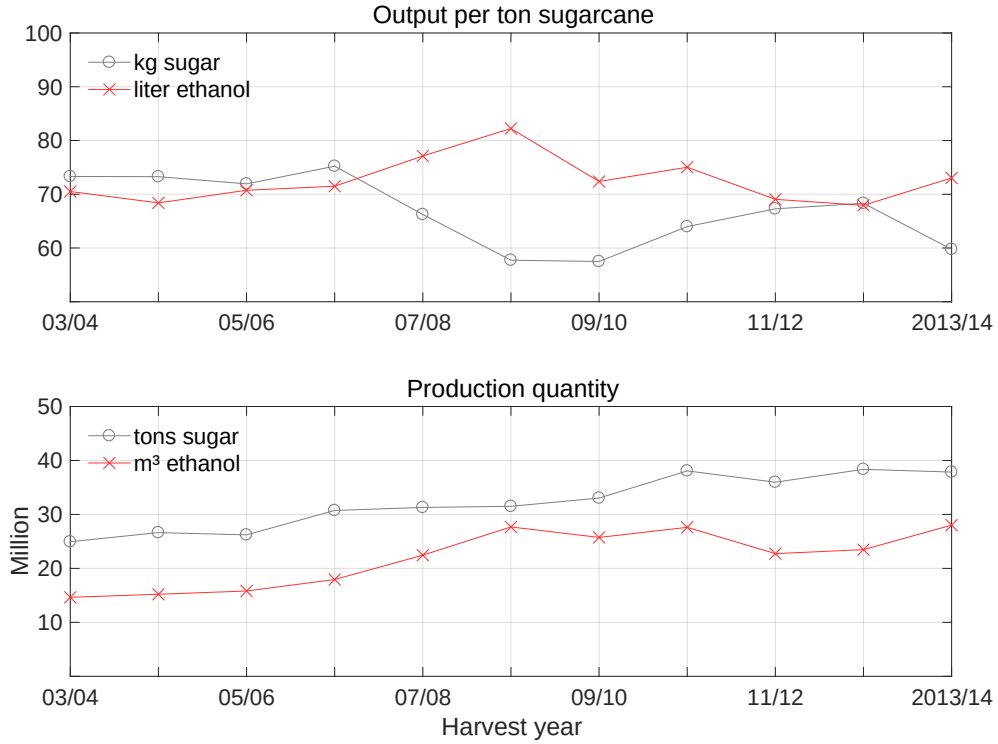

Figure 3.17: Sugar and ethanol [14]

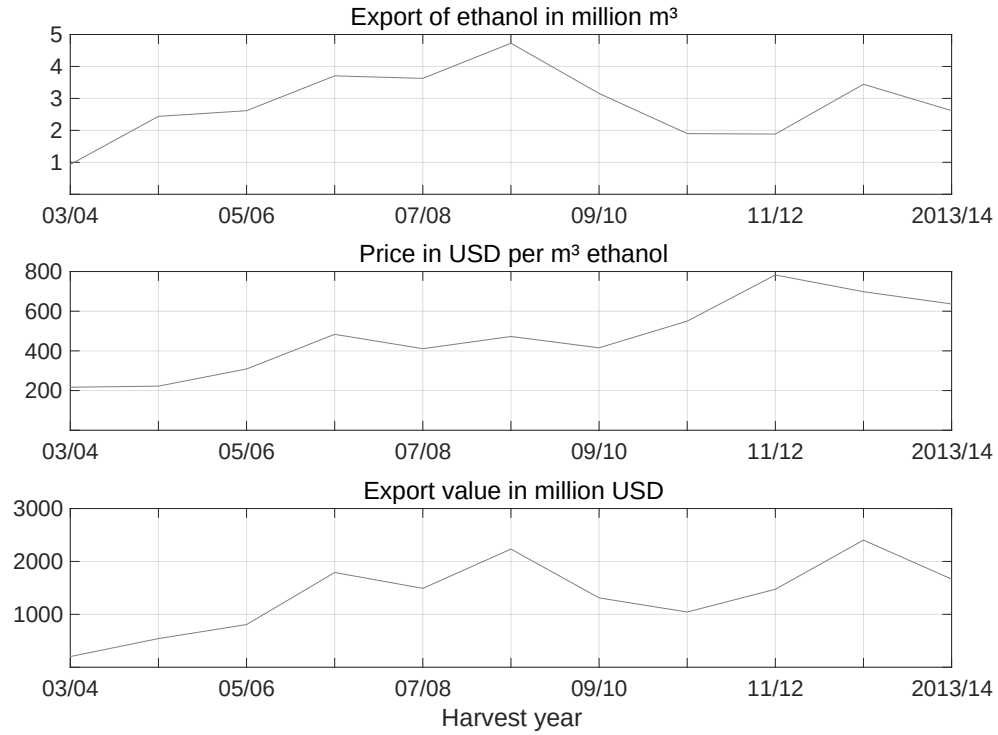

Figure 3.18: Relevance of ethanol export [14]

3.2.2 Estimation of photovoltaic area for transport supply

Since electric road vehicles gained importance in several national markets [83], this section discusses a possible photovoltaic power supply for the Brazilian transport sector. Main idea is at this point to compare the present land used for sugarcane acreage to produce ethanol as fuel with the size of a photovoltaic array to generate electricity as an alternative. The simplified supply chains for the "ethanol path" and the "electric path" are illustrated in figure 3.19.

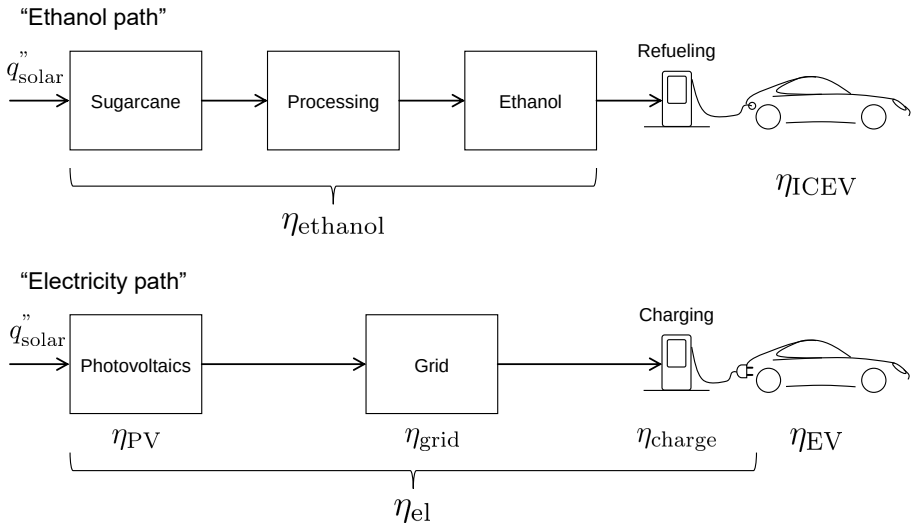

Figure 3.19: Supply chain of "ethanol path" and "electricity path"

Just like ethanol made from domestically cultivated sugarcane, solar power could provide distributed energy supply for transport. Moreover, electrified transportation systems using renewable power can also replace fossil fuels. Benefits of a higher share of renewable power in primary energy supply can be both lower carbon footprint and reduced price risks from global energy markets. As biogenic ethanol already is considered as renewable resource, the estimation below compares the space requirements for photovoltaic power generation with recent land use for sugarcane cropland. The estimation is based on preceding statistics for energy consumption with focus in the transport sector. Further necessary quantities for an electric supply chain are presented below, emphasizing on the operation of electric vehicles and not conducting a life-cycle assessment. In the result table 3.7 and in figure 3.20, the present Brazilian sugarcane acreage for ethanol is compared with the size of hypothetical photovoltaic arrays to replace with electricity the recent ethanol production, the total fuel consumption for road traffic, the gross electricity production and finally the total primary energy supply.
In order not to overestimate the benefits of an electrification, the less favorable parameters were chosen for the electricity system. For electric cars, an above average specific energy consumption of 0.20 kWh/km was used in the calculation or a below-average efficiency for the Brazilian distribution grid, see table 3.6. Subsequently, real results for electric transport would be at least as good as the values presented below. For the Brazilian energy sector and sugarcane-based ethanol, the recent values discussed in the preceding sections were taken. Main data sources were FAOSTAT, the database from the Food and Agriculture Organisation (FAO) from the United Nations [13], the Brazilian Energy Balance [8] and the statistical year-

Table 3.5: Values for efficiency estimation of ethanol production

	Symbol	Value	Unit	Source
Global horizontal irradiation	q''_{solar}	1,747	kWh/m^{2}a	[16]
Yield sugarcane per hectare	$m_{\mathrm{sugarcane}}/A$	76.1	t/ha	[13]
Conversion ratio ethanol to sugarcane	$V_{\mathrm{ethanol}}/m_{\mathrm{sugarcane}}$	72.5	l/t	[14]
Density ethanol	ρ_{ethanol}	0.79	kg/l	[84]
Heating value ethanol				
gravimetric	H_{l}	7.5	kWh/kg	[84]
volumetric	H_{l}	5.9	kWh/l	[84]

book about energy crops and biofuels from the Brazilian Ministry of Agriculture, Livestock and Supply [14]. Further assumptions are explained in the following paragraph.

The global horizontal irradiance in table 3.5 represents the mean of all measurement points in the state of São Paulo retrieved from a data set of INMET *(Instituto Nacional de Meteorologia)*, which is the national meteorological institute of Brazil. [16] The mean radiation sum for the state of São Paulo at 1,747 kWh/m^{2}a was chosen deliberately because of three reasons: Firstly, this value lies inbetween that of less sunny regions in the South and those of desertlike areas in the Northeast. Therefore, it represents approximately an average for Brazil. Secondly, a photovoltaic electricity production close to the biggest cluster of consumers would not necessarily require an expansion of the transmission grid. Generators and consumers could find themselves in relative proximity in the same or an nearby distribution grid. Subsequently, a consideration of transmissions grid losses is not necessary. Thirdly, most of the sugarcane croplands are located in the state of São Paulo or its neighboring states. [81] The results can be interpreted as a partly replacement of sugarcane cropland in São Paulo by photovoltaic arrays. Naturally, to prevent transmission grid expansion, solar power generators should be located close to consumers all over the country and not be concentrated in the state of São Paulo, what would mean even smaller arrays than calculated. For example, consumers in the sunny state of Bahia would need significantly less installed generation capacities to produce the same amount of electricity than those in São Paulo. The suboptimal for São Paulo are chosen here not to overestimate the benefits of a substitution of ethanol as fuel by photovoltaic electricity. The value for the yield of sugarcane per hectare represents the last ten-year average of the data illustrated in figure 3.16. During that period of time, one hectare delivered 76.1 tons of sugarcane. The conversion ratio from sugarcane to ethanol was derived in the same way. The average value for recent ten harvests was 72.5 liters of ethanol per 1 ton of sugarcane. Taking into account the heating value of the ethanol from every hectare makes the yield comparable to the annual sum of electricity produced by a photovoltaic array.
Using the values from the table 3.5 shown above, the efficiency η_{ethanol} for conversion of sunlight into ethanol is calculated as follows:

$$\eta_{\mathrm{ethanol}} = \frac{W_{\mathrm{ethanol}}}{Q_{\mathrm{sun}}} = \frac{m_{\mathrm{ethanol}} \cdot H_{\mathrm{l}}}{q'' \cdot A} \tag{3.6}$$

After expanding and rewriting, the fraction contains expressions for the yield of sugarcane per hectare and the conversion ratio of sugarcane to ethanol.

$$\eta_{\mathrm{ethanol}} = \frac{m_{\mathrm{sugarcane}}}{m_{\mathrm{sugarcane}}} \cdot \frac{\rho \cdot V_{\mathrm{ethanol}} \cdot H_{\mathrm{l}}}{q" \cdot A} = \underbrace{\frac{m_{\mathrm{sugarcane}}}{A}}_{\text{Yield}} \cdot \underbrace{\frac{V_{\mathrm{ethanol}}}{m_{\mathrm{sugarcane}}}}_{\text{Conversion ratio}} \cdot \frac{\rho_{\mathrm{ethanol}} \cdot H_{\mathrm{l}}}{q"} \tag{3.7}$$

Finally, the efficiency for conversion of sunlight into ethanol is $\eta_{\mathrm{ethanol}} \approx 0.2\ \%$ by applying above mentioned values.

$$\eta_{\mathrm{ethanol}} = 76.1\ \frac{\mathrm{t}}{\mathrm{ha}} \cdot \frac{1}{10^4}\ \frac{\mathrm{ha}}{\mathrm{m}^2} \cdot 72.5\ \frac{\mathrm{l}}{\mathrm{t}} \cdot \frac{0.79\ \mathrm{kg/l} \cdot 7.5\ \ \mathrm{kWh/kg}}{1,747\ \mathrm{kWh/m}^2} = 0.187\ \% \approx 0.2\ \% \tag{3.8}$$

It is worth mentioning, that this calculation does not consider additional energy input (e.g., fuel for agricultural machinery, processing, fertilizer, irrigation) or further outputs like energetic use residuals (e.g. bagasse). For analysis of energy flows related to ethanol production, see chapter 4 in [82].

The following passage provides an estimation of the efficiency for converting sunlight into electricity for electric vehicles. A photovoltaic array transforms solar energy at the efficiency η_{PV} into electricity, which then is distributed at η_{grid} over the grid to a charging point, where the electric vehicle is connected. Assuming a charging efficiency of η_{ch}, the total supply chain delivers electricity for the battery electric vehicle at the efficiency η_{el}. This energy is subsequently available for propulsion and auxiliary electrical systems.

$$\eta_{\mathrm{el}} = \eta_{\mathrm{PV}} \cdot \eta_{\mathrm{grid}} \cdot \eta_{\mathrm{charge}} = 0.15 \cdot 0.80 \cdot 0.80 = 9.6\ \% \tag{3.9}$$

The results above highlight, that there is a factor of approximately 50 between the efficiency of providing ethanol as fuel and supply of electric vehicles with solar power. Comparable results can be found in [85].

$$\frac{\eta_{\mathrm{el}}}{\eta_{\mathrm{ethanol}}} = 53.44 \approx 50 \tag{3.10}$$

Subsequently, this factor appears again, if comparing the area needed for a photovoltaic array to substitute ethanol as fuel. The necessary area A_{PV} to replace the sugarcane croplands with a photovoltaic power plant is calculated as follows:

$$\eta_{\mathrm{el}} = \frac{W_{\mathrm{el}}}{q" \cdot A_{\mathrm{PV}}} \ \rightarrow\ A_{\mathrm{PV}} = \frac{W_{\mathrm{el}}}{q" \cdot \eta_{\mathrm{el}}} \tag{3.11}$$

Table 3.6 contains the chosen values for estimation of the photovoltaic collector area to produce electricity as substitute for fuels. The value w_{el} for EVs in table 3.6 was estimated from recent models available on the global market.[12] The upper bound of approximately 20 kWh per 100 km was chosen not to underestimate the demand of electric vehicles. Real values for electricity consumption per vehicle kilometer traveled are likely to be lower.

In case of a substitution of gasoline, ethanol, diesel fuel etc. by electricity, the final energy consumption would be lower by a certain factor. Electric vehicles (EV) consume less energy per kilometer traveled due to significant higher conversion efficiencies η_{EV} of an electric powertrain

[12] BMW i3, Renault ZOE, Volkswagen e-Golf, Nissan Leaf, Tesla Model S

Table 3.6: Values for photovoltaic area estimation

	Symbol	Value	Unit	Source
Global horizontal irradiation	q”	1,747	kWh/m^{2}a	[16]
ICEV fuel consumption	w_{fuel}	0.56	kWh/km	[86]
EV electricity consumption	w_{el}	0.20	kWh/km	[87–91]
Efficiencies				
photovoltaic system	η_{PV}	0.15	-	[92]
distribution grid	η_{grid}	0.80	-	[93]
vehicle charging	η_{charge}	0.80	-	[94]

in comparison to the efficiency η_{ICEV} of an internal combustion engine vehicle (ICEV). This factor $w_{\mathrm{fuel}}/w_{\mathrm{el}}$ can be estimated as the ratio between specific energy consumption of an electric vehicle w_{el} to that of a conventional one consuming w_{fuel} per kilometer.

$$\frac{\eta_{\mathrm{EV}}}{\eta_{\mathrm{ICEV}}} = \frac{w_{\mathrm{fuel}}}{w_{\mathrm{el}}} \approx 2.8 \tag{3.12}$$

Following the idea above, the ratio $W_{\mathrm{ethanol}}/W_{\mathrm{el}}$ between the final demand of ethanol for road transport corresponding to figure 3.15 and electricity as substitute is 2.8 as well. That means, to replace 160 TWh of ethanol as final energy demand of the year 2016, approximately 57.1 TWh of electricity would be necessary for electric vehicles providing the same traffic performance.

$$\frac{W_{\mathrm{ethanol}}}{2.8} = \frac{160\ \mathrm{TWh}}{2.8} = 57.1\ \mathrm{TWh} \tag{3.13}$$

Applying equation 3.11 delivers the size A_{PV} of the photovoltaic array to generate this amount of electricity per year.

$$A_{\mathrm{PV}} = \frac{W_{\mathrm{el}}}{q” \cdot \eta_{\mathrm{el}}} = \frac{57.1 \cdot 10^9\ \mathrm{kWh}}{1,747\ \mathrm{kWh/m^2} \cdot 0.096} \approx 341\ \mathrm{km^2} \tag{3.14}$$

Under the meteorological conditions for the state of São Paulo, a photovoltaic array of 341 km^2 would be sufficient to produce enough electricity to substitute ethanol as fuel. A square with the same area has an edge length slightly above 18 km, see first case in table 3.7. In contrast to that, the harvested area of sugarcane for ethanol production was more than 50.000 km^2 in 2016, which would fill a square of more than 220 km edge length. This acreage was calculated using the data from table 3.5. Due to the figures illustrated in the bottom diagram of figure 3.16, around one half of the sugarcane cropland was used to produce ethanol as fuel. The planted area for sugarcane is by a factor of around 150 higher than the land needed for a corresponding photovoltaic array. Considering only the ratios of efficiencies of both paths, the factor 150 can be derived quickly by comparing the efficiencies of supply chain and powertrain.

$$\underbrace{\frac{\eta_{\mathrm{el}}}{\eta_{\mathrm{ethanol}}}}_{\text{Supply chain}} \cdot \underbrace{\frac{\eta_{\mathrm{EV}}}{\eta_{\mathrm{ICEV}}}}_{\text{Powertrain}} = 53.44 \cdot 2.8 = 149.6 \approx 150 \tag{3.15}$$

Table 3.7: Sizes of hypothetical PV arrays in comparison to sugarcane acreage

		Energy	Electricity	Area	Edge length
		TWh	TWh	km^2	km
(1)	Ethanol substitution	160	57	341	18
(2)	Fuel substitution for road traffic	900	321	1,917	44
(3)	Gross electricity production	600	600	3,578	60
(4)	Primary energy supply	3,600	3,600	21,465	147
	in comparison to				
(5)	Sugarcane acreage for ethanol	160	-	50,782	225

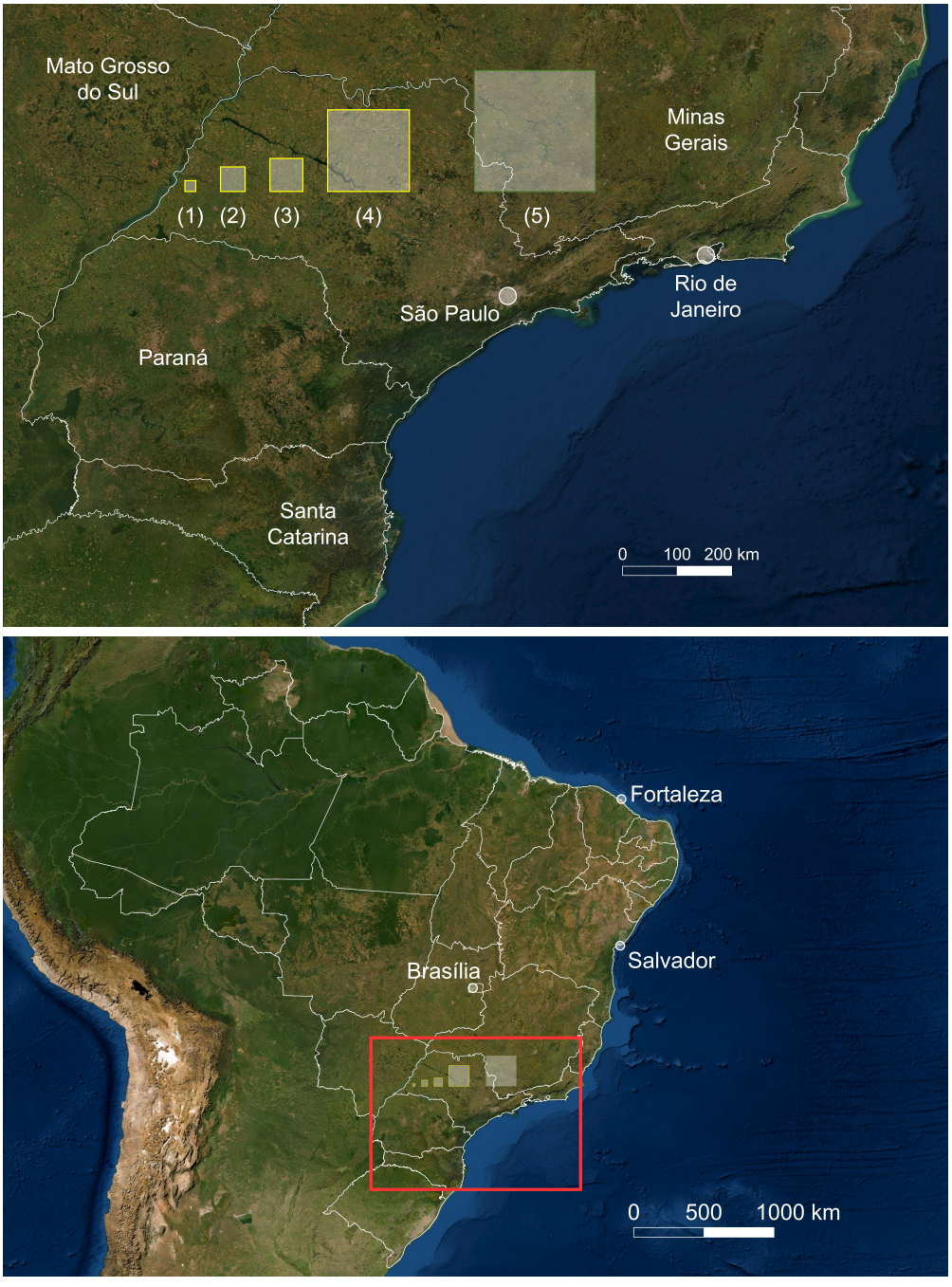

Figure 3.20: Hypothetical PV arrays in comparison to sugarcane acreage

The huge differences of efficiencies of both considered supply chains, ethanol vs. photovoltaic electricity and powertrain of ICEVs and EVs, explain the significantly different results for the space requirements. Assuming that the whole Brazilian road traffic would be electrified and therefore fuel being substituted by photovoltaic electricity, the second case in table 3.7 shows the size of this hypothetical photovoltaic array. In the shape of a share, its edge length would be 44 km. Over all categories, around 100 million motorized road vehicles existed in Brazil in the year 2016, including 54 million cars, 26 million motorcycles and scooters, 15 million trucks, buses, duty vehicles etc., see [95]. In order to supply every vehicle not differentiating the type, each one would need a PV collector area slightly less than 20 m^2. If the whole Brazilian gross electricity production of almost 600 TWh from the year 2016 would be produced by photovoltaics, the space requirement would be approximately a square of the size 60 km by 60 km, meaning around 100 m^2 per citizen. Even if the primary energy supply from the year 2014 would be delivered only by an PV array located in the state of São Paulo, this would have less than half of the size of the recent sugarcane acreage for ethanol. Figure 3.20 illustrates the previously mentioned cases on a map showing the state of São Paulo and its neighbors. The yellow squares represent the size of photovoltaic arrays in comparison to the recent acreage of sugarcane for ethanol. The largest square in green on the right is the latter mentioned acreage, the smallest square in figure 3.20 is the PV array to deliver the same energy in case of a switch from ethanol powered ICEVs to solar powered EVs. The factor of 150 between both space requirements gets clear in this image. For orientation, the metropolises of São Paulo and Rio de Janeiro are marked in this map with a white circle. The distance between both cities is around 360 km as the crow flies.

The real areas needed for photovoltaics to supply the transport sector would even be lower because of several reasons. More efficient modules can reduce the collector area needed to generate a certain amount of electricity. These modules do not need to be necessarily on the plain land. They can also be mounted on rooftops or covered parking, reducing the space requirements. As the values for energy consumption per kilometer traveled in table 3.4 indicate, a higher share of traffic performance on railways would provide further efficiency potentials. The general statement stays the same, if the specific energy consumption is derived for a country like Germany with long-distance trains and a high degree of railway electrification, see table 3.8. It is notable that only cars are considered as road vehicles for passengers in table 3.8 and only long-distance trains for passenger rail transport. To exploit the potentials of railways for Brazil, existing lines should be improved and electrified as well as new lines to be build. Brazil planned to construct a high-speed track to link Rio de Janeiro, São Paulo, and Campinas and their airports. [96] Besides gaining energy efficiency in transport, one purpose for this project was to relieve both airports and motorways and to increase travel comfort for the whole region. In terms of mitigation of environmental impacts, high-speed long distance trains are not in all scenarios the optimal solution. As an assessment revealed for a high-speed railway project in California [97], future occupancy as well as impacts for the life-cycle of both vehicles and infrastructure have to be considered. For the case of California, it turned out that railways linking cities over several hundred kilometers have the lowest specific energy consumption in an life-cycle assessment assuming high occupancy compared with cars and planes at the same conditions. A study for project for a high-speed railway service between São Paulo and Rio de Janeiro would likely deliver comparable results.

Table 3.8: Specific energy consumption for road and rail transport in Germany (2017) [21]

	Passenger	Freight
	kWh/pkm	kWh/tkm
Road	0.56	0.39
Rail	0.14	0.08

Going the "electric path" as described above would not only mean reduced land use, but also cost benefits in vehicle operation. A cost estimation was conducted only considering energy consumption and prices, not total costs of ownership, motorway tolls etc. For both ethanol and electricity consuming cars, the values from table 3.5 and table 3.6 were used, like the heating value of ethanol at 5.90 kWh per liter. The exchange rate as 3.00 Brazilian Real per US-Dollar was derived from the development displayed in 2.9 and the price for electricity from table 3.1 as 0.45 BRL/kWh or 0.15 BRL/kWh. Furthermore, a range of present and future total cost of photovoltaic electricity was assumed as 0.30 to 0.09 BRL/kWh. Due to the results presented in table 3.9, a 100 km journey costs almost 8.00 USD for ethanol but only 3.00 USD with an electric vehicle. If charging the car directly with solar power, the costs would be between 6.00 USD per 100 km or less than 2 USD in the future. For calculation of cost scenarios for photovoltaic electricity, see chapter 4.

Table 3.9: Energy cost comparison between ethanol ICEV and EV for a 100 km journey

	Energy price				Demand	Costs/100 km	
	USD/kWh	BRL/kWh	USD/l	BRL/l	kWh/km	USD	BRL
ICEV, ethanol	0.14	0.42	0.83	2.50	0.56	7.91	23.73
EV, grid charged	0.15	0.45	-	-	0.20	3.00	9.00
EV, PV	0.10	0.30	-	-	0.20	2.00	6.00
EV, PV future	0.03	0.09	-	-	0.20	0.60	1.80

One major component in total costs of ownership are the capital costs for the vehicle. In 2017, the expenses for purchasing an average electric car were significantly higher than those for a conventional one. Assuming a price convergence between electric and conventional vehicles, the "electricity path" will be an competitive option for road transport in the future. Furthermore, it is important to have in mind that this competitiveness photovoltaic combined with electric vehicles can strongly drive the demand for both technologies.

Chapter 4

Distributed integration

This chapter delivers an approach to quantify potentials for distributed generation in Brazil, focusing on photovoltaic application in the residential sector. Section 4.2 provides an approach for development of annual residential load profiles in hourly resolution. Since heating and cooling are important drivers for electricity consumption in private households, the load profiles consider dependency on ambient conditions. Since the possession of devices and climate conditions differ significantly within Brazil, the load profiles consider regional characteristics. Section 4.4 presents an approach including exemplary results for storage dimensioning followed by an economic assessment in section 4.5. Based on this assessment, one can estimate the potential on the demand side to integrate fluctuating power production.

4.1 Motivation

The focus lies on the residential sector because of several reasons. Firstly, Brazilian homes became the second-largest electricity consumer in the country, see figure 3.10 and were an essential driver of electricity demand in the past. In contrast to the industry sector, residential consumers can more accessible be generalized as people have similar habits and use a limited spectrum of typical home appliances. Due to that reason, standardized load profiles for German households are available for example, see [98], but also comprehensive data about Brazilian homes, see [15]. Industry companies are much more diverse, which can be made clear by comparing the quantity and temporal structure of an aluminum smelter's energy demand with that of a semiconductor factory or a food processing company. Statements for the industry are more specific in comparison to the residential sector. Furthermore, electricity had a significantly growing share during recent decades in the energy demand of the residential sector, see figure 3.13. The increasing penetration of electrical consumer devices and the substitution of other energy carriers such as firewood are the reasons for that. Apart from temporal reductions due to the economic crisis, continuing growth in electricity demand can be expected for the upcoming decades. On the one hand, population growth as a driver continues, see figure 2.4, but on the other hand also per capita consumption rises further. Latter can be explained with increasing per capita income and a higher purchase power for both devices and electricity. Especially more air conditioning systems like projected in [75] are considered to be responsible for future growth in electricity demand. Analyzing the residential sector is also important in

terms of social and economic issues. Since residential consumers are faced with the highest prices for electricity among other consumer groups, see figure 3.6, an investigation could reveal potentials for saving energy costs. Referring to the Brazilian tariff structure, see 3.1, economic benefits can come from shifting loads from peak to off-peak hours but predominately from the integration of photovoltaic power. As presented in the following sections in detail, photovoltaic electricity for distributed energy systems will likely increase its competitiveness significantly under Brazilian market conditions. One main source for this development will be the ongoing price erosion for photovoltaic modules, see Haegel et al. [99] The module price for solar cells came from around 100,000 USD/kW in the 1970s and decreased as a function of cumulative global shipments to around 1,000 USD/kW in 2015. It is projected that photovoltaic modules will fall soon to 250 USD/kW or less. The module prices constitute around 50 % of the total investment costs of a grid-connected photovoltaic system due to [92]. The downward trend for photovoltaic costs has a linear influence on the levelized cost of electricity (LCOE) as described in the appendix, see A.7. Decreasing costs for solar power supply can help stabilize electricity expenses, which is an essential factor to keep power affordable, especially for low-income groups in society.

4.2 Generation of residential load profiles

Electrical load profiles are necessary for several investigations in energy system analysis, including dimensioning of storage, transmission, or power generation capacities. However, load profiles for specific consumers are usually not available in the needed quality. Therefore, several approaches exist to fill this lack of data via simulation and prevent costly measurements. Apart from that, a simulation of load profiles can also be beneficial to evaluate the impact of upcoming consumer needs. For example, to answer, what will be the effect of higher penetration of air conditioning systems or electric road vehicles to grids. [100] Several approaches were conducted for the generation of load profiles. The following section presents a brief overview of recent contributions and their chosen methods.

Based on measured domestic electrical load profiles in Ireland for six months, McLoughlin, Duffy, and Conlon present in [101] a mathematical model based on Markov Chains to simulate the demand for several residential types, e.g., apartments and detached houses. In [102] these three authors conducted a parametric analysis of 4,000 measured Irish households to characterize the profiles with mean and maximum load, time of use, load factor, etc. For the time series generation via Markov Chains, the authors show that their simulated profiles deviate with an error of less than 10 % from the measured profiles. However, since long-term measurements of electricity demand for Brazilian homes were not part of this work, these approaches are not applied here.

With 1,300 residential electrical load profiles as a database, an approach is presented in [103] using clustering and Markov chains. Clustering is done to group similar load profiles, whereas the Markov models regenerate the synthetic time series for electrical load. This method again relies on a broad database of load profiles and differs from the lean approach described in this chapter.

For the case of Germany, Gobmaier developed in [100] a method to generate synthetic, national load profiles. The chosen bottom-up approach merges loads from different demand sectors,

subtracted feed-in time series, such as wind, photovoltaics, and combined heat and power units. The load curves show regional, calendrical and climatic dependencies by applying multivariate regression analysis, which are essential characteristics for the investigation conducted here, but without focusing on the residential sector. After defining the regression model parameters, real national load profiles are compared with synthesized time series, which show remarkable low deviations. Adopting this approach to Brazil would prerequisite the load profiles for the whole year in regional differentiation and the relevant meteorological time series for the same year for the same regions.
The authors of [104] used smart meter data from 1,072 Japanese households living in detached houses to identify relationships between personal lifestyle and electricity consumption. The frequency analysis of data covering 18 months revealed insights like lower electricity consumption when the residents' life follows a routine.
Besides [100, 104] for electrical profiles, frequency or Fourier analysis was also applied in [105] for heat loads of residential, government, business buildings. It prerequisites extensive time series, which were not available for the case of Brazilian households.

In this work, load profiles are used to determine costs of electricity supply by applying both the Brazilian net metering system, see section 3.1, and distributed energy storage, see figure 4.3. To cover a whole year with its seasonal characteristics, annual load profiles are needed representing typical effects in terms of electricity demand. Seasonal characteristics are peak loads caused by high air conditioning demand during hot phases, for instance. To derive the missing annual load profiles, an approach is presented in this section to generate them from available statistical and meteorological data. Figure 4.1 depicts schematically that source used: The green color indicates available data, the red color so far unknown time series to be generated.

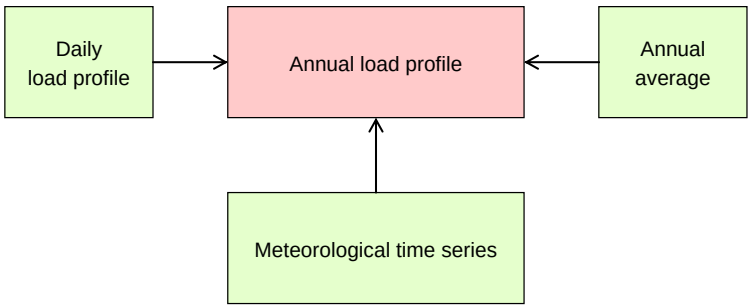

Figure 4.1: Data input for generation of annual load profiles

The daily load profiles in hourly resolution as well as the annual averages per Brazilian macro-regions North, Northeast, Central-West, Southeast and South, see figure 2.2, were retrieved from an investigation about possession of electrical devices and use of electricity in the Brazilian residential sector, see [15]. This research was conducted by the national electricity conservation program "PROCEL" *(Programa Nacional de Conservação de Energia Elétrica)* and the major Brazilian utilities company Eletrobrás under the patronage of the Brazilian Ministry of Mines and Energy (MME). The original daily load profile per Brazilian macro-region gathered from [15] are illustrated in figure 4.2.

Table 4.1: Categorization of electrical loads in Brazilian residential sector

Electric consumer	Load category
Television Lighting Audio devices Ironing Stove, oven Laundry machine Refrigerator Freezer	Non-shiftable load (B)
Hot water (esp. shower)	Hot water load (H)
Air conditioning	Air conditioning load (AC)

These profiles depict the consumption of common electrical devices in every hour of the day. A list of the electrical consumers in particular can be found in table 4.1. To derive not only potentials for storing electricity with batteries, but also applications for thermal storage, the load will be differentiated in three groups: Fix load (B), hot water load (H) and air conditioning load (AC). Idea behind that is the fact, that in a number of cases, thermal storage are the economically more favorable solution in comparison to batteries. Furthermore, by reducing the use of batteries the demand for both precious and critical battery materials can be avoided. The second column in table 4.1 shows the categorization of electrical consumers analyzed in [15] carried out in this chapter. In this work, the loads from devices in the left column from television to freezer are considered to be not shiftable. If their operation would be shifted for several hours within a day, it could restrict the consumer in his habits, require complex integration in an energy management system or even threaten the functionality of some devices. For example, the consumer is not free to choose anymore when to take out the laundry from the machine, an old freezer is costly to be integrated into an energy management system and an inappropriate inside temperate of a refrigerator could lead to earlier deterioration of food. For further investigations, latter mentioned devices can also be considered as flexible. In contrast to the group of non-shiftable loads, both electric hot water preparation and air conditioning have a significant impact to the daily load profile. Both categories are important for the power system since electricity is their main source of energy for air conditioning and hot water preparation. In 2009, 71 % of the Brazilian households used electricity for hot water preparation, only 4 % gas, around 1 % firewood and charcoal and less than 1 % solar energy. More than 24 % of the households did not have hot tap water, whereby regional differences are remarkable: 86 % in the tropical North region did not use hot water preparation, whereas only 0.9 % in the South with temperate climate. [24] The electric load of hot water preparation and air conditioning can be shifted relatively simple by integrating thermal storage without restricting consumer habits. A hot water storage "H" can be used to shift the load of an electric shower. Air conditioning loads can be shifted with an ice or cold water storage for cooling mode or with a hot water storage for heating mode. Air conditioning is abbreviated throughout this work with "AC". Electrical loads from the category "non-shiftable" can reduce their impact to the

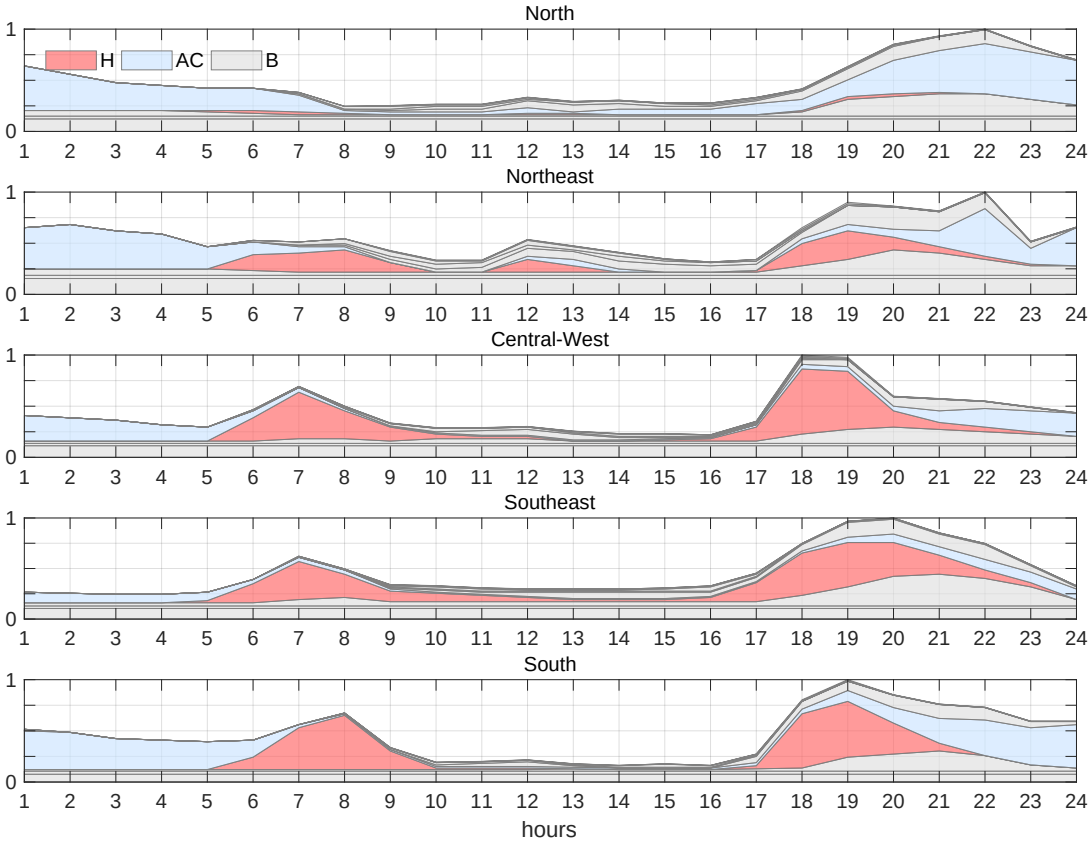

Figure 4.2: Normalized daily load profiles for the residential sector by macro-region [15]

grid if batteries are applied. This group and their corresponding storage technology is therefore abbreviated with "B". Figure 4.3 shows a general setup for distributed storage in the residential sector. The top sketch represents the configuration only considering one electric load, which can be shifted using batteries. In the lower configuration, the electric load is distinguished in the three categories and their corresponding storage. Under considering of distributed photovoltaic power generation, a dimensioning of storage capacities can be found in section 4.4 as well as economic evaluation in section 4.5. The regional profiles illustrated in figure 4.2 already take into account the classification in hot-water load (H), air conditioning load (AC) and non-shiftable load (B). The loads per category reveal on the first sight remarkable regional differences. In the tropical North region, electricity demand for hot water preparation does not play a significant role. In contrast to that, air conditioning causes a significant part especially from the evening hours until over the night until the morning. This electricity demand not only for room cooling is closely related to typical occupancy of homes. Since a number of people are not at home because of working, leisure or other outside activities. The impact of water heating is relatively low in the Brazilian Northeast, but is significantly higher in the Central-West, Southeast and South. Since hot water in the residential sector is mainly used for showering, the difference in demand can be explained with different climate depending habits. Under tropical and hot weather conditions, people consume less hot water for showering, whereas under cool conditions, the consumption is higher. This dependency is handled mathematically

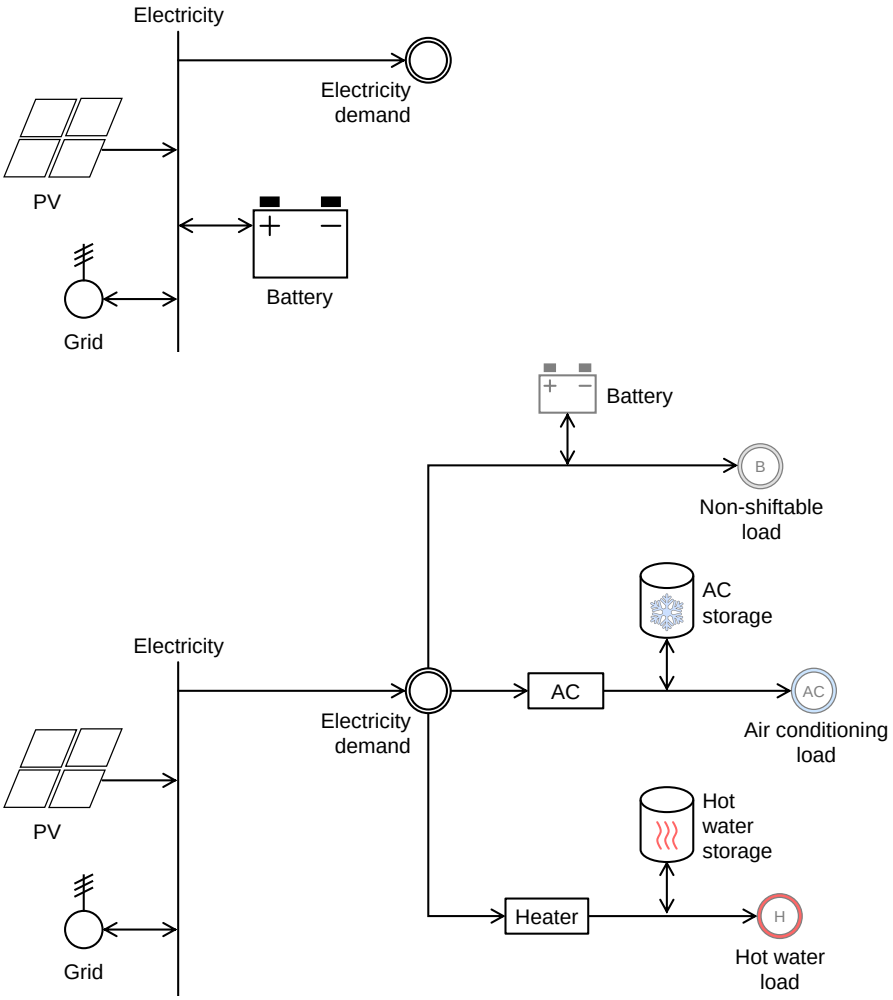

Figure 4.3: Distributed integration with batteries and thermal storage

in section 4.3.3. From the North region to the Southeast, one can recognize a decreasing air conditioning demand overnight. In contrast to the North, moderate temperatures during nights in the Southeast explain this difference. With a cooler climate in the southern states of Brazil, room heating gets an issue especially in the winter season. The electricity demand for room heating, which is captured here as air conditioning load, plays a certain role in the South, but a subordinate role in Brazil.

The daily profiles from figure 4.2 do not differentiate between seasons and their specific characteristics. Based on the daily load profiles presented above, the following passage describes an approach to develop annual load profiles, which reflect these seasonal, weather depended characteristics as well as essential calendar effects. The meteorological data used here originate from INMET *(Instituto Nacional de Meteorologia)* and were published by the LabEEE *(Laboratório de Eficiência Energética em Edificações)*, the laboratory of energy efficiency in buildings of the Federal University of Santa Catarina. [16]

4.3 Mathematical approach

The total annual electricity consumption W_{el} of a household is composed by the three above mentioned parts, namely the non-shiftable part $W_{\mathrm{B},t}$, the hot water load $W_{\mathrm{H},t}$ and the air conditioning load $W_{\mathrm{AC},t}$. The time series have each $t = 1, 2, ..., 8760$ elements, meaning for every hour per year one value. These time series are essential parts of the load profiles to be developed. The so called amplitude factors A_{B}, A_{H} and A_{AC} serve to scale the time series $W_{\mathrm{B},t}$, $W_{\mathrm{H},t}$ and $W_{\mathrm{AC},t}$ to meet real statistical shares. The total annual electricity consumption is then composed by the three load categories scaled by their amplitude factors in the following way:

$$W_{\mathrm{el}} = \sum_{t=1}^{8760} (A_{\mathrm{B}} \cdot W_{\mathrm{B},t} + A_{\mathrm{H}} \cdot W_{\mathrm{H},t} + A_{\mathrm{AC}} \cdot W_{\mathrm{AC},t}) \tag{4.1}$$

For the sake of brevity, the categories non-shiftable load (B), heating load (H) and air conditioning load (AC) are denoted below by $\mathrm{i} = \mathrm{B}, \mathrm{H}, \mathrm{AC}$. The time series $W_{\mathrm{H},t}$ in equation 4.1 are composed by daily vectors $d_{\mathrm{i},j}$. There are 365 vectors $d_{\mathrm{i},j}$ representing the days of one year, whereby every vector has $j = 1, 2, ..., 24$ elements, one for each hour per day. The daily vectors $d_{\mathrm{i},j}$ depend firstly on the original (o) daily load profiles $d^{\mathrm{o}}_{\mathrm{i},j}$ provided in [15], but also on calendar effects and meteorological conditions. The following subsections explain the modeling of daily load vectors $d_{\mathrm{i},j}$ for the three categories non-shiftable load (B), hot water load (H) and air conditioning load (AC).

Equation 4.2 represents the composition of the hourly load $d_{\mathrm{i},j}$ for each category $\mathrm{i} = \mathrm{B}, \mathrm{H}, \mathrm{AC}$. The hourly load is the sum of the original, hourly load value $d^{\mathrm{o}}_{\mathrm{i},j}$ and a calendar component $\Delta d_{\mathrm{i},j}$. The meteorological component $d^{\mathrm{m}}_{\mathrm{i},t}$ increases or reduces this sum.

$$d_{\mathrm{i},j} = (d^{\mathrm{o}}_{\mathrm{i},j} + \Delta d^{\mathrm{w}}_{\mathrm{i},j}) \cdot d^{\mathrm{m}}_{\mathrm{i},t} \tag{4.2}$$

4.3.1 Non-shiftable load

Basis for each hour of the daily load profile of non-shiftable loads is the original profile $d^{\mathrm{o}}_{\mathrm{B},j}$ for each region derived from [15]. The daily profiles differentiate by an hourly value $\Delta d^{\mathrm{w}}_{\mathrm{B},j}$ depending on weekday, Saturday or Sunday. For the non-shiftable load, meteorological conditions, holidays and other special occurrences are not considered for the sake of simplicity. Except of certain differences between weekday and weekend, the daily profile of non-shiftable load is repeated from one day to another. Expressed mathematically, the non-shiftable load $d_{\mathrm{B}}(n)$ for every day $n = 1, 2, ..., 365$ is calculated as follows:

$$d_{\mathrm{B}}(n) = \begin{pmatrix} d^{\mathrm{o}}_{\mathrm{B},1} + \Delta d^{\mathrm{w}}_{\mathrm{B},1} \\ d^{\mathrm{o}}_{\mathrm{B},2} + \Delta d^{\mathrm{w}}_{\mathrm{B},2} \\ \vdots \\ d^{\mathrm{o}}_{\mathrm{B},j} + \Delta d^{\mathrm{w}}_{\mathrm{B},j} \\ \vdots \\ d^{\mathrm{o}}_{\mathrm{B},24} + \Delta d^{\mathrm{w}}_{\mathrm{B},24} \end{pmatrix} \mathrel{\widehat{=}} \begin{pmatrix} \text{hour 1} \\ \text{hour 2} \\ \vdots \\ \text{hour j} \\ \vdots \\ \text{hour 24} \end{pmatrix} \tag{4.3}$$

All 365 daily profiles d_{B} with 24 elements each constitute the load profile for one year W_{B}, which can be denoted in the following way.

$$W_{\mathrm{B}} = \begin{pmatrix} d_{\mathrm{B}}(1) \\ d_{\mathrm{B}}(2) \\ \vdots \\ d_{\mathrm{B}}(n) \\ \vdots \\ d_{\mathrm{B}}(365) \end{pmatrix} \mathrel{\widehat{=}} \begin{pmatrix} \text{day 1} \\ \text{day 2} \\ \vdots \\ \text{day n} \\ \vdots \\ \text{day 365} \end{pmatrix} \tag{4.4}$$

The final profile for the non-shiftable load W_{B} is a vector with $t = 1, 2, ..., 8760$ elements. Each element in this vector represents the consumption of one certain hour t within one year.

$$W_{\mathrm{B}} = \begin{pmatrix} W_{\mathrm{B},1} \\ W_{\mathrm{B},2} \\ \vdots \\ W_{\mathrm{B},t} \\ \vdots \\ W_{\mathrm{B},8760} \end{pmatrix} \mathrel{\widehat{=}} \begin{pmatrix} \text{hour 1} \\ \text{hour 2} \\ \vdots \\ \text{hour t} \\ \vdots \\ \text{hour 8760} \end{pmatrix} \tag{4.5}$$

The profile W_{B} can then be used in equation 4.1.

4.3.2 Air conditioning load

Referring to the climate classification of Brazil, see figure 2.3, tropical conditions dominate most parts of the country. Apart from that, there are arid and semi-arid regions in the Northeast and subtropical climate in the southern parts. Especially in the South region, temperatures around the freezing point occur occasionally. Despite these cold periods in the South, room heating is of subordinate importance in Brazil in contrast to cooling. Due to the Brazilian meteorological conditions, main tasks of air conditioning systems are cooling and dehumidification of air.
The meteorological component $d_{\mathrm{i},t}^{\mathrm{m}}$ therefore considers both heating and cooling mode depending on different temperatures and humidities.

$$\text{AC operation in } \begin{cases} \text{cooling mode} & \text{if } t_{\mathrm{A}} > t_{\mathrm{AC,on}} \\ \text{heating mode} & \text{if } t_{\mathrm{A}} < t_{\mathrm{H,on}} \end{cases} \tag{4.6}$$

For the cooling mode, the specific demand $d_{\mathrm{AC}}(t_{\mathrm{A}}, \varphi_{\mathrm{A}})$ is derived from the specific electricity demand to enable the change of state of air running through an air conditioning system. Figure 4.4 displays a process diagram for an air conditioning system including most important quantities. The lower part illustrates schematically the way of the mass flow of air running through the system. For cooling and dehumidification, a certain heat flow has to be removed from the air flow. This heat flow $\dot{Q}_{\mathrm{in}}$ is removed by a chiller, which is commonly a vapor-compression refrigeration system, for example in split-system air conditioners. The electric power P_{el} is needed to enable the vapor-compression refrigeration system to take the heat flow $\dot{Q}_{\mathrm{in}}$ from the air flow $\dot{m}_{\mathrm{air}}$. The heat flow $\dot{Q}_{\mathrm{out}}$ is then released from the system as waste

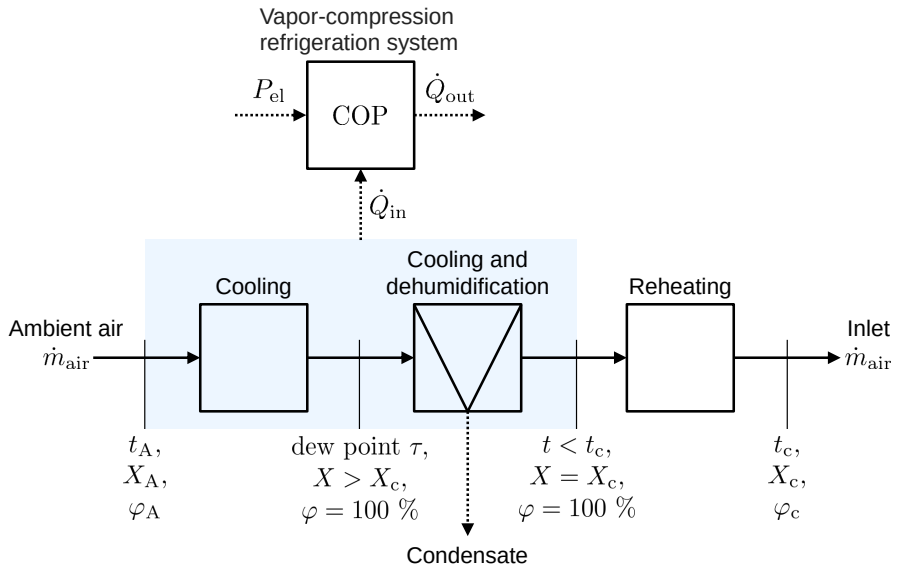

Figure 4.4: Process diagram of an air conditioning system

heat to the environment.
The specific electricity demand is derived from the coefficient of performance (COP), which characterizes the efficiency of the vapor-compression refrigeration system. The compressor of the refrigeration system is by far the biggest electricity consumer in an air conditioning system. Other minor consumers like fans and control devices are therefore neglected here.

$$\mathrm{COP} = \frac{\dot{Q}_{\mathrm{in}}}{P_{\mathrm{el}}} \tag{4.7}$$

The heat flow $\dot{Q}_{\mathrm{in}} = \dot{m}_{\mathrm{air}} \cdot \Delta h$ has to be taken from the air flow $\dot{m}_{\mathrm{air}}$ running through the process sketched in the lower part in figure 4.4. The enthalpy difference for this process is Δh. The specific electricity demand for the air conditioner can be written as follows:

$$\frac{P_{\mathrm{el}}}{\dot{m}_{\mathrm{air}}} = \frac{\Delta h}{\mathrm{COP}} \tag{4.8}$$

COP and h_{V} determine the electricity demand and are depended on the outside air conditions, namely ambient air temperature t_{A} and relative humidity φ_{A}. The real coefficient of performance COP can be derived from the ideal Carnot efficiency $\mathrm{COP}_{\mathrm{Ca}}$ and a quality grade η_{G}. Latter describes the ration between the real COP and the ideal $\mathrm{COP}_{\mathrm{Ca}}$ and is around 0.5.

$$\eta_{\mathrm{G}} = \frac{\mathrm{COP}}{\mathrm{COP}_{\mathrm{Ca}}} \approx 0.5 \tag{4.9}$$

The Carnot $\mathrm{COP}_{\mathrm{C}}$ can be directly derived from the operation conditions of an air conditioning system. In theory, the $\mathrm{COP}_{\mathrm{C}}$ depends two temperatures. Firstly, the temperature of heat input T_{in} and secondly, the temperature of heat output T_{out}.

$$\mathrm{COP}_{\mathrm{Ca}} = \frac{T_{\mathrm{in}}}{T_{\mathrm{out}} - T_{\mathrm{in}}} \tag{4.10}$$

In case of vapor-compression refrigeration, the input temperature T_{in} can be considered as the temperature of the evaporator, whereas the condenser operates at the output temperature T_{out}. Task of an air conditioner especially in tropical climate is not only to deliver cooled air at a certain temperature t_{c}, but also to dehumidify it. Dehumidification can be achieved by cooling air under the dew point τ. If a certain degree of relative humidity φ_{c} should be reached, the air flow has to be cooled to the corresponding dew point τ_{c}. This temperature τ_{c} determines the operation point of the evaporator. Assuming a temperature difference ΔT between the air and the refrigerant as driving potential for the heat transfer, the input temperature T_{in} is:

$$T_{\mathrm{in}} = \tau_{\mathrm{c}} + 273.15\ \mathrm{K} + \Delta T \tag{4.11}$$

In the same way, the temperature at the condenser needs to be at least for ΔT higher than the ambient t_{A}, so that a heat transfer from the condenser to the environment can be established at all time.

$$T_{\mathrm{out}} = t_{\mathrm{A}} + 273.15\ \mathrm{K} + \Delta T \tag{4.12}$$

Under the above-explained temperature levels, the $\mathrm{COP}_{\mathrm{Ca}}$ now considers the set points of the air conditioning and the ambient temperature. That means the $\mathrm{COP}_{\mathrm{Ca}}$ reacts on both set point values and meteorological conditions. Therefore, these parameters and conditions influence the electricity demand. The latter is here the main quantity of interest.

$$\mathrm{COP}_{\mathrm{Ca}} = \frac{T_{\mathrm{in}}}{T_{\mathrm{out}} - T_{\mathrm{in}}} = \frac{\tau_{\mathrm{c}} + 273.15\ \mathrm{K} - \Delta T}{t_{\mathrm{A}} - 2 \cdot \Delta T - \tau_{\mathrm{c}}} \tag{4.13}$$

Besides the $\mathrm{COP}_{\mathrm{Ca}}$, the ambient conditions also influence the specific electricity demand ${}^{P_{\mathrm{el}}}/_{\dot{m}_{\mathrm{air}}}$ over the enthalpy difference Δh. This enthalpy difference defines the heat flow, which has to be transferred from the air flow to reach the set point for inlet air temperature t_{C} and humidity φ_{c}.

$$\Delta h = c_{\mathrm{air}} \cdot (t_{\mathrm{A}} - t_{\mathrm{c}}) + \Big((X_{\mathrm{A}} - X_{\mathrm{c}}) \cdot \Delta h_{\mathrm{V}} + c_{\mathrm{vapor}} \cdot (t_{\mathrm{A}} - t_{\mathrm{c}}) \Big) \tag{4.14}$$

The ambient conditions appear in this equation in the shape of the temperature t_{A} and absolute humidity X_{A}. To calculate the absolute humidity X in kg water per kg air, see equation A.3 for approximation in the appendix. Further constants in equation 4.14 are the specific heat capacity for air $c_{\mathrm{air}} = 1.00$ kJ/kgK and for water vapor $c_{\mathrm{vapor}} = 1.86$ kJ/kgK and the enthalpy of vaporization of water $\Delta h_{\mathrm{V}} = 2500$ kJ/kg. The set points for the conditioned air at the inlet are indicated with the subscript c. The value for the absolute humidity X_{c} depending on a set point for relative humidity φ_{c} and temperature t_{c} can be calculated by applying the equations for saturation vapor pressure A.1 and dew point A.2 in the appendix. For the results shown in below, an inlet temperature of $t_{\mathrm{c}} = 20$ °C and a relative humidity of $\varphi_{\mathrm{c}} = 50$ % were chosen. Summarizing the equations above delivers the specific electricity demand for an air conditioning system in cooling mode depended on ambient conditions:

$$\frac{P_{\mathrm{el}}}{\dot{m}_{\mathrm{air}}} = \frac{c_{\mathrm{air}} \cdot (t_{\mathrm{A}} - t_{\mathrm{c}}) + \Big((X_{\mathrm{A}} - X_{\mathrm{c}}) \cdot \Delta h_{\mathrm{V}} + c_{\mathrm{vapor}} \cdot (t_{\mathrm{A}} - t_{\mathrm{c}}) \Big)}{\eta_{\mathrm{G}} \cdot \mathrm{COP}_{\mathrm{Ca}}} \tag{4.15}$$

Although room cooling is more important in Brazil than heating, latter is necessary as already mentioned occasionally in the Brazilian Southeast and South. Therefore, the heating mode of air conditioning systems is being considered as well. An air conditioning system operates in heating mode, if the ambient temperature t_{A} is under a certain switch-on temperature $t_{\mathrm{H,on}}$. Assuming that the air conditioning system operates as a heat pump under these conditions, its specific electricity demand is in that case:

$$\frac{P_{\mathrm{el}}}{\dot{m}_{\mathrm{air}}} = \frac{\Delta h}{\mathrm{COP}} = \frac{c_{\mathrm{air}} \cdot (t_{\mathrm{H}} - t_{\mathrm{A}})}{\eta_{\mathrm{G}} \cdot \mathrm{COP}_{\mathrm{Ca}}} \tag{4.16}$$

Whereby in equation 4.16 the Carnot-efficiency $\mathrm{COP}_{\mathrm{Ca}}$ for a heat pump is used.

$$\mathrm{COP}_{\mathrm{Ca}} = \frac{T_{\mathrm{out}}}{T_{\mathrm{out}} - T_{\mathrm{in}}} = \frac{t_{\mathrm{H}} + 273.15\ \mathrm{K} + \Delta T}{t_{\mathrm{H}} + \Delta T - t_{\mathrm{A}}} \tag{4.17}$$

To derive from the specific electricity demand the searched values $d_{\mathrm{AC}}(t_{\mathrm{A}}, \varphi_{\mathrm{A}})$, the time series for specific electricity need to be normalized and multiplied with the original daily load profile $d^{\mathrm{o}}_{\mathrm{AC}}$. The result is finally a weather depended time series W_{AC} for air conditioning with 8760 elements.

4.3.3 Hot water load

The hot water load $d_{\mathrm{H}}(n)$ depends not only from the original profile $d^{\mathrm{o}}_{\mathrm{H},j}$ and a difference depending on the weekday $\Delta d^{\mathrm{w}}_{\mathrm{H},j}$, but also from a meteorological component $d^{\mathrm{m}}_{\mathrm{H},1}$. The only weather depended quantity here is the ambient temperature. From the regional difference of hot water demand within Brazil [24], a factor $d_{\mathrm{H}}(t_{\mathrm{A}})$ between certain limits is derived, which represents the habits of using hot water for showering depended on ambient temperature. Referring to [15], hot water demand is considered here to be the same as demand for showering. Figure 4.5 depicts the dependency of relative hot water demand from ambient temperature, which will be explained in the following section.
In the first step, one can assume a linear relation between the relative hot water demand $d_{\mathrm{H}}(t_{\mathrm{A}})$ for showering and the ambient temperature t_{A}, see equation 4.18.

$$d_{\mathrm{H}}(t_{\mathrm{A}}) = a \cdot t_{\mathrm{A}} + b \tag{4.18}$$

The parameters a and b are determined under consideration of certain habits following [106]. At a maximum temperature $t_{\mathrm{A,max}}$, the hot water demand reaches a certain minimum $d_{\mathrm{H,min}}$. In the same way, if it is cold outside, people prefer to take hot showers. Therefore, at a minimum ambient temperature $t_{\mathrm{A,min}}$, the hot water demand reaches its relative maximum $d_{\mathrm{H,max}}$.

$$d_{\mathrm{H}}(t_{\mathrm{A}}) = \begin{cases} d_{\mathrm{H,max}}, & \text{if } t_{\mathrm{A}} = t_{\mathrm{A,max}} \\ d_{\mathrm{H,min}}, & \text{if } t_{\mathrm{A}} = t_{\mathrm{A,max}} \end{cases} \tag{4.19}$$

Therefore, the parameters a and b can be determined.

$$d_{\mathrm{H}}(t_{\mathrm{A}}) = \frac{d_{\mathrm{H,min}} - d_{\mathrm{H,max}}}{t_{\mathrm{A,max}} - t_{\mathrm{A,min}}} \cdot t_{\mathrm{A}} + d_{\mathrm{H,max}} \frac{d_{\mathrm{H,min}} - d_{\mathrm{H,max}}}{t_{\mathrm{A,max}} - t_{\mathrm{A,min}}} \cdot t_{\mathrm{A,min}} \tag{4.20}$$

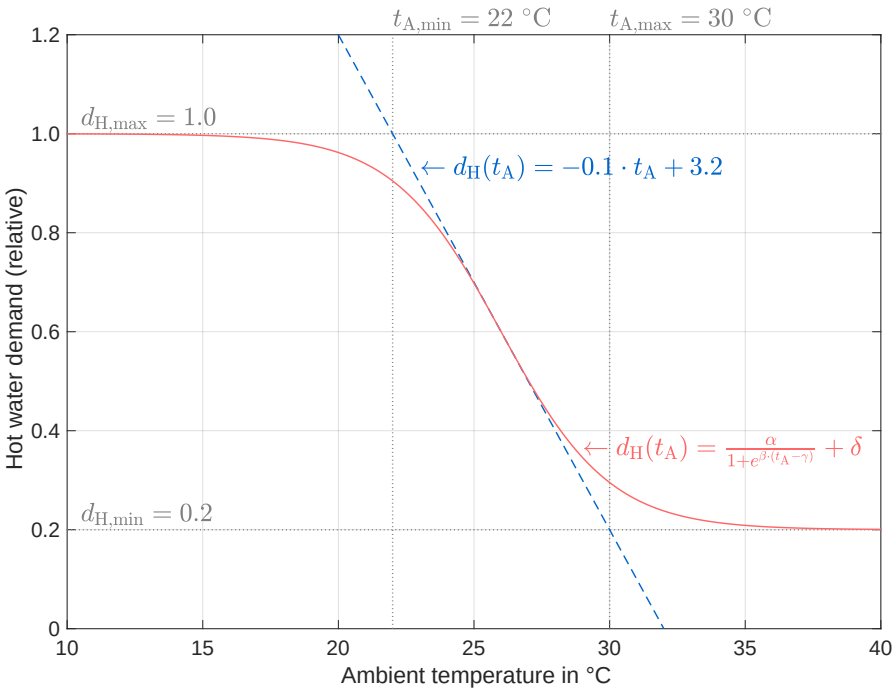

Figure 4.5: Modeled dependency between hot water demand and ambient temperature

Taking into account the regional characteristics of the tropical North with temperatures close to 30 °C throughout the year, less than 20 % use hot water for showering, one can determine the limiting values to $t_{A,max} = 30$ °C and $d_{H,min} = 0.2$. In similar way, almost all people in the relatively cool southern states use water heating, therefore the limiting values can be chosen as $t_{A,min} = 22$ °C and $d_{H,max} = 1.0$. In that case, the linear function is:

$$d_H(t_A) = -0.1 \cdot t_{A,min} + 3.2 \tag{4.21}$$

Obviously, a further increasing energy demand for showering is unrealistic in case of colder outside temperatures than $t_{A,min}$ as well as some people will remain, who use hot water even in hot regions. For example, if they spend the whole day in air conditioned buildings at low inside temperatures. To represent the convergence to $d_{H,min}$ and $d_{H,max}$ at extreme temperatures, a logistic function reflects the relation better than a linear function. Equation 4.22 shows the general formulation of a logistic function with parameters α, β, γ and δ being determined below.

$$d_H(t_A) = \frac{\alpha}{1 + e^{\beta\cdot(t_A-\gamma)}} + \delta \tag{4.22}$$

For extreme high ambient temperatures t_A, the relative hot water demand will not fall under the threshold $d_{H,min}$. Therefore, a limit value observation delivers the value for δ.

$$\lim_{t_A \to \infty} d_H(t_A) = \delta = d_{H,min} \tag{4.23}$$

The parameter α can found in a similar way by considering extreme low outside temperatures.

$$\lim_{t_A \to -\infty} d_H(t_A) = \alpha + \delta = d_{H,max} \tag{4.24}$$

$$\rightarrow \alpha = d_{H,max} - d_{H,min} \tag{4.25}$$

The development of the relative heat demand $d_{\mathrm{H}}(t_{\mathrm{A}})$ can be approximated in the range between $t_{\mathrm{A,min}}$ and $t_{\mathrm{A,max}}$ with the linear function mentioned above. That means, both curves pass in the middle through the same point at same gradient or in reality, that half of the consumers reduced the hot water demand at $(t_{\mathrm{A,max}} + t_{\mathrm{A,min}})/2$.

$$d_{\mathrm{H}}\left(\frac{t_{\mathrm{A,max}} + t_{\mathrm{A,min}}}{2}\right) = \frac{d_{\mathrm{H,max}} + d_{\mathrm{H,min}}}{2} \tag{4.26}$$

In case of both the linear and the logistic function have the same gradient, the last missing parameter can be determined.

$$d'_{\mathrm{H}} = \frac{\partial}{\partial t_{\mathrm{A}}}\left[\frac{\alpha}{1 + e^{\beta\cdot(t_{\mathrm{A}}-\gamma)}}\right]_{t_{\mathrm{A}}=\frac{t_{\mathrm{H,max}}+t_{\mathrm{H,min}}}{2}} = \frac{d_{\mathrm{H,max}} + d_{\mathrm{H,min}}}{t_{\mathrm{H,max}} + t_{\mathrm{H,min}}} \tag{4.27}$$

By using the specific values displayed in figure 4.5, the logistic function to reflect the meteorological dependency of hot water demand can be written as follows.

$$d_{\mathrm{H}}(t_{\mathrm{A}}) = \frac{0.8}{1 + e^{0.5\cdot(t_{\mathrm{A}})-26}} + 0.2 \tag{4.28}$$

These values were also used for calculation of annual load profiles for the Brazilian macroregions North, Northeast, Central-West, Southeast and South, see section 4.3.5.

4.3.4 Determination of amplitude factors

After applying the methods described above to derive annual profiles for the three categories non-shiftable, hot water and air conditioning load, these profile have to be recombined to one annual electrical load profile. The profiles have to be rescaled by using the amplitude factors, so that every load category maintains its annual share corresponding to statistics. For example, if air conditioning accounts for 32 % of the annual electricity demand, this share has to reappear in the newly generated annual load profile.

The amplitude factors are determined by solving the linear equation system, under consideration of the s_{B}, s_{H} and s_{B} due to statistics.

$$s_{\mathrm{i}} = \frac{s_{\mathrm{i}}}{W_{\mathrm{el}}} \tag{4.29}$$

The linear equation system to determine the amplitude factors can be denoted as follows:

$$A_{\mathrm{B}} \cdot (W_{\mathrm{B}} - \frac{W_{\mathrm{B}}}{s_{\mathrm{B}}}) + A_{\mathrm{H}} \cdot W_{\mathrm{H}} + A_{\mathrm{AC}} \cdot W_{\mathrm{AC}} = 0 \tag{4.30}$$

$$A_{\mathrm{B}} \cdot W_{\mathrm{B}} + A_{\mathrm{H}} \cdot (W_{\mathrm{H}} - \frac{W_{\mathrm{H}}}{s_{\mathrm{H}}}) + A_{\mathrm{AC}} \cdot W_{\mathrm{AC}} = 0 \tag{4.31}$$

$$A_{\mathrm{B}} \cdot W_{\mathrm{B}} + A_{\mathrm{H}} \cdot W_{\mathrm{H}} + A_{\mathrm{AC}} \cdot W_{\mathrm{AC}} = W_{\mathrm{el}} \tag{4.32}$$

After this finale step, the initial equation 4.1 can be applied to calculate the load profile for the residential sector. The profiles have following characteristics:

- annual electrical load profile in hourly resolution (8760 time steps)

- differentiation of three load categories:
  - non-shiftable load (B)
  - water load (H)
  - air conditioning load (AC)
- different influence of meteorological conditions and weekdays for every category
- statistical shares for each category are maintained

4.3.5 Application for Brazilian macro-regions

Figure 4.6 illustrates for five Brazilian macro-regions the generated load profiles with the mathematical approach described above. The same data sources as mentioned in section 4.2 were used for original daily load profiles, statistical shares of load categories and meteorological data. The values listed in table A.2 were chosen as set points and switch-on temperatures for air conditioning to generate the results depicted in figure 4.6.

The diagrams in the left column of figure 4.6 show seven days (168 hours) in January, beginning with Monday. It is worth to mention, that January is a summer month, since the Brazilian territory is mainly located on the southern hemisphere. According to that, the profiles in the right half show seven days in August, which is a winter month in Brazil. This first day in this example is a Tuesday. As mentioned above, the winter temperatures are very moderate in all parts in Brazil. Temperatures around or under the freezing point are very rare.

Taking a closer look to the profile for the North region, the almost absence of a seasonality is remarkable. The peaks for air conditioning do not differ considerably from January to August. From the Northeast region over the Central-West down to the Southeast, seasonal effects in air conditioning demand can be recognized. For latter mentioned regions, the period in January shows a higher air conditioning demand, which is caused by higher temperatures in the summer and moderate climate in the winter. Contrary to that, the air conditioning in the South region is higher in August in comparison to January. Reason for that are the relatively low ambient temperatures in the South during winter, which make the air conditioning system operate in heating mode.

The differences within the illustrated days not only come from different weather conditions, but also from weekday depending usage of electric consumers. Since the occupancy of homes during daytime on weekend is implied to be higher than on weekdays, the air conditioning demand is higher in that time. A meteorological dependency of non-shiftable load has not been implemented in this approach, but it could be one step for further improvement.

Adapted to the year 2017 by taking into account the total electricity demand in the residential sector, the countrywide load profiles were simulated. A comparison of these times series with the real load in Brazil over all sectors can be found in the appendix, see figure A.12.

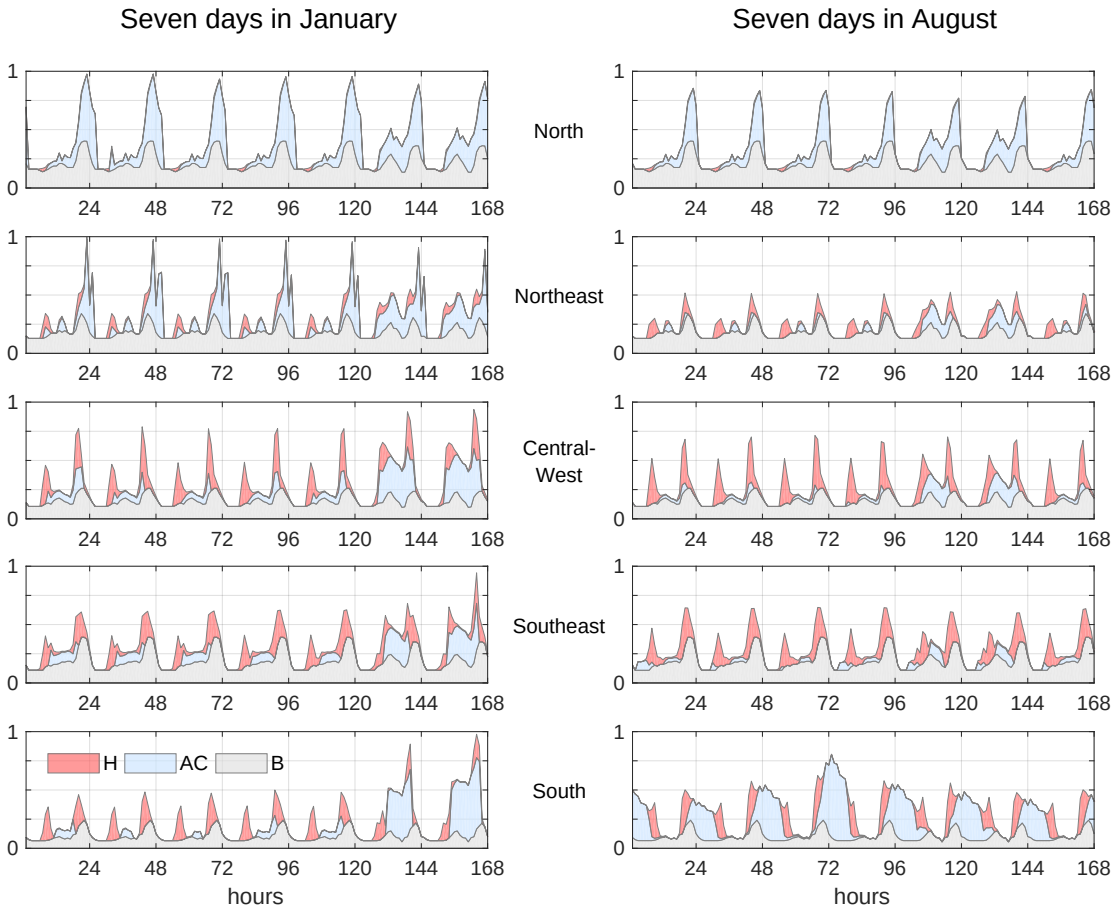

Figure 4.6: Generated load profiles for Brazilian macro-regions

4.4 Derivation of storage capacities

This section presents an approach for storage dimensioning based on the regional load profiles developed in section 4.2. It is assumed, that the storage operates on consumer side in the residential sector, see figure 4.3. They are dimensioned in that way to maximize the self-consumption of distributed photovoltaic generation. A comparable approach can be found for example in [107]. Storage dimensioning as an outcome of a linear optimization model is presented in section 5.2 of the following chapter. The photovoltaic peak capacity per consumer unit is dimensioned to generate the annual electricity consumption of each unit. Basis for the dimensioning of both photovoltaic system and storage are normalized load profiles. Therefore, the annual maximum hourly value is one for each profile. An excerpt of the used profiles in regional resolution is illustrated in figure 4.6.

In the first step of storage dimensioning, only batteries are considered. This approach is displayed in figure 4.7. In the second step, the load is differentiated in three categories, including the electrical load caused by hot water demand and operation of air conditioning systems, see figure 4.9. Motivation for the investigation of thermal loads and their corresponding potential for thermal storage is to reveal possible economic benefits. A financially more favorable solution

can possibly be found, if storage requirements can be satisfied by relative cheap water or ice storage instead of relative costly batteries. The economic evaluation can be found in section 4.5.
The first column of diagrams in figure 4.7 depicts in gray the electrical load profile and the photovoltaic generation for an average day differentiated by Brazilian macro-region. The second column shows the residual load for each of the five regions, from which the storage capacity can be derived. Red bars for the residual load mean a deficit of electricity production, whereas green bars stand for a surplus. The required storage capacity for an average day is than determined by integration of the residual load $W_{\mathrm{j}}^{\mathrm{res}}$. The residual load $W_{\mathrm{j}}^{\mathrm{res}}$ for each time step j has to be calculated as a difference between generation $W_{\mathrm{j}}^{\mathrm{gen}}$ and demand $W_{\mathrm{j}}^{\mathrm{dem}}$.

$$W_{\mathrm{j}}^{\mathrm{res}} = W_{\mathrm{j}}^{\mathrm{gen}} - W_{\mathrm{j}}^{\mathrm{dem}} \tag{4.33}$$

$$W_{\mathrm{j}}^{\mathrm{sto}} = W_{\mathrm{j-1}}^{\mathrm{sto}} + W_{\mathrm{j}}^{\mathrm{res}} \tag{4.34}$$

$$\text{for } j = 1, 2, ..., 24$$

The maximum reached during this representative period is the required storage capacity C_{n}.[1]

$$C_{\mathrm{n}} = \max(W_{\mathrm{j}}^{\mathrm{sto}}) \tag{4.35}$$

$$\text{for } j = 1, 2, ..., 24$$

Applying a battery storage with this capacity under the above described conditions, the consumer would neither need electricity from the grid nor feed-in. During one average day per region, the storage level follows the curve illustrated in the third column in figure 4.7.
The dimensioning of storage capacity was conducted using average hourly values for both photovoltaic generation and load. In reality, generation and load show differences from one day to another. Consequently, a storage capacity derived from an average day would not cover all supply and demand of all days of the year, depending on the extend single days differ from the average. Figure 4.8 shows in the first column again the battery storage level for an average day. These diagrams also contain the capacity required to provide enough storage capacity for 100 % self-consumption for an average day. The specific values in red represent this storage capacity in kWh. For example, 6.1 kWh are required to satisfy the storage needs derived from the profile for the North region. For further explanations, this explicit value of storage capacity for each profile is expressed as relative storage capacity r.

$$\text{Relative storage capacity } r = \frac{\text{Real applied capacity } C_{\mathrm{real}}}{\text{Normal capacity } C_{\mathrm{n}}} \tag{4.36}$$

C_{real} denotes the real storage capacity applied in each case, whereas C_{n} is the "normal" capacity to fulfill the requirements of an average day, meaning 100 % self-consumption, no electricity exchange with the grid. For later evaluations, the real storage capacity C_{real} is varied relative to the normal storage capacity C_{N} in discrete steps.

The column in the middle of 4.8 shows the ratio of self-consumption s depending on the relative storage capacity. The self-consumption ratio s denotes here the share of directly

[1] For a storage level, only positive values or zero makes sense. To force all values of $W_{\mathrm{j}}^{\mathrm{sto}}$ for j = 1,2,...,24 to be non-negative, the lowest value $\min(W_{\mathrm{j}}^{\mathrm{sto}})$ must be added to all $W_{\mathrm{j}}^{\mathrm{sto}}$ before determining C_{n}

consumed electricity W_{dir} produced by the photovoltaic system to the total electricity demand per year W_{dem}. If the storage is empty or not available, the amount of electricity W_{grid} is received from the grid. Therefore, the self-consumption ratio can be written as follows:

$$s = \frac{W_{\mathrm{dir}}}{W_{\mathrm{dem}}} = \frac{W_{\mathrm{dem}} - W_{\mathrm{grid}}}{W_{\mathrm{dem}}} = 1 - \frac{W_{\mathrm{grid}}}{W_{\mathrm{dem}}} \tag{4.37}$$

For calculation of the self-consumption ratio, the profiles for the whole year in hourly resolution were taken, reflecting daily and seasonal differences. The underlying concept for storage operation was to minimize exchange with the grid. By using the same notation as in figure 3.7, the strategy to determine storage level and grid exchange is described in the following lines. Depending on a surplus, a deficit or equilibrium, the residual load $W_{\mathrm{t}}^{\mathrm{res}}$ can be positive, zero or negative. Table 4.2 shows a simple case distinction. This rule delivers when to charge or discharge the storage and when electricity is purchased from or fed into the grid. The following intertemporal storage balance reveals where to put the residual load $W_{\mathrm{t}}^{\mathrm{res}}$:

$$W_{\mathrm{t}}^{\mathrm{res}} = W_{\mathrm{t}}^{\mathrm{gen}} - W_{\mathrm{t}}^{\mathrm{dem}} \tag{4.38}$$

$$\Delta W_{\mathrm{t}} = W_{\mathrm{t-1}}^{\mathrm{sto}} + W_{\mathrm{t}}^{\mathrm{res}} \tag{4.39}$$

In the equation above, $W_{\mathrm{t-1}}^{\mathrm{sto}}$ denotes the storage level from the previous time step $t-1$. The value ΔW_{t} can be regarded as the storage content in time step t, but this new storage level is only possible, if none of the two conditions in table 4.2 is violated. The first condition indicates

Table 4.2: Case distinction for operation strategy

		Full storage (1)	Empty storage (2)	Charge or discharge
		if $\Delta W_{\mathrm{t}} \geq C_{\mathrm{real}}$	elseif $\Delta W_{\mathrm{t}} \leq 0$	else
Storage level	$W_{\mathrm{t}}^{\mathrm{sto}}$	$W_{\mathrm{t-1}}^{\mathrm{sto}}$	$W_{\mathrm{t-1}}^{\mathrm{sto}}$	$W_{\mathrm{t-1}}^{\mathrm{sto}} + W_{\mathrm{t}}^{\mathrm{res}}$
Feed-in	$W_{\mathrm{t}}^{\mathrm{in}}$	$W_{\mathrm{t}}^{\mathrm{res}}$	0	0
Purchase	$W_{\mathrm{t}}^{\mathrm{out}}$	0	$W_{\mathrm{t}}^{\mathrm{res}}$	0

that the storage already reached its capacity limit. Therefore, the residual load must be fed into the grid. The second condition means, that a discharge for $W_{\mathrm{t}}^{\mathrm{res}}$ of the storage would lead to a negative level. That means practically, the storage is empty or almost empty. Therefore, the necessary residual load $W_{\mathrm{t}}^{\mathrm{res}}$ has to be purchased from the grid.

For the economic evaluation conducted in section 4.5, predominantly the self-consumption ratio is an interesting result for further calculations. It determines the cost composition between purchased electricity and expenditures for generation on consumer side. The middle column in figure 4.8 illustrates the self-consumption ration depending on the relative storage capacity. As complementary quantity to the self-consumption ratio s corresponding to equation 4.37, the feed-in ratio f is shown in the third column.

$$f = 1 - s = \frac{W_{\mathrm{grid}}}{W_{\mathrm{dem}}} \tag{4.40}$$

The amount of electricity fed into the grid is relevant when considering centralized integration of photovoltaic power generation or other fluctuating renewable sources of electricity. The green

bar in the diagrams for both self-consumption ratio s and feed-in ratio f highlights the result for the relative storage capacity $r = 1$, see figure 4.8. The results for both are calculated for different relative storage capacities r varied in increments of $\Delta r = 0.25$. As explained above, the storage capacity for the case $r = 1$ was derived from the average day and applied to each consumer unit. The capacities in kilowatt-hours can be found in red font in the first column of figures 4.8 and are summarized together with following results in table A.3, see appendix.

Except for the Brazilian South, for all other macro-regions a self-consumption ratio greater than 90 % is possible for the case $r = 1$. Due to its considerable seasonality in the South, the days from one season to another differ significantly, therefore a storage sized with an average day only provides a self-consumption ratio close to 80 %. Without applying an energy storage at all $(r = 0)$, a self-consumption ratio around 30 % is possible for the North and the South under the conditions described above, whereas approximately 40 % in the Northeast, the Central-West and the Southeast. Between $r = 0$ and $r = 1$, a significant gain in self-consumption can be recognized from one step to another, whereas storage sizes of $r > 1$ only deliver very small improvements. The economic evaluation conducted in section does not provide strong arguments for a relative storage capacity above $r > 1$, when discussing grid-connected systems.

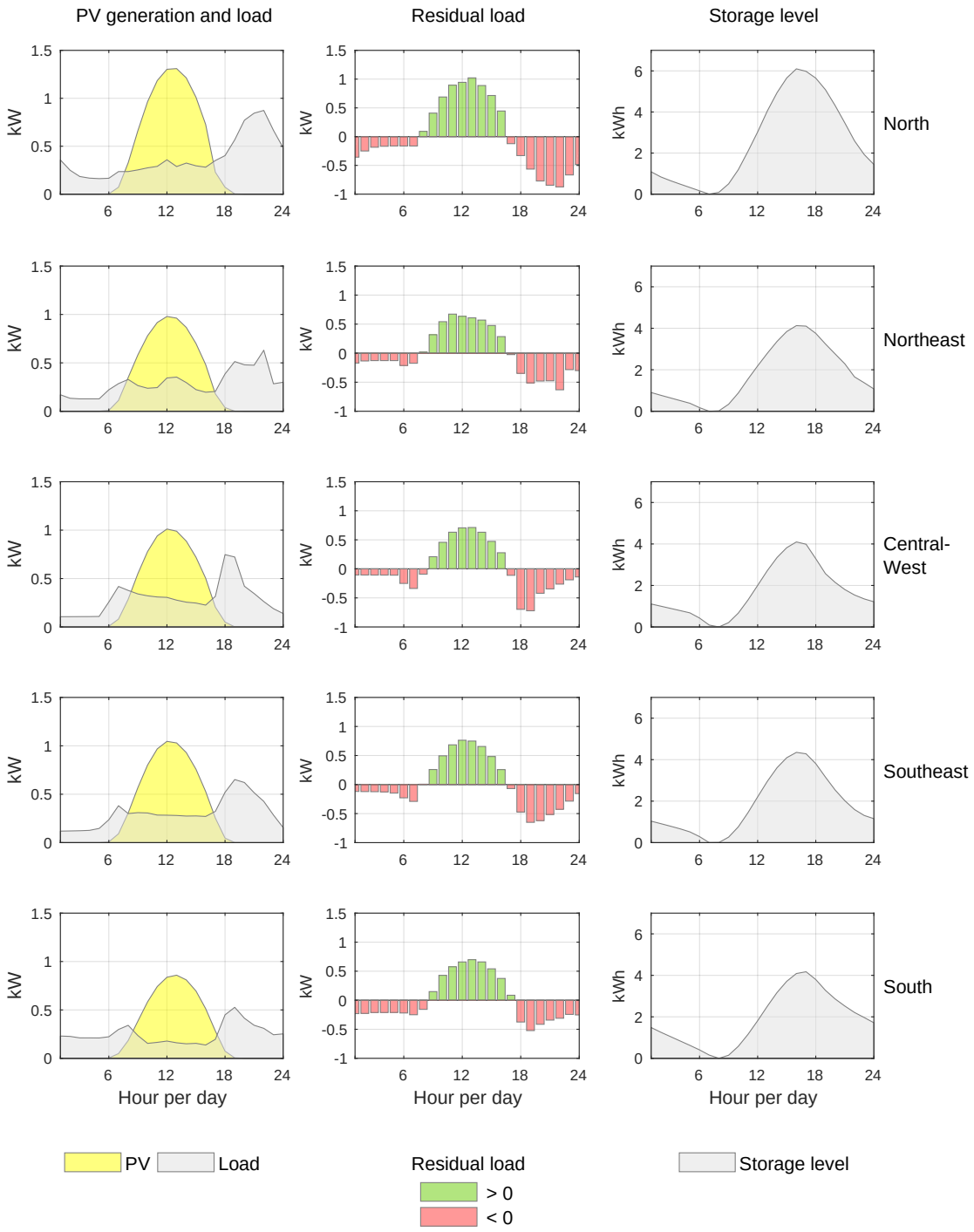

Figure 4.7: Regional profiles and battery storage level

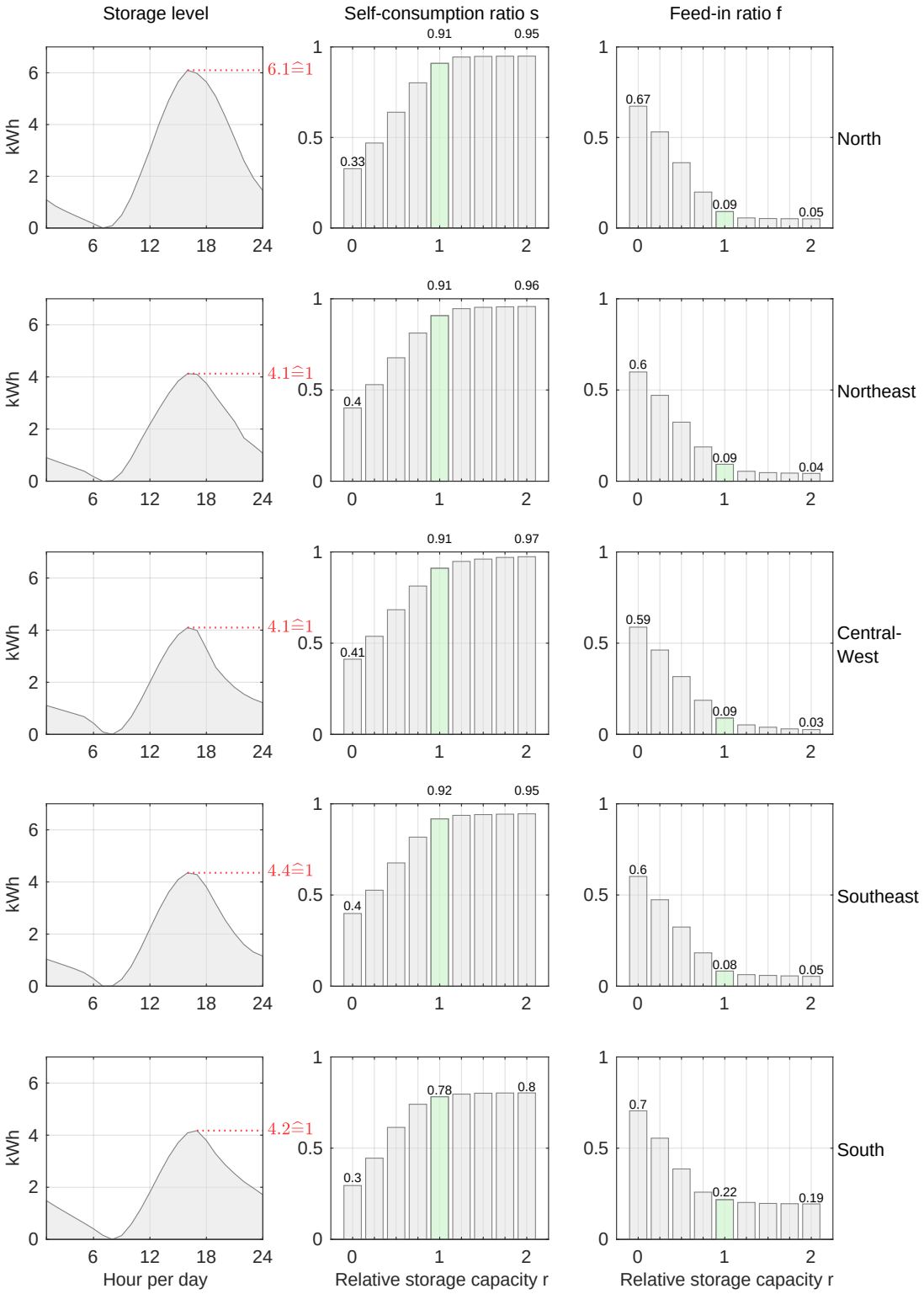

Figure 4.8: Self-consumption rates depending on battery size

Figure 4.9 and figure 4.10 illustrate the same approach as described before, but under consideration of thermal storage in the residential sector besides batteries. The setting for a households energy system is sketched in the lower half in figure 4.3. One remarkable difference to batteries is the consideration of self-discharge in case of thermal storage. The effect of loosing energy from one hour to another with the self-discharge rate κ is modeled here as follows:

$$W_{\mathrm{t}}^{\mathrm{sto}} = (1 - \kappa) \cdot W_{\mathrm{t-1}}^{\mathrm{sto}} + W_{\mathrm{t}}^{\mathrm{res}} \tag{4.41}$$

Since the self-discharge of common stationary accumulators is around 5 % per month, see for example [108], an hourly self-discharge is neglected here. For the presented results, a self-discharge rate for thermal storage of $\kappa = 3\ \%$ was chosen, what leads to a loss of around 30 % of the storage content within 12 hours. The temporal energy loss of a thermal storage of daily 30 % has a completely different magnitude compared to the 5 % per month of batteries. Figure 4.10 shows the results for storage sizing in the first column as well as the corresponding self-consumption ratios in the second column. The third column in figure 4.10 displays a ranking of the best selection of storage types sorted by self-consumption ratio. Under application of all three types for storage, namely battery (B) and thermal storage for hot water (H) and air conditioning (AC), lower self-consumption ratios are reached in contrast to the case only using batteries. A tabular comparison can be found in the appendix, see table A.4. Self-consumption rates are lower in the case of thermal storage applications compared to battery-only applications. Two reasons explain these differences. Firstly, the flexibility of several storages is lower in comparison to one single battery since the conditions of table 4.2 restrict storage operation more often. Secondly, the self-discharge of thermal storage has a remarkable impact.

As expected, the usage of all three types of storage allows the highest self-consumption rates right after the scenarios only with batteries. This result is illustrated in third column in figure 4.10. The second best position in terms of the self-consumption rate depends on the region and is related to the prevailing climate conditions. Due to the negligible role of hot water demand in the North region, the waiving of hot water storage has a marginal impact on the self-consumption ratio, whereby an air conditioning storage contributes considerably to a high self-consumption ratio. In all other macro-regions, the second-best composition is the combination of battery and hot water storage. Because of the relatively simple and cost-effective implementation of hot water storage, its effect on the self-consumption ratio is remarkable. Just by adding hot water storage on the consumer side into a residential energy system, the self-consumption ratio could be increased by around 15 % in the Central-West, the Southeast, and the South. The results also show the possible increases in self-consumption if only thermal storage were used. In contrast systems without storage, over 50 % of self-consumption are possible in all regions. Since self-consumption ratios are usually subordinate criteria after cost considerations, an economic evaluation for the presented cases is conducted in the following section taking into account the Brazilian market environment and tariff structure as well as possible future developments. Considered future developments are decreasing costs for both battery and photovoltaic systems and the possible abolition of net metering.

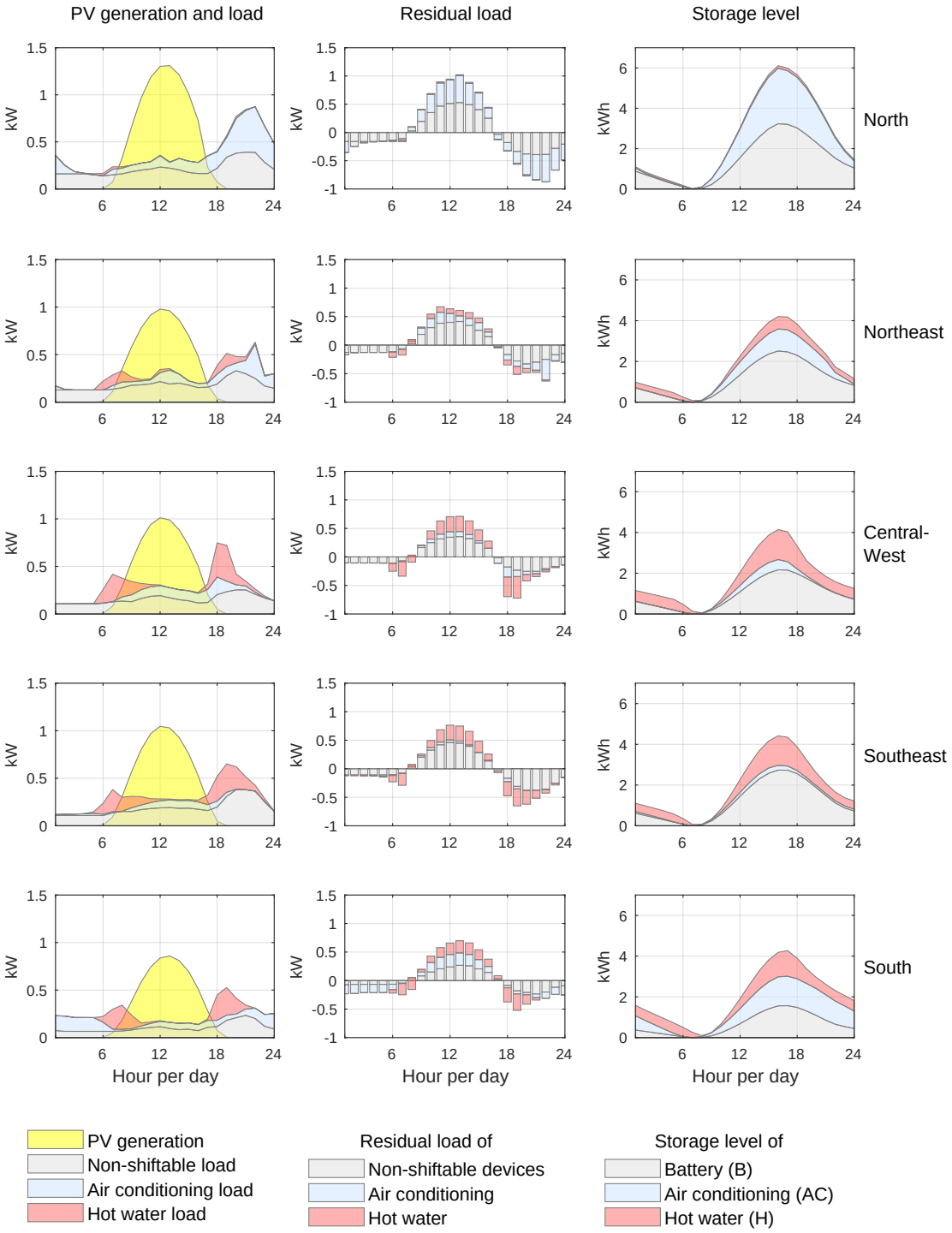

Figure 4.9: Regional profiles, battery and thermal storage levels

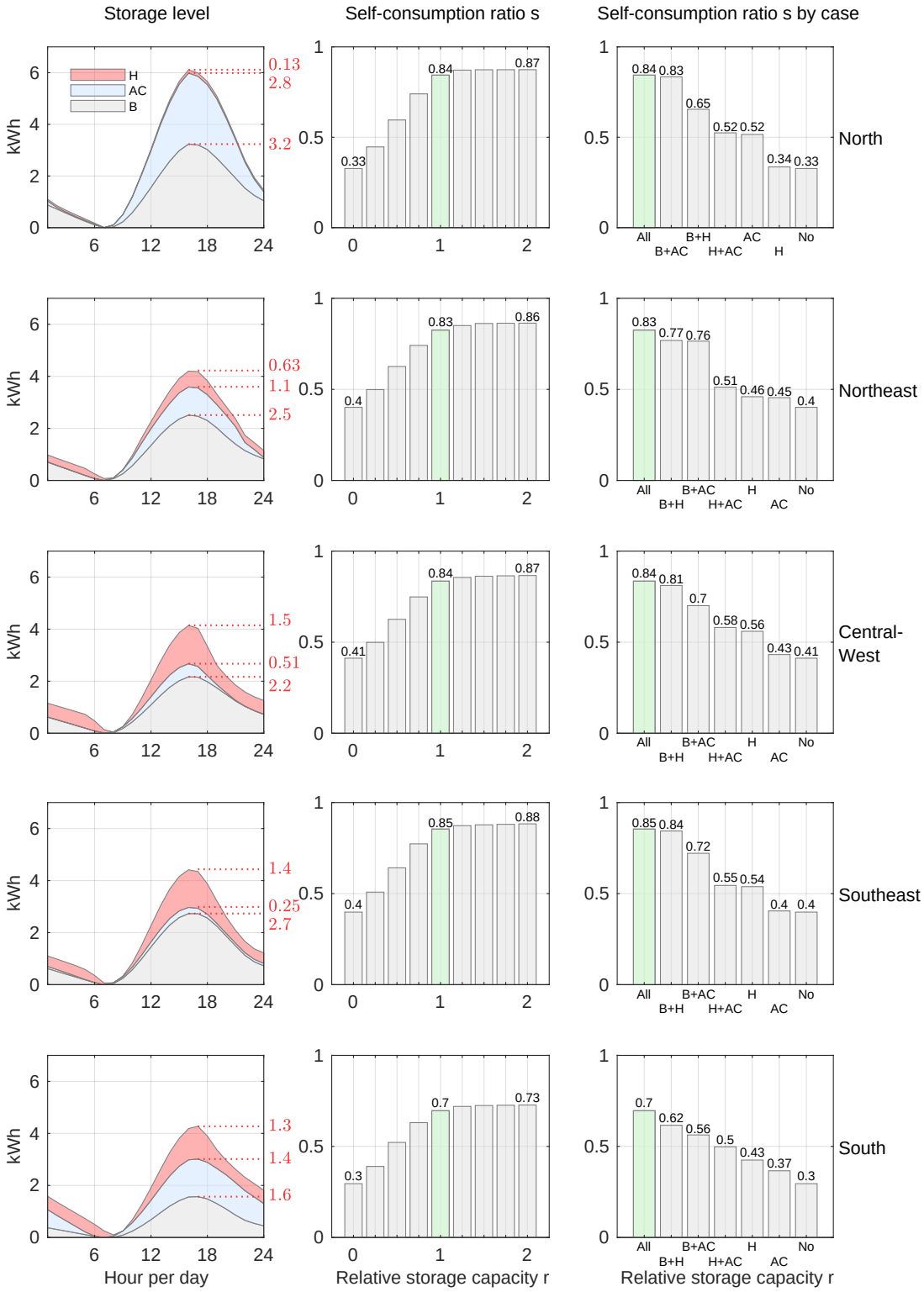

Figure 4.10: Self-consumption ratios depending on applied storage

4.5 Economic evaluation by Levelized Cost of Electricity

The economic evaluation of this section follows the common approach of Levelized Cost of Electricity (LCOE) [109]. The main components for LCOE calculation are initial investment costs I_0, period of use T of the involved technologies, and interest rate i. The total initial investment I_0 is calculated as the product sum of the capacities C multiplied with their specific costs k of all technologies applied in each case. The considered technologies are a photovoltaic system (PV), battery storage (B), and thermal storage for hot water (H) and air conditioning systems (AC). For the sake of simplicity, other costs besides initial investment are not considered here. Since no fuel is necessary and only low-maintenance appliances are considered, real results should not differ too much from these calculations.

$$I_0 = C_{\mathrm{PV}} \cdot k_{\mathrm{PV}} + C_{\mathrm{B}} \cdot k_{\mathrm{B}} + C_{\mathrm{H}} \cdot k_{\mathrm{H}} + C_{\mathrm{AC}} \cdot k_{\mathrm{AC}} \tag{4.42}$$

The LCOE is then calculated with the formula A.7 derived in the appendix from the net present value (NPV).

$$\mathrm{LCOE} = \frac{I_0}{W_{\mathrm{el}}} \cdot \mathrm{ANF}(i, T) \tag{4.43}$$

The factor $\mathrm{ANF}(i, T)$ in this equation considers the annuity value of the investment. Assuming the interest rate i over the period of use or investment period T, the factor $\mathrm{ANF}(i, T)$ for the annuity is:

$$\mathrm{ANF}(i, T) = \frac{(1+i)^T \cdot i}{(1+i)^T - 1} \tag{4.44}$$

For results depicted below, the investment period of $T = 20\ a$ was chosen, a common product lifetime for photovoltaic systems. Other components are considered here to have the same lifetime, which leaves room for more detailed investigations. Interest rates are varied in the range of $5\ \% < i < 15\ \%$ to reflect the observed volatility illustrated in figure 2.9.

The following heat maps illustrate the results of the economic evaluation. Figure 4.11 acts as a reading example. The top heat map in figure 4.11 shows for the load profiles and solar radiation of the Southeast region the results for the LCOE in USD per kWh. From left to right, the capacity prices for batteries get gradually cheaper, from 600 to 100 USD/kWh. From the bottom to the top, the specific prices for systems decrease from 1,000 to 500 USD/kWh. This methodology for visualization is applied miniaturized in the following figures. Slightly different to read is the heat map to investigate the impact of varying interest rates, see bottom chart in figure 4.11. The horizontal axis represents decreasing interest rates from 15 to 5 %. The vertical axis combines increasing investment prices for both photovoltaic systems and batteries, gradually increasing within the same interval as described above.

Southeast: Variation of price for battery (B) and photovoltaic (PV)

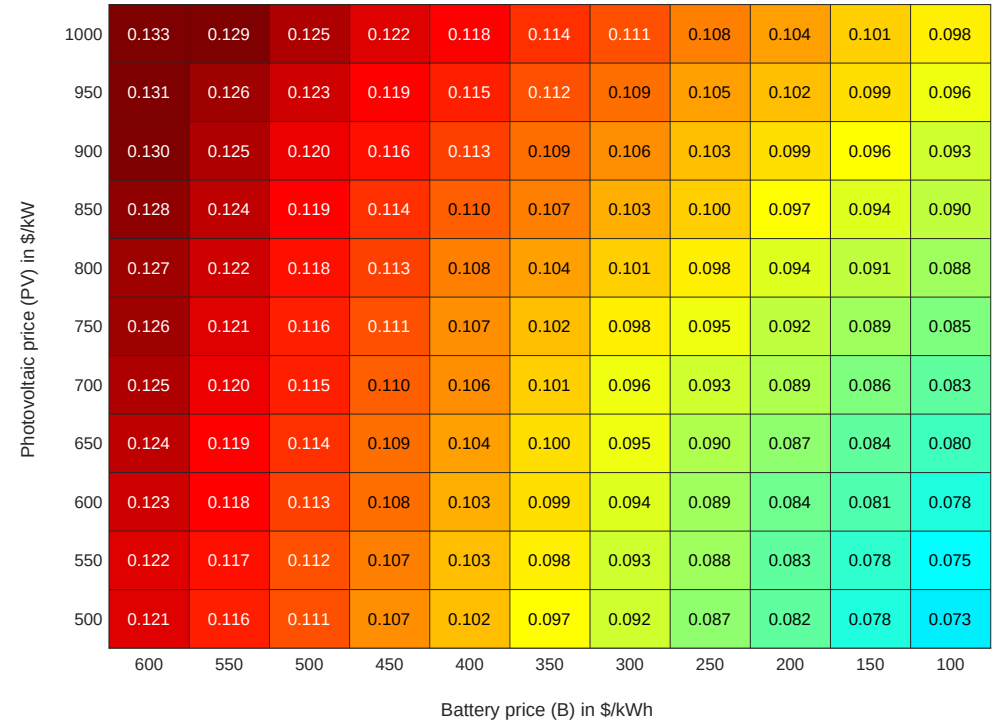

Northeast: Variation of interest rates (i) and prices for photovoltaic (PV), battery (B)

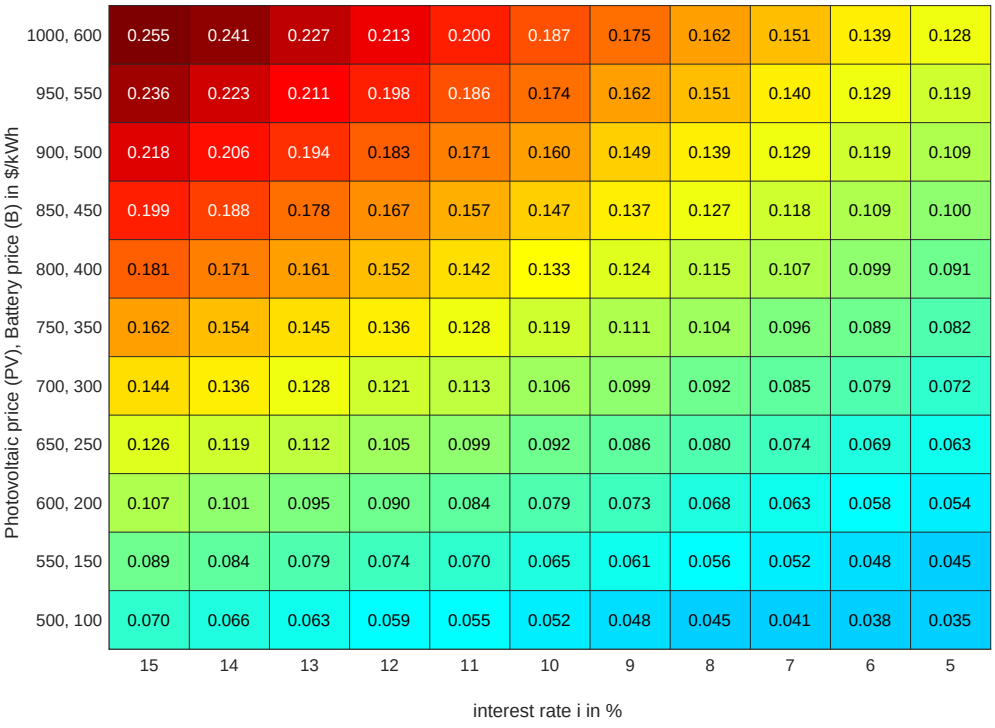

Figure 4.11: Reading example for LCOE heat maps

The tables of heat maps from figure 4.12 do not display the pure LCOE, but the electricity price a consumer would see when net metering is not applied. In the presence of net metering, the use of distributed storage would mainly increase supply reliability but with no or very limited economic benefit to residential customers. A summary on the net metering in Brazil, see section 3.1 in chapter 3. The displayed electricity price p_{el} is the weighted average of the self-produced electricity by the distributed system and the additional electricity purchased from the grid at the price p_{grid}. The price p_{grid} used here is the average electricity tariff by the specific Brazilian macro-region. In the equation below and the following graphs, the self-consumption rate from equation 4.37 is denoted with s.

$$p_{\mathrm{el}} = s \cdot \mathrm{LCOE} + (1 - s) \cdot p_{\mathrm{grid}} \tag{4.45}$$

Unlike the reading example of figure 4.11, figure 4.12 and the ones of the following pages do not contain specific values for electricity costs. The color bar at the bottom provides the range of weighted electricity prices for each plot. One can find a tiny legend in each figure at the top right, which describes the horizontal and vertical axis. The columns of all plots show the results for each Brazilian macro-region, starting with the North region on the very left over the Northeast, Central-West, Southeast, and South at the very right. The rows stand for different or no storage capacities. All subplots contain in the bottom line the range of calculated weighted electricity costs in USD/kWh and the self-consumption rate s. A household must purchase the remaining share of power $1 - s$ from the grid at p_{grid}. With every price drop for PV or battery, an iterative electricity price increase by 5 % for p_{grid} is assumed. The mean tariffs by region for residential customers derived from [9] are summarized in the table below.

Table 4.3: Mean tariff by Brazilian macro-region

Region	p_{grid} in USD/kWh
North	0.154
Northeast	0.147
Central-West	0.149
Southeast	0.132
South	0.104

The following paragraphs describe the main findings of the economic evaluation for distributed integration for selected parameters. The following results differ by different storage options, namely only battery for figure 4.12 and 4.13. The underlying system composition for the two latter mentioned is sketched in the top section of figure 4.3 in section 4.2, whereas the bottom scheme is the basis for the results displayed in figure 4.13 and 4.14. For those, also the thermal storage options hot water (H) and air conditioning (AC) are considered. Therefore, the applied battery capacities are lower compared to the cases with batteries as the only storage option.

Figure 4.12 depicts the results for the weighted average of LCOE and the regional price of electricity in USD/kWh. With batteries as the only storage option, the range goes from 0.06 to 0.24 USD/kWh. As the tiny legend in the top-right subplot shows, the horizontal axes represent varying prices for battery capacity from 600 to 100 USD/kWh, and the vertical axis

covers the price range of photovoltaics from 1000 to 500 USD/kWh. From one row to another, the relative storage capacity r according to equation 4.36 increases by 0.25, starting from 0 in the top row to 1.5 in the bottom row. The first row shows the range of electricity costs for all regions depending on the price reduction of photovoltaics and price increase of p_{grid} by 5 % for each step. The relative storage capacity $r = 0$ indicates that no battery is applied here. According to these calculations, a self-consumption rate s between 30 % (South, North) and around 40 % (Northeast, Southeast, and Central-West) is possible without batteries. The costs for power supply are above 0.13 USD/kWh in all cases, showing a high impact of the increase of p_{grid} due to the low self-consumption rate s. When assuming a price development to 100 USD/kWh for batteries and 500 for PV, a relative storage rate of $r = 0.75 - 1.0$ appears to be the best solution in terms of lowest supply cost. Self-consumption rates above 74 % are possible under these conditions in all regions with electricity costs down to 0.06 USD/kWh, significantly below the regional electricity tariffs. Relative storage capacities above $r = 1.0$ are economically unfavorable. In the North and Northeast, PV and battery storage systems provide comparable costs per kWh as power purchased from the grid. In contrast, meager costs for PV and batteries are a condition for grid parity for the South. Noteworthy that PV and battery systems not only provide lower costs, but also prevent interruptions in electricity supply, which happen occasionally, see figure 3.8.

The impact of varying interest rates on the weighted average of LCOE and regional price of electricity is illustrated in figure 4.13. The horizontal axes represent the range 15-5 % for the interest rates. The vertical axis combines the price interval 1000-500 USD/kW for photovoltaics and 600-100 USD/kWh for batteries. One important finding is that the influence of interest rates on the supply costs is much lower compared to varying investment costs.

The economic feasibility under consideration of further storage options besides batteries depicts figure 4.14. Under these conditions, applied battery capacities are significantly lower, what can be seen by comparing figure 4.8 and 4.10. When using all storage options, see the first row of figure 4.14, electricity costs are on the same level or lower compared to p_{grid}, except for the South. Suppose batteries are no component in distributed systems. In that case, the use of hot water (H) storage or thermal storage for air conditioning (AC) is only attractive at higher prices compared with table 4.3. The combination B+H standing for battery and hot water storage seems economically favorable in the Central-West and the Southeast due to regional climatic and seasonal characteristics. The same applies to the case battery and air conditioning storage B+AC for distributed systems in the North and the Northeast. For the South region, the low prices for p_{grid} caused by the highest Brazilian shares of hydropower in electricity production make the economic feasibility of distributed storage challenging.

Figure 4.13 displays the impact of varying interest rates and investment costs on distributed systems relying on both batteries and thermal storage. One can recognize a remarkable impact where relatively costly batteries are applied; see the cases abbreviated with All, B+H, and B+AC. Therefore, the interest rates and their projections can act as decision variables for investments in distributed systems.

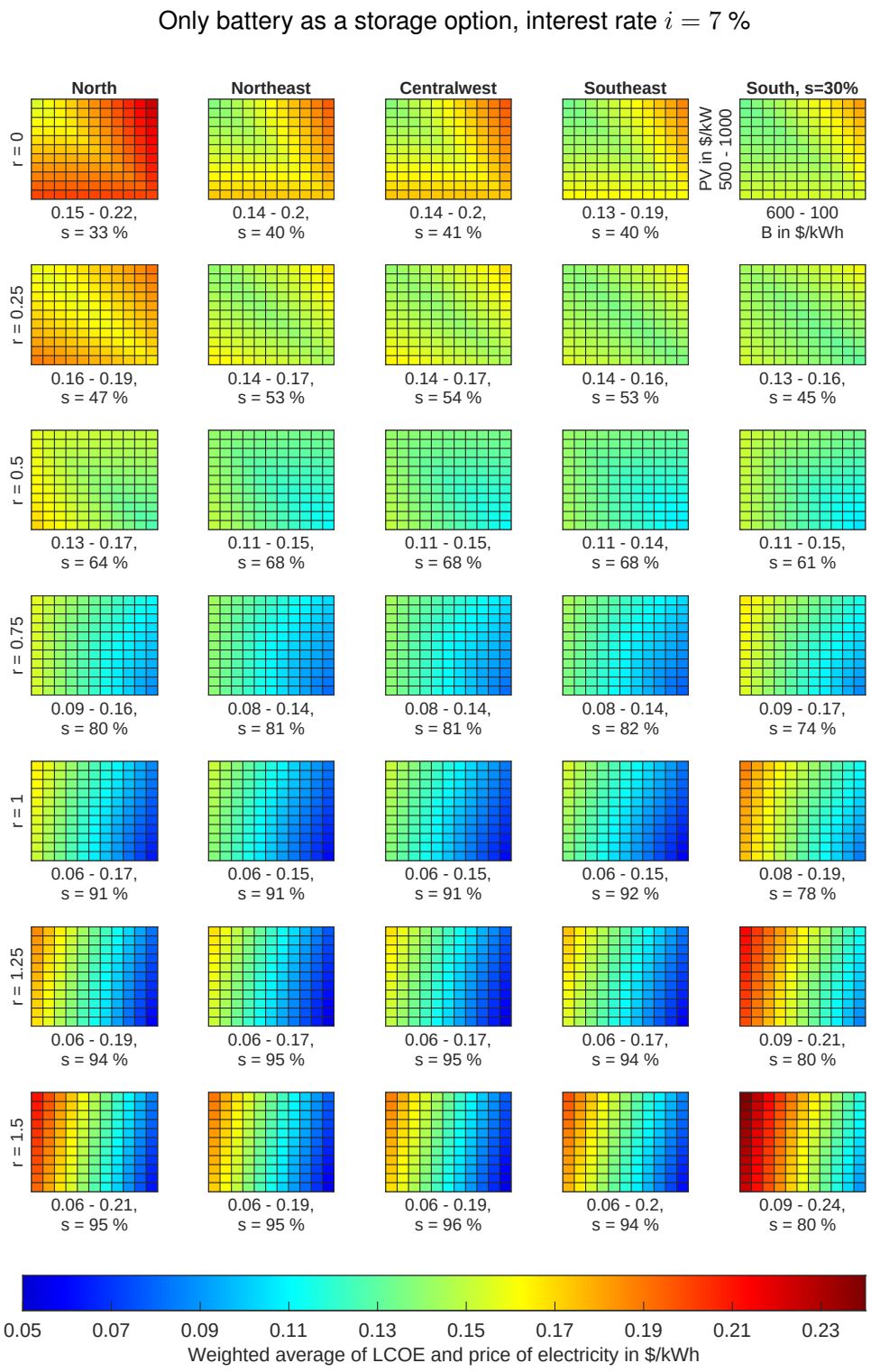

Figure 4.12: USD/kWh depending on prices for battery and PV

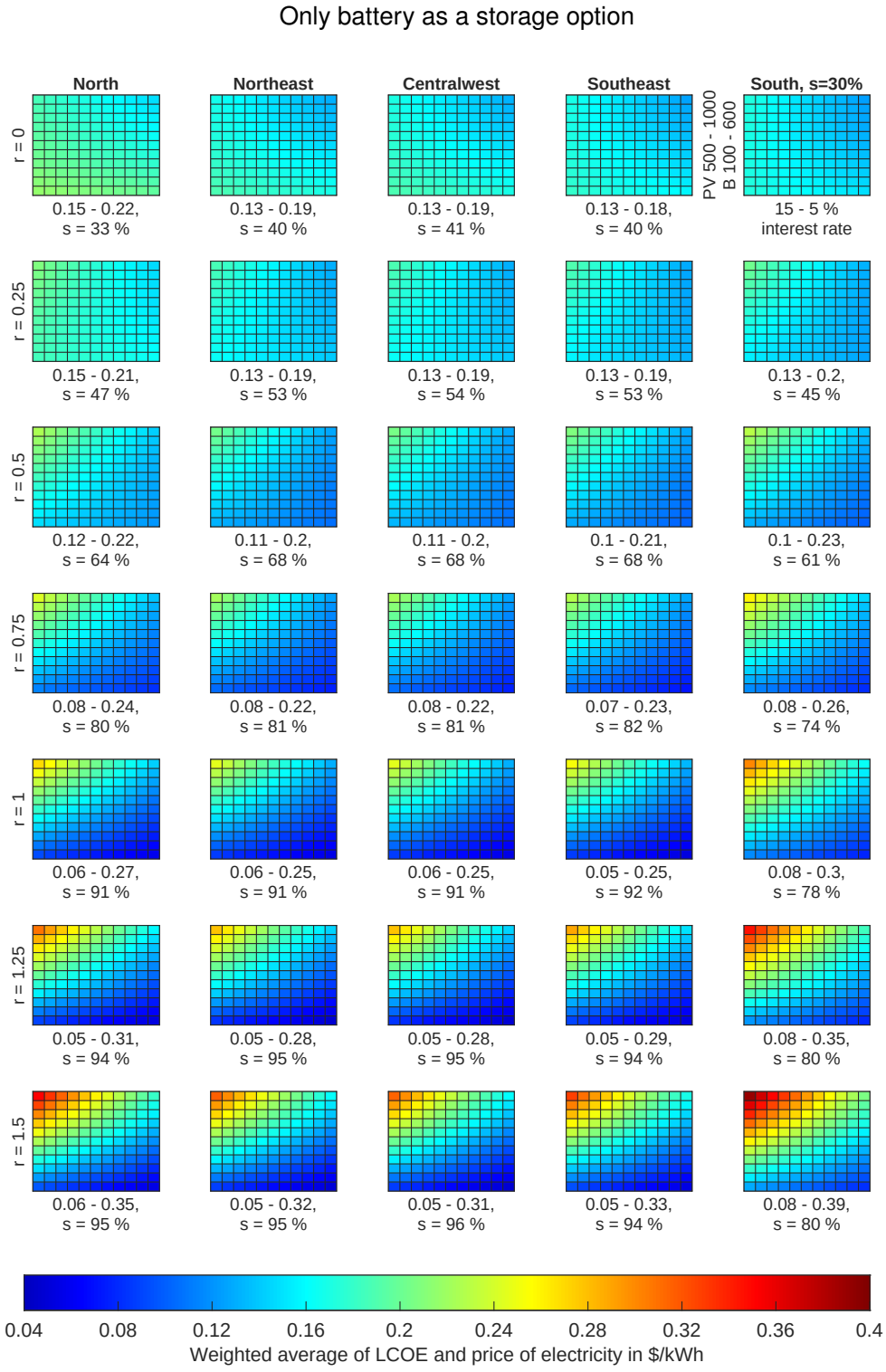

Figure 4.13: USD/kWh depending on interest rates and investment costs

Battery (B), hot water (H), and air conditioning (AC) as storage options, interest rate $i = 7$ %

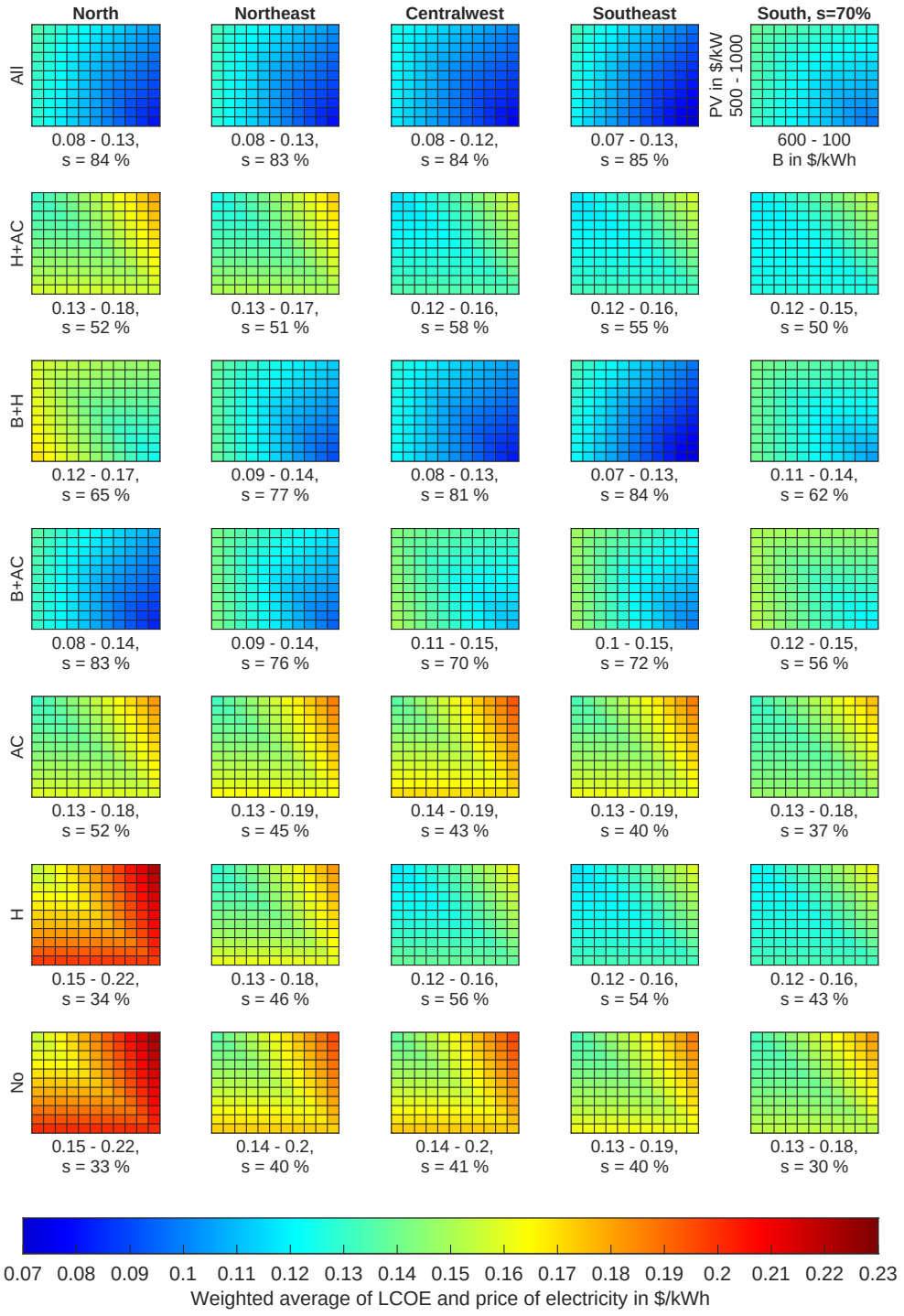

Figure 4.14: USD/kWh with thermal storage depending on prices for batteries and PV

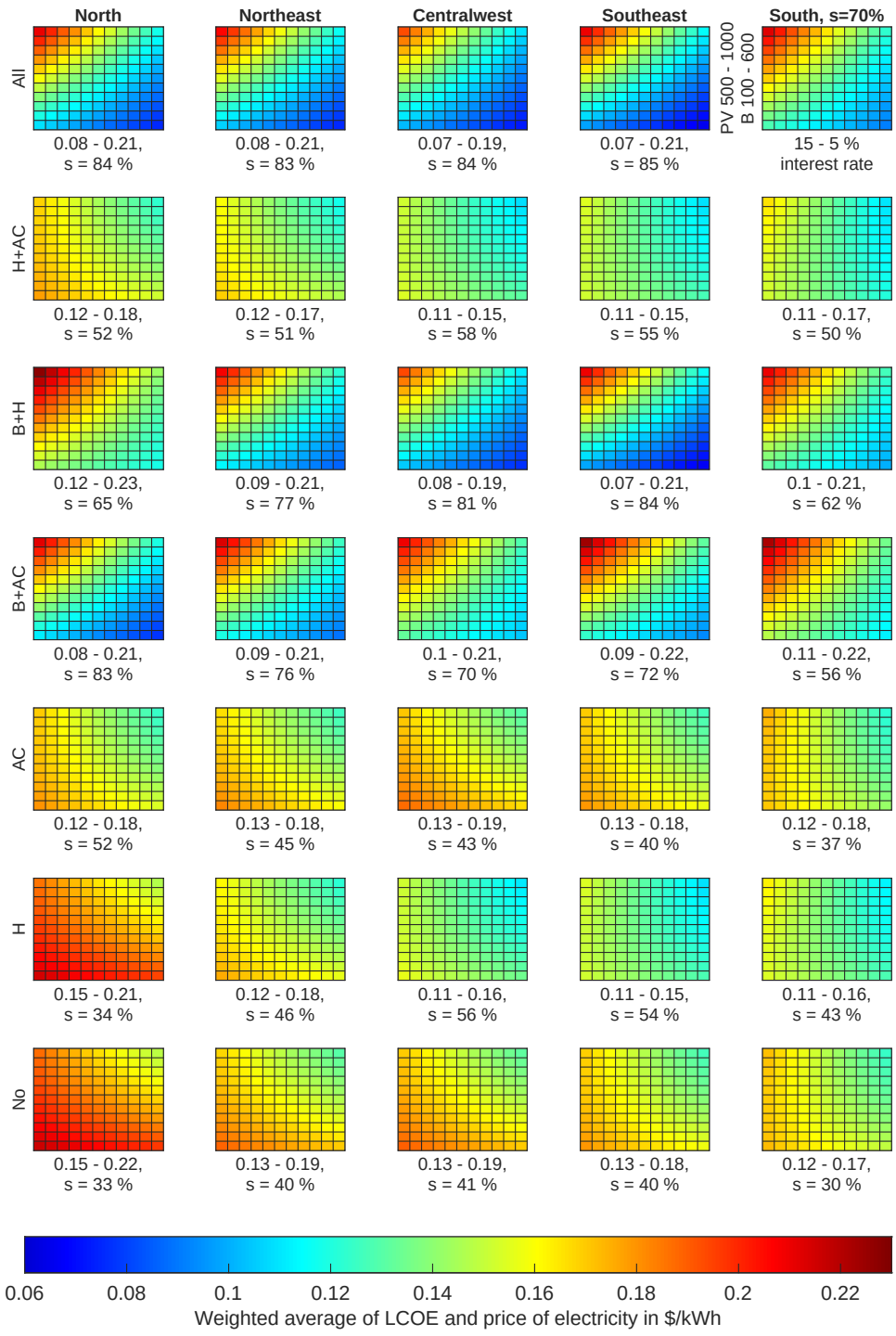

Figure 4.15: USD/kWh with thermal storage depending on interest rates and investment costs

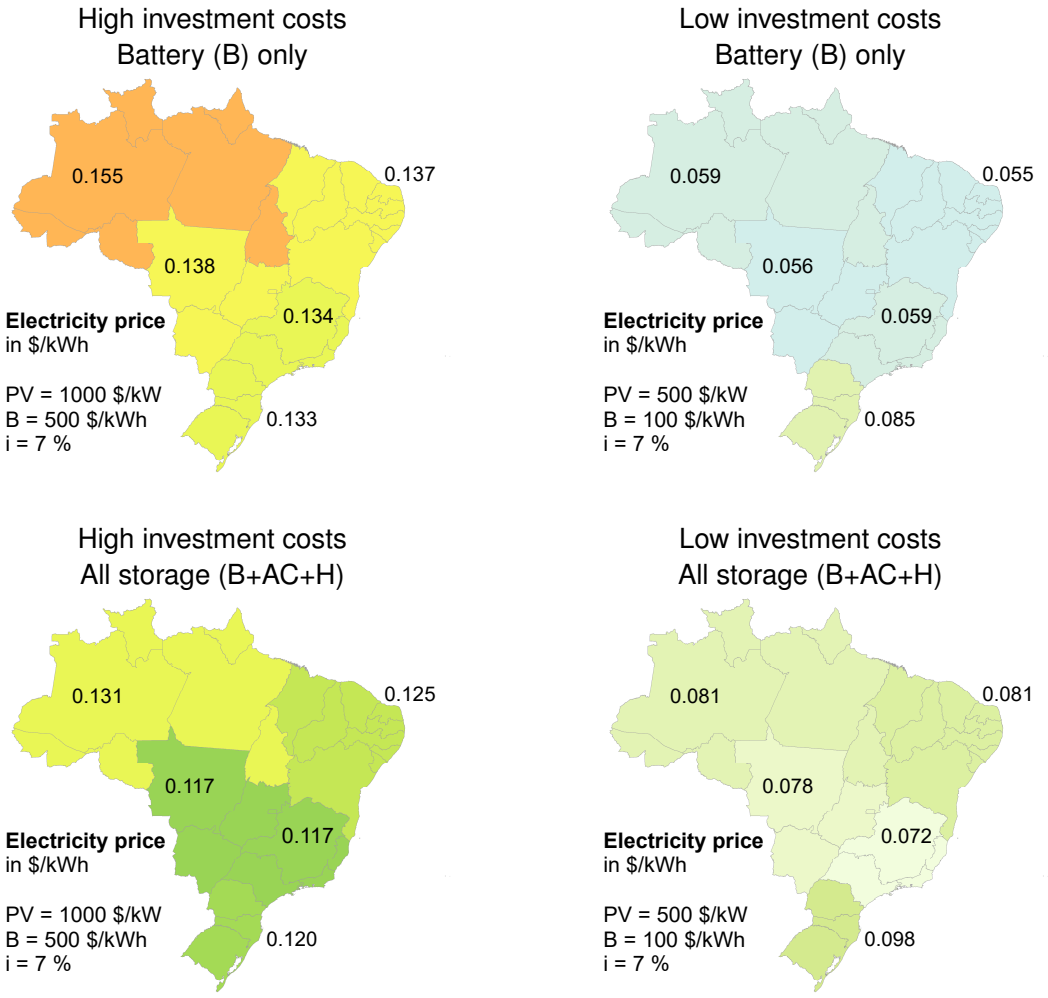

Figure 4.16: Electricity prices for residential customers without net metering

The figures 4.12 to 4.15 showed detailed results for electricity supply costs under the absence of net metering. Under consideration of net metering, the energy system with its large hydropower balances the supply of distributed generation and demand. It might be possible that net metering is abolished in the future. One reason can be that in growing distributed generation capacities, the flexibility needs might overpass the system capabilities. Assuming that net metering is not possible anymore, electricity feeds into the grid does not create any refund or right to retrieve electricity at another time. Therefore, the whole amount of electricity received from the grid needs to be paid, and high self-consumption rates unfold their commercial benefits. As described above, distributed integration with storage technologies on the consumer side allow high self-consumption rates. The maps in figure 4.16 above summarize the regional costs per kWh depending on the five macro-regions North, Northeast, Central-West, Southeast, and South. When comparing these values with the mean residential electricity tariffs by region, see table 4.3, it gives an estimation where distributed integration of photovoltaic would be economically favorable even without net metering. Assuming high investment costs, it is not attractive in the South and close to parity in the other regions. A more detailed analysis is needed for the South at low investment costs, whereas in all other

regions, distributed integration is likely an attractive business case even without net metering.

Under the presence of net metering, distributed integration is not relevant from an economic perspective. For maximum profit under net metering, optimal photovoltaic system dimensioning means producing each household's annual demand precisely. An annual overproduction would not be favorable since no feed-in tariffs exist. In the environment of net metering, the following maps show how attractive photovoltaic systems are for residential customers. The top map in figure A.14 displays the LCOE for each Brazilian state at specific investment costs for photovoltaics of 1,000 USD/kW and an interest rate of 9 %. Even under these conditions, LCOE is way lower in all states compared to the official electricity tariffs. Photovoltaic systems get even more favorable under net metering conditions when assuming specific investment costs of 500 USD/kW. In the Northeast, LCOE below 0.03 USD/kWh are possible in the upcoming years.

For decision-makers, the internal rate of return of an investment project acts as a relevant figure. The internal rate of return needs to be higher than the interest rate at a particular market to make an investment attractive. Under consideration of state-wise electricity tariffs of 2018 and average solar radiation, figure 4.18 displays the internal rates of return of distributed photovoltaic power for residential customers. The top map shows the internal rate of return at 1,500 USD/kW for investment in photovoltaics, and bottom map for 1,000 USD/kW. At specific costs of 1,500 USD/kW, the internal rate of return ranges from 6 % in the southern state of Santa Catarina up to 21 % in the Northeastern state of Piauí. At 1,000 USD/kWh, this interval goes from 12 to 33 %. One should not prematurely conclude economic attractiveness from these relatively high interest rates. Since the interest rates set by the Central Bank of Brazil act as a baseline for investments in real assets, the difference between both rates is an important criterion. The interest rates alternated from over 25 % in 2003 to less than 7 % in 2018, see figure 2.9. High interest rates on the capital market lower the profitability of the aforementioned investments in photovoltaic systems and constitute an additional risk. But even when assuming the highest interest rates of recent years, photovoltaic systems are economically attractive in many Brazilian regions. With continuing price erosion described by Haegel et al. in [99], this will be the case almost everywhere in the country.

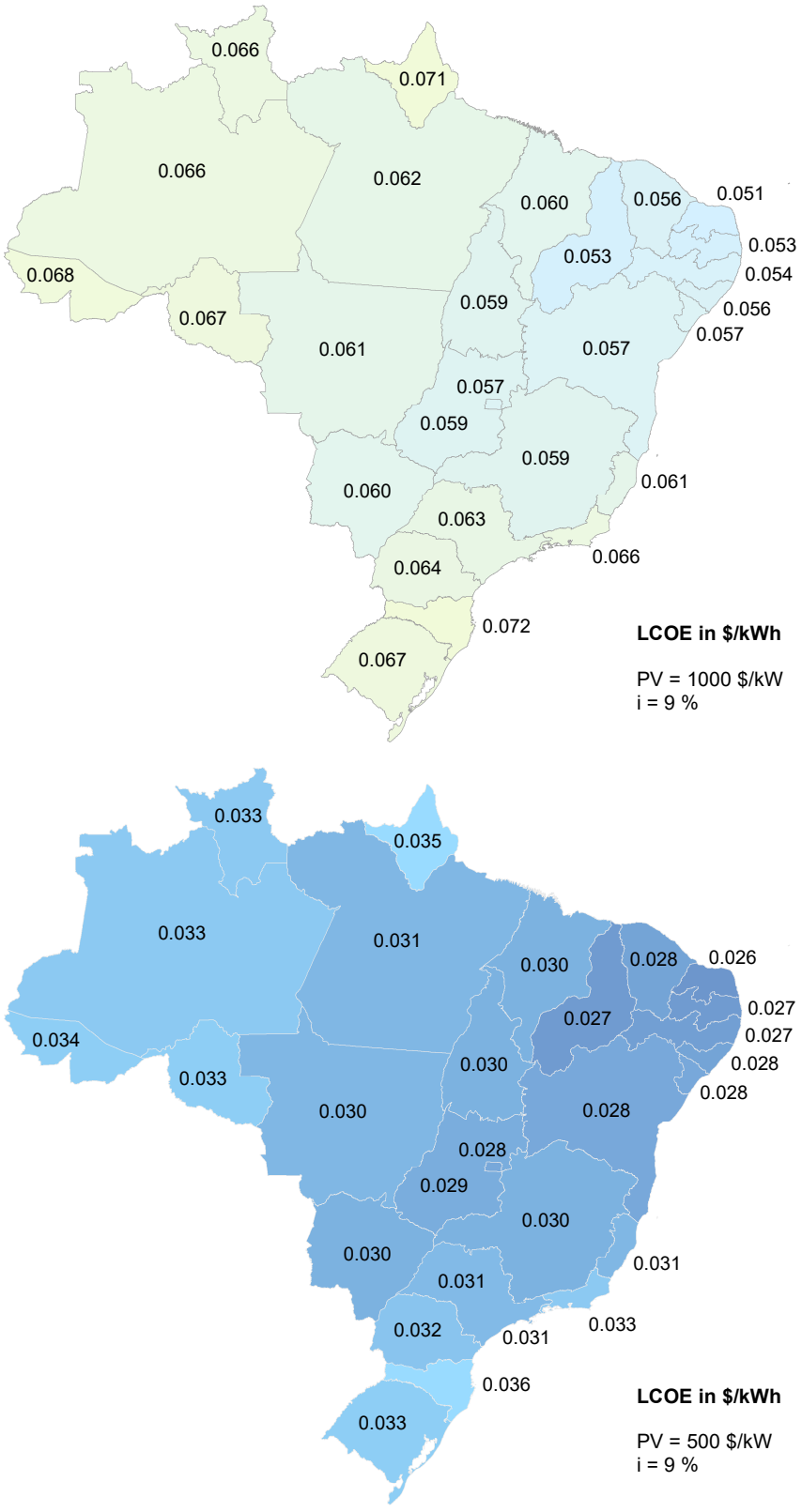

Figure 4.17: LCOE of PV systems using net metering

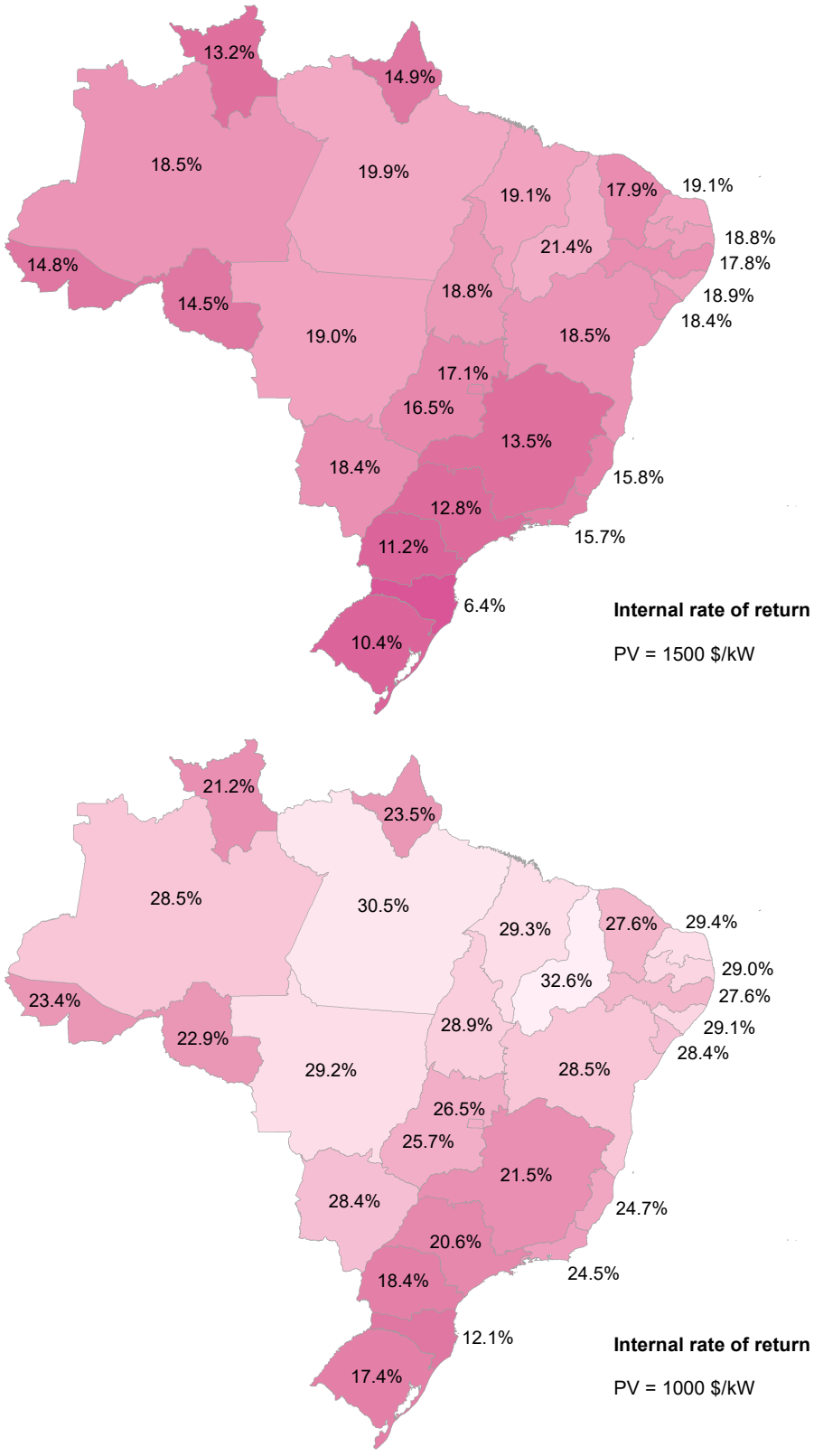

Figure 4.18: Internal rate of return of PV systems using net metering

4.6 Summary for distributed integration

This chapter provided a concept for the dimensioning and economic evaluation of distributed energy systems focusing on the residential sector based on time series. Ambient conditions, statistical possession and usage of specific devices determined the load profiles. As a result, the load profiles show plausible temporal, seasonal, and regional characteristics for each Brazilian macro-region.

The economic evaluation revealed that the existing net metering system makes distributed storage economically unattractive. Unlike that, distributed photovoltaic power will provide significantly cheaper electricity compared to regional electricity tariffs with ongoing price erosion for photovoltaic modules. It is worth mentioning that the photovoltaic systems do not need to be necessarily on the consumer side as shown in figure 3.7. As described in [69] it is also possible due to the framework to compensate generation and demand between several prosumer units. These conditions provide huge growth potential for solar power systems, which might lead to a discussion or even to the elimination of net metering. When assuming the elimination of net metering, distributed integration becomes economically relevant. For that reason, battery and thermal storage technologies on the consumer side were considered to increase the rate of self-consumption. The results revealed remarkable regional characteristics as well as paths to reduce needed battery capacities.

In the absence of net metering, economically reasonable storage application lead to self-consumption rates from 70 % in the South to more than 90 % in the North, Northeast, Central-West, and Southeast. Self-consumption rates above 50 % are possible in all regions when considering only thermal storage for hot water and air conditioning. Hot water storage is a very cost-effective and technologically simple solution compared to a battery, which helps furthermore to save the use of precious resources for use cases where batteries are difficult to be substituted, e.g., mobile applications. The relevance of flexible, renewable-powered air conditioning will increase when the market penetration continues as projected in [75].

Under the assumption of net metering, the Brazilian power system balances the supply and demand of photovoltaic generation. The following chapter 5 focuses on hydropower and its storage capacities, to which extent the system can integrate fluctuating power.

Chapter 5

Centralized integration

The main topic of this chapter is the centralized integration of intermittent renewable power. Centralized integration of intermittent power generation originating from wind and refers in the context of this work to two main possibilities: Flexibility operation of power stations and centralized energy storages. In contrast to the previous chapter addressing flexibility on the consumer side, this chapter focuses on the supply side of the energy system. Since the Brazilian energy system relies predominantly on hydropower generation, including enormous storage capacities provided by reservoir lakes, the assessment of hydropower is one important part of this chapter. Sources, approaches, and ideas are presented to derive the most important figures for assessing hydropower stations' storage capacity and flexibility. The most relevant source of information for several aspects of the Brazilian power system is the Operador Nacional do Sistema Elétrico abbreviated with ONS, the national Brazilian grid operator [17]. ONS provides, on the one hand, general information on the composition of the Brazilian power energy system and its development during the recent years, but also detailed information including time-series on operation, even partly countrywide in hourly resolution. In contrast to many other Brazilian statistics being published for the five macro-regions defined by IBGE, the system operator ONS structured Brazil into four regions: North, Northeast, and South correspond to the Brazilian macro-regions, whereas Southeast and Central-West are merged to one region.

The main goal of all investigations of this chapter is to gather sufficient knowledge about the Brazilian power system to draw a possible future development. Essential characteristics are an increased demand mainly for electricity as a forwarding projection of past trends. For the energy demand and supply since 1970, see chapter 3. The outlook is conducted by applying a linear optimization model considering selected possible development paths, see the model-based outlook in section 5.2 of this chapter.

The optimization model relies on a brought set of input data, such as technological and economic limitations and parameters and time series for the supply of hydropower, wind, and solar. Assumptions, calculations, and sources to gather the relevant information are presented below and supplemented by appendix A1 from section A and appendix A2, see A. Several publications addressed the question about integrating intermittent electricity production in the Brazilian energy systems.

Hunt and his co-authors propose seasonal-pumped-storage plants for a Brazilian electricity system, which relies on around 80 % on hydroelectricity in its energy mix. Since dams in

the Amazon region such as the Belo Monte provide an insignificant storage capacity due to their nature as run-of-the-river power plants, seasonal storage capacities are needed due to the authors to balance the unequal potential between the wet and the dry season. [110] Seasonal-pumped-storages should also increase the overall power production of existing cascades of hydropower plants since they can avoid spillage during the rain period. For that reason, the reservoir lakes of seasonal-pumped-storages need to be integrated into the proper position of the dam cascades, wherefore the authors provide a selection process in [111], and some potential locations in [112]. For a dam cascade in the Paraná river basin proposed by Hunt in [110] as a location for seasonal-pumped-storage, Machado analyzes in [113] how this type of storage technology can both reduce intermittence of wind power generation and increase hydropower efficiency. Unlike these investigations, the work here does not assume that hydropower will stay the majoritarian electricity producer in Brazil. When extrapolating trends in electricity consumption of the past decades to the future, significant growth in electricity demand is very likely. However, one may doubt that hydropower will cover the future increase in demand. As discussed in [114], the potentials for hydropower dams are almost exploited in populated regions, and the negative impacts of a further expansion of hydropower in the Amazon region will overweight its positive effects. In addition to that, a predominant share of hydropower will probably reduce the security of supply and make power production less predictable. Stickler argues in [115] that ongoing deforestation in the Amazon basin could considerably reduce evapotranspiration leading to dramatically lower precipitation even in distant regions and consequently to a lower power output of hydroelectric plants. As severe droughts appear more frequent in the context of climate change, Melo discusses in [59] their hydrological impact on the important Paraná river basin. A higher diversified generation portfolio could meet the discussed challenges.

Several publications consider photovoltaic power generation to be an appropriate supplement of hydropower in Brazil. Following the argumentation of Schmidt in [116], the solar potentials are not as concentrated available across the country as, for example, wind and hydropower. With a view on the map for solar radiation by state, the nature-given potentials make use of photovoltaics attractive almost everywhere, see figure A in the appendix. At a total domestic demand up to 800 TWh, the optimization model applied by Schmidt delivers under the made assumption a share of 50 % for hydropower, 37 % for photovoltaic and 9 % for wind power to be optimal. Not mentioning distinct numbers, storages are necessary to shift generation within 24 hours, for example, from day to night. The work of Barbosa [117] delivers up to 270 GW of installed photovoltaic power at a total electricity generation of around 1,100 TWh. In comparison to that, the installed hydropower capacity is in the investigated scenarios close to 100 GW. Wind power plays with less than 17 GW in her scenarios a subordinate role. Additional to the existing reservoirs' storage capacity, around 240 GWh of batteries are needed and electrolyzers and compressors for hydrogen or compressed air storage, respectively. Barbosa used for her publication a linear optimization model, which is comparable to the one used in this work for the model-based outlook. In contrast to recent publications, the model-based scenario analysis here investigates more the regional differences of Brazil, the system composition by power source, storage needs, and transmission capacity under different conditions, and an estimation of land requirements for selected scenarios.

The sections of this chapter before the model-based outlook contain sources, references, and

approaches to gather input data and justification of assumptions. Some of them are used for the outlook, and others are rejected due to their limitations.

5.1 Determinants of power supply

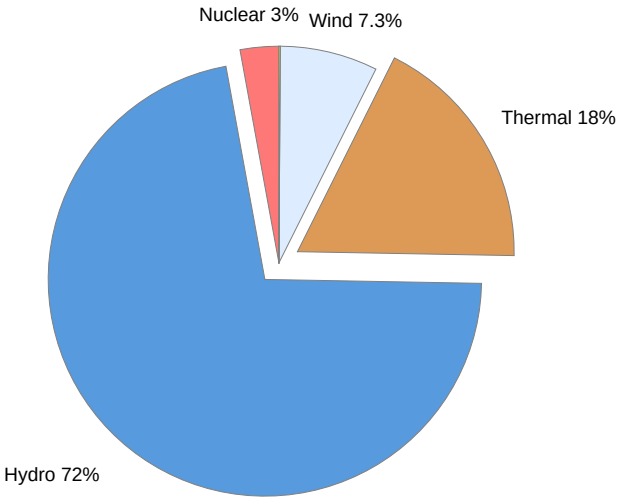

Figure 5.1: Power generation of 546.8 TWh in 2017 by source

The Brazilian National Grid Operator ONS provided the data displayed in table 5.1.[1] The table shows the real composition of power generation capacity in December 2017 and the officially planned expansion for the years 2021 and 2025. All shown numbers display the state of December of each year.
According to these numbers, the total share of hydropower will decrease until 2025 to approximately 60 % from 68 %, thermal power remain almost in its position, whereas wind and solar power outline the highest growth rates, but on a low level. The total generation capacity is planned to grow from 155 GW in 2017 to 180 GW in 2025.
Corresponding to the generation capacity listed in table 5.1 for 2017, the piechart in figure 5.1 displays the power generation by source summing up to 548.8 TWh. Hydropower was with 72 % by far the most relevant contributor, followed by thermal power with 18 %. Thermal power summarizes all power stations relying on fuel, whether fossil, biomass, or residuals. For details, see 5.1.4. The share of wind power production was at around 7 % in 2017, whereas the only two Brazilian nuclear reactors in Rio de Janeiro state accounted for 3 %. Photovoltaic power generation was significantly under 1 % and is therefore not detectable in the chart. The color scheme for the different sources is used throughout this work.

5.1.1 Hydropower

The basic idea for the application of hydropower in the following outlook is not the operation as pumped hydroelectric energy storage as proposed in [110–113], but to provide flexibility

[1] The historical data were retrieved in early 2021 from http://www.ons.org.br/paginas/resultados-da-operacao/historico-da-operacao

Table 5.1: Installed and officially planned expansion of power generation capacity

	2017		2021		2025	
	GW	%	GW	%	GW	%
Hydropower	105.1	67.9	108.6	64.0	109.3	60.4
Thermal	34.4	22.2	37.2	21.9	42.0	23.2
Nuclear	2.0	1.3	2.0	1.2	2.0	1.1
Wind	12.3	8.0	18.2	10.7	22.5	12.4
Solar	0.9	0.6	3.7	2.2	5.3	2.9
Total	154.7	100.0	169.7	100.0	181.1	100.0

in a power system with wind and solar power as dominating sources. One can describe the operation mode simplified with the following distinction of cases:

- **Case 1:** Wind and photovoltaic power generation lower than demand $\rightarrow$ turbines consume water from the reservoirs
- **Case 2:** Wind and photovoltaic power generation greater than or equal to demand $\rightarrow$ water turbines (almost) stop, natural inflow increases reservoir level

In the first case, hydropower has to fill the gap between the demand and the meteorological given supply of wind and photovoltaics and possible contributions from thermal power. Whether the reservoir level h_{nom} lowers depends mainly on the relation between natural inflow $\dot{V}_{\mathrm{in}}$ and the technical outflow $\dot{V}_{\mathrm{out}}$, see figure 5.2. A surplus in power production is possible for the second case, which hydropower cannot tackle since pumped-storages are not considered. Curtailment of wind turbines or solar farms can avoid a surplus or excess electricity is stored, for example, in batteries or other storage technologies on the demand-side as described in the previous chapter. In which extend batteries are necessary for the system is one outcome of the model-based outlook. For further investigations, the most relevant characteristics of hydroelectricity need to be determined quantitatively. The following paragraphs provide references and approaches to assess natural inflow, evaporation losses, and storage capacity. Figure 5.2 contains the physical quantities to calculate the storage capacity of a single reservoir based on the potential energy of the water stored according to [118]. The reservoir with the volume V is fed by the natural inflow $\dot{V}_{\mathrm{in}}$. The outflow $\dot{V}_{\mathrm{out}}$ rushes from the reservoir through the turbine, which is attached to a generator to produce electrical power P_{el}. For a single hydroelectric power plant, the power production P_{el} is calculated with the following equation, wherein η denotes the total efficiency of the plant, ρ the density of water, g the gravity of Earth, and h_{eff} the effective head.

$$P_{\mathrm{el}} = \eta \cdot \rho \cdot \dot{V}_{\mathrm{out}} \cdot g \cdot h_{\mathrm{eff}} \tag{5.1}$$

When using this physical description, the stored energy W_{el} of a hydropower plant is determined by the equation 5.2

$$W_{\mathrm{el}} = \eta \cdot \rho \cdot \Delta V \cdot g \cdot h_{\mathrm{eff}} \tag{5.2}$$

The appendix 5.1.1 contains an assessment of the storage capacity by using the physical description above considering stand-alone reservoirs. Brazil's reservoirs' total storage capacity is, according to ONS data at 211 TWh, significantly higher than the numbers estimated in the appendix. Reasons for that are likely the incompleteness of the used data set, the too conservative assumptions, and ignoring the fact, that the reservoirs are connected to large cascades within one drainage basin. Paragraph 5.1.1 shows the reservoir storage capacities used for the model-based outlook, including their regional distribution.

One can derive the outflow of a drainage basin mainly from the local amount of rain and

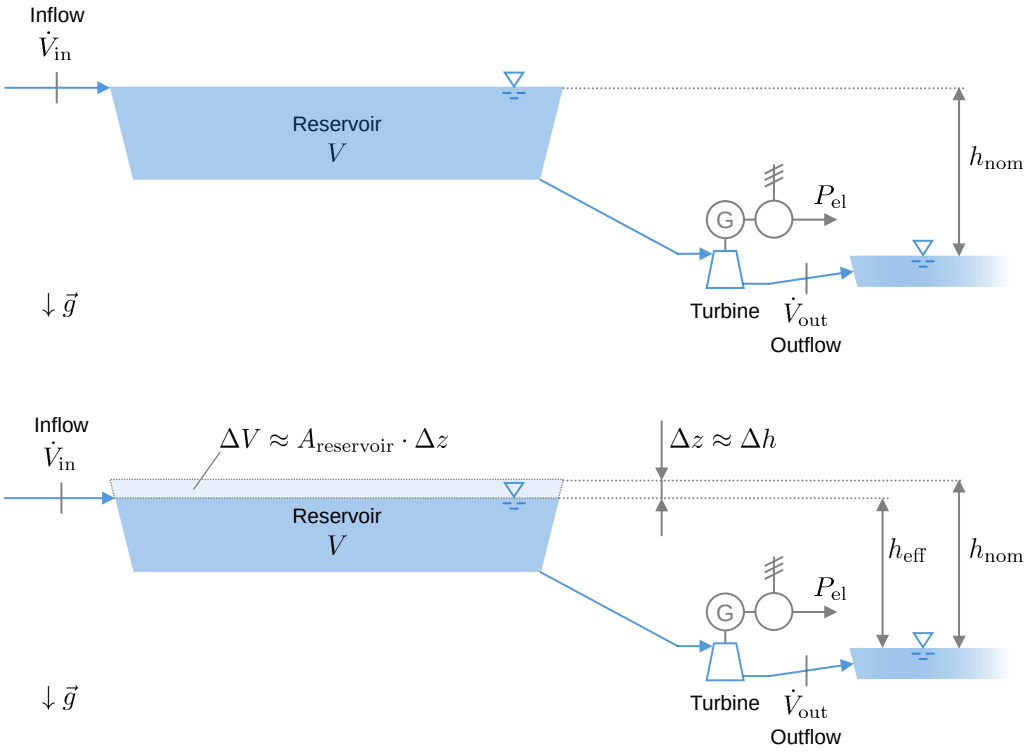

Figure 5.2: Full and partly discharged reservoir

some other meteorological and hydrological characteristics. That is the main idea of the paragraph below, with the help of a model designed to reproduce the hydrological behavior of a drainage basin. The sketch in figure 5.3 is the basis for the considerations in paragraph 5.1.1 to calculate the inflow $\dot{V}_{\mathrm{in}}$ to a reservoir lake. As argued below, this approach is not used for later considerations since it did not deliver reliable results for every case, is relatively complex to apply, and its high spatial resolution is unnecessary for the investigations conducted here.

Calculation of inflow

The water flow of a river naturally feeds a hydropower reservoir. However, the inflow depends mainly on inflow from an upper reservoir or drainage basin, precipitation, evaporation, and other gains and losses from human activities. Knowing the inflow is necessary to quantify the electricity generation potential of dams. Therefore, two approaches are presented below.

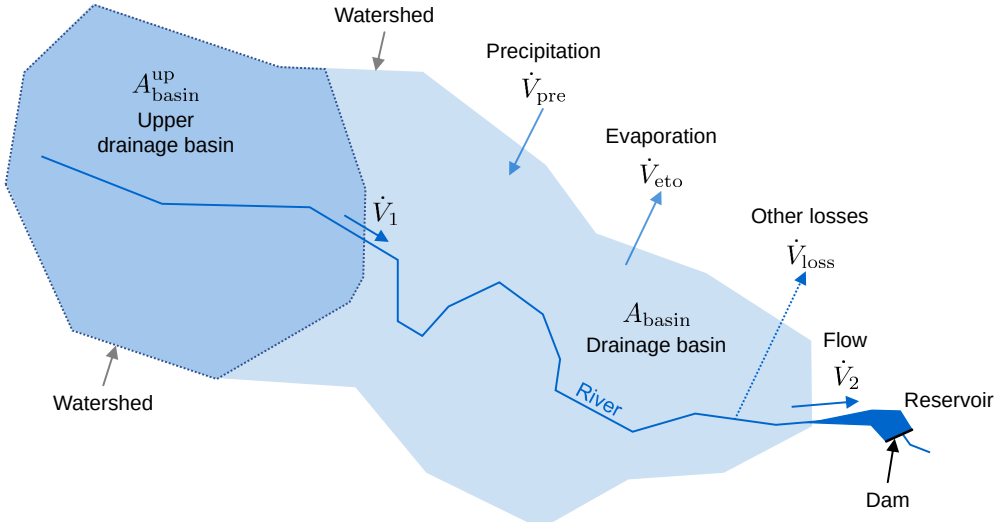

Figure 5.3: From precipitation to reservoir inflow

Rejected approach: State-space model

Inspired by the approach of Crawford and Thurin [119] on hydrological estimates for small hydroelectric power plants, one can derive the outflow of a drainage basin from a model of three coupled water storage as illustrated in the sketch below: moisture storage (1), a groundwater storage (2) and the surface water (3) as third storage. Since for a certain drainage basin the precipitation, the inflow, the outflow, and the meteorological data defining the evaporation are known, a so-called state-space model can be applied to identify the dynamic behavior of a real hydrological system. The state-space representation has been used for example in [120] to identify and to predict the thermal inertia of building components. For the case of a hydrological system, the model represents a system of coupled mass balances for water. The existence of three different types of water storage in this model causes different degrees of delay between the inputs (inflow from an upper part of a river, precipitation, evaporation) and the outflow of a certain drainage basin. The discharge of the drainage basin is the flow that feeds the power station's reservoir. This approach shall deliver the time series for total discharge.

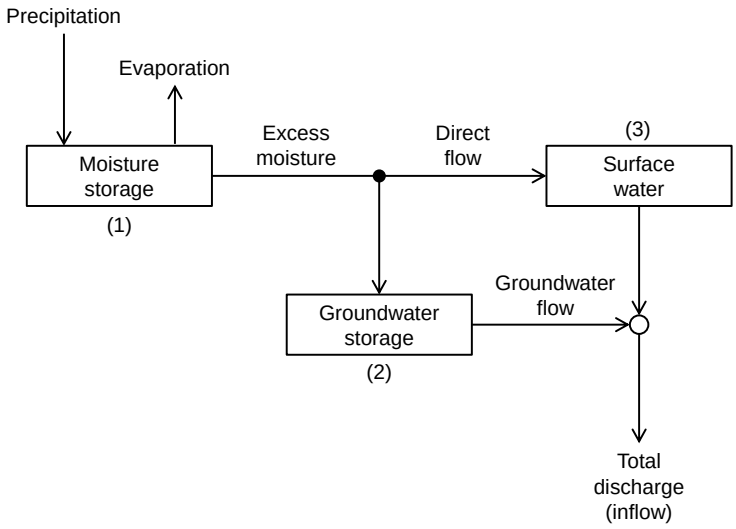

Figure 5.4: Concept to derive inflow from precipitation by Crawford and Thurin

The block diagram in figure 5.5 depicts the basic composition of a state-space model. The general mathematical notation is the following:

$$\dot{x} = \mathbf{A} \cdot x + \mathbf{B} \cdot u \tag{5.3}$$

$$y = \mathbf{B} \cdot x + \mathbf{D} \cdot u \tag{5.4}$$

The vector x represents the states of a system. Concerning the hydrological behavior of a drainage basin, the state is quantified by the water content of the three above-mentioned different kinds of storage, moisture and groundwater storage, and surface water. The input signals of the system are summarized in the input vector u. In this case, the input signals consist of time series for inflow from the upper river sections, rain and, evaporation. The only output time series is the discharge of the considered area, which feeds the reservoir. Therefore, the output vector y is a one-dimensional time series. The interactions between the types of storage, the inputs and outputs are the parameter matrices **A**, **B**, **C** and **D**. The components of these matrices represent physical parameters like the soil's storage capacity and permeability for water, flow resistance, vegetation affecting evaporation, etc. The values of these parameters are estimated in a system identification process conducted via MATLAB [121]. The number of assumed coupled storage, the dimensions of the time series for inputs and outputs define the dimension of the state-space model, see table 5.2.

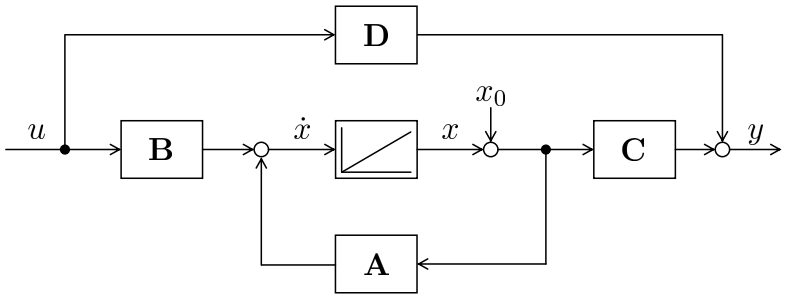

Figure 5.5: Block diagram for a state-space model for reservoir inflow calculation

Table 5.2: Components of a state-space model for description of hydrological behavior

Component	Description
$\boldsymbol{A}(3 \times 3)$	system matrix
$\boldsymbol{B}(3 \times 2)$	input matrix
$\boldsymbol{C}(1 \times 3)$	output matrix
$\boldsymbol{D}(1 \times 2)$	feedthrough matrix
$u(365 \times 2)$	input vector for precipitation, evaporation
$y(365 \times 1)$	output vector for discharge (inflow to reservoir)
$\dot{x}(3 \times 1)$	derivative of state vector
$x(3 \times 1)$	state vector, e.g. water content
$x_0(3 \times 1)$	initial values

The approach to derive the reservoirs inflow by using a state-space shows several advantages, such as a good accuracy for discharge calculation for selected sites and the overall possibility to predict the reservoir feed flow based on meteorological data. An example for good estimation is depicted in figure A.15. The approach was tested for 10 further specific locations in total, see table A.8 in the appendix. It could be transferred to many other areas with sufficient availability of time series for inflow, outflow, and corresponding meteorological data. The necessity for time series in relatively high temporal resolution depending on each location makes this approach relatively hard to apply. Identified hydrological behaviors also cannot be transferred to many other sites, most likely because of characteristics related to soil and vegetation differ too much from one drainage basin to another. During this investigation also cases showed up, where a prediction of the outflow seemed to be not predictable at all. One possible explanation for the unpredictability of the discharge of a drainage basin can be seen in poor quality of input data or not covered water flows mainly of technical origin. One might think about water extraction for irrigation needs or for supply of municipalities or inflow from ground and waste water. This is likely the case for a river section of Rio Uruguai located close to the border to Argentina in the state Santa Catarina in the South of Brazil. The sharp gradients of the volume flow probably come from uncovered technical flows, see penultimate diagram in figure A.17 in the appendix. The model output does not follow at all the real volume flow, see bottom chart in figure A.17. The high effort for gathering data in both temporal and spatial resolution, the partly inaccuracies for discharge calculation lead the rejection of this approach in the proceeding of this work. Most importantly, the high spatial resolution of inflow is not necessary in the following investigation, since reservoir inflow, level of reservoirs, and hydropower generation are considered aggregated for the above mentioned regions structured by ONS, see first paragraph in chapter 5.

Inflow calculation from ONS-data

For the model-based outlook towards the future Brazilian electricity system conducted in section 5.2 input data is only necessary in region-wise resolution, the aggregated data for regions provided by the National Brazilian grid operator ONS is used for further investigations. The database of ONS does not contain the inflow profiles for the reservoir lakes directly, but the amount energy produced by hydropower for each day is available as well as the energy

content of all reservoirs. The reservoirs energy content is available aggregated for the four ONS regions North, Northeast, and South and for Southeast and Central-West as one region. Since the below used optimization model uses also the same four macro-regions, this spatial resolution for inflow and storage content is sufficient. The aggregated inflow per day and for each region is calculated following the equation below, in which all units are an amount of energy, e.g. GWh.

$$\text{inflow}(\text{day}) = \text{content}(\text{day}+1) + \text{generation}(\text{day}) - \text{content}(\text{day}) \tag{5.5}$$

A higher temporal resolution than daily is necessary, because one purpose of the optimization model applied in section 5.2 is the investigation of the interaction between intermittent renewable energies. In case of a daily resolution, differences between day and night cannot be revealed, for example, the impact of high power generation peaks caused by photovoltaics. Therefore, an hourly resolution was chosen for the optimization model. The daily inflow profile consisting of 365 values for each of the four regions is therefore expanded via linear interpolation into hourly creating four time series vectors with 8760 elements each. Missing: Reference to inflow time series or the diagram itself.

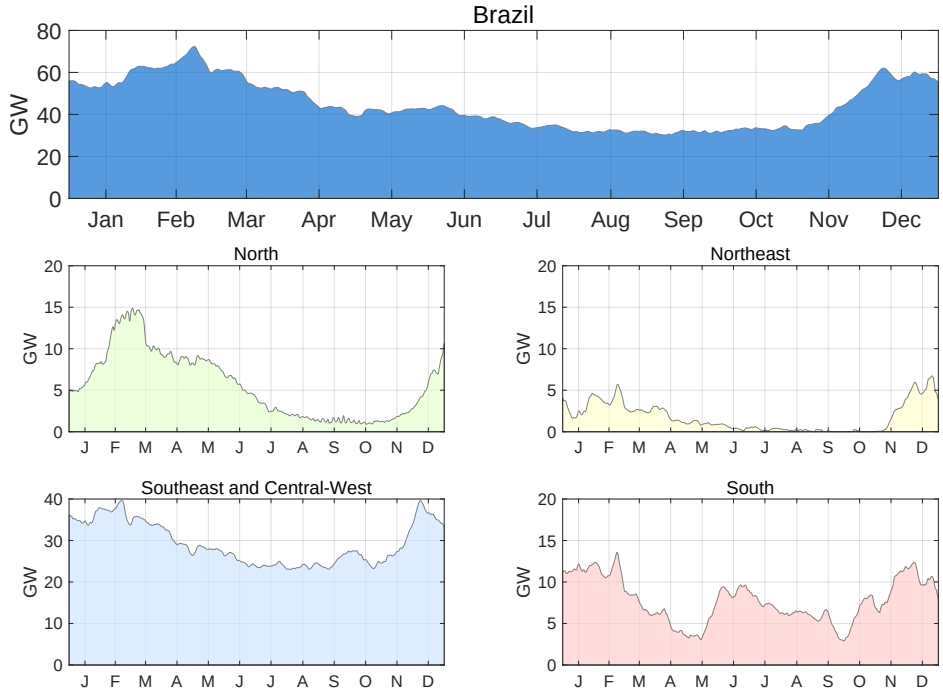

Figure 5.6: Hydropower inflow per region (2017) in GW per hour

Estimation of evaporation losses

Due to the importance of hydropower in the Brazilian electricity system, possible losses of hydropower potential need to be assessed. For the sake of simplicity, losses caused by technical water extraction are not considered here. Moreover, one could assume that technical water extraction from rivers is compensated to a large extent by the inflow of wastewater discharge in the same area. In contrast to that, losses caused by evaporation need to be taken

into account, since these losses are not necessarily compensated by rain in the same drainage basin and may have a relevant magnitude especially in dry regions and seasons. The topic of evaporation from artificial lakes and reservoirs was also addressed in a report by the FAO, the Food and Agriculture Organization of the United Nations [122]. The estimation provides global estimations for the annual evaporation volume as well as helpful estimated equations to gather missing figures to characterize reservoirs. These equations were derived from the Global Reservoir and Dam Database (GRanD)[2]. For the evaporation loss calculation presented below, the three most important sources were the meteorological data set from INMET [16], detailed information about Brazilian hydropower stations retrieved from ANEEL [123], and the calculation method for Penman-Monteith evaporation (FAO-56 Method) described in [124]. The appendix provides further details about the used sources on weather data, see A, and for the hydropower system, see 5.1.1.
For each Brazilian state, average evaporation losses in millimeter per day were calculated considering the quantities mentioned in figure 5.7, namely solar radiation $\dot{q}''_{solar}$, wind speed v_{w}, relative humidity φ, ambient temperature t_{A}, and total atmospheric pressure p. The average

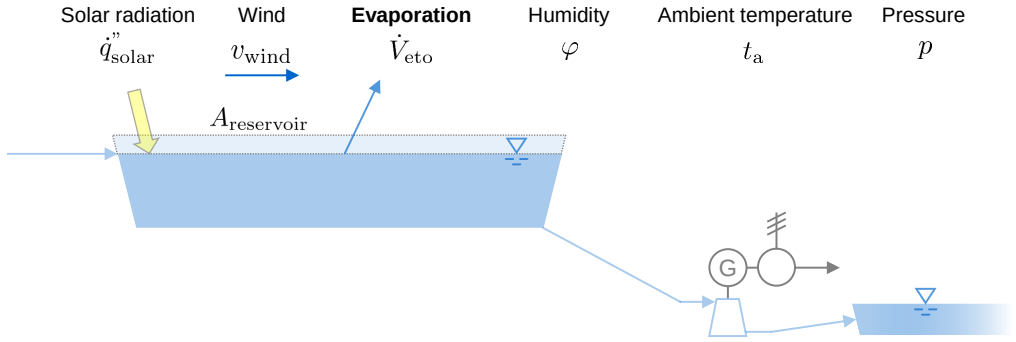

Figure 5.7: Full and partly discharged reservoir

evaporation loss over all states is around 5 mm/d, which can be considered as a reduction of level of the reservoir. During dry, sunny and windy days, maximum values in level loss up to 10 millimeters are reached following the mentioned approach. Expressed in annual losses, highest levels are reached in the states of Pernambuco and Rio Grande do Norte with around 2500 mm/a and the lowest losses in Santa Catarina with approximately 1500 mm/a. The unweighted average for the 27 federal states is at 2000 mm/a. Other investigations for loss of water of hydropower reservoirs deliver for the case of Norway around 450 mm/a, for Ethiopia around 1600 mm/a and 1700 mm/a for Central India, see [125]. The data set described in consists of 489 data sets for hydropower stations, which have an installed capacity of 105 GW in total. For 125 out these 489 hydropower stations, all relevant data is known to apply the equations below. These 125 sites together account for 70 GW installed capacity out of 105 GW. For area $A_{\mathrm{reservoir}}$ the value given for the maximum level of each site is used while being conscious of the fact, that the full level is only rarely or never reached during the year. Thus, the lost flow $\dot{V}_{\mathrm{eto}}$ due to evaporation is overestimated compared to reality. For the factor eto the value

[2]Global Reservoir and Dam Database (GRanD) http://globaldamwatch.org

specific for each federal state is used where the particular hydropower station is located.

$$\dot{V}_{\mathrm{eto}}\ [\mathrm{m^3/s}] = A_{\mathrm{reservoir}}\ [\mathrm{km^2}] \cdot \mathrm{eto}\ [\mathrm{mm/a}] \cdot \frac{1}{8760} \cdot \frac{1}{3.6} \tag{5.6}$$

$$P_{\mathrm{loss}}\ [\mathrm{kW}] = \dot{V}_{\mathrm{eto}}\ [\mathrm{m^3/s}] \cdot \rho\ [\mathrm{kg/m^3}] \cdot g\ [\mathrm{m/s^2}] \cdot h_{\mathrm{nom}}\ [\mathrm{m}] \tag{5.7}$$

The loss of power P_{loss} results finally from the potential energy from the evaporated water $\dot{V}_{\mathrm{eto}}$, where ρ stands for the density of water, g for the gravity of the earth, and h_{nom} for the nominal gross head. Since the effective head h_{eff} the water flows from the reservoir through the turbine to the river, see figure 5.2, calculating with h_{nom} leads to one further overestimation. This calculation methodology applied for 125 hydropower stations considering their spatial distribution results in an average loss of power during the year of around $P_{\mathrm{loss}} = 700$ MW, meaning approximately 1 % of 70 GW. A loss of around 1 % of hydropower caused by evaporation can be kept in mind for the discussion below of the model-based outlook, see section 5.2. This share is also relevant when estimating a self-discharge rate, which reduces the capacity of hydropower storage. The following paragraph is about the storage capacity of all reservoirs and their regional distribution, anticipating the aggregation in table 5.3. [17]

Table 5.3: Aggregated storage capacities by region

Region	TWh	%
North	11.1	5.2
Northeast	38.4	18.2
Southeast and Central-West	147.0	69.7
South	14.5	6.9
Total	211	100.0

Distribution of hydropower

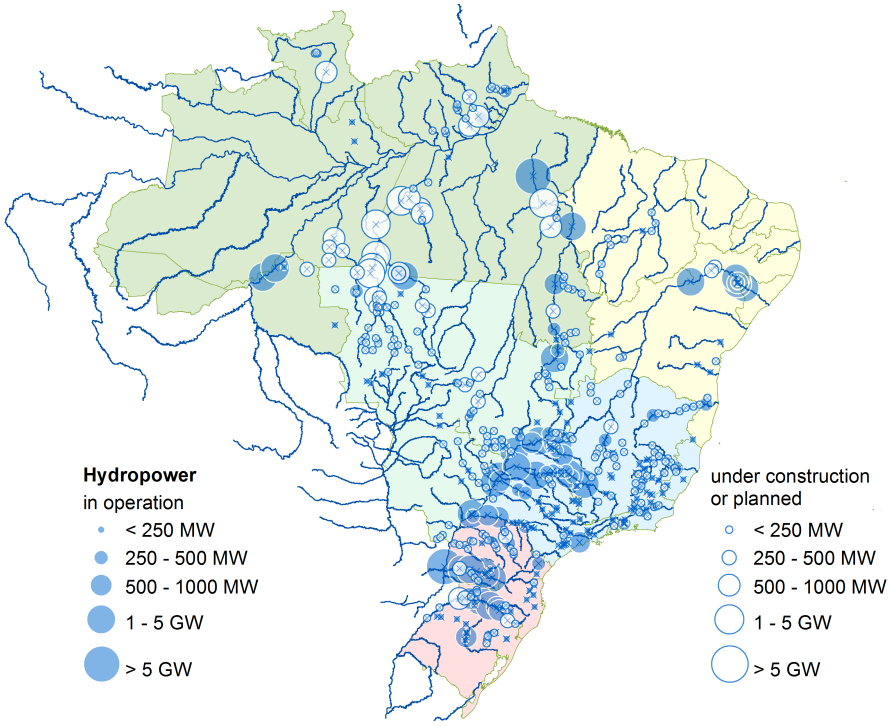

Figure 5.8: Distribution of hydropower generation capacity

The main source for the data on hydropower in Brazil, including characteristics of the reservoirs, is the system for georeferenced information called *(Sistema de Informações Georreferenciadas do Setor Elétrico)*, abbreviated with SIGEL, which is provided by ANEEL [123]. A database containing 489 data sets was the foundation for a detailed analysis, which is presented in the appendix, see 5.1.1. Each data set describes a hydropower plant. This analysis also includes an estimation of missing values for the rivers' drainage basins. The knowledge of the drainage basins acts as a basis for the outflow estimation proposed in the paragraph above. Like the approach to estimating the reservoirs' inflow with a state-space model, the results gathered from the detailed analysis of the reservoirs were not used in the model-based outlook. The storage capacities are underestimated when calculating them from the given database, see figure A.11 in the appendix in comparison to table 5.3. Furthermore, the high degree of spatial resolution is unnecessary for the consideration below.
Figure 5.8 shows the distribution of hydropower plants. Most of the sites, which are under construction or planned, are located in the Amazon Basin. As Hunt pointed out in [110], the Northern dams are predominantly designed as run-off-the-river plants to mitigate the impact on the Amazon rain forest. Therefore, the additional construction of hydropower capacity does not lead in the same way to new storage capacities. For the below conducted model-based outlook, the aggregated storage capacities by region listed in table 5.3 used. The national grid operator ONS provided these data and the time series for storage operation during the year. Latter are displayed in figure A.18 in the appendix.

5.1.2 Wind

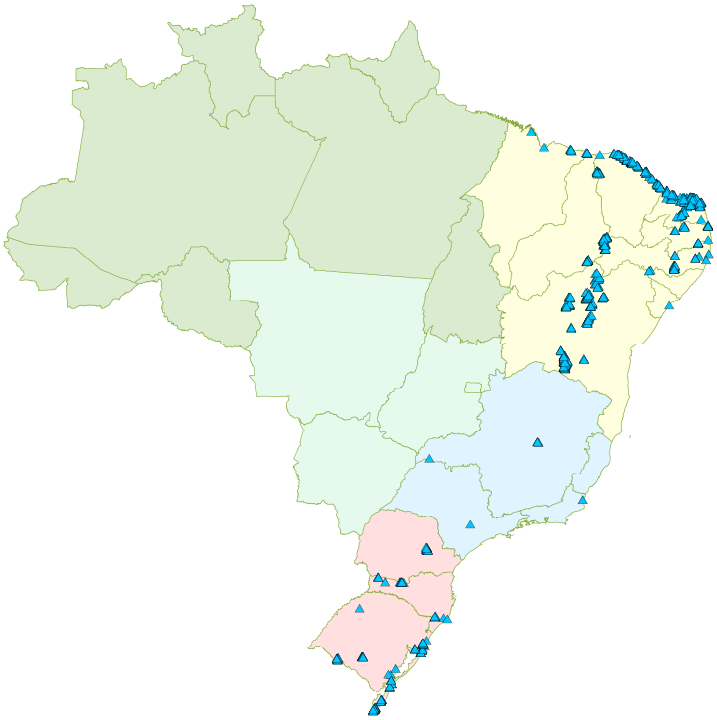

Figure 5.9: Distribution of wind power generation capacity in December 2017

By the end of 2017 slightly more than 12 GW of wind power generation capacity were installed in Brazil. The Northeast contributed with approximately 10 GW the vast majority. Another 2 GW of wind turbines were located in the South Region. Good locations for wind farms are situated mostly in coastal regions and exposed, elevated terrains of the Northeast and South. With more than 2,500 full load hours many sites there are very attractive for onshore wind power lying often in sparsely populated regions. In contrast to that, with less than 1,000 full load hours at almost all locations, the Brazilians North covering the Amazon basin is relatively unattractive for wind power with no installed capacity reported until 2017. The potential for wind energy in Central-West is also quite low with only a few locations over 1000 full load hours. Unlike the North and the Central-West, the densely populated Southeast offers several good locations above 1600 full load hours per year in hilly terrain and close to the cost, but also in proximity to possible customers. The full load hours presented in this section were calculated based on the wind speed in hourly resolution contained in the INMET data [16]. How to derive wind power generation and full load hours from given measured wind time series is described around figure A.1 in the appendix. Due to the planning of ONS installed wind capacity will grow over 22 GW until 2025, see table 5.1. The overall potential for wind energy was assessed in the Brazilian Atlas in 2001 to more than 140 GW considering wind speed in 50 meters above ground and rotor diameters between 40 and 80 meters. The technical potential to be harvested with recent wind turbines is surely significantly higher, since wind turbines grew continuously in height and diameters in the past years with this trend likely to proceed, see [126].

5.1.3 Solar

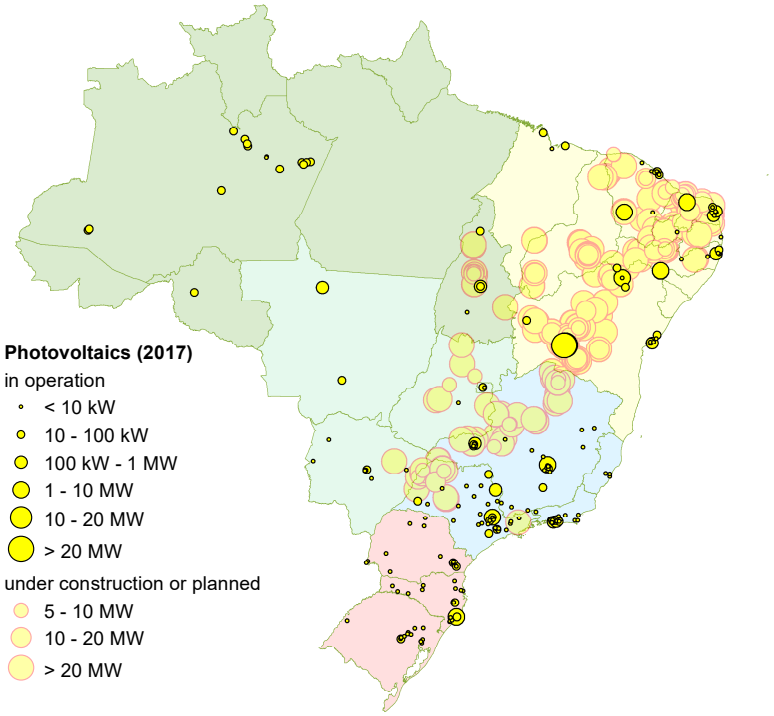

Figure 5.10: Distribution of photovoltaic power generation capacity

The distribution of existing and planned installations depicted in figure 5.10 of photovoltaic power correlates visibly with the spatial differences of solar radiation. The state-wise average annual sum of global horizontal irradiance was calculated from the the INMET time series and is displayed in figure A in the appendix. The values range from around 1,500 kWh square meter and year in the very South and 1,600 kWh/m²a the North over 1,800 kWh/m²a in the Central-West and Southeast to more than 2,000 kWh/m²a in some near-equator states of the Northeast. Approximately 1 GW of photovoltaics were installed by the end of 2017 with more than 70 % in the Northeast. More than 3 GW were installed in early 2021 and the capacity is officially expected to grow to around 5 GW countrywide by 2025. Expressed in relation to the Brazilian population around 20 Watt of photovoltaic per capita were installed by 2021 in comparison to Germany with around 600 Watt per capita in 2019. [127] In Germany, the annual sum of global radiation in 2020 was between 1,000 and 1,300 kWh/m². [128] In the light of these figures and increasing economic attractiveness resulting from an ongoing price erosion for photovoltaic modules [99] under 250 USD/kW with its impact on LCOE, the officially expected expansion due to table 5.1 seems to be very conservative. Assuming 600 Watt installed PV per capita in Brazil would result in more than 120 GW of photovoltaic power nationwide. These numbers are in the magnitude of the model-based outlook presented below and emphasize the relevance to investigate the integration of fluctuating solar power in the Brazilian electricity system. For the model-based outlook, the specific investment costs for photovoltaic systems are assumed to be 500 USD/kW, see table 5.6, composed of 250 USD/kW for the modules and the same amount for other cost components as recommended in [92].

5.1.4 Thermal power

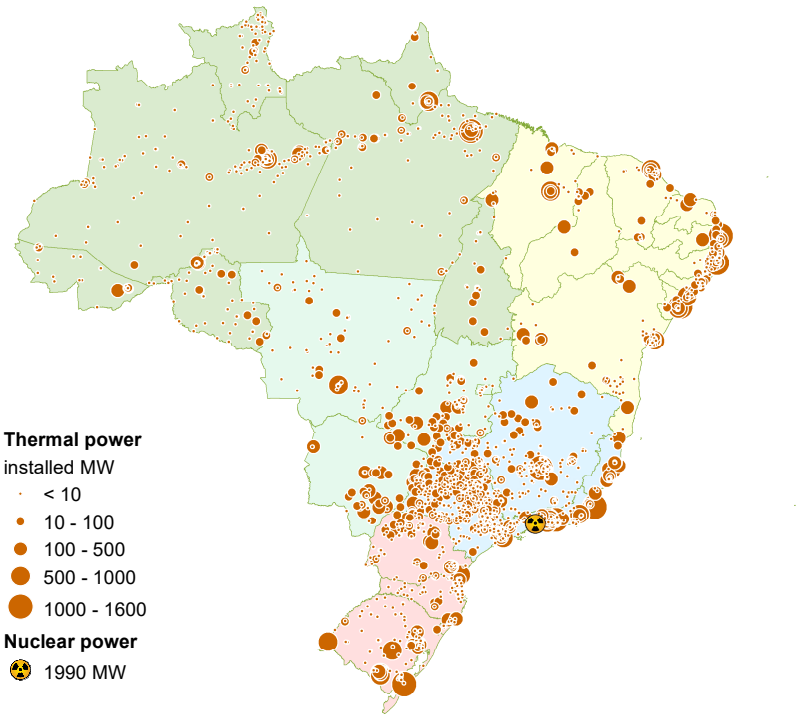

Figure 5.11: Generation capacity of hydro and thermal power

By the end of 2017, in total 34.4 GW of conventional fired thermal plants were installed in Brazil and 37.2 GW in 2021, basically distributed similarly to the Brazilian population. In 2021, natural gas fired plants contribute 15.2 GW or a bit less than 41 % to thermal power generation capacity, 14.1 GW or 38 % are for combustion of biomass including residuals from sugarcane processing. Fuel oil and diesel power systems are often located in remote regions in the Amazon basin for example and have a total capacity of 4.3 GW and share of 12 %. Coal-fired power stations account another 3 GW or 8 % and other types fuel less than 2 %. Due to official plans, power plants firing natural gas will be expanded by 3.4 GW until 2025, biomass by 1 GW, fuel oil and diesel by 0.3 GW. Coal and other fuel types remain unchanged. Not included in these percentage figures are the 1990 MW installed capacity of Brazil's one nuclear power station in the state of São Paulo. Its installed capacity will neither be expanded nor reduced until 2025.

For the model-based outlook, several assumptions concerning thermal power generation were made and are summarized in section A in the appendix. Apart from the nuclear power plant, all thermal power plants are considered to have similar characteristics, converting the same fuel to the same costs into electricity at a constant efficiency of 36 %. It is further assumed, that thermal power plants can change their power output by $\Delta P/P_{\mathrm{inst}} = 30\ \%$ per hour in relation to the installed capacity. Further limitations such as lower bounds for operation due to combined heat and power production are not considered.

5.1.5 Transmission

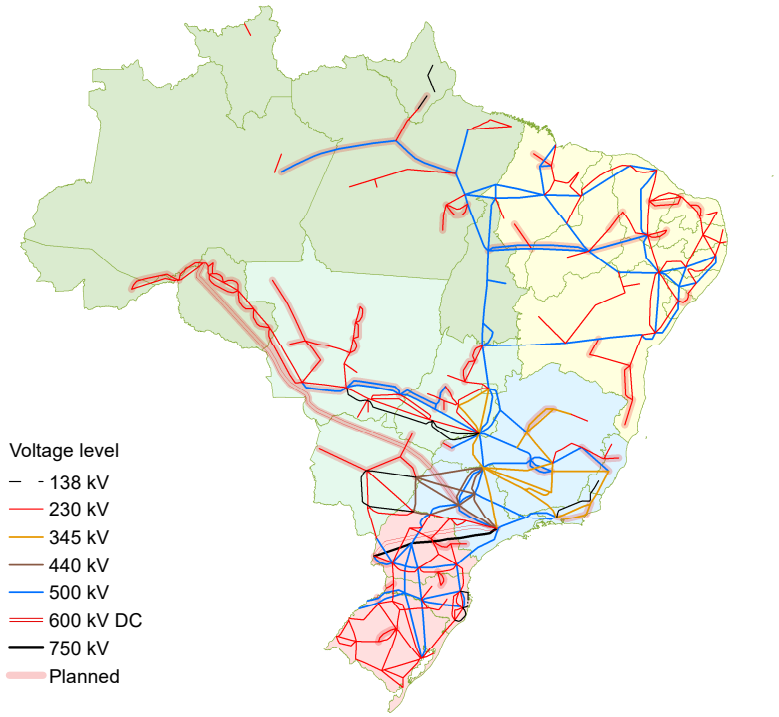

Figure 5.12: Existing transmission grid 2017 and planned expansion

The map above shows the Brazilian transmission grid as it was by the end of 2017. The planned grid expansions correspond to the planned expansions of the generation capacity linking partly remote power stations with the consumers. In the model-based outlook, a simplified transmission grid is implemented. The initial capacities were estimated from the maximum difference of demand and supply in each region, see figure 5.20. The North (NO) is able to transfer up to 3 GW with the Northeast (NE) and the Central-West (CW) and Southeast (SE) combined. Northeast on the one hand, Central-West and Southeast on the other hand can exchange up to 3 GW with each other. The link to the South (SO) is assumed to have a capacity of 1.5 GW. The transmission capacity can be expanded by the model at given, simplified conditions, see section A.

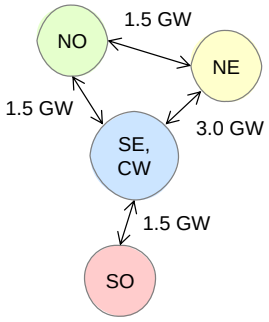

Figure 5.13: Simplified transmission system for model-based outlook

5.1.6 Time series for wind, sun, and inflow

The model applied in the following section 5.2 uses normalized profiles for intermittent renewable energies. As mentioned above, wind and solar profiles were derived from the INMET database [16] providing between 1 (Roraima) and 51 (Minas Gerais) annual time series per Brazilian federal state in hourly resolution. Since the model uses only four regions, see figure 5.13, average profiles from normalized time series were calculated. The value of 1 is not reached in the time series for wind and sun within, see figure 5.14 below, since maximum wind speed or solar radiation is obviously not reached in the same hour per year over several states. For the case of wind power time series, the wind speed profiles were transformed for each location into wind power as described in the appendix around figure A.1 and then normalized summarizing all time series within one macro-region.

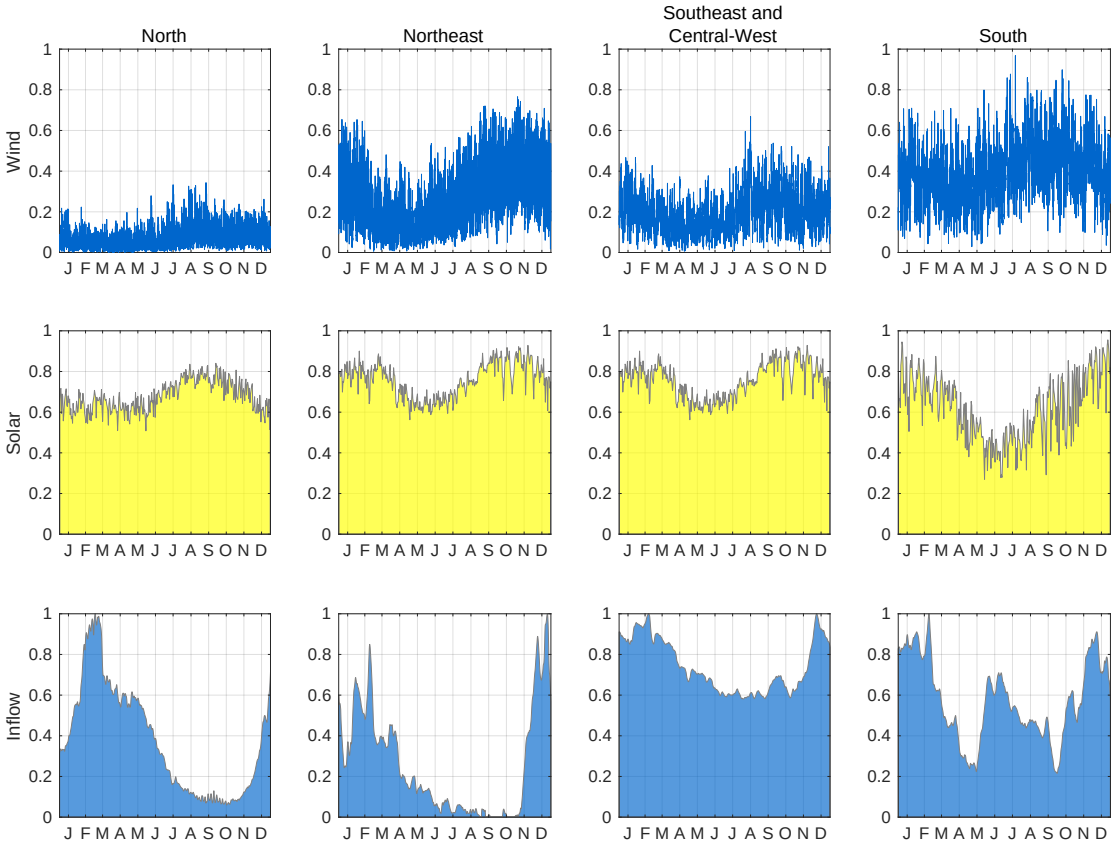

Figure 5.14: Normalized supply profiles

Unlike wind and sun, the inflow time series displayed above were not derived from precipitation as described in the rejected approach, see paragraph 5.1.1, but calculated from given time series for hydropower production and storage level per macro-region as described above. With varying extent depending on the macro-region, the time series for wind show a higher level in the second half of the year. The windiest conditions appear predominantly from August to October. A comparable but less pronounced maximum can be found for solar radiation

around September and October for the regions North, Northeast, Southeast, and Central-West. The South with a distance of at least 2500 km to the equator shows a distinct seasonality in terms of solar radiation. Peaks occur around the turn of the year and the lowest values in June and July.

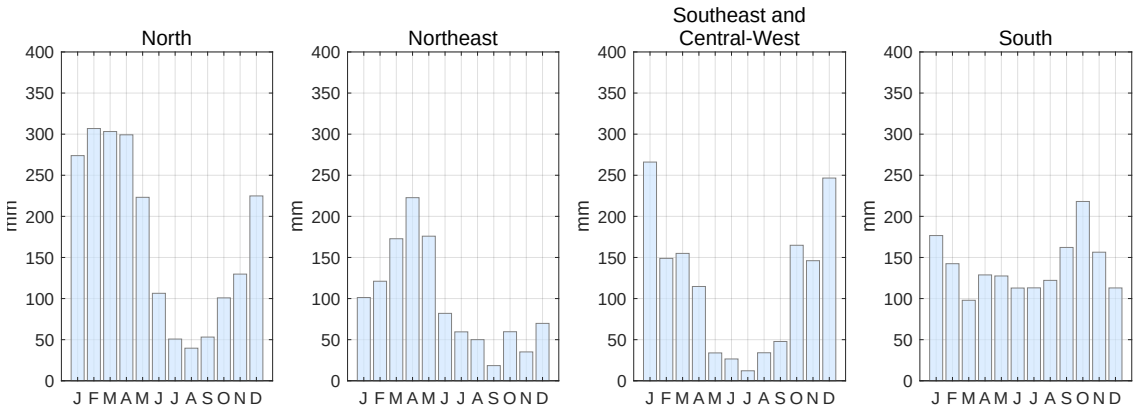

Figure 5.15: Precipitation per month

In contrast to the wind and sun, the inflow time series for the North and the Northeast show higher levels in the first half of the year with a second peak time around December. The inflow time series depicted in figure 5.14 were derived from 2017 data show lowest inflows between July and October for all Brazilian regions except for the South. For the latter region, a remarkable phase of high inflows can be seen by the mid of the year. One has to keep in mind, that the inflow time series are from 2017 only, whereas the other meteorological time series from the years between 2007 and 2011. More generalizable effects can be detected in the monthly precipitation, see figure 5.15, which was calculated from the same source as the profiles for wind and sun. To a certain degree, the driest periods occur simultaneously with the highest potential for wind and sun, namely between June and October. Temporal opposite availability of renewable energy resources are promising preconditions for a both economical and stable electricity system mainly relying on wind, solar and hydropower. A quantitative investigation of such a system can be found in the following section.

5.2 Model-based outlook

For the model-based outlook, a linear optimization model designed in context of this work for the Brazilian electricity system is applied. At the beginning of this section, a brief insight into linear optimization is given as well as description of the particular model used in this work. Optimization in general refers to the identification of the best solution out of a space of possible solutions. The best solution is defined as the set of variables to achieve the maximum value of an objective function, for example maximum profit or minimal costs. The solution space is limited by restrictions that can represent any given limits, e.g. physical, technological, economical, regulatory, or temporal nature. An optimization problem in which the objective function and all the constraints are linear is called a linear optimization problem or linear programming (LP). The main advantage in contrast to other kinds of optimization problems such as non-linear or mixed-integer optimization problems is its reliable solvability towards its global maximum. For more information about optimization, see chapter 14 in [129].

$$\begin{aligned} \text{Maximize} \quad & z = c^{\mathrm{T}} x \\ \text{subject to} \quad & \mathbf{A}x \leq b \\ & x \geq 0 \end{aligned} \tag{5.8}$$

The equations above show the general mathematical formulation of a linear optimization problem. The scalar z represents the value of the objective function $c^{\mathrm{T}}x$ consisting of the transposed cost vector c and the variable vector x, whereby the latter is determined while solving the optimization problem. The components of the variable vector can be chosen subject to the constraints represented by the inequalities $\mathbf{A}x \leq b$ and $x \geq 0$. The vectors c and b as well as the matrix $\mathbf{A}$ contain the input data of the the model, whereas the variable vector x stands for the model output.
The groundwork for the model-based outlook conducted in this section is the energy system model called *urbs*, which has its roots in the early 2000s at the Max Planck Institute for Plasma Physics in Garching and the University of Augsburg, Germany. [130] A broad overview of energy system models including examples for the application of the model urbs, its predecessors, and its derivatives can be found in the doctoral thesis of Johannes Dorfner from 2016. [131] Dorfner's work contains also an extensive model documentation for urbs, see p. 77 ff.
Figure 5.16 below shows the adaption of urbs to the electricity system of Brazil. Model inputs are the time series and several technical and economical parameters. Input time series in regional dependency are the electricity demand, profiles derived from meteorological data for wind and sun as well as the time series for hydropower inflow. Available processes for both are characterized by costs for investment and operation as well as technical parameters, which are displayed in the appendix, see chapter A. Since an outlook should be provided based on the system optimization, the most interesting model output in this case are the capacities for power generation, storage technologies and transmission to meet the electricity demand assumed for upcoming years or decades. The different assumptions for future costs and demand are summarized in table 5.7. The region South is displayed exemplary in figure 5.16 in detail, but all other regions can be represented in a similar way. For transfer of electricity between the regions, all of them are considered to be linked with initial capacities shown in the simplified, spatial grid model, see figure 5.13. Each region in that setting is represented as a node in

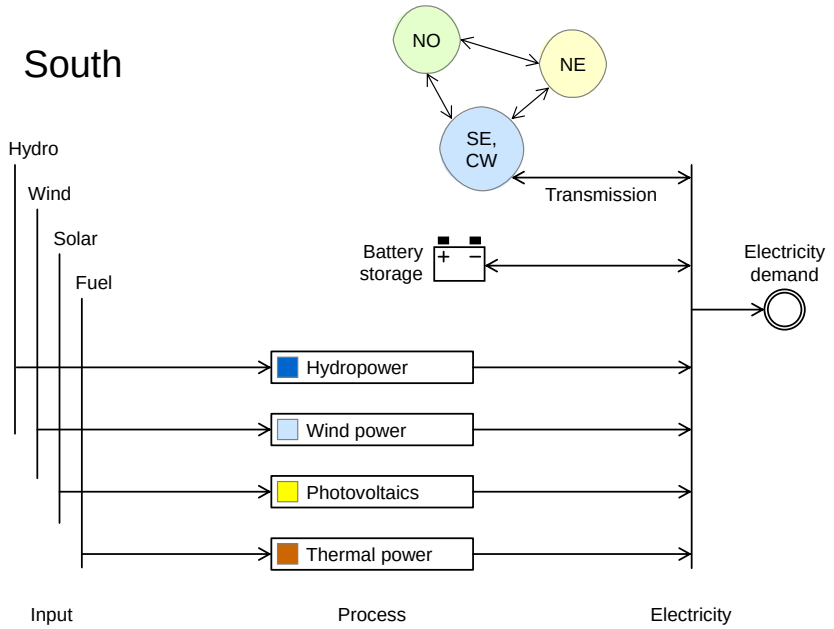

Figure 5.16: Model representation of processes

the energy system, without costs or losses for electricity distribution within this node. One single exception has to be mentioned for the Southeast region including Central-West, where a process for nuclear power exists, additionally. The nuclear power process equals the thermal power process, but with another kind of fuel, other costs and different technical parameters, see table A.10 and table A.11. The hydropower process is modeled differently and more precisely

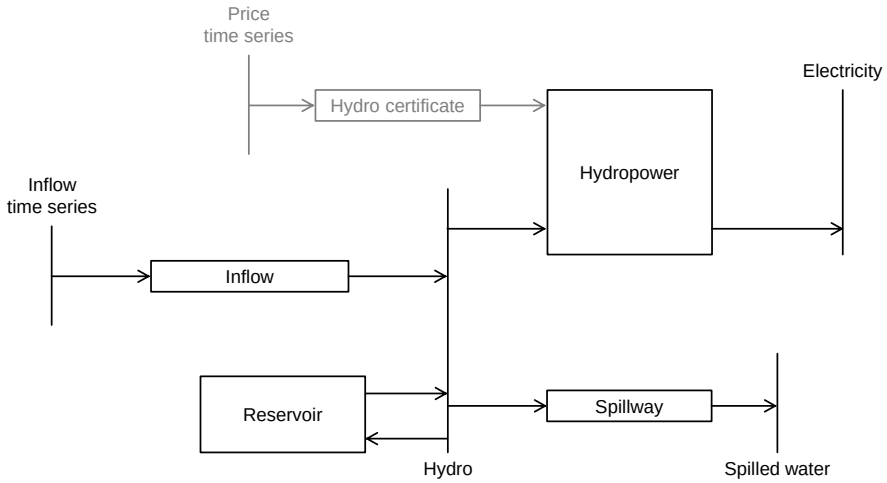

Figure 5.17: Modeling of hydropower in optimization model urbs

compared to other conversion processes, not only because of the overwhelming importance of hydropower in the Brazilian electricity with a share of more than 60 % by installed capacity and around 70 % by produced power in 2017, see table 5.1. Figure 5.17 shows the hydropower process more in detail as it is implemented in each region of the model, see figure 5.16. Three

important characteristics are reflected by the following approach. The intermittent inflow time series as input, the storage capacity in the scale of terawatt hours of the hydropower reservoirs, and the controllability of hydropower production comparable to conventional thermal power generation. The lossless inflow process displayed in figure 5.17 converts the normalized inflow time series into an intermediate product here designate as *hydro* and megawatt hour as a unit. The vertical line for hydro has the character of a mass or energy balance, whereby all inputs and outputs per time step must sum up to zero. The inflow time series itself are derived from given time series for regional storage levels and hydropower power production as described in section 5.1.1. There are three options for the further use of the intermediate product hydro. Which option is used to what extent is determined as part of the optimization process described above and expressed as time series for each region. The first option and main purpose is to consume the intermediate product hydro and convert it via the hydropower process into electricity. The second option for the use of hydro is to fill the reservoir with water. Practically, a filling of the reservoir happens in reality always when the inflow is greater than all outflows combined. Besides evaporation and technical losses, which are not addressed in the model, but discussed above in section 5.1.1, the third possibility to use water is the spillway. Both in reality and in this model, the spillway is used when the reservoirs are at their top level and the inflow is higher than the outflow through the turbines. Since multiple-input and multiple-output (MIMO) processes can be represented in this model, the hydropower process has the price time series as a further input. Time-dependent prices for hydropower utilization can represent upcoming scarcity of water in case of foreseeable droughts, for example.

5.2.1 Reference model 2017

Table 5.4: Installed capacity in GW by December 2017

	Brazil	North	Northeast	Southeast and Central-West	South
Hydropower	105.1	15.5	11.0	62.1	16.5
Thermal	34.4	3.6	7.2	19.3	4.4
Nuclear	2.0	-	-	2.0	-
Wind	12.3	0.2	10.0	0.03	2.0
Solar	0.9	-	0.7	0.2	0.004

Brazil's electricity system of the year 2017 acts as a reference model for the outlook conducted in this section. Table 5.4 lists the installed power generation capacity by region. To justify the credibility of the model-based outlook, the optimization process was applied to the 2017 electricity system to compare the real data retrieved from ONS with the model output. Input data for the reference model were the installed capacities by the end of 2017, see table 5.1, the demand time series from 2017, and the profiles for the intermittent resources wind, sun and water inflow as described in section 5.1.6, whereby all time series are different depending on the Brazilian region. For comparison of the real data and the reference model, the total power generation is displayed in figure 5.18 as well as the generation profiles by source including load profile for each region, see figure 5.20.

When directing the attention to the total generation depicted in figure 5.18, one can note that the reference model reproduces relatively good the mix of electricity from 2017. All displayed shares for power production differ for around 1 % or less between the real data and the model. Similarly, the modeled total power production deviates by only around 4 TWh, which less than 1 % difference from reality. The remaining slight differences between the real data and the

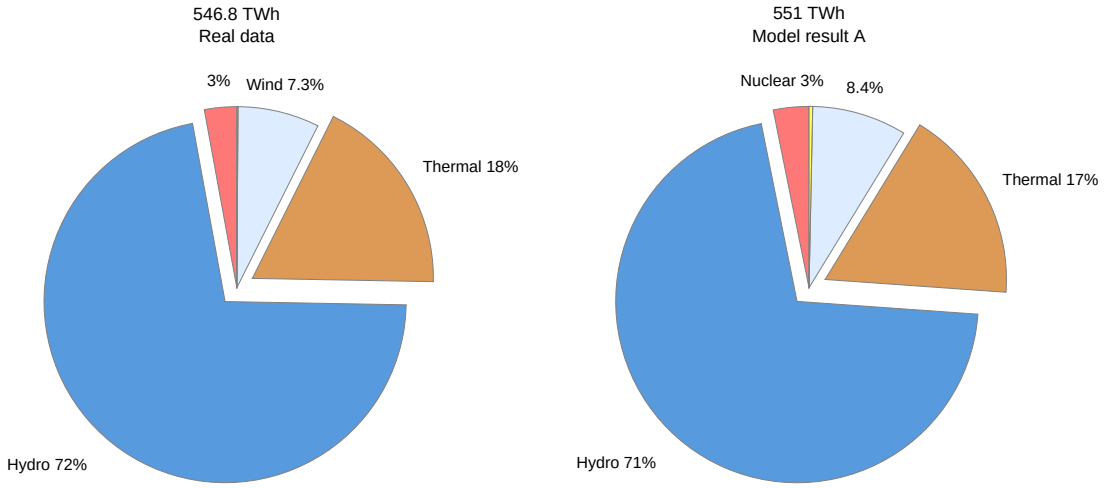

Figure 5.18: Comparison of real total power generation in 2017 with model A

linear optimization might be explained in the following way: For the case of wind and solar, the reference model considers the existing installed capacity by the end of 2017. This leads to an overvaluation of wind and solar power, since the average installed capacity for both was remarkably lower than the end value. The diagrams of figure A.19 in the appendix illustrate the referred development of power generation capacity of 2017. One further source of deviation can be, the time series for wind and sun do not originate from 2017, but from 2001 between 2010. The share of hydropower is gradually higher in the real data compared to the model

Table 5.5: Initial and end level of hydropower reservoirs by region

	Total capacity	Initial state	Final state	Δ
Region	TWh	%	%	TWh
North	11.1	19	23	0.4
Northeast	38.4	16	13	-1.2
Southeast and Central-West	147.0	34	23	-16
South	14.5	62	57	-0.7
Total	211	67.2	49.6	-17.6

result. This might be related to the final level of the reservoirs. In reality, the energy content of all reservoirs together is 17.6 TWh lower by December 31, 2017 in comparison to the initial state on January 1, 2017, see table 5.5. In contrast to that, the model contains a condition, that the aggregated level of all reservoirs by region has to be equal to or greater than the initial

state. This *storage content condition* reduces the possible electricity production by stored water, which can be expressed as follows.

$$\text{storage content}(\text{t} = \text{end}) \geq \text{storage content}(\text{t} = 0) \tag{5.9}$$

In case of ignoring this restriction, the reservoir lakes are emptied until the end of the optimization period due to the objective function for cost minimization or profit maximization, respectively. The causation of higher costs in one following year, for example, due to substitution of hydropower production with other energy carriers, is not considered in this constellation. The resulting energy mix is displayed in figure 5.19, see model result B. A system operation that empties the reservoirs at the expense of future generation costs cannot be considered as realistic. To ensure a realistic system behavior, the above mentioned inequality 5.9 has been introduced.

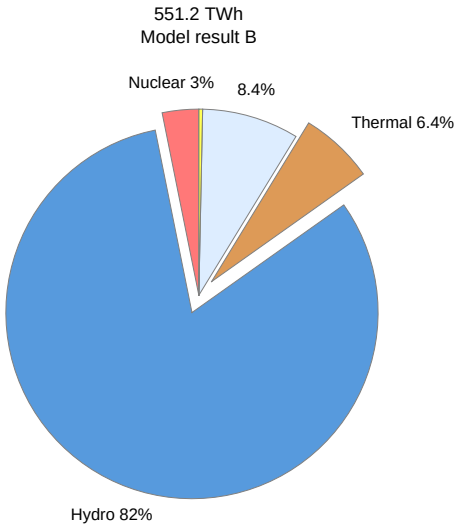

Figure 5.19: Modeled power generation in 2017 without storage content condition

Furthermore, import from countries outside Brazil is not considered in the optimization model. In 2017, 547 TWh or 99.5 % of Brazil's electricity demand were produced domestically and around 2 TWh were imported from neighboring countries. Due to the low share of imported electricity and for the sake of simplicity, it is assumed that only power production within Brazil can be used for fulfilling the domestic electricity demand.
Figure 5.20 shows a comparison between real profiles for generation and load by region in the top section and their modeled counterpart in the bottom section. The above-described model A was used to create the results in the bottom section, including the consideration of the storage content condition 5.9. The load profiles are input time series and therefore in both cases the same. As already expressed in the pie chart in figure 5.18 for the total mix of power generation, the modeled shares of electricity sources resemble relatively good to the real data. A similar conclusion can be derived from the comparison of the generation profiles. However, there are some remarkable differences between the real and the modeled profiles, which are mentioned and explained in the following paragraph.

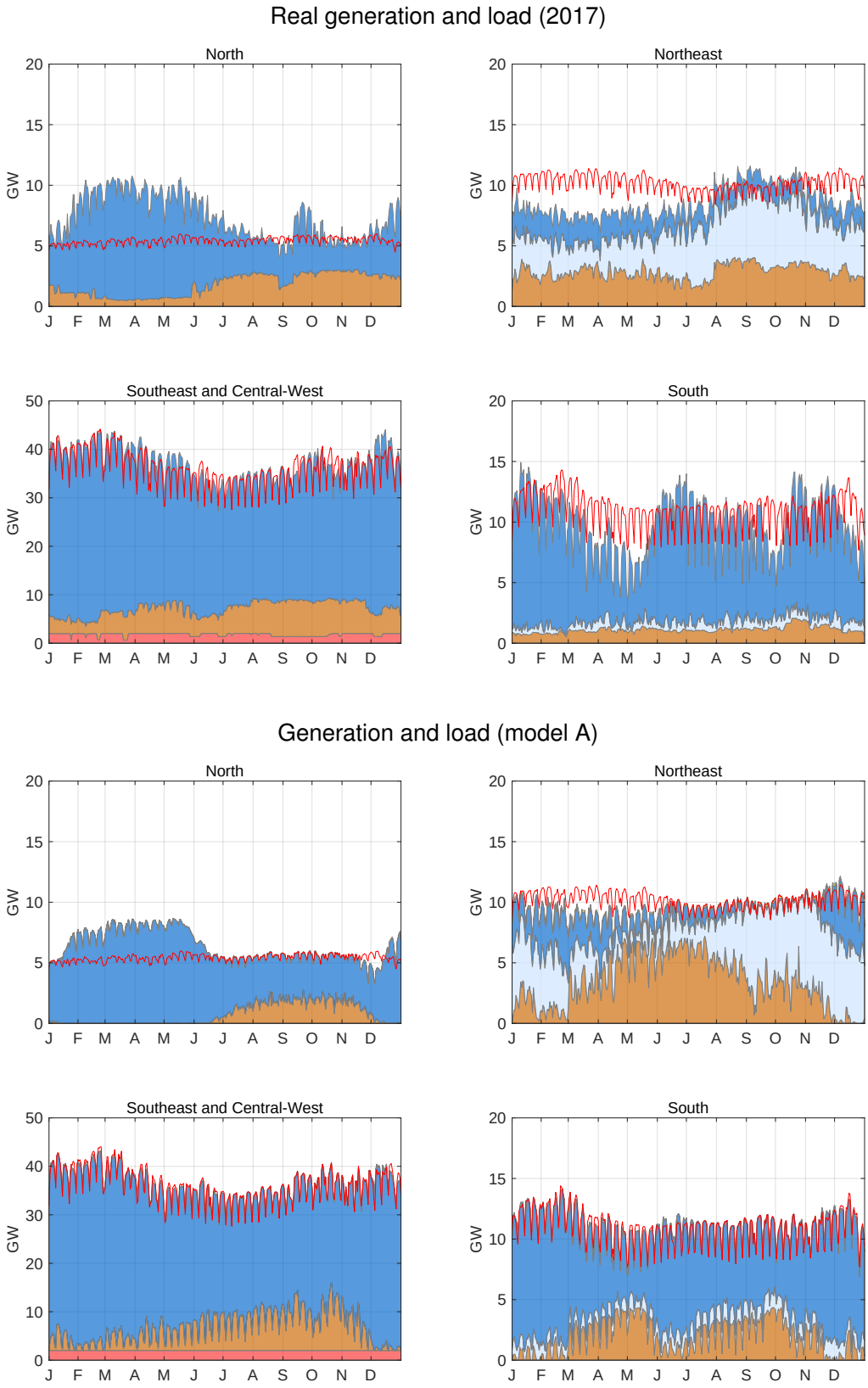

Figure 5.20: Comparison of real and modeled generation profiles

As already mentioned above, the input time series for wind used in the model are derived from meteorological data from 2017, but from 2001 between 2010, see A in the appendix. For the case of hydropower generation, the gradients are in reality higher than in the modeled time series. This fact can be clearly detected when comparing the hydropower generation profiles of the North and the South region. The high volatility of hydropower generation can be observed in the real time series almost throughout the whole year in both regions. In contrast to that, the generation follows in the modeled time series to a larger extent the demand profile. Both in North and South, the power production mainly relies an hydroelectricity and thermal power generation. Especially in the modeled time series of the South region, the gradients of thermal electricity generation are significantly higher than in the real time series. This means, that thermal electricity is used in the model more flexible than hydropower. The assumed variable costs for thermal power in the model are higher than those for hydropower, see table A.10. Therefore, thermal power stations are only ramped-up when cheaper sources are unavailable and ramped-down otherwise. This explains higher gradients in the modeled time series for thermal electricity. Furthermore, a certain base load provided by thermal power can be observed in the real data in contrast to the model results. During January and June in the North region, thermal power stations operate on a low level, whereas almost no contribution of electricity produced by fuels is the outcome of the model for the same time and region. Not only for the North region, the following three aspects can act as an explanation for the thermal baseload in the real data, which is not observable in the modeled time series.

1. Thermal power stations are necessary for the local power supply. Due to bottlenecks in the grid within a region, abundantly available but remote resources such as hydropower cannot be transferred to the consumers. Since grid restrictions are only modeled in-between the regions, but not within the regions, this effect is not represented in the model.
2. As depicted in figure 3.2 in chapter 3, residuals from sugarcane production such as bagasse and black liquor are fuels with a significant share in Brazil's thermal power production. These plants for conversion of residuals into electricity and heat underlie other rules for the operation, which are not covered by the represented in the model.
3. Unlike reality, no minimal operation is considered for thermal power plants in the model, e.g. for heat-driven co-generation.

More detailed modeling of the characteristics of thermal power stations in the Brazilian electricity system can be a relevant subject for future investigations. Since one focus of this work is the interaction between hydropower and fluctuating renewable energies such as wind and sun, the detailed operation of thermal power plants plays a secondary role. Additionally, most of the results presented below imply a minor share of thermal power in the future electricity production of Brazil. Subsequently, inaccuracies in the modeling of this minor share will not change the overall statements.

5.2.2 Scenario results

The setting of model A described above is taken as a reference for the model-based outlook. Table 5.6 shows the main differences between the reference model representing 2017 and the scenario base (1a). The trends for price erosion found in [126] for wind, in [99] for photovoltaics,

and in [132] for lithium-ion batteries are extrapolated roughly to derive plausible values for the future scenarios. Scenario base (1a) considers an increase by 100 % for demand, which means in absolute values a growth from 550 TWh to 1,100 TWh. With an eye on figure 3.2 showing the development of the Brazilian electricity production from 1970 until 2016, it took in the past between 10 and 20 years to double the electricity demand. Since the pace of growth in demand decelerated in recent decades, one can estimate that Brazil will reach 1100 TWh of electricity demand between 2030 and 2040. Therefore, the sketched future scenarios are located in the forth decade of this century when extrapolating past developments. However, these assumptions are subject to considerable uncertainty due to the difficult predictability of occurrences influencing the electricity demand, such as economic crises or faster than expected technological shifts. One of these relevant technological developments is investigated in scenarios 2 and 3, where a significant extra load is added for hydrogen production.

It is known from the past, that fuel prices vary within a broad range affecting the costs for

Table 5.6: Main differences between input data for 2017 and for future scenarios

		Year 2017	Scenario Base (1a)	
Investment costs for	Wind	1600	1000	$/kW
	Photovoltaics	1000	500	$/kW
	Battery	200-800	50-200	$/kWh
Electricity demand	Total	550	1100	TWh

thermal power production. Similarly, it is unclear for the case of batteries, if and to which extent their prices will drop. Therefore, all scenarios are split up into sub-scenarios to investigate the impact on the optimal system composition depending on fuel and battery prices. These scenarios with a variation of fuel and battery prices are indicated with (a) after the number in table 5.7. For each scenario three different prices for fuel and three for batteries are considered, which results in nine sub-scenarios per scenario. Scenarios with a variation of fuel price (F) by battery price (B) are shortly denoted with the type FxB, see table 5.7.

Due to the high importance of hydropower for the Brazilian electricity system, the impact of the flexibility of hydropower is also examined more in detail. Flexibility here is characterized as difference of power output of a process from one time step to the following time step divided by the installed process in this region. The following inequality defines the upper limit for flexibility:

$$\frac{\Delta P}{P_{\mathrm{inst}}} \leq \frac{\Delta P^{\max}}{P_{\mathrm{inst}}} \tag{5.10}$$

As a numerical example, at a time step duration of one hour and given hydropower flexibility of 10 % and installed power of 20 GW per region, the change of power production has to be lower or equal to 2 GW per hour. To investigate the impact of different values for hydropower flexibility, each scenario indicated with (b) after the number is split up into nine sub-scenarios with different flexibility for each. Scenarios with a variation of hydropower flexibility and stable prices for fuel and batteries are shortly denoted with the type H100, see table 5.7.

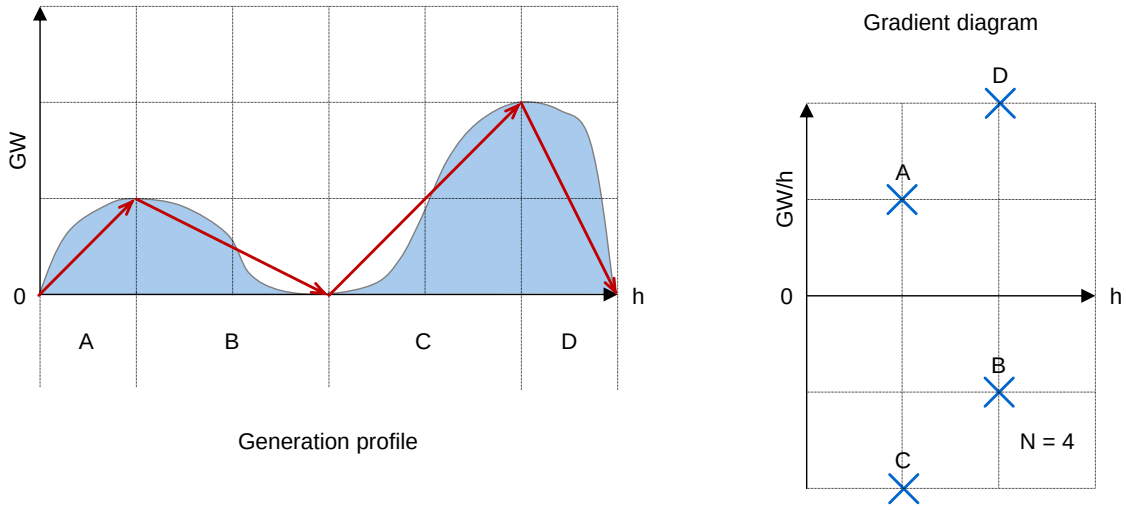

Figure 5.21: Transformation from generation profile to gradient diagram

To which extent the flexibility of hydropower is used in each scenario is a matter of interest and display in a dedicated graph, here named *gradient diagram*. The idea for the transformation of a hydropower generation profile into a gradient diagram is described with the help of a simple example, see figure 5.21. A steady increase of power output, blue curve in interval A, is simplified in the first into a linear ramp, see red arrow. Then, the ramp is translated into a cross in the gradient diagram, whereby the horizontal position of the cross represents the duration of the steady increase in hours, the vertical position describes the power increase in GW until the next turning point. Interval B shows the same relation for a steady decrease in power output. The same shall apply for intervals C and D, accordingly. Subsequently, a detailed generation profile is transformed into a compact scatter plot, which gives a fast insight into the volatility of hydropower production of a certain scenario, including a quantification via height, duration, and number of ramps. Each ramp is represented by a cross, the total number of ramps is N. The results discussed below show the impact of different system configurations for hydropower volatility, which gives a foresight on possible challenges in terms of the flexibility of Brazil's future electricity system.
For all scenarios summarized in table 5.7 the following results are provided:

1. Total power production in TWh and power generation by source in %
2. Installed generation capacity of thermal, wind and solar power by source in GW, differentiated by existing and new
3. Installed battery storage capacity by Brazilian region in GWh
4. Power generation and load per region in GW
5. Gradient by ramp length for hydropower generation
6. Transmission capacity between regions, differentiated by existing and new

Due to the large number of graphics illustrating these results, the images are moved to the appendix, see chapter A, following the order of table 5.7. The key findings in the optimization results are described in the following section, with references to the relevant point in the appendix.

Table 5.7: Overview of scenarios for model-based outlook

No.	Scenario name	Type	Prices	Characteristics and main differences
1a	Base	FxB	F=25-100 $/MWh, B=50-200 $/kWh	Base scenario for the future energy system. In contrast to 2017, doubled demand, lower investment costs for wind, photovoltaics, and batteries.
1b	Base	H100	F=25 $/MWh, B=50 $/kWh	Like 1a, but with varying flexibility of hydropower $\Delta P/P_{\mathrm{inst}}$ from 1 % to 100 %. All other input data remain unchanged.
2a	Hydrogen	FxB	F=25-100 $/MWh, B=50-200 $/kWh	Additional constant electrical load of 120 GW in Northeast for hydrogen production. A total of 120 GW · 8760 h = 1,051 TWh of electricity is used for hydrogen production.
2b	Hydrogen	H100	F=25 $/MWh, B=50 $/kWh	Like 2a, but with varying flexibility of hydropower. All other input data remain unchanged.
3a	Green hydrogen	FxB	F=25-100 $/MWh, B=50-200 $/kWh	Additional electrical load of 120 GW peak reduced by thermal power generation profile of sub-scenario F1B1 from scenario 2a. A total of 787 TWh of electricity is used for hydrogen production.
3b	Green hydrogen	H100	F=25 $/MWh, B=100 $/kWh	Like 3a, but with varying flexibility of hydropower. All other input data remain unchanged.

5.2.3 Key findings by scenario

The following sections discuss the results of the scenarios listed in table 5.7. Not displayed results can be found in the appendix A. For selected extreme outcomes, the space requirements are estimated and illustrated on a map, see section 5.2.4.

Scenario 1a "Base"

As argued above and summarized in table 5.6 above, the assumed main differences between 2017 and the future energy system are lower investment costs for wind energy converters, photovoltaic power systems, battery storage, and a doubled demand for electricity. The scenario 1a is considered as bases scenario for the following five ones, listed in table 5.7.
The first result graph for this scenario, see figure A.21, shows the power generation by source at an annual demand of 1099 TWh. One can see nine pie charts representing sub-scenarios.

Each sub-scenario displays the cost-optimal composition of power supply, whereby each sub-scenario differs from another by a different price for fuel and batteries. As depicted in figure 5.16, fuel is used in thermal power plants and batteries are considered to be grid-connected. The order of the pie charts follows the rule symbolized in the small scheme, see also figure 5.22 below.

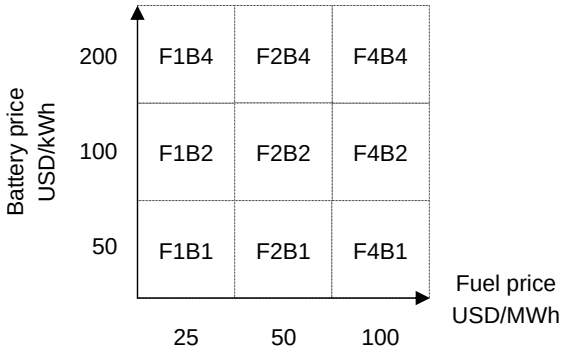

Figure 5.22: Scheme FxB for differentiation of prices for fuel (F) and batteries (B)

That means, at the bottom left, one can find the sub-scenario with the lowest prices for both fuel and batteries. The three sub-scenarios in one horizontal line are all calculated with the same battery price, but with an increasing price for fuel in the right direction. The lowest considered fuel price here is 25 USD per MWh, which is 2.5 cents per kWh or approximately 0.25 USD per liter of diesel fuel or light fuel oil. In the right direction, the fuel price increases by the factor of two or four to the values of 50 USD/MWh or 100 USD/MWh, respectively. As in the horizontal direction for fuel, the same applies for battery costs in the vertical direction, starting with the lowest investment cost of 50 USD/kWh over doubled costs of 100 USD/kWh to the fourfold price in the top line. The naming convention is derived from the factors for the price increase, meaning from F1B1 with the lowest prices to F4B4 the highest, meaning by a factor of four higher prices compared to the lowest. With this method, one can investigate the influence of fuel and battery price on the composition and operation of future electricity systems. The fuel price might not only vary because of the volatility of energy markets but also because of policies such as subsidies for fuel or certificates for pricing of CO_2. For the sake of simplicity, both are considered here to be part of the gross price.

For the case of power generation by source in scenario 1a "Base", one can identify the following aspects. Independently from chosen fuel or battery prices, wind and photovoltaic power combined will contribute more than 50 % to Brazilian electricity production. For the case of expensive fuel and cheap batteries, the share of wind and sun reaches up to 68 %, see F4B1 in figure 5.23. With a high battery price of 200 USD/kWh and a low fuel price of 25 USD/MWh, see F1B4, thermal power has the highest share in the energy mix among all sub-scenarios with around 14 %. In all other sub-scenarios, thermal power is substituted mainly by wind or sun, since nuclear and hydropower are not considered here for expansion. Moreover, it is not foreseeable with a view to the official expansion plans, see table 5.1, that an increase in demand up to 1100 TWh within the upcoming one or two decades can be covered with an expansion of generation capacities of nuclear or hydropower. The highest share of photovoltaics with 41 % shows up in scenario F4B1. F4B1 is the case of expensive

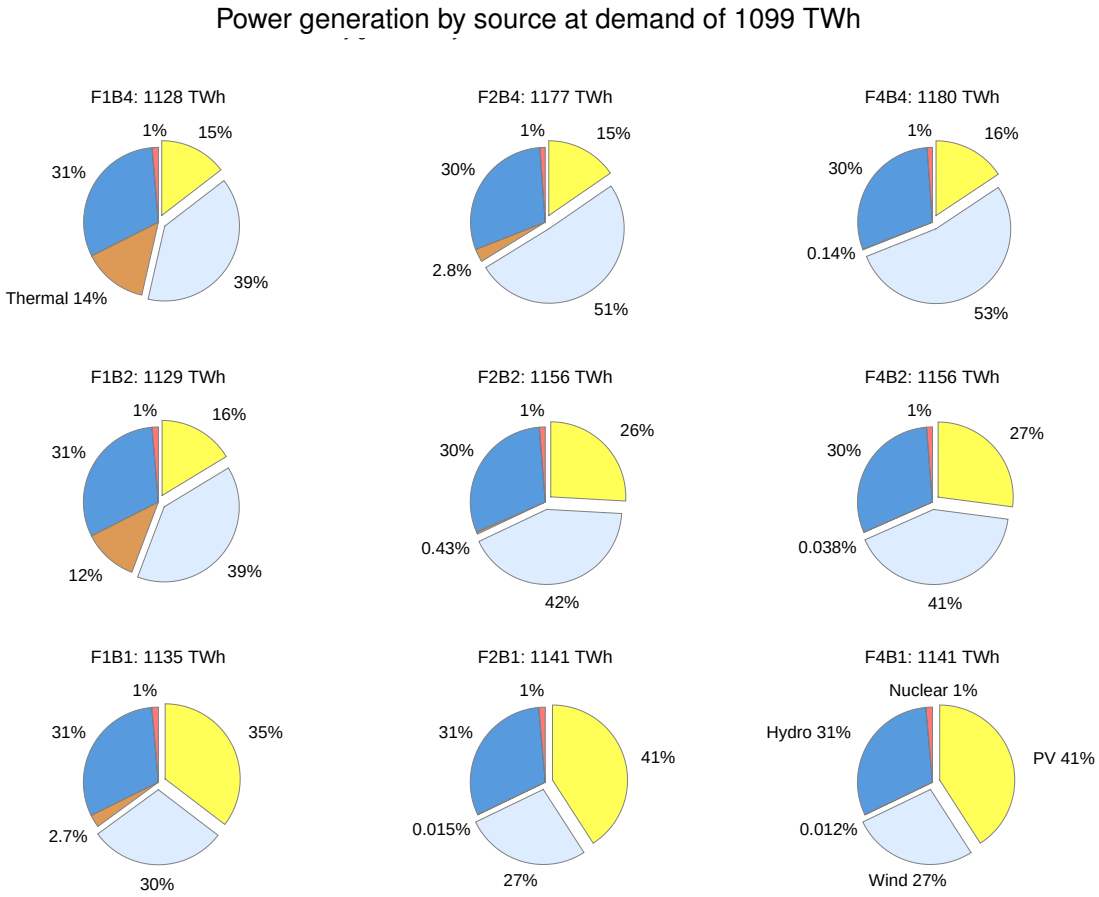

Figure 5.23: Scenario 1a "Base", scheme FxB

fuel to 100 USD/MWh and cheap batteries to 50 USD/kWh. In this case, thermal power production almost disappears completely. A scenario without thermal power at all will likely not become reality, since thermal power plants are partly used for converting residuals into electricity or necessary as combined heat and power plants. The latter mentioned sub-scenario F4B1 expresses an appropriate interaction between photovoltaics and batteries, which means that the availability of cost-effective batteries supports the penetration of photovoltaic power. An explanation for that is the good applicability of battery storage for day-night balancing of photovoltaic power production. At the top of each pie chart, one can find the total annual electricity generation for each sub-scenario. Both thermal plants and batteries provide flexible power supply, therefore, generation and demand are close together when flexibility options are affordable. The lowest surplus is generated for the case of cheap fuel and expensive batteries, with 29 TWh in total or 2.6 % in relation to the total demand. In the case of cheap fuel and cheap batteries, see sub-scenario F1B1, the surplus is with 36 TWh or 3.3 % slightly higher due to the losses during charging and discharging of batteries. When both mentioned flexibility options are more expensive like in sub-scenario F4B4, a higher surplus 7.4 % is the cost-minimal solution leading to an annual curtailment of 81 TWh.

For scenario 1a "Base", figure 5.24 depicts the installed generation capacity by source in GW.

Figure 5.24: Scenario 1a "Base", scheme FxB

Since nuclear and hydropower are not considered for significant expansion, both technologies are not included in the graphs. The focus of this result plot is on the existing and newly installed capacity of thermal power, wind, and solar, where the the results differ significantly depending on each sub-scenario. One important finding is, that only in one sub-scenario a considerable gain can be seen for thermal power plants. To the existing 34.4 GW of another 28.0 GW are added when assuming a low fuel price of 25 USD/MWh and a high battery price of 200 USD/kWh, see sub-scenario F1B4. With a price of 100 USD/kWh for batteries while all other conditions remain unchained the growth of thermal power shrinks from 28.0 GW in scenario F1B4 to 8.4 GW in F1B2. In the further four sub-scenarios, thermal power grows between 0.1 GW (F2B2) and 2.2 GW (F1B1), whereas it is not expanded in the remaining three sub-scenarios. When it comes to the expansion of wind and photovoltaic power, one can observe not only an enormous growth compared to the energy system of 2017 but also significant dependencies of capacity expansions from fuel and battery prices. Corresponding to ONS data in table 5.1, according to which 12.3 GW of wind were installed in 2017, the lowest projected total generation capacity of wind energy converters is above 83 GW, see sub-scenario F4B1. For low battery prices of 50 USD/kWh, the installed capacity of wind stays in the same magnitude, which means that it does not exceed 100 GW. But when battery storage are assumed to be more expensive, the optimal system composition relies to a larger extent

on wind power. At a price of 100 USD/kWh for battery storage systems, the wind generation capacity ranges from around 130 to 150 GW, in case of expensive batteries and expensive fuel, the system optimization delivers more than 190 GW of wind power, see sub-scenario F4B4. The lowest value with around 85 GW of solar power can be seen for the case of fuel the lowest gross price of 25 USD/MWh and the highest battery price of 200 USD/kWh, see sub-scenario F1B4. In contrast to that, ideal economic conditions for photovoltaics are high fuel and low battery prices, leading to around 240 GW of installed solar power generation capacity according to sub-scenario F4B1. Bringing these numbers in relation to the Brazilian population in 2018 of around 210 million people, the installed capacity for wind reaches from around 400 Watt per capita in sub-scenario F4B1 to around 900 Watt per capita in sub-scenario F4B4. For photovoltaic power, the corresponding numbers range from 400 Watt in sub-scenario F1B4 to around 1150 Watt per capita in sub-scenario F4B1. The values per capita are likely to be overestimated since one can expect a higher population than 210 million until the future state described in scenario 1a "Base" is reached. For comparison, in 2019 the installations per capita in Germany for wind power were above 700 Watt per capita, and for photovoltaics around 600 Watt per capita, see [127]. Even if these optimization results for installed capacity seem enormously high in absolute values, the specific numbers in relation to the population show that the optimization results vary around the present values for Germany. The shift towards wind and sun in Brazil can be expected to be way more economical compared to past investments in Germany.

Batteries are likely to be an important component of future energy systems to bring fluctuating renewable electricity supply into balance with the consumers' demand. To which extent batteries are needed for both reliable and cost-minimal supply is highly dependent on the prices for flexibility options. As depicted in the scheme of figure 5.22, the two-dimension fuel price for flexible thermal power generation is investigated here on the horizontal axes and battery prices on the vertical axis. Figure 5.25 displays for these dimensions the results for battery storage capacity broken down into three by three sub-scenarios. The stacked bar charts show the total installed capacity of battery storage depending on each sub-scenario, whereby the color code indicates the regional distribution, see legend top left. In the case of low fuel and high battery prices represented by sub-scenario F1B4, only 51 GWh of battery storage are part of the cost-minimal future electricity system, with the highest utilization of storage in the South of Brazil. As shown and explained above, thermal power plays an important role in this sub-scenario. In contrast to that, when assuming high prices for fuel and low prices for batteries, see sub-scenario F4B1, the total installed storage capacity around 700 GWh is by a factor of 14 higher compared to the opposite case F1B4. In this sub-scenario, around two-thirds of photovoltaic generation capacity and correspondingly battery storage are installed in the Southeast and Central-West, which is the most populous region with the highest share of demand among the Brazilian macro-regions. In relation to the population of 210 million people, the installed capacity ranges in scenario 1a "Base" from 0.24 kWh per capita in sub-scenario F1B4 to 3.3 kWh in sub-scenario F4B1. 3.3 kWh per person or 700 GWh for the whole country might seem a lot, but these numbers do not seem unrealistic for the future when compared with the storage capacity of electric road vehicles or with the present capacity of hydropower reservoirs. Assuming 20 million electric cars with a range of 300 km and a battery capacity between 40 and 60 kWh each, that would lead to a total capacity between 800 and 1200 GWh

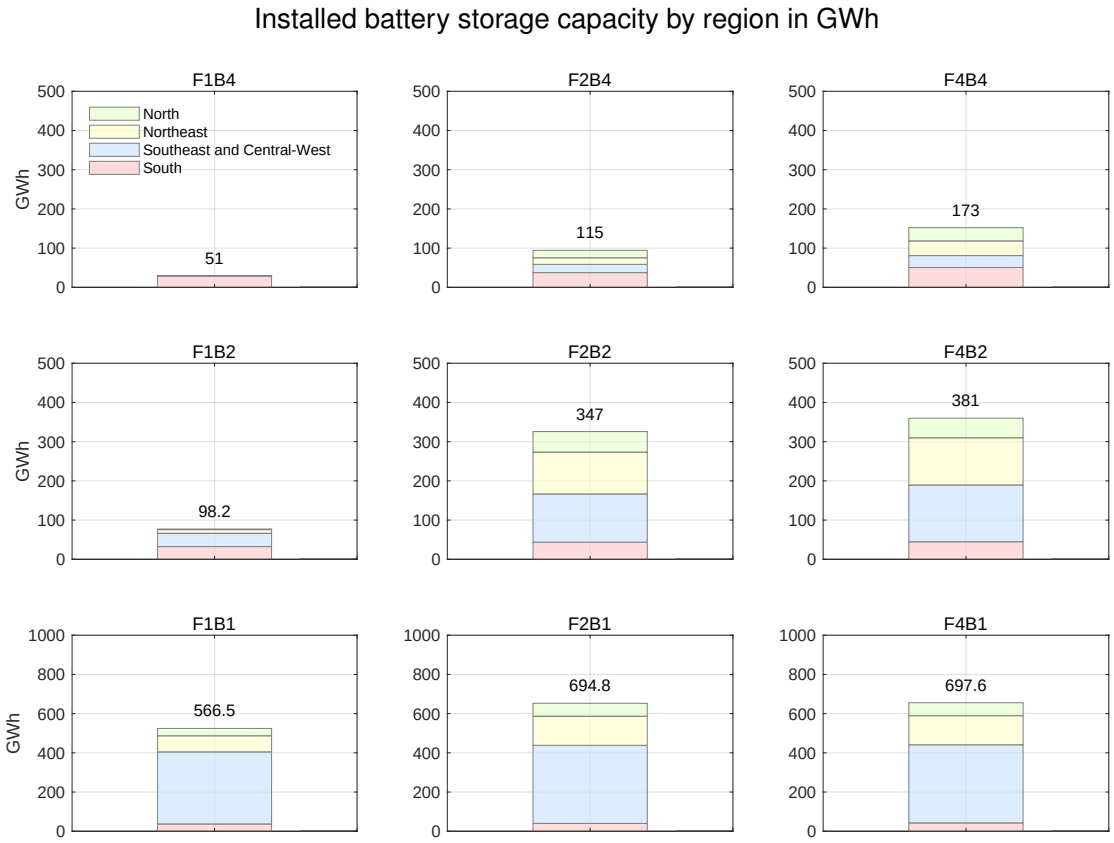

Figure 5.25: Scenario 1a "Base", scheme FxB

on the road. 20 million cars are less than one-half of the Brazilian passenger vehicle stock from 2016 with 54 million cars. [95] One can summarize, that a power supply without the use of any conventional thermal electricity and without expansion of nuclear and hydropower would need much less battery capacity than the electrification of the transport sector. The capacity of 700 GWh or 0.7 TWh shown in sub-scenario F4B1 appears to be even smaller when comparing it with the total storage capacity of all Brazilian hydropower reservoirs. The storage capacity of all lakes was 211 TWh in 2017, which is almost exactly 1000 kWh per inhabitant.

The time series for power generation and load for sub-scenario F1B1 differentiated by region are displayed in figure 5.26. Remarkable differences between this future scenario and the real profiles shown in figure 5.20 are most above all different compositions by sources. Solar power has a large impact on the energy mix in all regions throughout the year, except for the South region, where wind power is the dominating source. Despite the assumption of low prices for fuel, thermal power plays only in the North and the Northeast a considerable role with seasonal differences. Thermal electricity comes in mainly during the dry season in the North, where the availability of hydropower is lower, which can be seen in the normalized profiles for the inflow, see figure 5.14. Since wind and photovoltaic power play the predominant role in the Northeast, thermal power is only necessary to contribute a minor share before August or September. Between March and August, both wind and solar radiation are on a lower level in

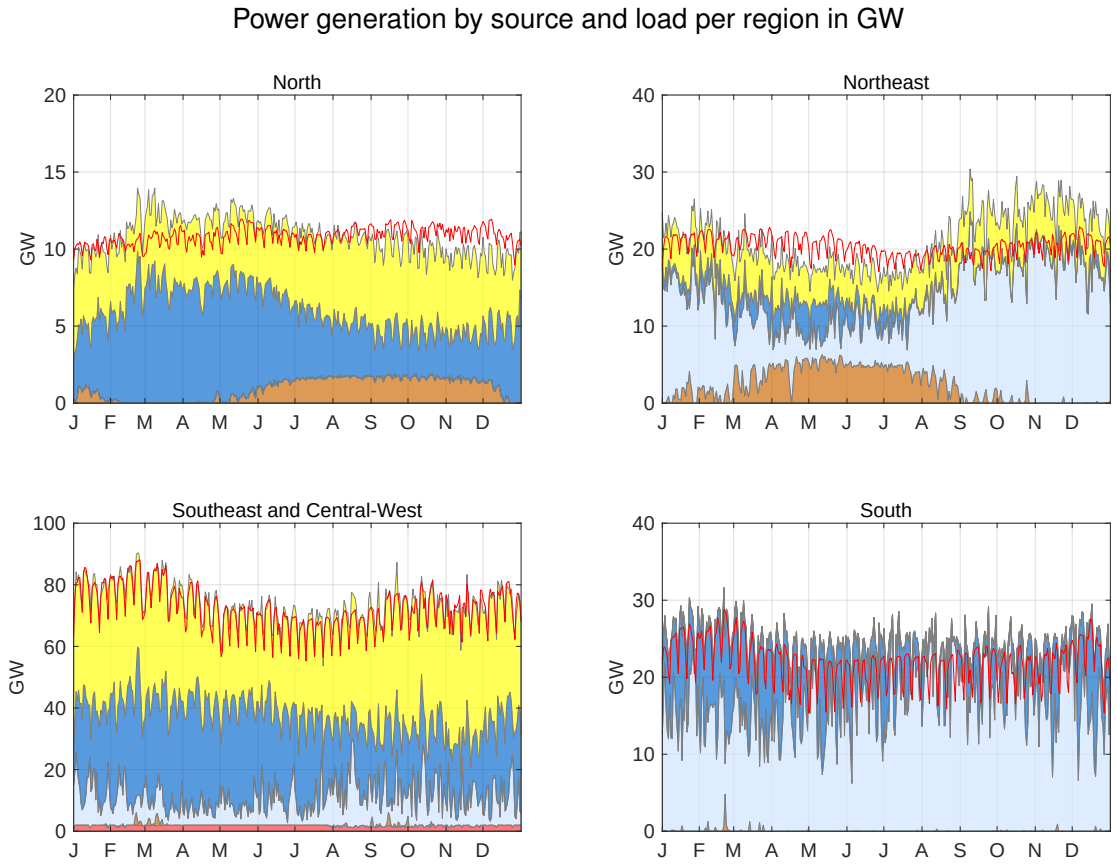

Figure 5.26: Scenario 1a "Base", sub-scenario F1B1

the Northeast compared to the rest of the year. Hydropower cannot fulfill the demand during this time due to a partly simultaneous scarcity of precipitation in the same period. For the regions North, South, Southeast, and Central-West hydropower was in 2017 by far the most important contributor of baseload supply, see 5.20. Whereas in this future scenario depicted here, hydropower turns more into the role to balance the highly volatile electricity production of wind and sun, leading partly to high fluctuations in hydropower production. The dynamic characteristics of hydropower are described more in detail below.

Figure 5.27 shows the volatility of hydropower all over Brazil for scenario 1a "Base", in which each ramp is symbolized by a small cross depending on the gradient and duration of a ramp. The way how to derive this kind of diagram was described in subsection 5.2.2 above and illustrated simplified in figure 5.21. The sub-scenario results considering the lowest prices for fuel and batteries can be found in the bottom left, see F1B1, with increasing prices for fuel in the horizontal direction and for batteries in the vertical direction, analogous to the result plots presented previously.

When considering only fuel and battery prices, one cannot detect a simple impact of these two dimensions on hydropower volatility. The bottom three graphs appear very similar, pointing out around N = 2800 ramps per year, even though fuel prices increased fourfold from sub-scenario F1B1 to F4B1. The number N of ramps differs only by approximately 3 %. In the first column of

plots in figure 5.27, the impact of battery prices on hydropower volatility can be investigated at constant fuel price at the lowest level of 25 USD/MWh. When doubling the battery price from 50 to 100 USD/kWh, the number of ramps decreases by less than 3 %. But when doubling the battery price once again to 200 USD/kWh, the number of ramps increases by 20 % to N = 3300 in comparison to the initial state. There is obviously a turning point when considering the number of ramps N as a function of the battery price B for a constant fuel price of 25 USD/MWh. At fuel prices of 50 USD/MWh or 100 USD/MWh, the number of hydropower ramps decreases significantly, when increasing the battery price, as can be seen in the middle and the right column of the plots. The lowest number of ramps of around N = 1800 appears under the conditions of sub-scenario F4B4, meaning at the highest fuel and battery prices assumed here. As stated initially, there is no clear relation between the two price dimensions and the hydropower volatility.

One might assume intuitively, that a higher share of wind and photovoltaics in the energy mix leads to higher volatility of hydropower including more hydropower ramps. When comparing the results of scenario 1a "Base" for the composition of power generation by source, see figure 5.23 with the hydropower ramps, see figure 5.27, one cannot find evidence for this hypothesis. One can state, that to a certain degree the opposite is the case. The lowest number of ramps appears in sub-scenario F4B4, where wind and photovoltaics have a share of 69 % in total, whereas the highest number of ramps shows up for the sub-scenario with the lowest share of 54 %, see sub-scenario F1B4. Other scenario results are part of the explanation of the dynamic behavior of the hydropower generation. Besides the composition of power generation, important factors for hydropower behavior are the expansion of the transmission grid in between the regions and the installed battery capacity. For the sake of clarity, the most relevant numerical results for electricity generation, battery capacity, and transmission grid expansion are summarized in figure 5.28. According to these results, the most important factor to maintain moderate hydropower volatility is a capacitive expansion of the transmission grid. For all cases with increased transmission capacity in between the regions, the number of ramps was 20 % or lower compared to sub-scenarios without expansion. The transmission capacity is expanded in the sub-scenarios F2B2, F4B2, F2B4, and F4B4. One further finding is, that expansion leads to fewer ramps, but more ramps with a duration longer than 15 hours, see the scatter plots for the latter mentioned sub-scenarios in figure 5.27. These sub-scenarios have also in common, that the share of wind power is above 40 % in contrast to all other sub-scenario results. The generation profiles of wind power obviously favor the expansion of the transmission grids and require less short-term flexibility from hydropower.

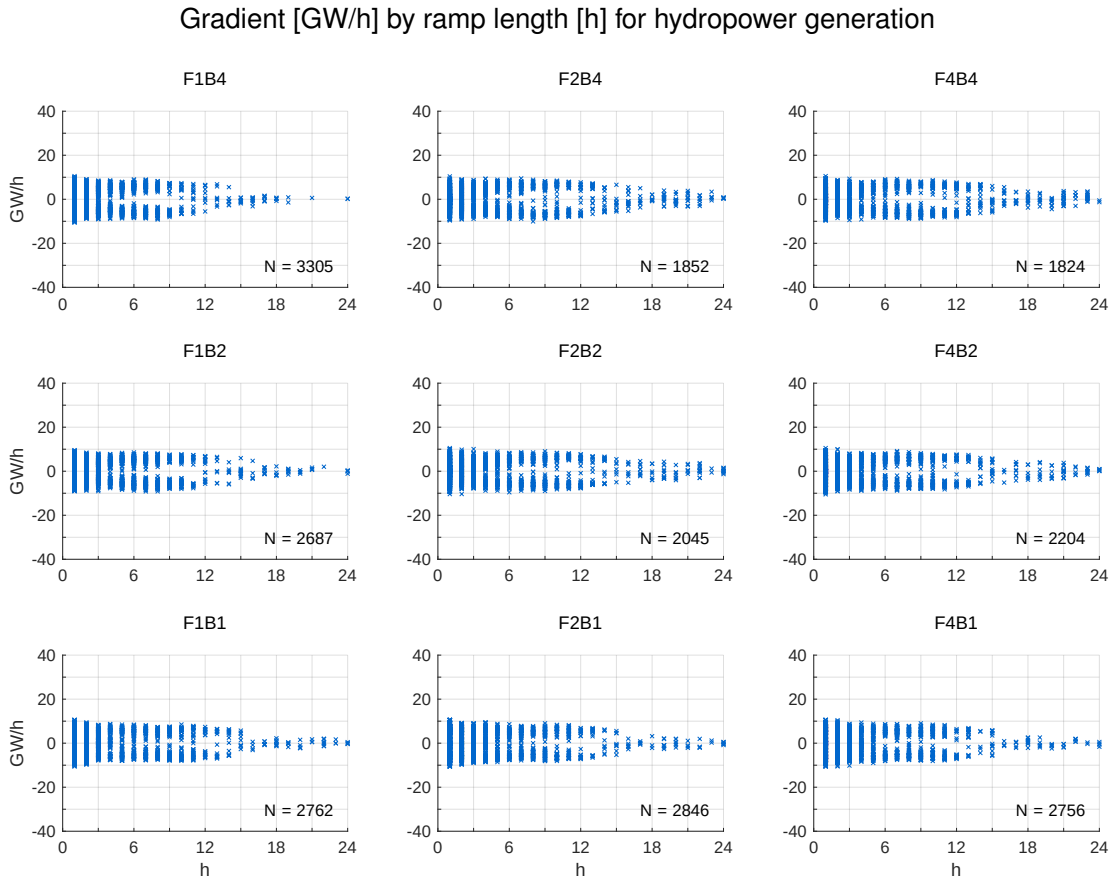

Figure 5.27: Scenario 1a "Base", scheme FxB

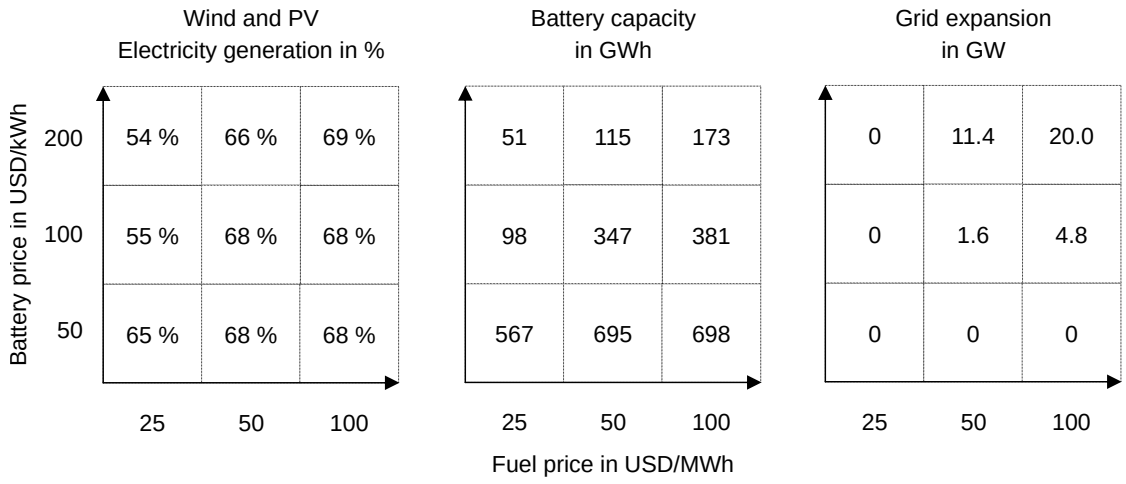

Figure 5.28: Summary of scenario 1a "Base" for wind, PV, battery, and transmission grid

The optimization results presented here show, that the availability of cost-effective batteries, see sub-scenarios in the lower third, leads to a share of photovoltaics in power generation of at least 30 %. A high proportion of photovoltaic electricity production requires day-night balancing. Both batteries and hydropower provide this short-term flexibility. That explains the high number of ramps in the hydropower profiles with a duration under 12 hours.
In the case of expensive batteries and cheap fuel, see sub-scenario F1B4, both thermal and hydropower provide the flexibility needed in an almost absence of batteries. This explains the highest number of ramps of more than 3300 per year in scenario 1a "Base".
In brief, the impact on hydropower volatility seen in the scenario results above can be summarized as follows:

1. High transmission capacities in between the regions, fewer hydropower ramps in total, but more ramps longer than 15 hours
2. High proportion of photovoltaic power generation, more ramps with shorter than 12 hours
3. Highest hydropower volatility in case of cheap fuel, expensive batteries, and without transmission capacity expansion

In scenario 1a "Base", the maximum change in power generation per time step has been limited to 10 %. Due to the definition of flexibility used here, see equation 5.10, that means for Brazil a maximum increase or decrease of hydropower generation of 10.51 GW per hour, since the total installed hydropower capacity is 105.1 GW. The value of 10 % is an assumption derived from the volatility of hydropower production in 2017. To investigate the impact of a lower or higher hydropower flexibility of 10 % the results of scenario 1b "Base" are presented below.

Scenario 1b "Base"

Scenario 1b "Base" uses the same assumptions as scenario 1a "Base", which is described above. Sub-scenario F1B1 of 1a and H010 of 1b are in detail the same, above all with the same assumption for flexibility of hydropower of 10 %. The other sub-scenarios of scenario 1b "Base" were calculated to investigate the impact of different hydropower flexibility, especially on optimal battery and transmission capacity. Each assumption for hydropower flexibility is indicated with the abbreviation for each sub-scenario. The short name H010 stands for the sub-scenario with the flexibility of 10 % based on the definition in equation 5.10, H001 for 1 %, H050 for 50 %, and so forth. The name of the scenario scheme is H100 in contrast to the scheme FxB presented above. The resulting plot is sorted in the order presented below, see figure 5.29. Hydropower flexibility increases from right-to-left and from top-to-bottom, starting at a minimum value of 1 % (H001) up to a maximum value of 100 % (H100).

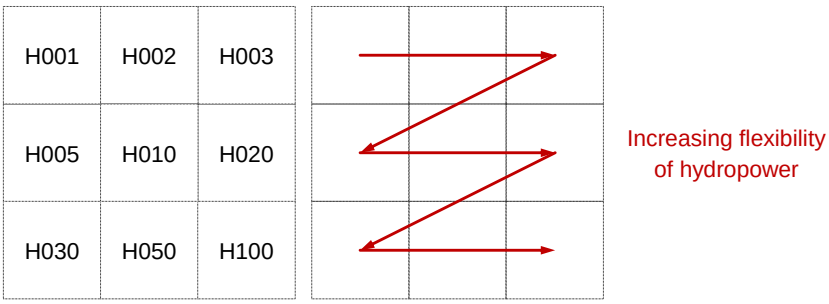

Figure 5.29: Scheme H100 for different flexibility of hydropower

The impact of varying hydropower flexibility on the energy mix is relatively low, as can be seen in the results for power generation by source figure A.24 in the appendix. In case of allowed variations of 5 % or less, one can observe shares of thermal power between 3.3 and 3.9 %, whereas 2.7 % in all sub-scenarios with the flexibility of hydropower of 10 % or more. In general, no share of any source differs more than 2 % compared to sub-scenario H010. A comparable summary can be drawn for the installed capacity by source, see figure A.30 in the appendix. Similarly, the transmission capacity is not expanded in any sub-scenario. In contrast to that, a remarkable influence on the results can be seen when the installed battery capacity is considered, see figure 5.30 below. At hydropower flexibility of 10 % in the sub-scenario H010, the optimization for the Brazilian electricity system delivers 567 GWh as cost-optimal battery storage capacity. The optimal battery storage capacity is with 746 GWh around 32 % more when assuming a possible change of power output by 1 % from one hour to another in relation to the installed hydropower. At 20 % flexibility, with 545 GWh around 4 % fewer battery storages are the cost-minimal result. A further increase of hydropower flexibility does not lead to any further significant reduction of necessary battery capacity. When assuming a possible change of hydropower output from 100 % to 0 % or the other way around within one hour, the installed battery capacity only goes down to 538 GWh or around 1 % less than a system with 20 % hydropower flexibility. Corresponding to these results, one can summarize that under the made assumptions and conditions, hydropower flexibility over 20 % is sufficient, and any further increase does not lead to significantly fewer battery storages. In addition, it is doubtful that flexibility well over 20 % can be reconciled with other uses of rivers than power generation. Excessive, short-term changes in the production of hydropower electricity could cause tidal waves, which could negatively affect human activities related to rivers and harm the habitats of plants and animals. Therefore, the impact of increased volatility of hydropower needs to be investigated in more detail. The ramp plots derived from the hydropower generation profiles for scenario 1b "Base" provide an insight into the hydropower flexibility found in the appendix, see figure A.48.

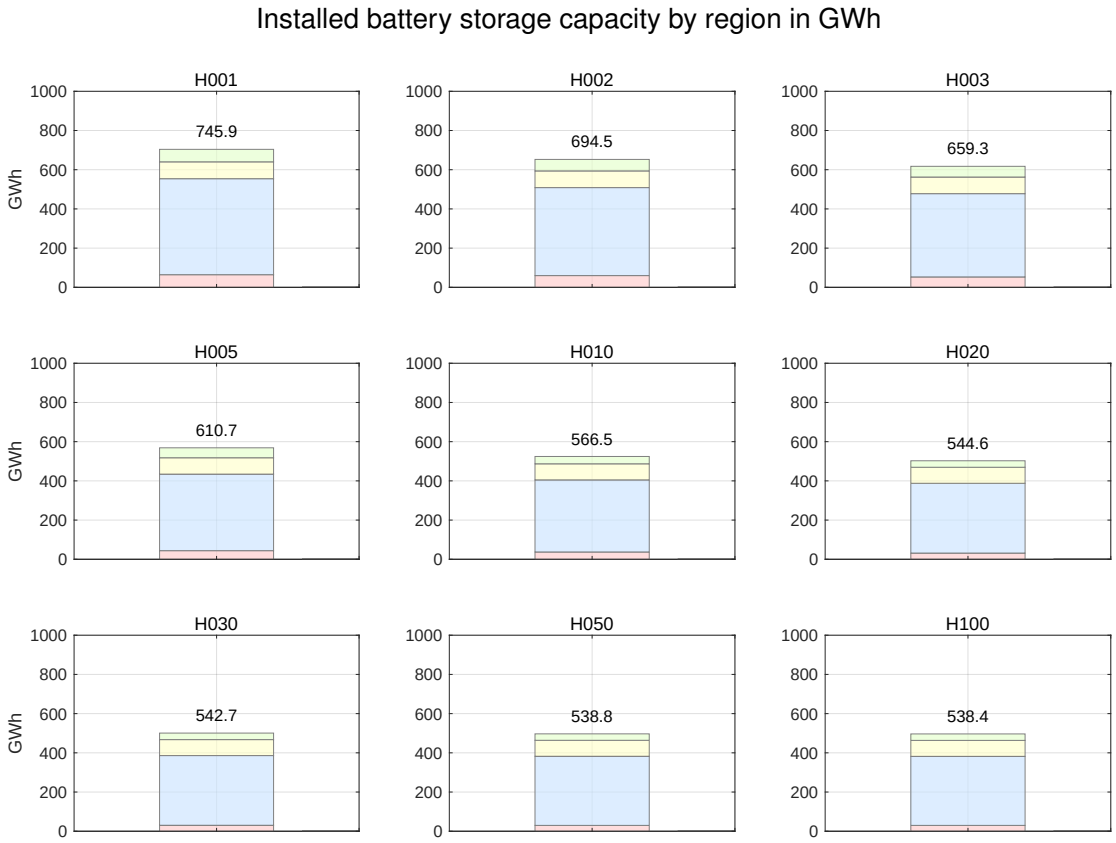

Figure 5.30: Scenario 1b "Base", scheme H100

Scenario 2a and 2b "Hydrogen"

To meet the goals for reducing carbon dioxide emissions, some energy fossil fuels such as jet fuel, marine diesel, or coke for steel production might be replaced by chemical energy carriers based on hydrogen produced by electrolysis. To investigate the impact of hydrogen production on the Brazilian electricity system, a constant load of 120 GW is added to the electricity demand time series of the Northeast region. The Northeast region is proposed here since three important characteristics are fulfilled. Firstly, it is sparsely populated in large parts, and secondly, it offers for both wind and solar power above-average full-load hours. The third characteristic which applies partly to the Northeast is related to the typical landscapes there. In comparison to Brazilian ecosystems like the Mata Atlântica or the Amazon rainforest, see figure 2.3, one can expect in the semi-arid, scrubland Caatinga fewer conflicts between photovoltaic parks, wind farms, and nature.
The electrical load of 120 GW was derived from the following consideration related to a possible hydrogen export to Germany. According to [133], the demand for hydrogen-based, synthetic fuels in Germany will be between 530 and 930 TWh in 2050. Domestic production at this scale in Germany will likely exceed spatial potentials. Therefore, the import of energy carriers is necessary to a certain degree, which could generate economic perspectives for hydrogen-producing countries. When assuming 500 TWh of hydrogen to be imported from Brazil to

Germany at an efficiency of 50 %, 1,000 TWh of electricity need to be produced in Brazil. This efficiency considers losses for electrolysis, hydrogen conversion into a transportable form, and propulsion energy for the transport itself. This leads to an electrolyzer capacity of almost 120 GW, running 8760 hours per year constantly. An amount of electricity in the same magnitude is needed when replacing 2016s whole Brazilian mineral oil demand of the transport sector with a hydrogen-based fuel, see figure 3.9 in section 3.2 of chapter 3. So not only an export opportunity might lead to the realization of one of the hydrogen scenarios sketched here.
Production of hydrogen with constant output might be a favorable operation mode for electrolyzers, but it leads to environmental and cost disadvantages in the system operation and its composition. With a view on the results for power generation by source, see figure A.22 in the appendix, one can see a significantly increased use of thermal power in comparison to scenario 1a "Base". If hydrogen production relies largely on thermal power generation based on fossil fuels, that counteracts the initial objective of hydrogen usage to reduce greenhouse gas emissions. The battery storage capacity reaches depending on the sub-scenario up to 2,663 GWh, which is more than a factor of three more compared to 1a "Base", see figure A.34 in the appendix. Such a large-scale application of battery storage likely antagonize sustainability goals in terms of used materials. A sustainability assessment of battery materials in the context of electric vehicles is conducted for example in [134]. Furthermore, there are surely more cost-effective solutions described in the following scenario 3, "Green hydrogen." Scenario 2b displays the results for hydrogen production with 120 GW constant load in the Northeast with varying flexibility of hydropower depending on the sub-scenario, see appendix.

Scenario 3a and 3b "Green hydrogen"

As described above, hydrogen production with a constant electrical load of 120 GW results either in significantly higher use of thermal power or in a larger increase necessity for battery storage capacity. Scenario 3 "Green hydrogen" is designed to mitigate these less favorable outcomes. Green hydrogen indicates here, that hydrogen is mainly produced by renewable energies. The chosen approach to accomplish this here is the following. From sub-scenario F1B1 as part of scenario 2a "Hydrogen", the time series of thermal power generation in the Northeast was taken and subtracted from the constant load of 120 GW. The resulting load curve of the electrolyzers in scenario 3 "Green hydrogen," correlates temporally with the production of wind and sun predominantly. Figure 5.31 shows a direct comparison of the load curves displayed as the red line of scenarios 1, 2, and 3. All production profiles are taken from sub-scenario F1B1. Table 5.8 depicts the key figures for electricity demand and hydrogen production in the scenarios discussed. Most importantly, the electricity used for hydrogen production in scenario 3 "Green hydrogen", is with 787 TWh 25 % lower than in scenario 2 "Hydrogen" with 1,051 TWh. This reduction leads to dramatically lower needs for photovoltaic and battery storage capacity by more than 50 %, see figure A.29 and figure A.35 in the appendix. Accordingly, the expansion of the transmission capacity between the regions is a way lower or even not necessary, when the hydrogen production follows the supply of wind and sun, see A.53. In this investigation, no clear statement is made about the hydrogen output under these conditions. The dependency of efficiency of electrolyzers with the assumed high volatile production profile can be a subject of further research.

Table 5.8: Electricity demand in the Northeast by scenario

	1a "Base"	2a "Hydrogen"	3a "Green Hydrogen"
Total demand in Northeast	178 TWh	1,230 TWh	966 TWh
Demand for H_2 production	0 TWh	1,051 TWh	787 TWh
H_2 production in relation to 2a	0 %	100 %	75 %

5.2.4 Comparison of space requirements

This section covers the space needed for wind farms and solar arrays since space requirements affect the feasibility of a scenario. For the sake of conciseness, the focus is on extreme scenario outcomes. Figure 5.32 shows hypothetical areas needed when concentrating all wind energy converters and photovoltaic arrays in sparsely populated regions in the Northeast with good meteorological conditions for both. In reality, the power generators are likely distributed over the country and located much closer to consumption centers. The following results consider 10 MW of installed wind power per km² and 100 MW per km² for the case of photovoltaics. The authors of [135] recommend a distance between two wind turbines of the three to five-fold of the rotor diameter, which leads roughly to the named value. 100 MW rated photovoltaic power per km² is the product of an assumed peak solar radiation of 1 kW/m² multiplied with an overall efficiency of 10 %. This efficiency summarizes all possible losses and includes the fact that an area is not entirely covered with solar panels. Both densities are likely conservative estimations. Subsequently, higher values per km² will lead to less required space. In the same way, roof-top or floating systems and offshore wind turbines will reduce installations on the plain land. As indicated simplified in figure 5.32, wind parks and solar farms can use the same land so that the area needed does not count separately. Therefore, the provided results in table 5.9 express upper estimates for space requirements.

Table 5.9 shows under the assumptions described above the sub-scenarios with extreme results for photovoltaic arrays or wind farms, respectively. One has to remember that Brazil's total electricity production W_{el} was at 547 TWh in 2017, whereas the scenarios here start at a power production of 1,135 TWh and reach up to 2,469 TWh. It is noteworthy here that the W_{el} includes all sources of electricity, not only wind and sun. The area A needed for photovoltaic systems ranges from 950 km² up to 4,400 km². To make these values more understandable, the column next to the calculated area show the edge length l of hypothetical squares. Analogous to that, the space required for wind farms ranges from 8,000 km² up to 43,000 km² in rounded values. Sub-scenario F2B4 of the "2a Hydrogen" outlines the highest land requirements of 45,000 km² counted the space for wind turbines and PV together. The top map shows the hypothetical squares in a selected section in the Northeast. The bottom map shows this map section in the context of the whole country. Remarkably, even the highest land requirements calculated here are lower than the acreage of sugarcane of the year 2016 for ethanol production. The sugarcane acreage for ethanol was 50,782 km² which produced 160 TWh of fuel, see figure 3.20 in chapter 3. A shift from sugarcane-based ethanol towards electric propulsion would make land use much more energy efficient. Moreover, environmental benefits are possible from such a transition. Most of the sugarcane acreage is located in

the Southeast region [59], where the natural vegetation was the Atlantic rain forest called Mata Atlântica. When assuming that the mobility sector does not need sugarcane-based fuel anymore, the natural vegetation could be reestablished by reforestation of former sugarcane acreage.

Table 5.9: Estimated space requirement for wind and photovoltaics by selected scenario

				PV		Wind	
No.	Name	Sub-scen.	W_{el} in TWh	A in km²	l in km	A in km²	l in km
1a	Base	F4B1	1,135	2,400	49	8,000	89
1a	Base	F2B4	1,177	950	31	18,500	136
2a	Hydrogen	F2B4	2,469	1,800	42	43,000	207
3a	Green hydr.	F4B1	1,992	4,400	66	21,300	146

5.3 Summary of model-based Outlook

This chapter provided an overview of the Brazilian electricity system of around 2020. The linear optimization model was calibrated with generation and storage capacities from 2017, with time series for hydropower and demand from the same year. The mean profiles for wind and sun were calculated from data covering the years 2001 to 2010. All data were applied in hourly resolution for one whole year and are unique for four regions. The Brazilian grid operator ONS structured the country into the regions the North, Northeast, Central-West and Southeast, and South. The model delivered a deviation of around 1 % compared to the real values for electricity generation of 2017 at around 550 TWh, which justifies the credibility of the outlook.

The scenario "1a Base" for the outlook assumed a total electricity demand of 1,100 TWh, including sub-scenarios to investigate the impact of a wide range for fuel and battery prices. High fuel prices might originate from oil market conditions and a carbon tax implementation. Key findings of this scenario are that wind and photovoltaic power contribute more than 50 % to the Brazilian future electricity production in all sub-scenarios. Under these conditions, existing thermal power plants and hydroelectricity ensure the supply during calm and darkness. Cheap batteries support PV penetration, whereas expensive fuel and batteries expand transmission capacities within the regions. Assuming low prices for fuel and costly batteries, the market for the latter almost disappears. In this sub-scenario, existing thermal power plants and hydroelectricity ensure the supply during calm and darkness.

Scenarios 2 and 3 investigate the impact of additional electricity demand in the Northeast between 787 TWh and 1,051 TWh for hydrogen production. Hydrogen can be used for synthetic fuels or direct application in Brazil or export. Scenario 2 assumes an additional constant load of 120 GW, which leads to an enormous increase in thermal power production or battery capacity. Both outcomes would likely thwart the sustainability goals of hydrogen use. Therefore, scenario 3 was designed, where the electricity demand for hydrogen production more or less follows the generation profile of renewable sources. At only 25 % less electricity used for hydrogen

production, the need for battery and generation capacities is far over proportional lower.

Since wind and solar farms require considerable space, selected scenarios are compared and drawn simplified as squares on a map. The most extreme case assumes a power production with around 2,500 TWh of almost five times higher than 2017 but with 43 thousand square kilometers less space requirement than the sugarcane acreage of 2015 at 51 thousand square kilometers, which delivers 160 TWh of ethanol. All other scenarios calculated in this work show a significantly lower need for space.

Not investigated in this work was the impact of different meteorological conditions, which would reveal how robust these results are in the context of climate variations. It is also worth considering the influence of flexible loads as described in the previous chapter. In every case, the thermal storage capacities on the consumer side would further reduce the demand for batteries, which likely makes futures scenarios possible without batteries at all. Furthermore, it is necessary to assess in detail on a regional level whether rivers and hydropower cascades can handle the upcoming flexibility needs arising with shares over 50 % of wind and sun in the Brazilian electricity mix.

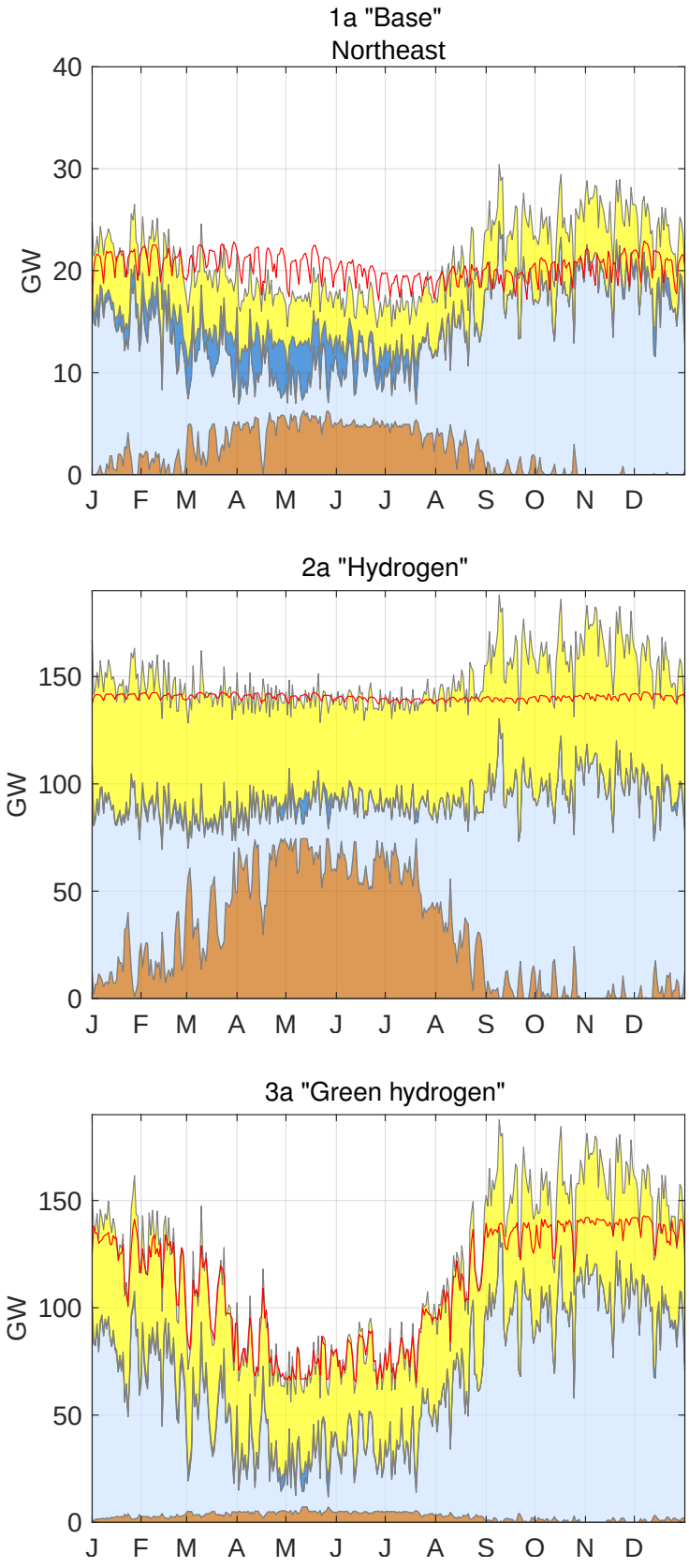

Figure 5.31: Load (red) and power generation by source in Northeast for sub-scenario F1B1

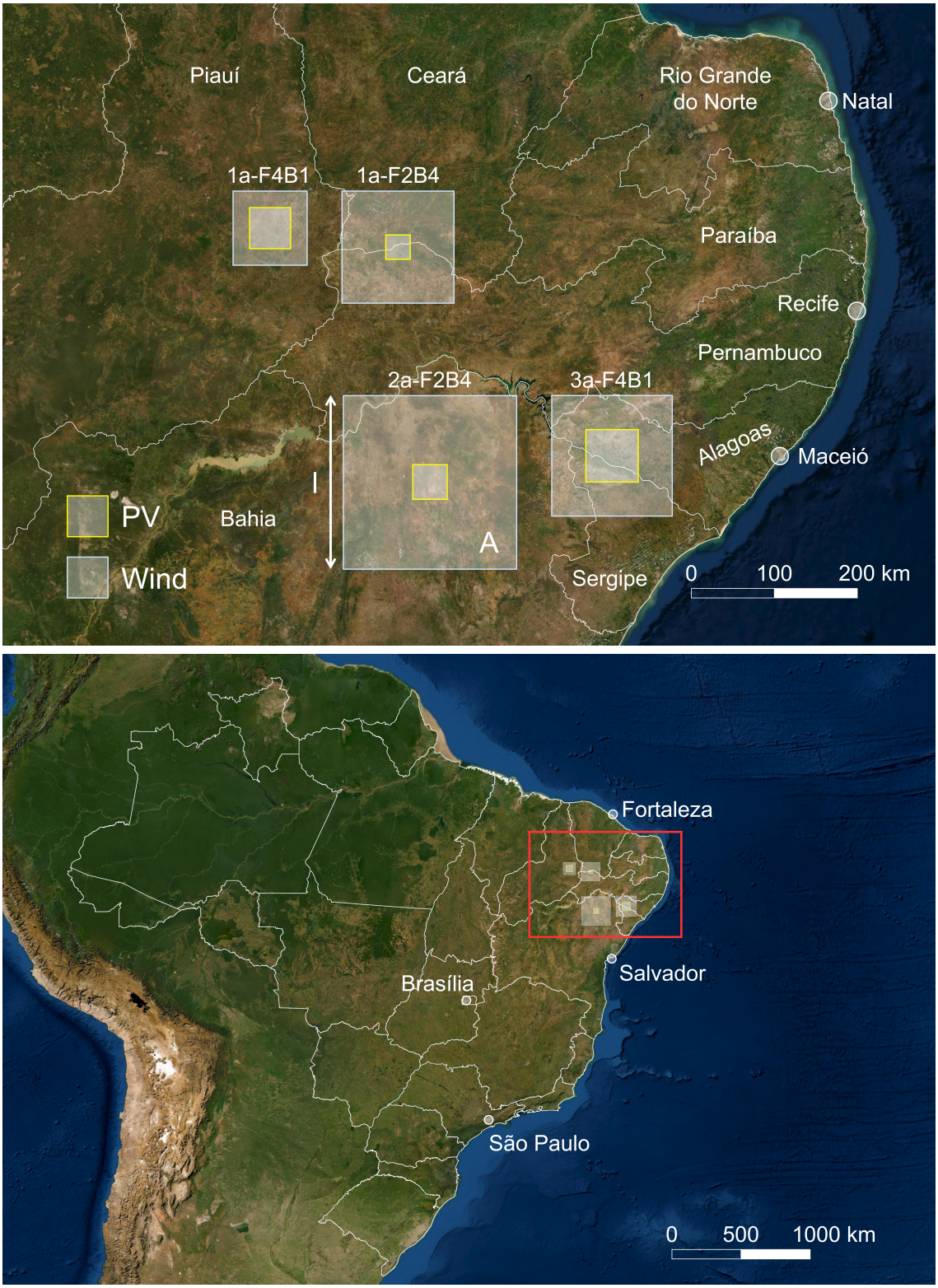

Figure 5.32: Space requirement for wind and photovoltaics for selected scenarios

Chapter 6

Summary

The key findings of this work originate predominantly from the model-based outlook in chapter 5. Assuming ongoing trends in demand, wind and photovoltaic power together will contribute the majority to Brazil's electricity generation in the following decades. The total market size for grid-connected batteries is highly dependent on the price relation between fossil fuel and battery storage capacity. At low fuel prices and expensive batteries, integrating fluctuating generation at a total demand of 1,100 TWh is probably possible mainly by using existing hydropower reservoirs without additional large-scale storage capacities. Since solar and wind power integration leads to higher volatility in hydropower production, further investigations are relevant to evaluate the impact on dam outflows and their possible negative effects. Depending on the scenario, the total battery capacity can also reach several one-digit terawatt hours, which is still magnitudes below the storage capacity of the existing hydropower reservoirs of more than 211 TWh in 2017. Wind farms and solar arrays will need considerable land of several thousand square kilometers. However, the spatial requirements of all calculated scenarios up to a total demand of 2,500 TWh are lower than the sugarcane acreage of 2015 for 160 TWh fuel production. In contrast to sugarcane, solar and wind power can be harvested in regions with less conflicts with other types of land-use and nature. Moreover, the substitution of sugarcane-based fuel would provide the potential for reforestation, for example.

Chapter 4 provided a concept for the dimensioning and economic evaluation of distributed energy systems focusing on the residential sector based on time series. Ambient conditions, statistical possession, and usage of specific devices determined the load profiles. The load profiles show plausible temporal, seasonal, and regional characteristics for each Brazilian macroregion but should be validated in future investigations. The economic evaluation revealed that the Brazilian net metering system makes distributed storage economically unattractive. When assuming the elimination of net metering, distributed integration becomes economically relevant. For that reason, battery and thermal storage technologies on the consumer side were considered to increase the self-consumption rate. The results revealed remarkable regional characteristics as well as paths to reduce needed battery capacities. In the absence of net metering, economically reasonable storage application lead to self-consumption rates from 70 % in the South to more than 90 % in the others. Self-consumption rates above 50 % are possible in all regions when considering only thermal storage for hot water and air conditioning. Thermal storage can be a more attractive low-tech solution, helping to save precious materials

for applications like electric vehicles where batteries are difficult to be substituted. Flexible thermal and hydropower production, expansion of transmission capacities, and thermal storage on the consumer side are the main factors to reduce batteries.

Both market conditions and technological developments form an attractive environment for a shift towards described scenarios, leading to considerable investments in the renewable energy sector. Addressing Brazilian challenges, including corruption and bureaucracy described in the final section of chapter 2 would facilitate necessary investments. One further important field of research arising from the results presented here is the circular economy in wind turbines, photovoltaic systems, batteries, and additional system components. Before transforming the energy system towards the scenarios presented in this work, solutions for the recycling of technical plants on a gigawatt-scale are essential for sustainable development.

Acknowledgements

This work was made possible by funding the Bavarian Ministry of Economic Affairs and the Bavarian University Center for Latin America (BAYLAT). Many thanks to Thomas Hamacher for the opportunity to work as a researcher and lecturer at the Technical University of Munich for the scientific support, inspiration, motivation, and fruitful discussions. In the same way, thanks to Gilberto de Martino Jannuzzi for the instructive time at the Federal University of Campinas (UNICAMP) in São Paulo. I am also really grateful for my colleagues in Brazil and Germany, namely Anahi Molar-Cruz, Manuella Pereira, Magdalena Stüber, Dennis Atabay, Matthias Huber, Humberto Jantim Neto, Johannes Jungwirth, Johannes Dorfner, Philipp Kuhn, Philipp Tünte, Rodolfo Damásio de Castro, Ricardo Rüther, Roberto Lambertz for their enrichment of my work in various ways. Thanks to the Technical University of Munich for providing me with an excellent research environment, including free access to advanced software used in this work, such as MATLAB, ArcGIS, and Gurobi. Most importantly, I want to thank my family and friends for their emotional support and patience.

Appendix A

Appendix

A1: Auxiliary calculations

This chapter provides the calculation methods of below mentioned quantities.

A1.1 Saturation vapor pressure

Due to equation 21 in [136], the saturation vapor pressure p_{sw} can be approximated for the temperature range $-40\,^{\circ}\mathrm{C} < t_{\mathrm{A}} < 50\,^{\circ}\mathrm{C}$. This range covers all occurring outside temperatures in Brazil. Relevant time series for ambient temperature t_{A} can be gathered from the INMET data, see [16].

$$p_{\mathrm{sw}}(t_{\mathrm{A}}) = K_1 \cdot e^{\frac{K_2 \cdot t_{\mathrm{A}}}{K_3 + t_{\mathrm{A}}}} \tag{A.1}$$

K_1, K_2 and K_3 are time invariant constants in equation A.1, whereas can t_{A} depend on time and location. The values for the constants can be found in table A.1.

Table A.1: Constants for approximation of saturation vapor pressure

Constant	Value	Unit
K_1	61.10	Pa
K_2	17.62	-
K_3	243.04	°C

A1.2 Dew point

The dew point τ is the temperature to which humid air must be cooled to become saturated with water vapor. The relative humidity $\varphi = 100\ \%$ at the dew point. Further cooling below the dew point leads to condensation of liquid water and is therefore used to dehumidify air to reach a specific water content. Referring to [137], the temperature τ at the dew point can be approximated with the equation below.

$$\tau(\varphi, t) = K_3 \cdot \frac{\frac{K_2 \cdot t}{K_3 + t} + \ln \varphi}{\frac{K_2 \cdot t}{K_3 + t} - \ln \varphi} \tag{A.2}$$

Table A.1 contains the constants K_2 and K_3. The equation for approximation of the dew point temperature can be applied also in a range from -40 °C to 50 °C and is therefore valid for meteorological conditions occurring on ground-level in Brazil.

A1.3 Absolute humidity

The absolute humidity X in kg water per kg dry air can be calculated corresponding to p. 97 in [138] by the following equation:

$$X = \frac{M_{\mathrm{w}}}{M_{\mathrm{air}}} \cdot \frac{p_{\mathrm{sw}}}{p/\varphi - p_{\mathrm{sw}}} = 0.622 \cdot \frac{p_{\mathrm{sw}}}{p/\varphi - p_{\mathrm{sw}}} \; \frac{\mathrm{kg\ w}}{\mathrm{kg\ air}} \tag{A.3}$$

The constant molar masses of water $M_{\mathrm{w}} = 18.015$ kg/kmol and air $M_{\mathrm{air}} = 28.963$ kg/kmol can be summarized to 0.622 kg water per kg dry air. Equation A.1 can be applied to get the saturated water pressure p_{sw}. The total pressure p and the relative humidity φ can be gathered from meteorological data.

A1.4 Parameters for air conditioning

Table A.2: Set points and switch-on temperatures for air conditioning

Property	Symbol	Value
Cooling mode		
Set point temperature	t_{c}	20 °C
Set point humidity	φ_{c}	50 %
Switch-on temperature	$t_{\mathrm{AC,on}}$	24 °C
Heating mode		
Set point temperature	t_{c}	40 °C
Switch-on temperature	$t_{\mathrm{H,on}}$	16 °C

A1.5 Results for storage dimensioning

The table A.3 contains essential numbers for the derivation of storage capacities of section 4.4, such as generation and demand of electricity, the peak capacity of photovoltaics, and storage capacities to cover an average day. The electricity amount W_{el} per region equals the sum of normalized profiles, see section 4.3.5. Since the photovoltaic generators were sized to generate exactly the annual demand for electricity, W_{el} means both the generation and demand. Assuming the profiles to be representative for each specific region, the values can be used for estimating storage requirements for distributed integration. Under the presented assumptions, the self-consumption ratios s shown in figure 4.8 for the case "Battery only" can be reached. Those self-consumption ratios s displayed in figure 4.10 consider besides batteries, thermal storage for hot water and air conditioning. The self-consumption ratios s are summarized and listed in the table A.4. For comparison, the first column of table A.4 contains the self-consumption ratios without using distributed storage. The subscript "e" in table A.3 for the capacity of thermal storages in kWh_e indicate, that this is the equivalent electricity which can be stored. The corresponding thermal capacity can be different. In case of a hot water storage, the thermal storage capacity would be almost the same like for electricity,

since conversion from electricity to heat can be achieved at very low energy losses. Electrical resistance heating is a common technology for that. To determine the thermal storage capacity of a cold storage for air conditioning systems, the thermal capacity would be significantly higher, because the coefficient of performance COP has to be taken into account.

Table A.3: Demand, generation and storage capacities

	Gen. & dem.		Battery only	All storage types		
	W_{el}	P_{PV}	B	B	AC	H
	kWh	kW_p	kWh	kWh	kWh_e	kWh_e
North	3,314	1.62	6.1	3.2	2.8	0.1
Northeast	2,539	1.20	4.1	2.5	1.0	0.6
Central-West	2,559	1.25	4.1	2.2	0.5	1.5
Southeast	2,678	1.44	4.4	2.7	0.3	1.5
South	2,198	1.31	4.2	1.6	1.4	1.3

Table A.4: Self-consumption ratios s

	Without storage	Battery only	All storage types
	%	%	%
North	33	91	84
Northeast	40	91	83
Central-West	41	91	84
Southeast	40	92	85
South	30	78	70

A1.6 Calculation of LCOE

The calculation method for the levelized cost of electricity (LCOE) is derived from the net present value (NPV) of an investment. More background about the net present value is provided on p. 49 ff. in [139]. In case of the investment in a photovoltaic system for example, the cash flow can be considered as the value of the electricity $p_{\mathrm{el}} \cdot W_{\mathrm{el}}$ produced by the solar generator within one year. The photovoltaic system has a period of use of T and the discount rate i is the return of an investment with similar risk.

$$\mathrm{NPV} = -I_0 + \sum_{t=1}^{T} \frac{p_{\mathrm{el}} \cdot W_{\mathrm{el}}}{(1+i)^t} \tag{A.4}$$

Assuming constant interest rates i over the investment period T, the series can be rewritten by introducing the factor for the annuity value $\mathrm{ANF}(i, T)$.

$$\frac{1}{(1+i)^t} = \frac{(1+i)^T - 1}{(1+i)^T \cdot i} = \frac{1}{\mathrm{ANF}(i, T)} \tag{A.5}$$

After setting the net present to zero, the electricity price p_{el} is just cost covering and represents therefore the levelized cost of electricity (LCOE). In this formulation for every year the same cash flow is considered.

$$\mathrm{NPV} = -I_0 + p_{\mathrm{el}} \cdot W_{\mathrm{el}} \cdot \frac{(1+i)^T - 1}{(1+i)^T \cdot i} \stackrel{!}{=} 0 \tag{A.6}$$

$$\rightarrow \mathrm{LCOE} = \frac{I_0 \cdot \mathrm{ANF}(i,T)}{W_{\mathrm{el}}} \tag{A.7}$$

Further information about levelized cost of electricity of renewable electricity sources can be found on p. 29 ff. in [109].

A1.7 Calculation of wind power from wind time series

Wind power generated by a wind turbine from measured wind time series can be calculated in the following steps.

1. Logarithmic wind profile: The equation below allows the calculation of the wind speed $v(z)$ in a certain height z depending on the wind speed v_{m} measured at the height z_{m}, see p. 575 ff. in [140].

$$v(z) = v_{\mathrm{m}} \cdot \frac{\ln {}^{z}/_{z_0}}{\ln {}^{z_{\mathrm{m}}}/_{z_0}} \tag{A.8}$$

The parameter $z_0 = 0.1\ \mathrm{m}$ assuming a cropland like environment permeated by bushes, small forests and some buildings. The wind speed was measured by INMET [16] at a height of $z_{\mathrm{m}} = 10\ \mathrm{m}$. For the rotor hub height $z = 100\ \mathrm{m}$ was chosen referring to the growth trend of recent years, see p. 26 in [126]. The calculation method is illustrated in the top diagrams in figure A.1.

2. Performance curve of a wind energy turbine: The power output of a wind turbine depending on the wind speed can be calculated by taking into account the performance curve of this turbine. The performance curve applied here was derived from a Enercon E-126, which is a wind turbine model of recent state of art, see [141]. Its specifications are above the market average, see [126]. Therefore, this model is assumed to be representative for wind turbines in upcoming years.

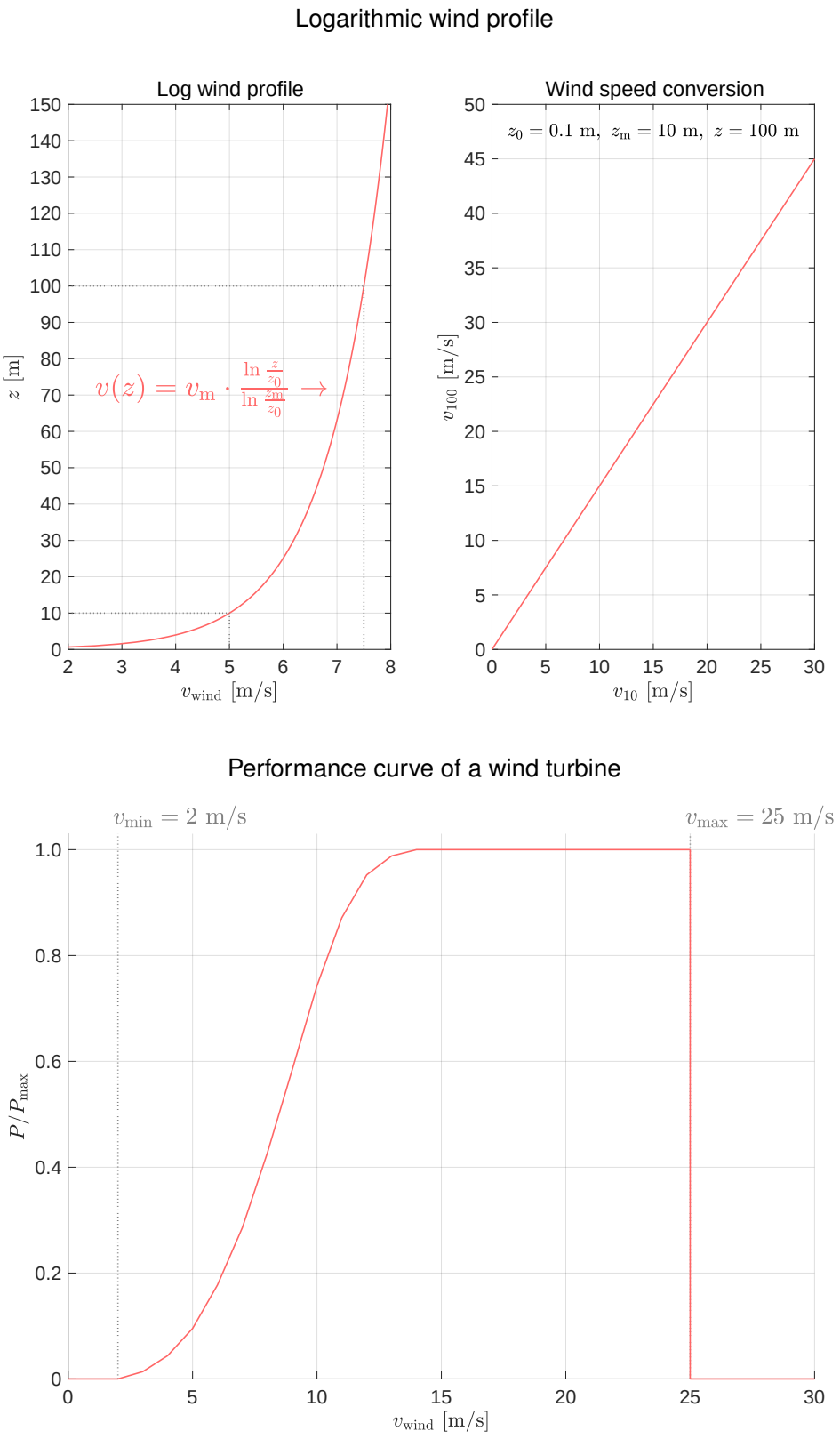

Figure A.1: Conversion of wind time series to wind power

A2: Reservoirs

A2.1 Data availability

Table A.5 contains an overview of the data availability of hydropower plants. The system for georeferenced information "SIGEL" *(Sistema de Informações Georreferenciadas do Setor Elétrico)* provided by ANEEL, see [123], contains in total 489 hydropower plants. However, the estimation of every reservoir's storage capacity does not rely on all data sets for several reasons. These reasons are explained below. Please note, the model-based outlook conducted in section 5.2 uses the aggregated storage capacities by region of table 5.3 as input data. The estimations presented here are not used for the system optimization in 5.2.

Table A.5: Data availability for Brazilian hydropower plants

Property	Unit	Available data sets	Share
Installed capacity	kW	489	100 %
Minimum flow rate	m^3/s	11	2 %
Efficiency of turbine	%	15	3 %
Efficiency of generator	%	15	3 %
Full maximum level	m	179	37 %
Maximum level	m	384	79 %
Minimum level	m	35	7 %
Downstream level	m	381	78 %
Nominal gross head	m	383	78 %
Area at maximum level	km^2	452	92 %
Area at minimum level	km^2	10	2 %
Area of drainage basin	km^2	301	62 %
Volume of reservoir at maximum level	km^3	155	32 %
Volume of reservoir at mimimum level	km^3	137	28 %

A2.2 Estimation of reservoir level difference

Incomplete data require the estimation of differences between the maximum level and minimum level of each reservoir. The maximum level in meters above sea level is known for 79 % of the reservoirs. The minimum level is also necessary to calculate the level difference, but only 7 % of the data sets for reservoirs had a non-zero value. Zero as the minimum level is implausible because no reservoir discharges itself down to sea level. However, considering the N = 35 data sets out of 489, where both maximum and minimum levels are available, one can calculate the difference. This difference of maximum and minimum reservoir levels is illustrated in figure A.2. These results show that even most of them are not applicable for determining the reservoir's storage capacity. Notable reasons:

- No negative difference possible, because the maximum level cannot be lower than the minimum-
- Equal levels are not typical for a reservoir-
- Lowering the level of a lake for several hundred meters is very unlikely. Therefore the calculated difference of 756 meters is implausible.

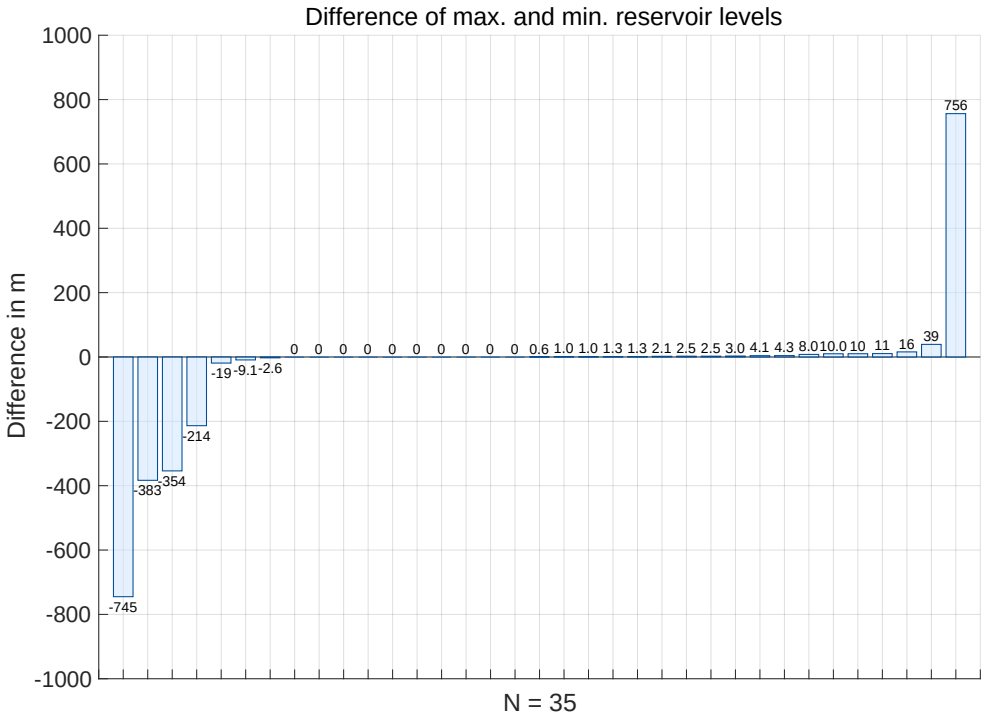

Figure A.2: Implausible ratio of reservoir area to installed capacity

A2.3 Implausible ratio of reservoir area to installed capacity

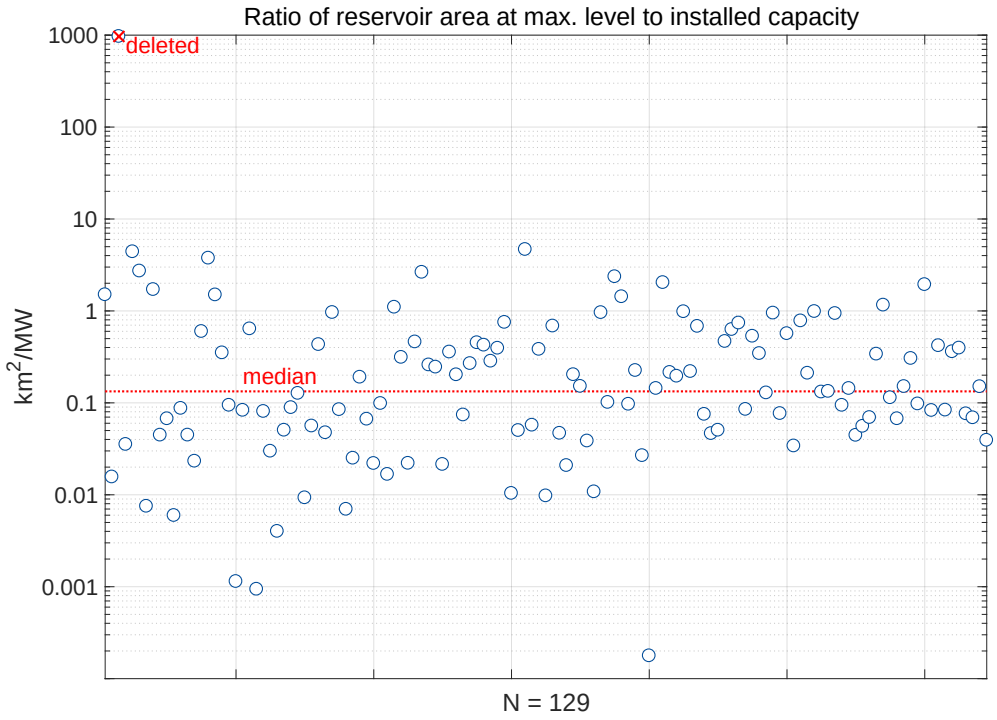

Figure A.3: Implausible ratio of reservoir area to installed capacity

A2.4 Implausible ratio of reservoir volume to installed capacity

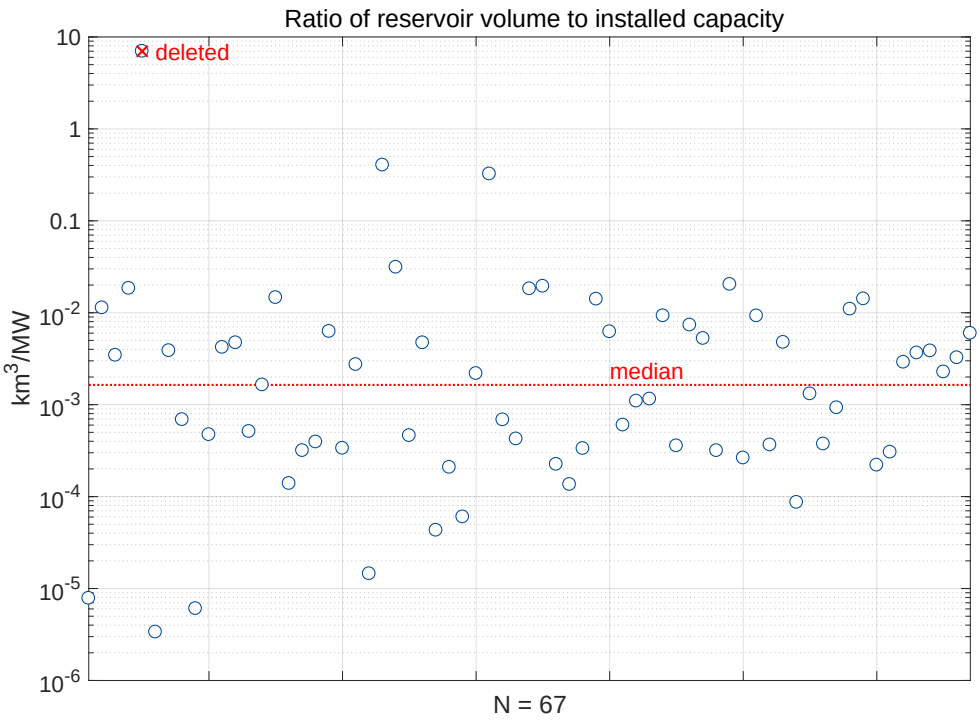

Figure A.4: Implausible ratio of reservoir volume to installed capacity

A2.5 Estimation of reservoir specific storage capacity

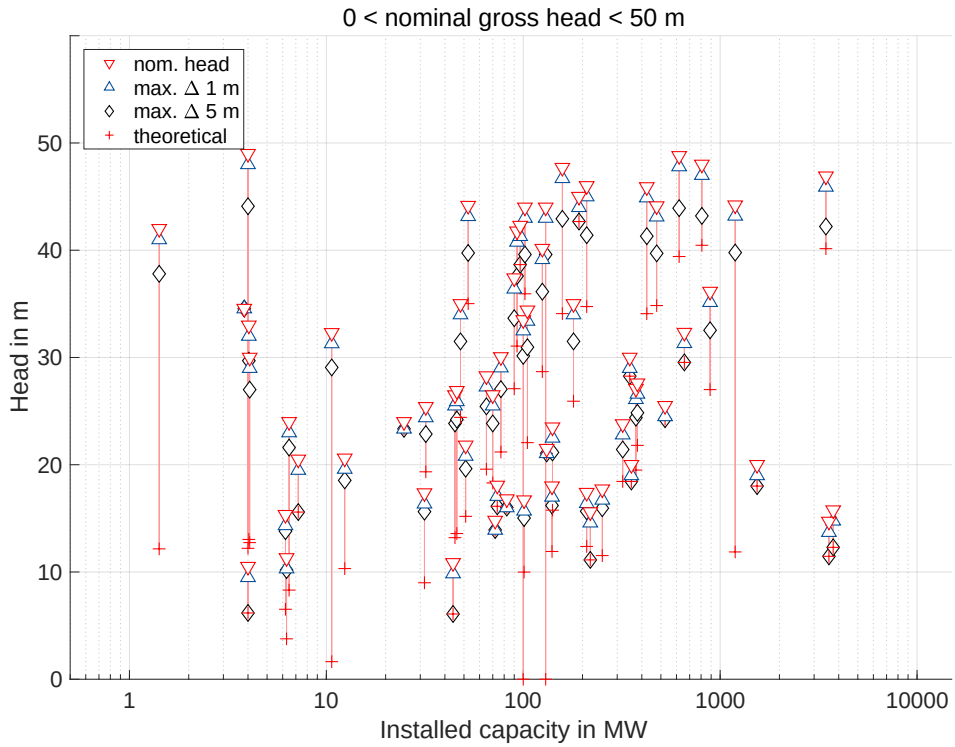

Figure A.5: Hydropower plants (head < 50 m)

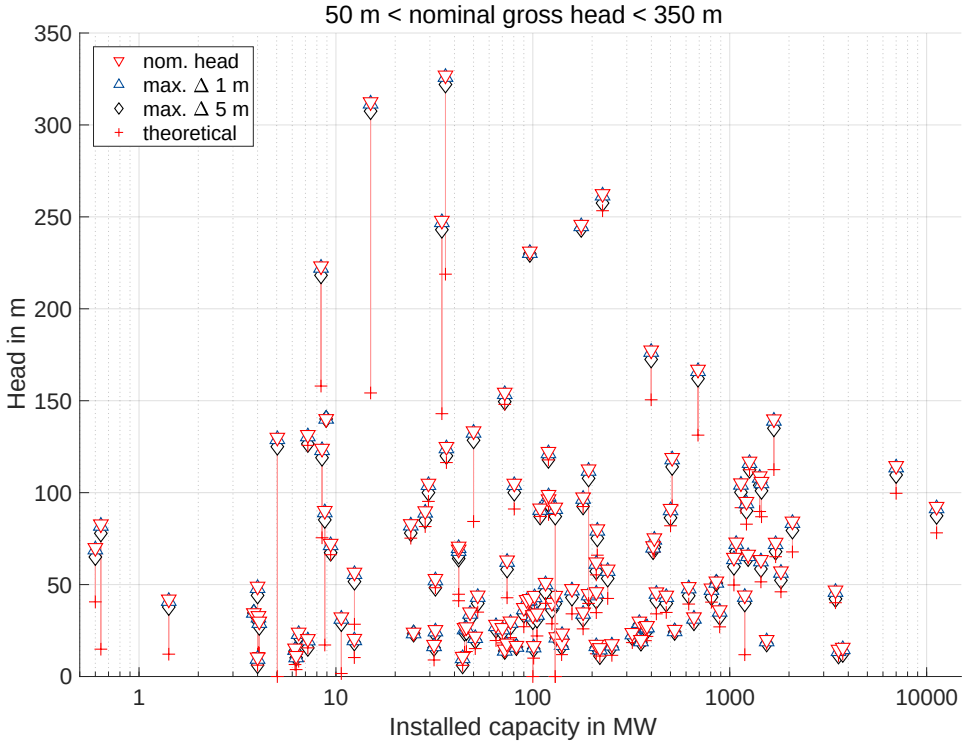

Figure A.6: Hydropower plants (50 m < head < 350 m)

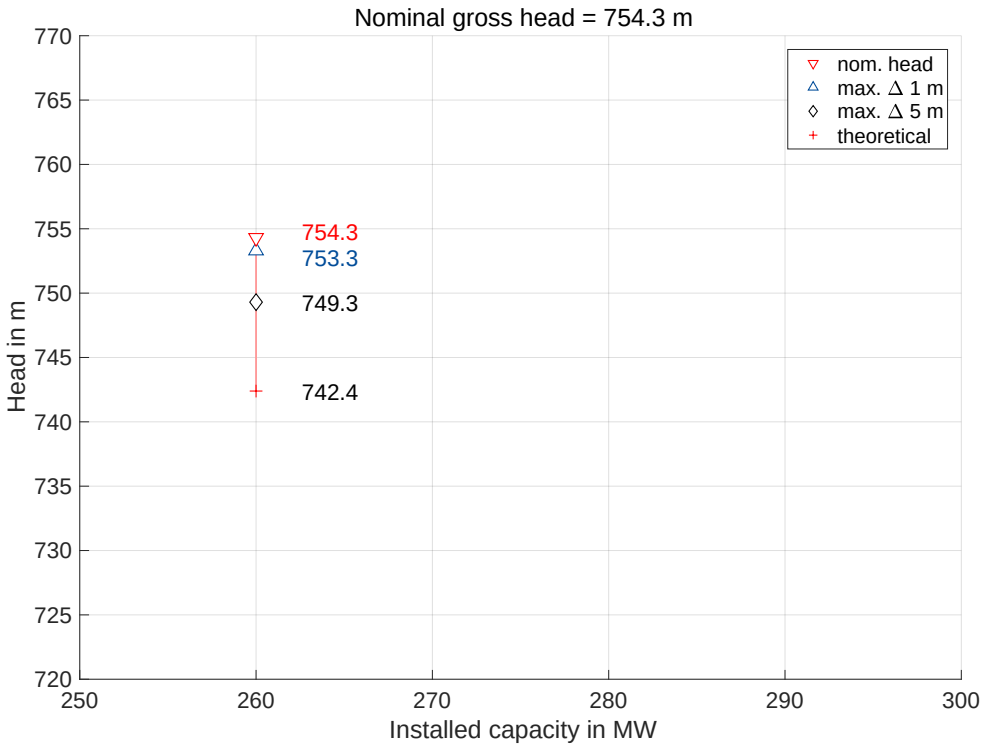

Figure A.7: Hydropower plants (head = 754 m)

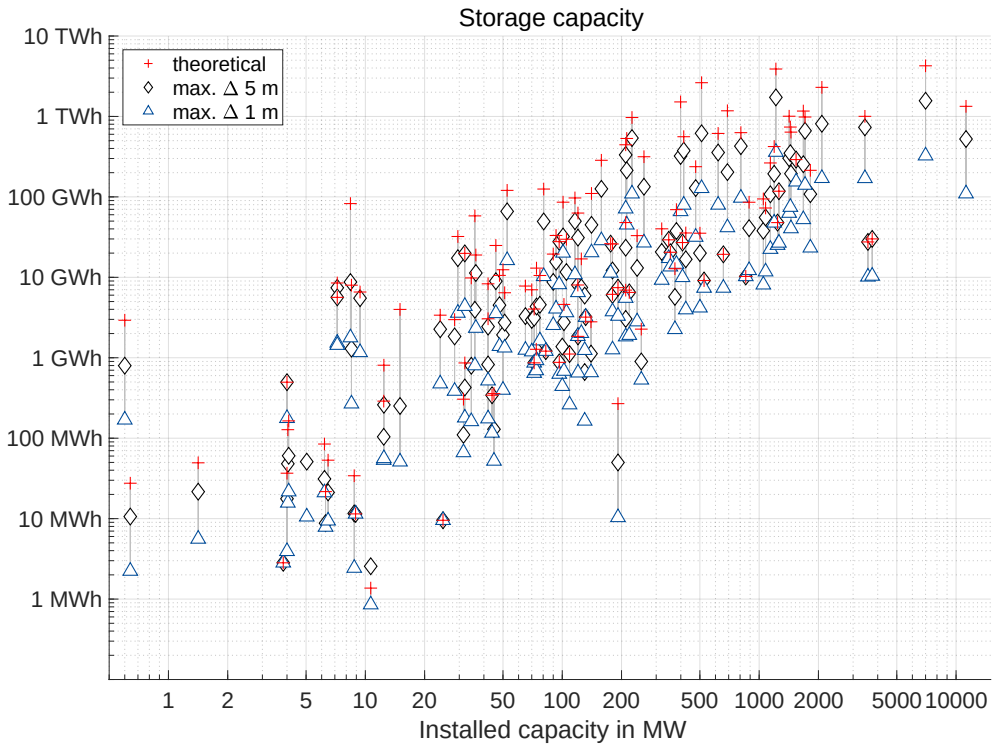

Figure A.8: Storage capacity by installed power

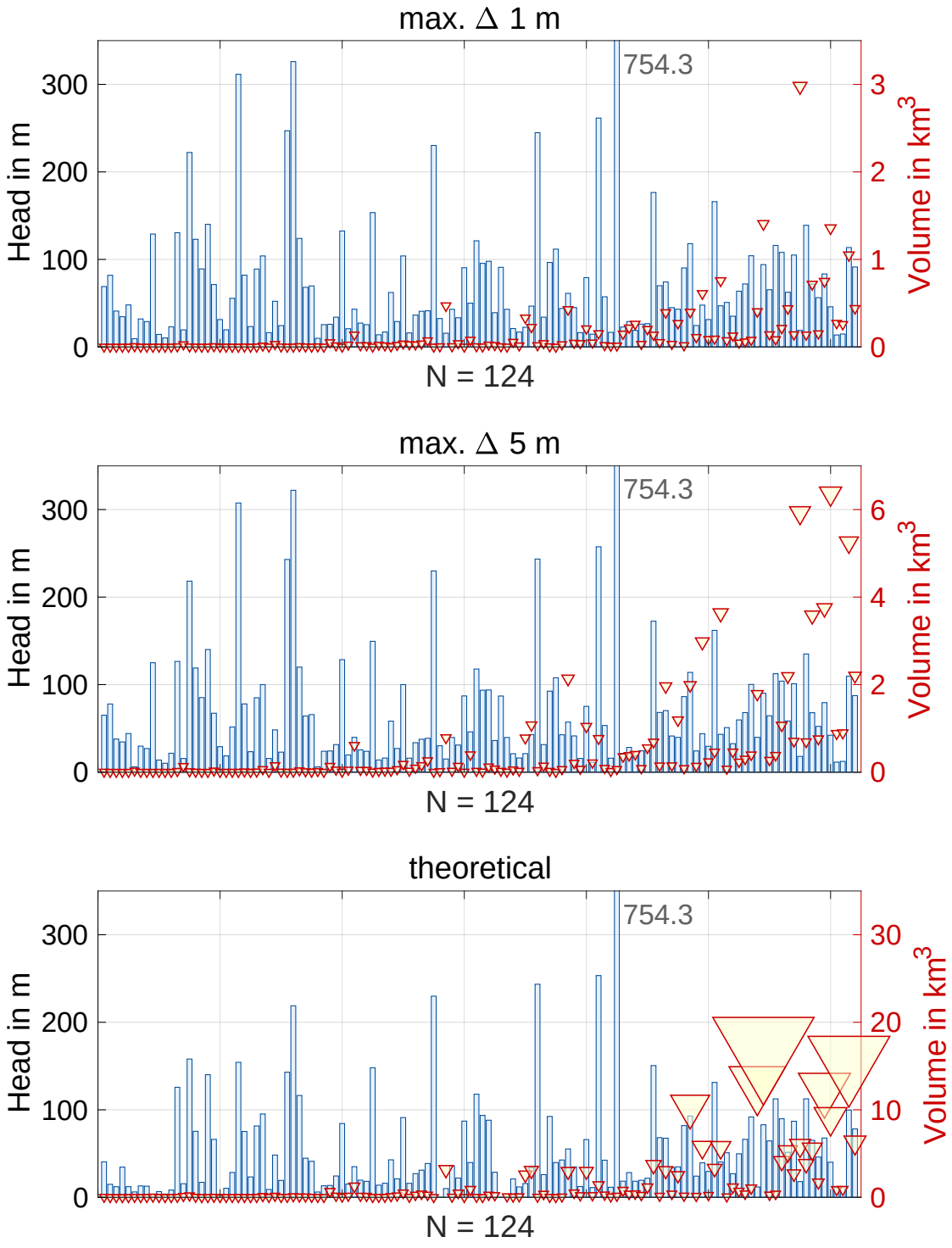

Figure A.9: Data for calculation of weighted head

A2.6 Estimation of drainage basin

$$A_{\mathrm{Basin}}(P_{\mathrm{inst}}) = p_1 \cdot P_{\mathrm{inst}} + p_2 \tag{A.9}$$

Table A.6: Intervals and parameters for linear estimation of drainage basin

Installed capacity P_{inst}		Parameter p_1	Parameter p_2	sum of square error
min. MW	max. MW	1000 km²/MW	1000 km²	
1	10	0.190	0.209	155.3
10	100	0.066	0.101	121.8
100	1000	0.141	-0.306	4573.1
1000	10000	0.057	-1.449	6958.9

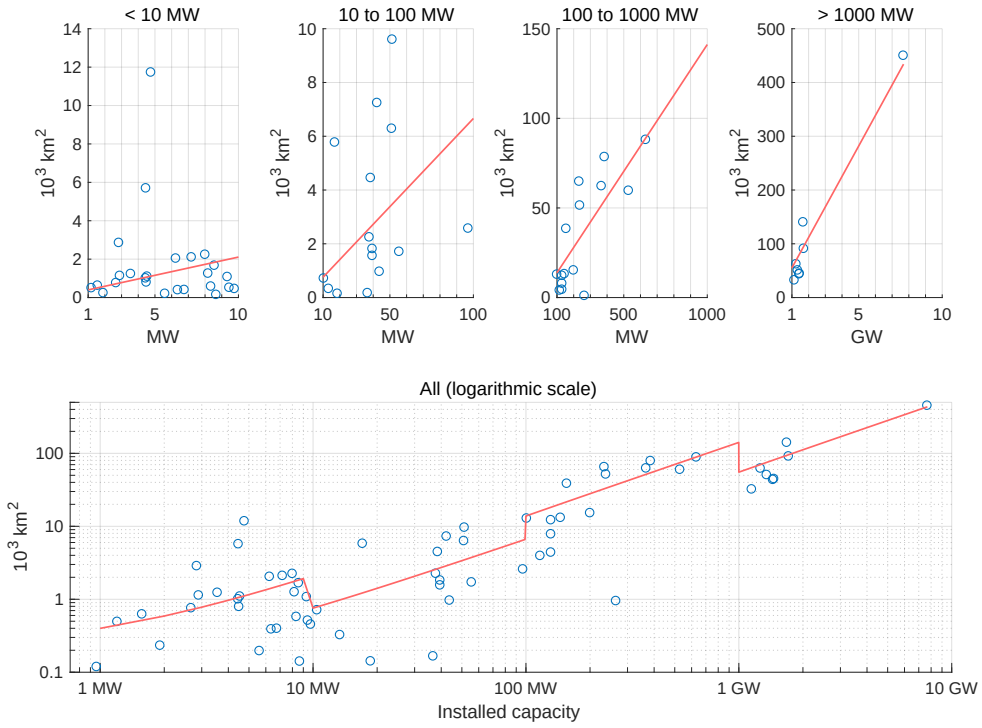

Figure A.10: Ratio of area of drainage basin to installed capacity

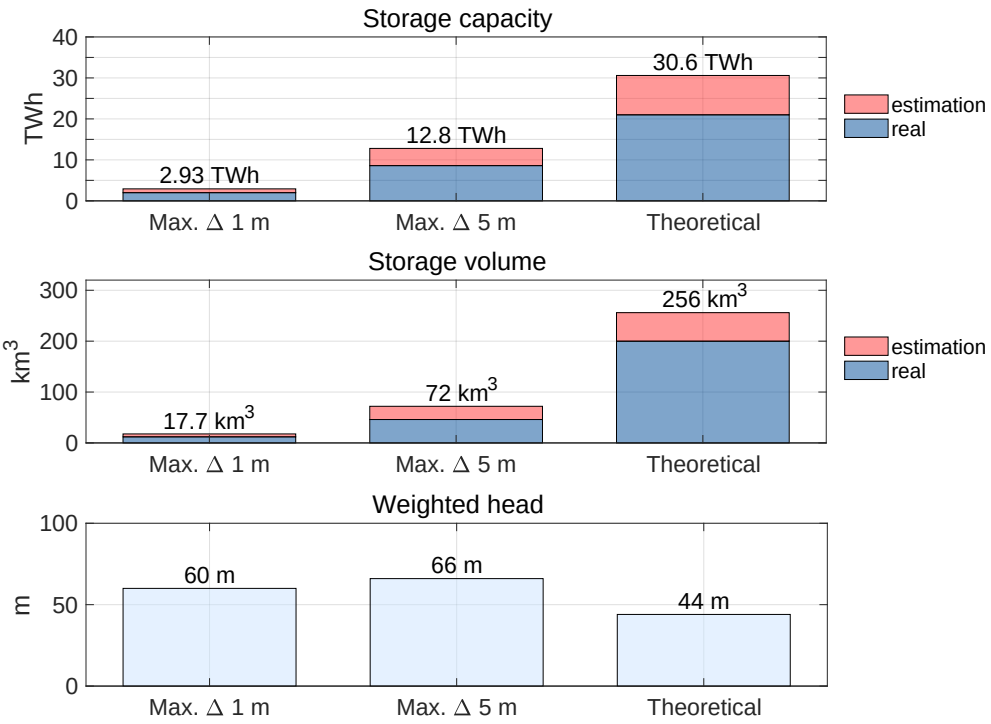

Figure A.11: Storage capacity considering individual reservoirs

A3: Additional results and data

A3.1 Comparison of real load with simulation

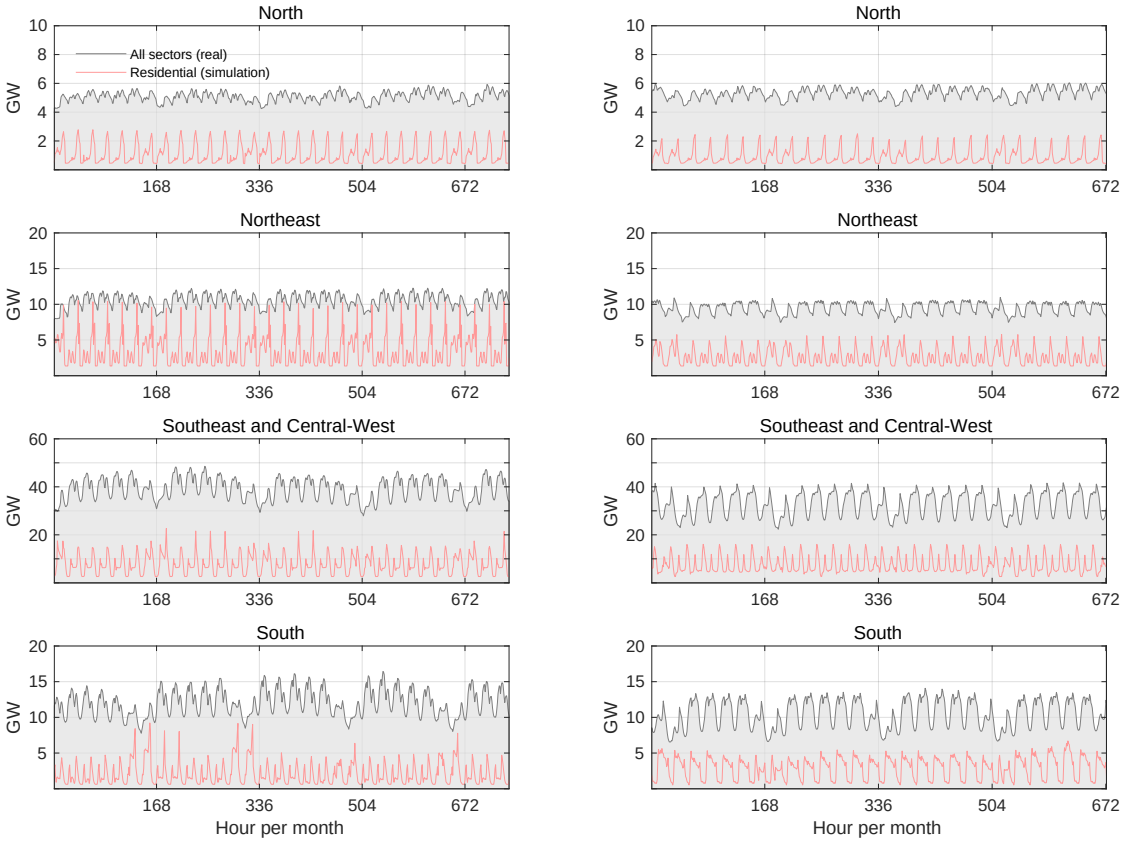

Figure A.12: Comparison of real load with simulated residential load profiles

A3.2 Meteorological data from INMET

The meteorological time series from INMET *(Instituto Nacional de Meteorologia)* contain in total 428 locations, see table A.7, and were gathered between 2001 and 2010. [16] Following meteorological quantities were retrieved from this archive:

- ambient temperature t_{A}
- global horizontal radiation q_{solar}

- total atmospheric pressure p
- relative humidity φ
- precipitation pre
- wind speed v_{w}

Table A.7: Meteorological data: Arquivos climáticos INMET 2016

State	Abbreviation	Region	INMET data sets
Acre	AC	North	4
Alagoas	AL	Northeast	7
Amapá	AP	North	4
Amazonas	AM	North	12
Bahia	BA	Northeast	40
Ceará	CE	Northeast	14
Distrito Federal	DF	Central-West	3
Espírito Santo	ES	Southeast	9
Goiás	GO	Central-West	21
Maranhão	MA	Northeast	17
Mato Grosso	MT	Central-West	31
Mato Grosso do Sul	MS	Central-West	16
Minas Gerais	MG	Southeast	51
Pará	PA	North	19
Paraíba	PB	Northeast	8
Paraná	PR	South	23
Pernambuco	PE	Northeast	12
Piauí	PI	Northeast	18
Rio de Janeiro	RJ	Southeast	14
Rio Grande do Norte	RN	Northeast	7
Rio Grande do Sul	RS	South	33
Rondônia	RO	North	4
Roraima	RR	North	1
Santa Catarina	SC	South	19
São Paulo	SP	Southeast	27
Sergipe	SE	Northeast	5
Tocantins	TO	North	9
Brazil	BR	-	428

A3.3 Solar radiation by state

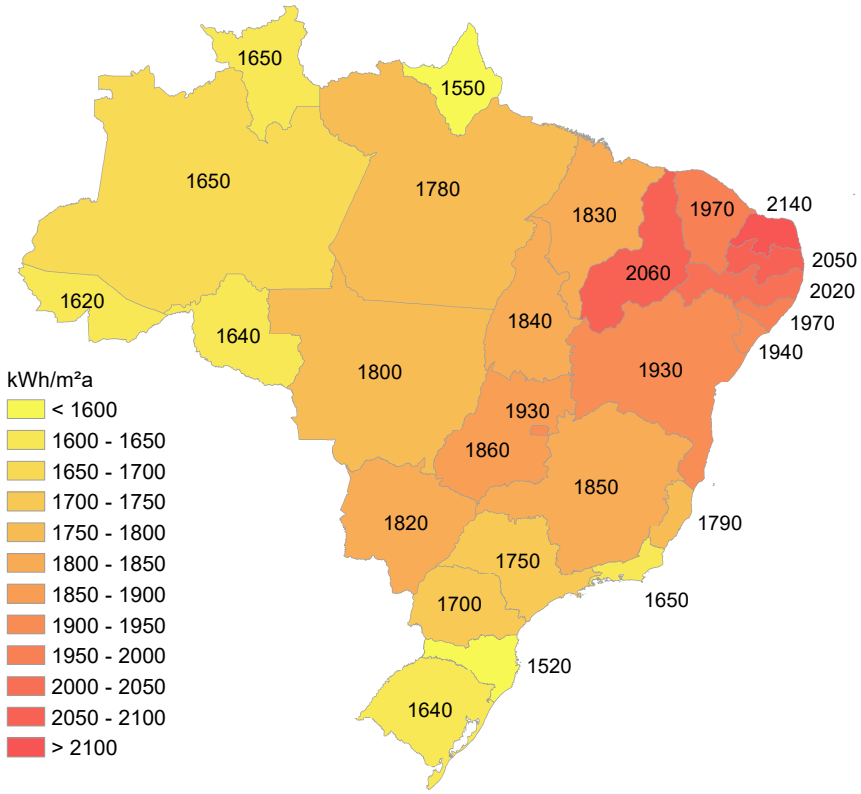

Figure A.13: Mean global horizontal radiation by state [16]

Assumption: Numerical value for annual sum of global horizontal radiation Q_{ghr} per square meter equals full load hours τ_{PV} for photovoltaic power.

The annual sum of global horizontal radiation Q_{ghr} results from the integral of solar radiation $\dot{q}"_{\mathrm{ghr}}(t)$ over the time of the year.

$$Q_{\mathrm{ghr}} = \int \dot{q}"_{\mathrm{ghr}}(t)\,\mathrm{d}t \tag{A.10}$$

Assuming the same annual radiation is received over the time τ_{PV} with maximum radiation $\dot{q}"^{\max}_{\mathrm{ghr}} \stackrel{!}{=}$ **1 kW/m²**, the equation above can be simplified to the following product:

$$Q_{\mathrm{ghr}} = \dot{q}"^{\max}_{\mathrm{ghr}} \cdot \tau_{\mathrm{PV}} \tag{A.11}$$

Multiplication of both sides with the efficiency η_{PV} of the photovoltaic system leads to the the linear relation between full load hours τ_{PV}, installed capacity P_{PV}, and annual sum of produced electricity W_{el}.

$$W_{\mathrm{el}} = P_{\mathrm{PV}} \cdot \tau_{\mathrm{PV}} \tag{A.12}$$

A3.4 LCOE of PV using net metering

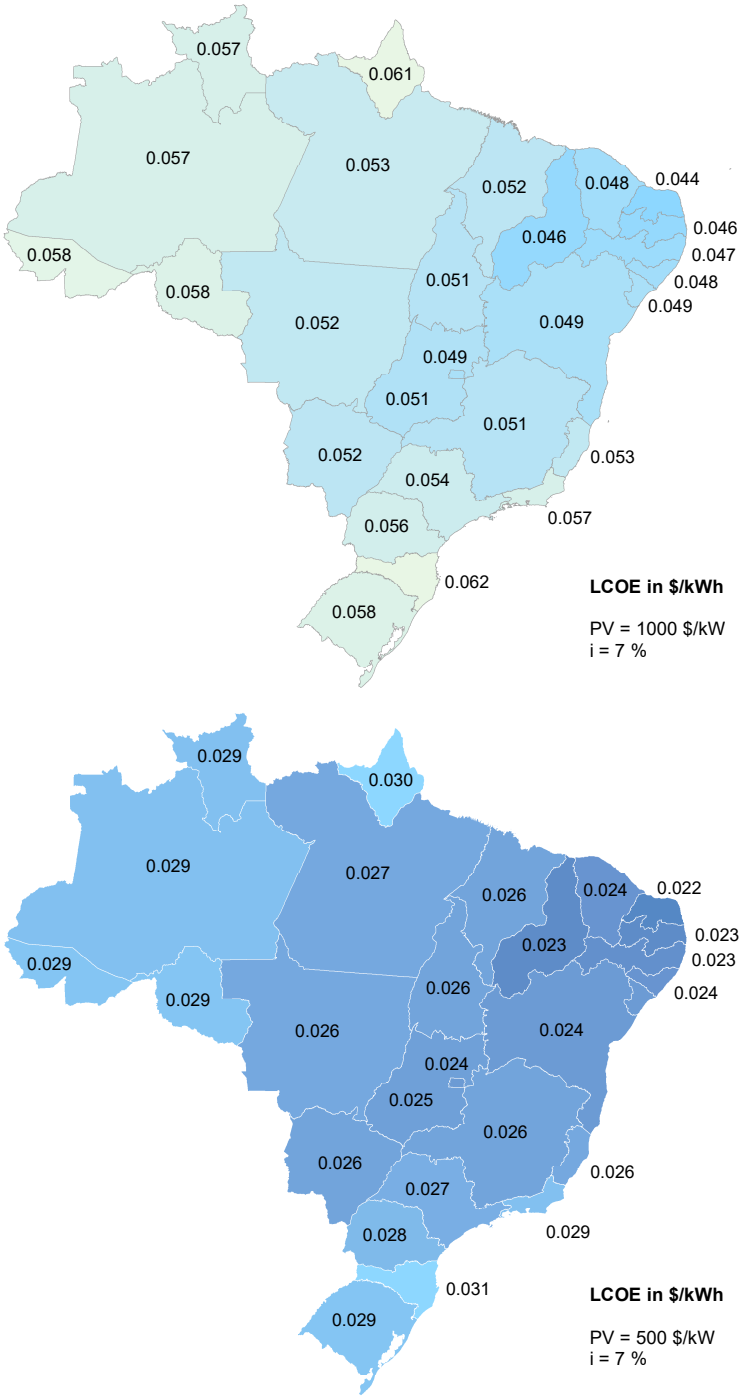

Figure A.14: LCOE of PV systems using net metering

A3.5 Precipitation and hydropower inflow

Table A.8: Investigated locations for inflow calculation via state-space model

No.	Pos.	Location	Rio (River)	State	Year
1	l	Cassilândia	Aporé	Mato Grosso do Sul	2003
	u	Aporé	Aporé	Goiás	2003
2	l	Colonia dos Americanos	das Almas	Goiás	1997
	u	Serra da Mesa	das Almas	Goiás	1997
3	l	São Félix do Araguaia	Araguaia	Mato Grosso	2005
	u	Luiz Alves	Araguaia	Goiás	2005
4	l	Traipu	São Francisco	Alagoas	2004
	u	Pão de Açúcar	São Francisco	Alagoas	2004
5	l	Ibó	São Francisco	Pernambuco	1997
	u	Santa Maria da Boa Vista	São Francisco	Pernambuco	1997
6	l	Fazenda Vista Alegra	Madeira	Amazonas	2006
	u	Manicoré	Madeira	Amazonas	2006
7	l	Belo Horizonte	Xingu	Pará	1997
	u	Pombal	Xingu	Pará	1997
8	l	Indiaporã	Grande	São Paulo	1953
	u	Rifaina	Grande	São Paulo	1953
9	l	Passo do Itaum	Ibicuí	Rio Grande do Sul	2011
	u	Jacaquá	Ibicuí	Rio Grande do Sul	2011
10	l	Itapiranga	Uruguai	Santa Catarina	2016
	u	Iraí	Uruguai	Rio Grande do Sul	2016

The hydrological data used for identification of a hydrological system by applying a state-space model described in paragraph 5.1.1 was retrieved from several sources provided by the Agência Nacional de Águas e Saneamento Básico (ANA), the Brazilian agency for water and sanitation [142], see `https://dadosabertos.ana.gov.br`. To analyze the relation between meteorological conditions with a drainage basins' outflow, the hydrological data was merged with the weather time series from INMET, see table A.7. The state-space model approach described in section 5.1.1 was tested for the following ten locations, see table A.8. For each location, two data points were considered. One lower point indicated with "l" attached to the location number and one further point upstream, indicated with "u". Lower and upper points where chosen in that way, that no dam is between both. Such a technical barrier between both sites would make the identification of the hydrological behavior impossible without considering the operation of the dam.

The volume flow displayed in figure A.15, figure A.16, and figure A.16 represents the gain of water within the drainage basin. That means the difference between inflow from the upper point and the outflow from the lower point. Subsequently, negative values are possible for this volume flow, for example, in case of a loss of water due to evaporation or water extraction.

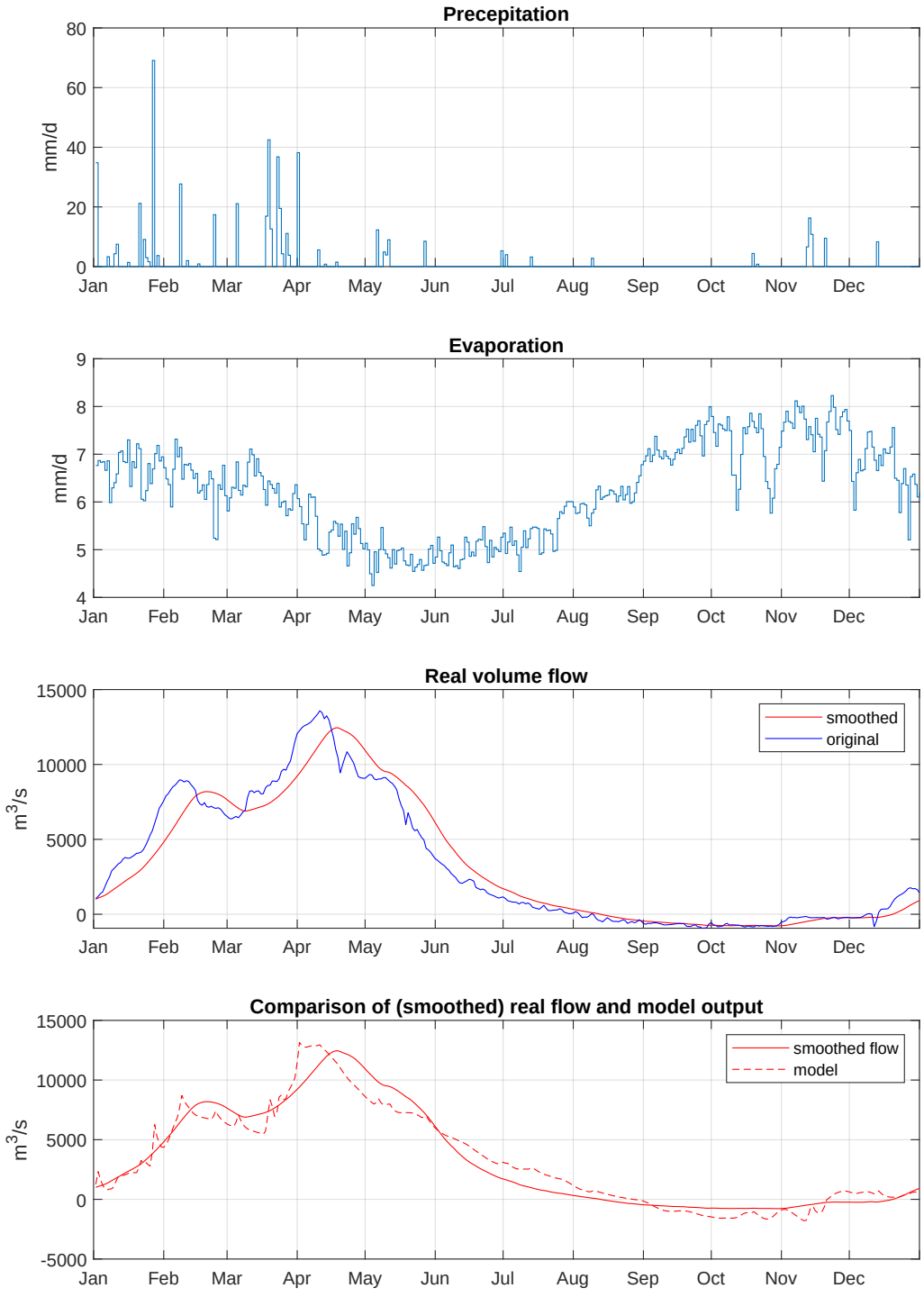

Figure A.15: Rio São Francisco in Pernambuco: Good identification of hydrological behavior

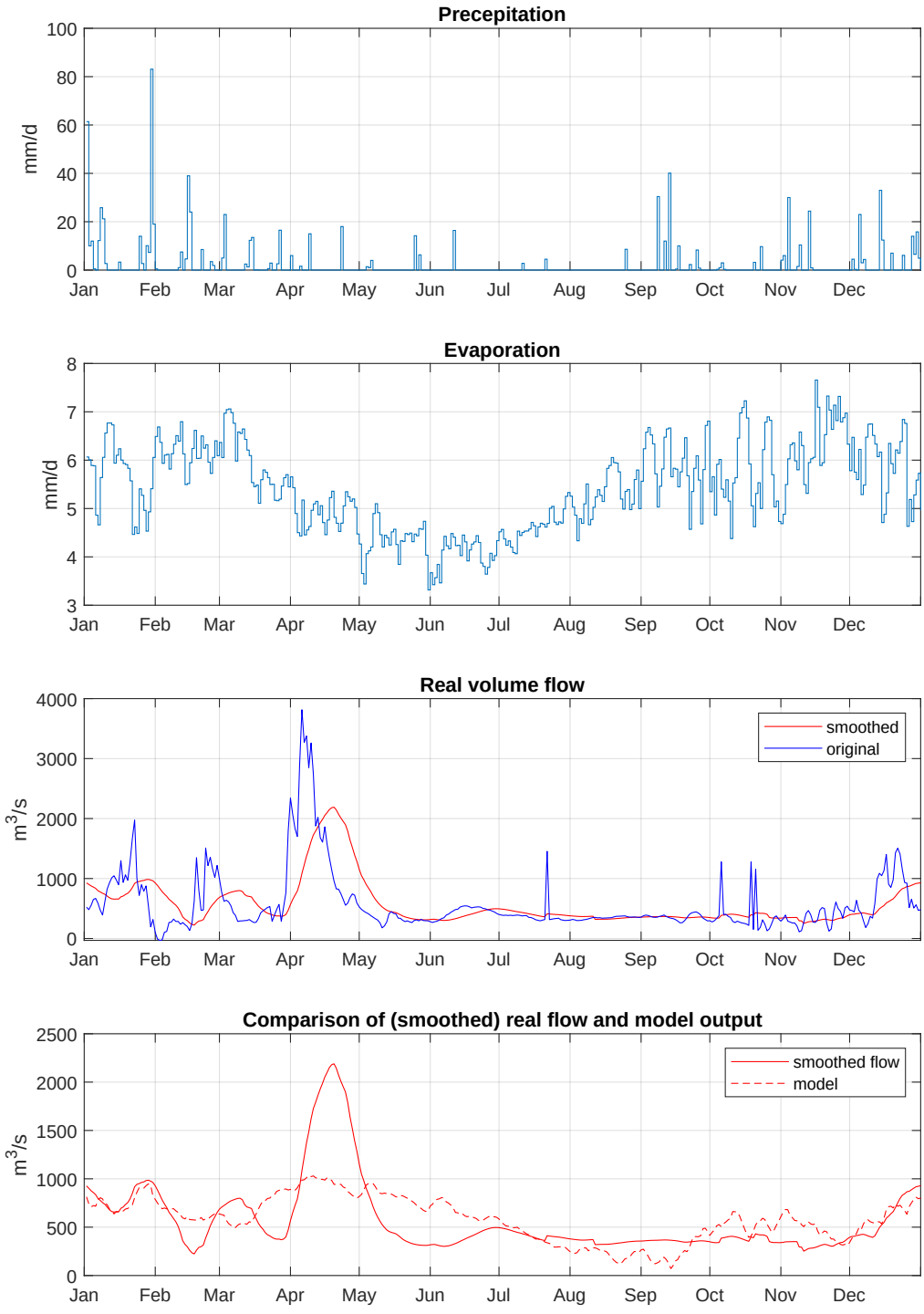

Figure A.16: Rio Grande in São Paulo: Example for weak identification of hydrological behavior

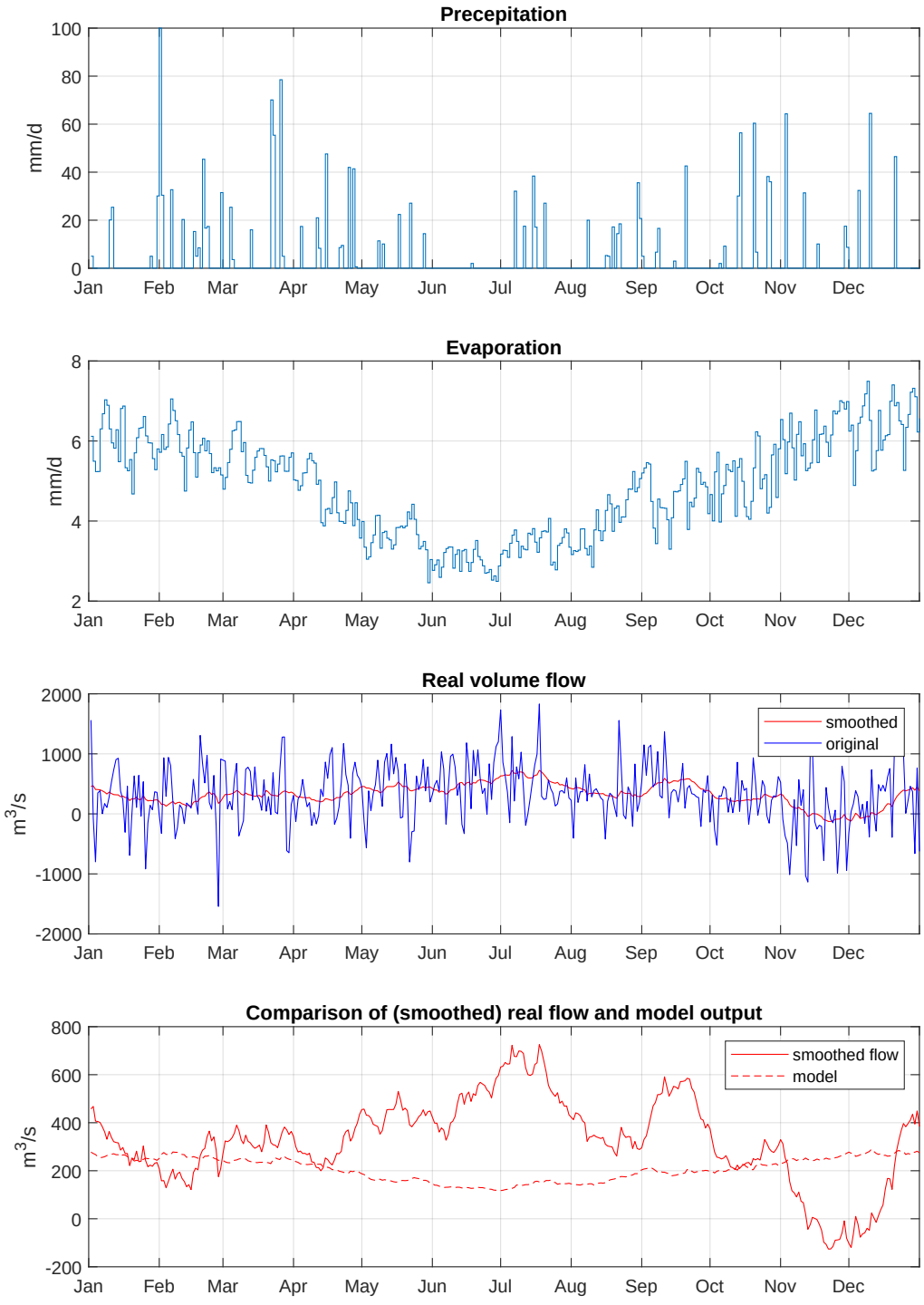

Figure A.17: Rio Grande in São Paulo: Example for unpredictable hydrological behavior

A3.6 Reservoir level

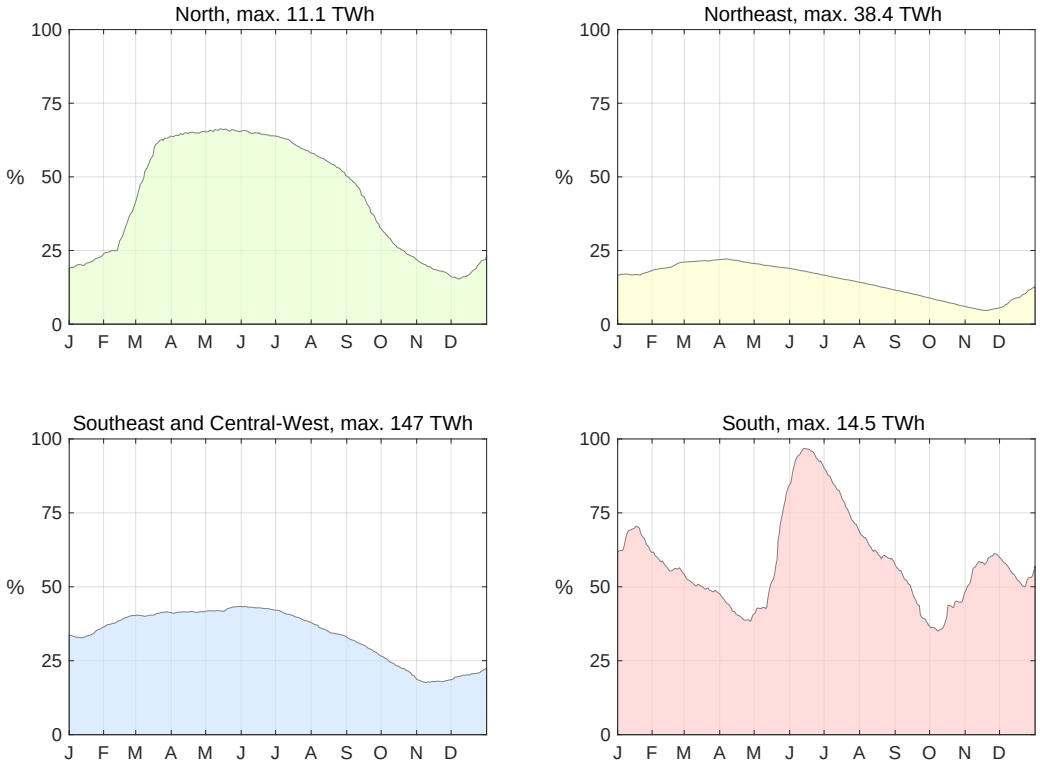

Figure A.18: Storage level in 2017 per region [17]

A3.7 Generation and load for 2017

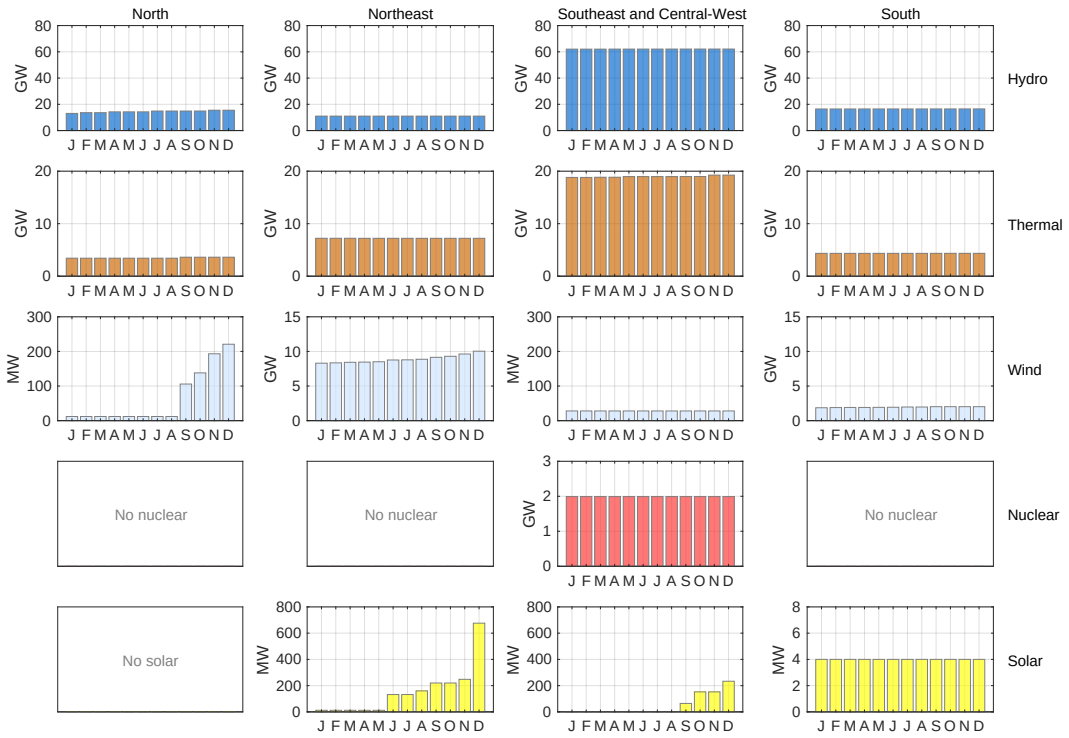

Figure A.19: Power generation capacity by region during 2017 [17]

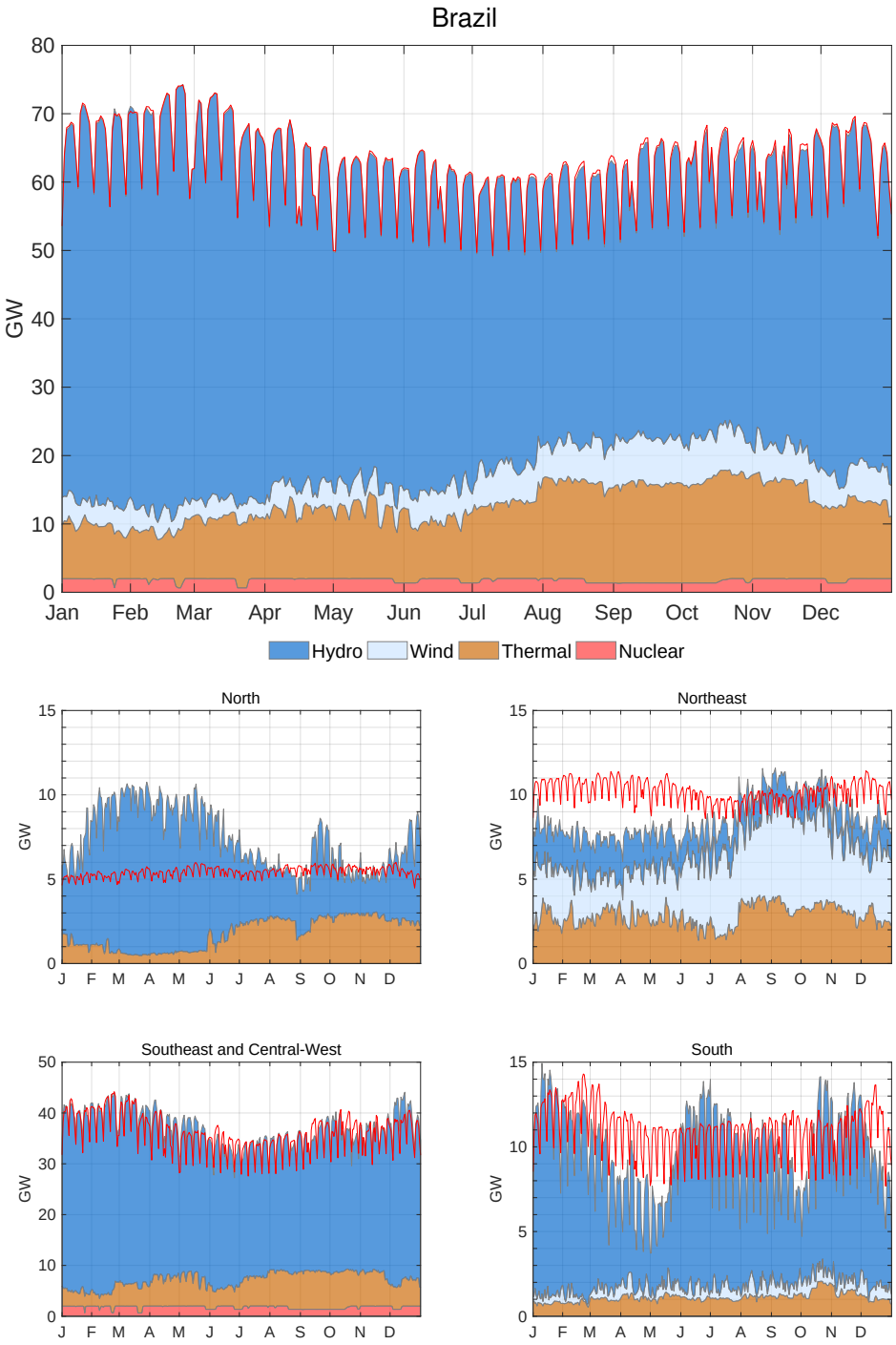

Figure A.20: Real generation and load in 2017 [17]

A4: Optimization results

Section A of this appendix contains values used as input for the model-based outlook in section 5.2 of chapter 5. The model-based outlook delivered results for the scenarios summarized in table A.9. The following sections include a collection of all optimization results of the scenarios described in section 5.2.

Table A.9: Overview of scenarios for model-based outlook

No.	Scenario name	Type	Prices	Characteristics and main differences
1a	Base	FxB	F=25-100 $/MWh, B=50-200 $/kWh	Base scenario for the future energy system. In contrast to 2017, doubled demand, lower investment costs for wind, photovoltaics, and batteries.
1b	Base	H100	F=25 $/MWh, B=50 $/kW/h	Like 1a, but with varying flexibility of hydropower $\Delta P/P_{\mathrm{inst}}$ from 1 % to 100 %. All other input data remain unchanged.
2a	Hydrogen	FxB	F=25-100 $/MWh, B=50-200 $/kWh	Additional constant electrical load of 120 GW in Northeast for hydrogen production. A total of 120 GW · 8760 h = 1,051 TWh of electricity is used for hydrogen production.
2b	Hydrogen	H100	F=25 $/MWh, B=50 $/kWh	Like 2a, but with varying flexibility of hydropower. All other input data remain unchanged.
3a	Green hydrogen	FxB	F=25-100 $/MWh, B=50-200 $/kWh	Additional electrical load of 120 GW peak reduced by thermal power generation profile of sub-scenario F1B1 from scenario 2a. A total of 787 TWh of electricity is used for hydrogen production.
3b	Green hydrogen	H100	F=25 $/MWh, B=100 $/kWh	Like 3a, but with varying flexibility of hydropower. All other input data remain unchanged.

A4.1 Model assumptions

Table A.10: Costs, prices, and depreciation period

	Investment costs	Depreciation	Variable costs	Comment
	USD/kW	a	USD/MWh	
Hydropower	-	-	10+10	(1), (2)
Thermal	300	20	25+10	(3)
Nuclear	-	-	1	(1)
Wind	1000	20	10	
Solar	500	20	10	
Transmission	1500	50	1	

(1) No expansion is considered for hydroelectricity and nuclear power. Therefore, no investment costs are assumed.
(2) One part of the variable costs can be adapted for hourly time dependency, e.g., to represent the higher value of stored water in lakes during droughts.
(3) One part of the variable costs can be adapted for time dependency, e.g., to represent a variation of fuel prices, if necessary, in hourly resolution.

Table A.11: Technical data for power generation and storage technologies

	Installed capacity in GW						
	BR	NO	NE	SE, CW	SO	η	$\Delta P_{\max}/P_{\text{inst}}$
Hydropower	105.1	15.5	11.0	62.1	16.5	-	0.1
Thermal	34.4	3.6	7.2	19.3	4.4	0.36	0.3
Nuclear	2.0	-	-	2.0	-	0.33	-
Wind	12.3	0.2	10.0	0.03	2.0	-	-
Solar	0.9	-	0.7	0.2	0.004	-	-
	Storage capacity in TWh						
	BR	NO	NE	SE, CW	SO	η	
Reservoir	211.0	11.1	38.4	147.0	14.5	0.9	
Battery	-	-	-	-	-	0.9	

– Brazil (BR), North (NO), Northeast (NE), Southeast (SE), Central-West (CW), South (SO).
– Operador Nacional do Sistema Eletrico (ONS), the national Brazilian grid operator [17] provided the numbers for generation and storage capacities.
– Generation and storage capacities represent December 2017.
– Efficiencies η and flexibility $\Delta P_{\max}/P_{\text{inst}}$ are assumptions.
– The impact of different hydropower flexibility is further investigated in 5.2.2.

A4.2 Power generation

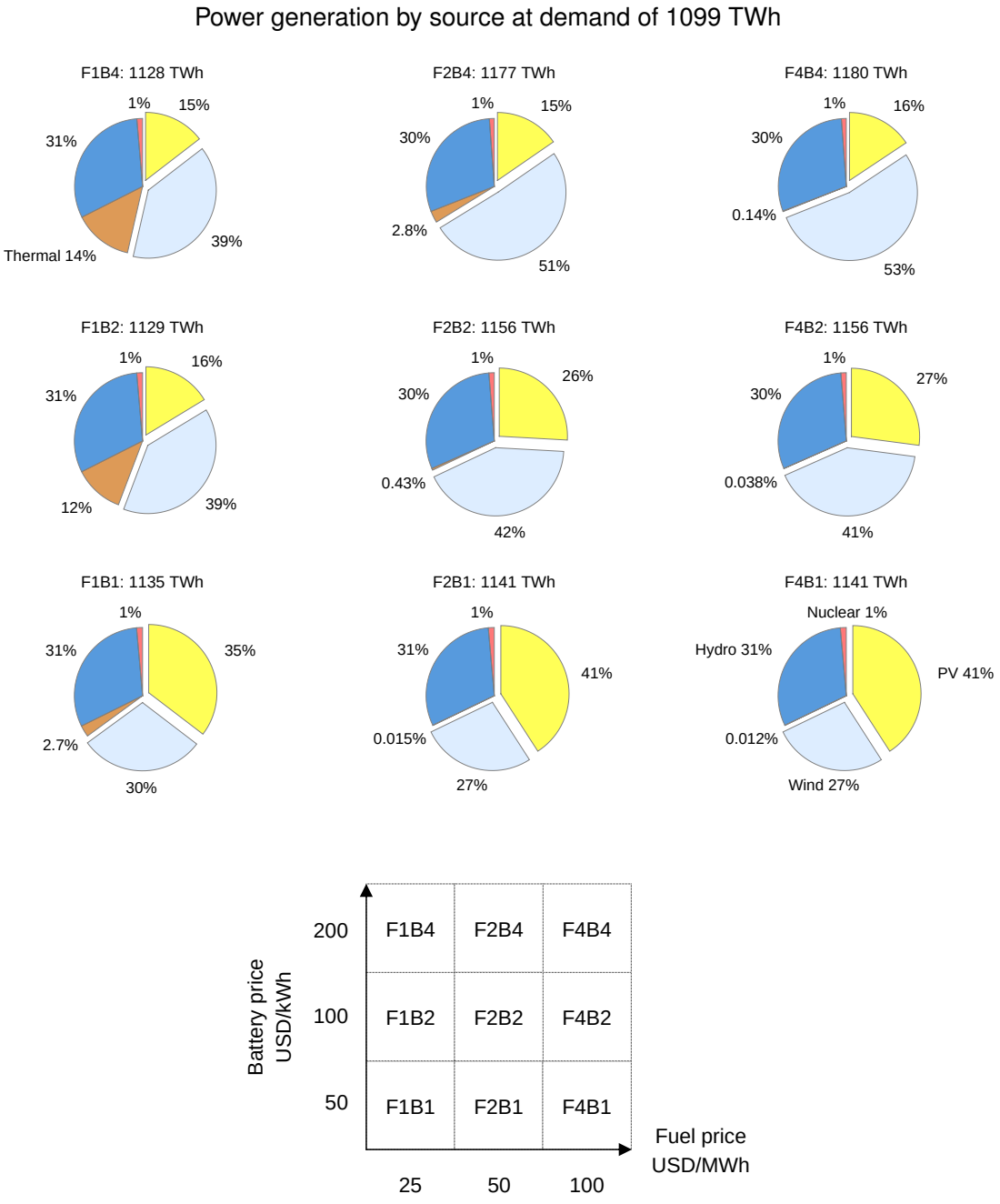

Figure A.21: Scenario 1a "Base", scheme FxB

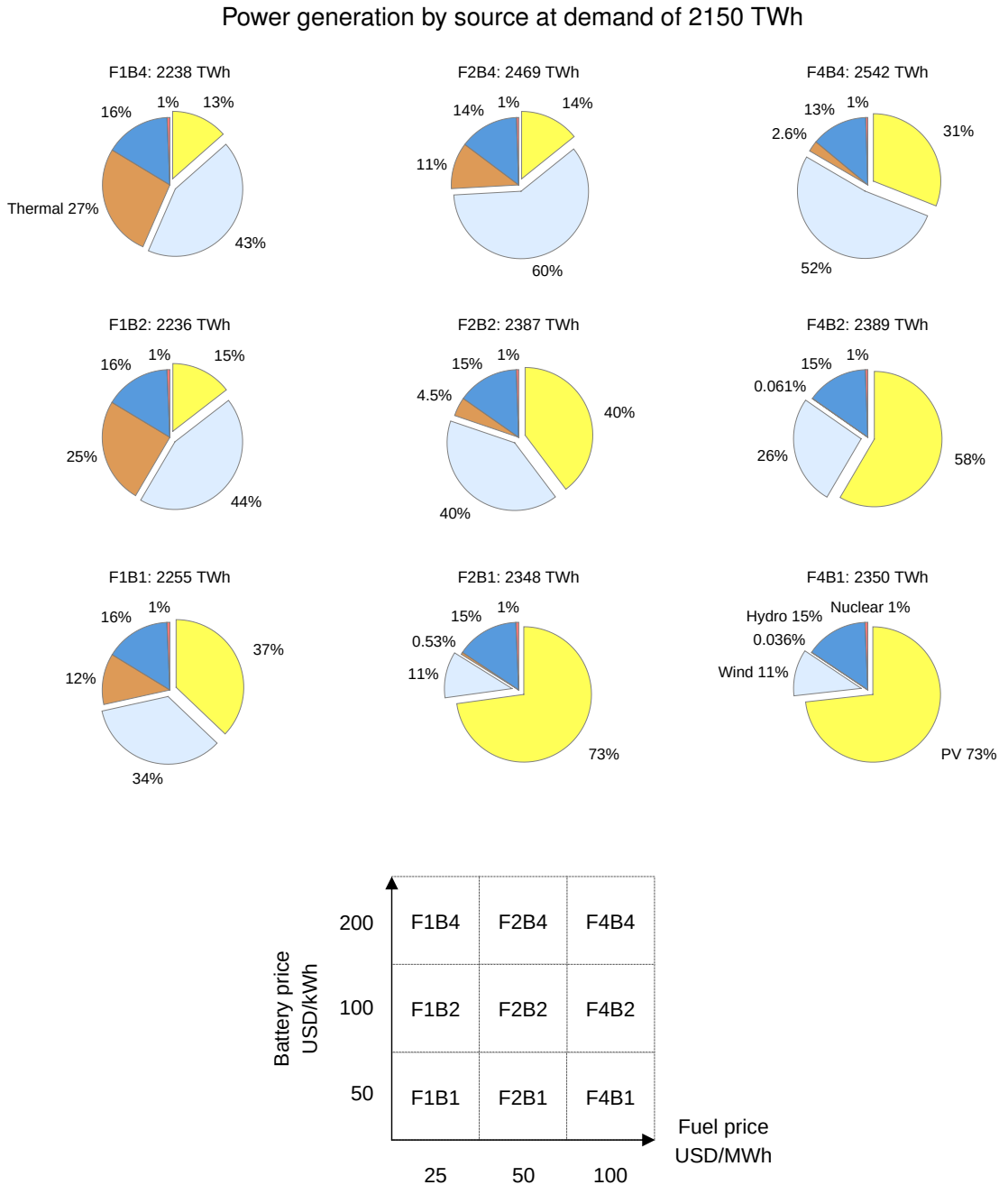

Figure A.22: Scenario 2a "Hydrogen", scheme FxB

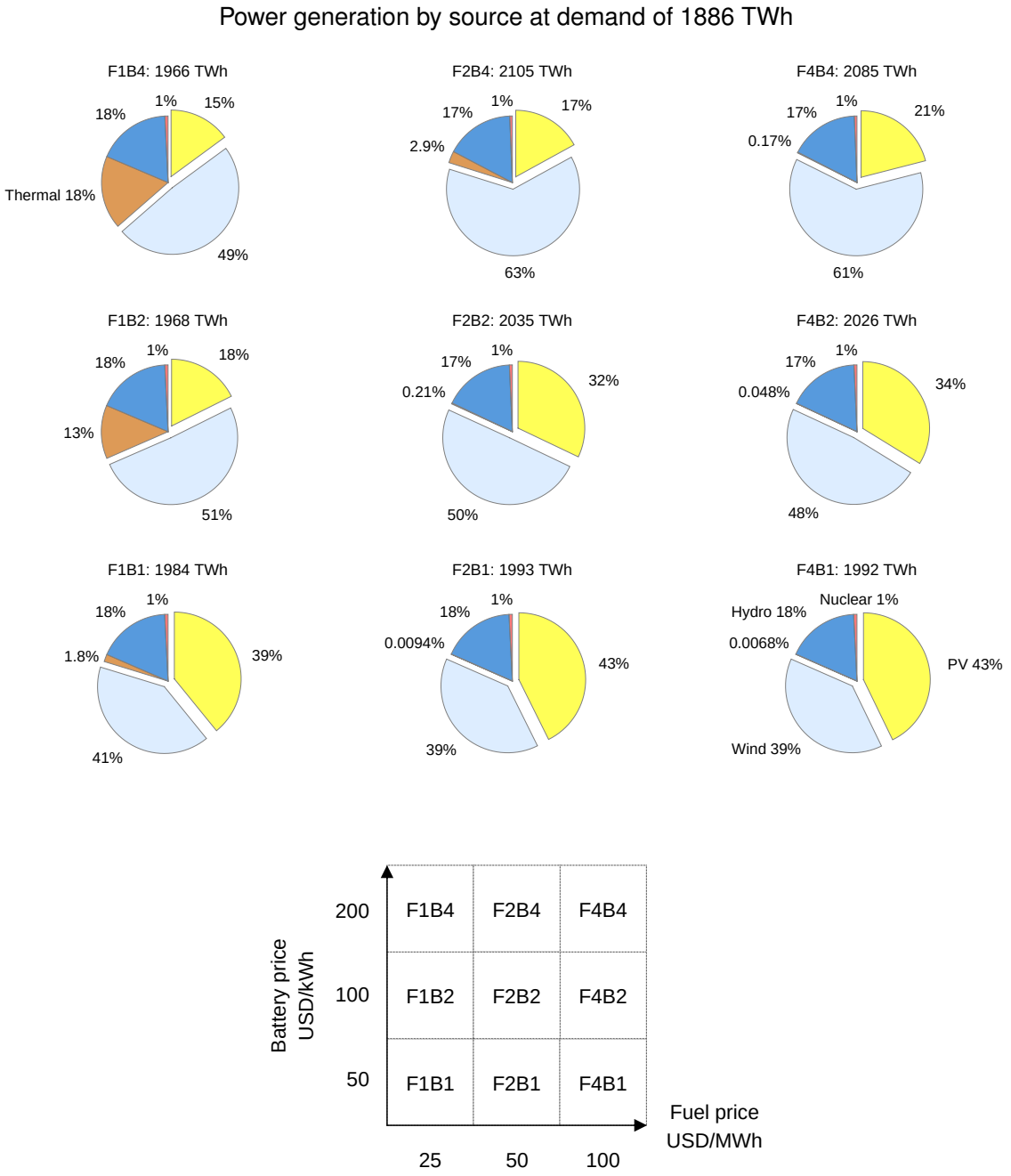

Figure A.23: Scenario 3a "Green hydrogen", scheme FxB

Figure A.24: Scenario 1b "Base", scheme H100

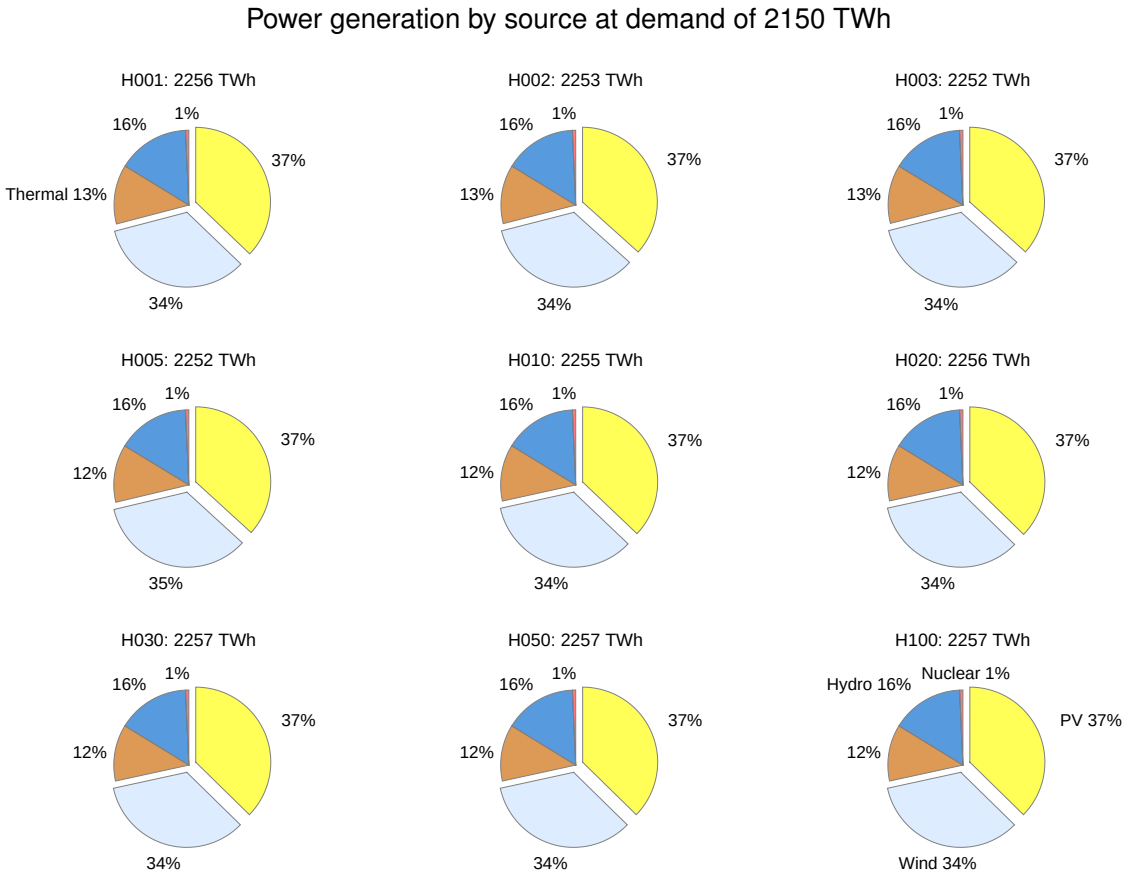

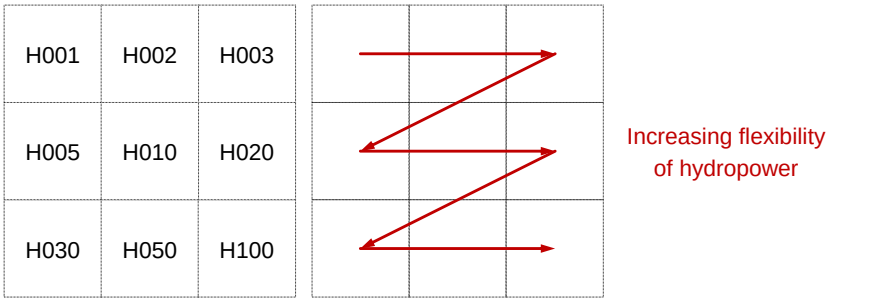

Figure A.25: Scenario 2b "Hydrogen", scheme H100

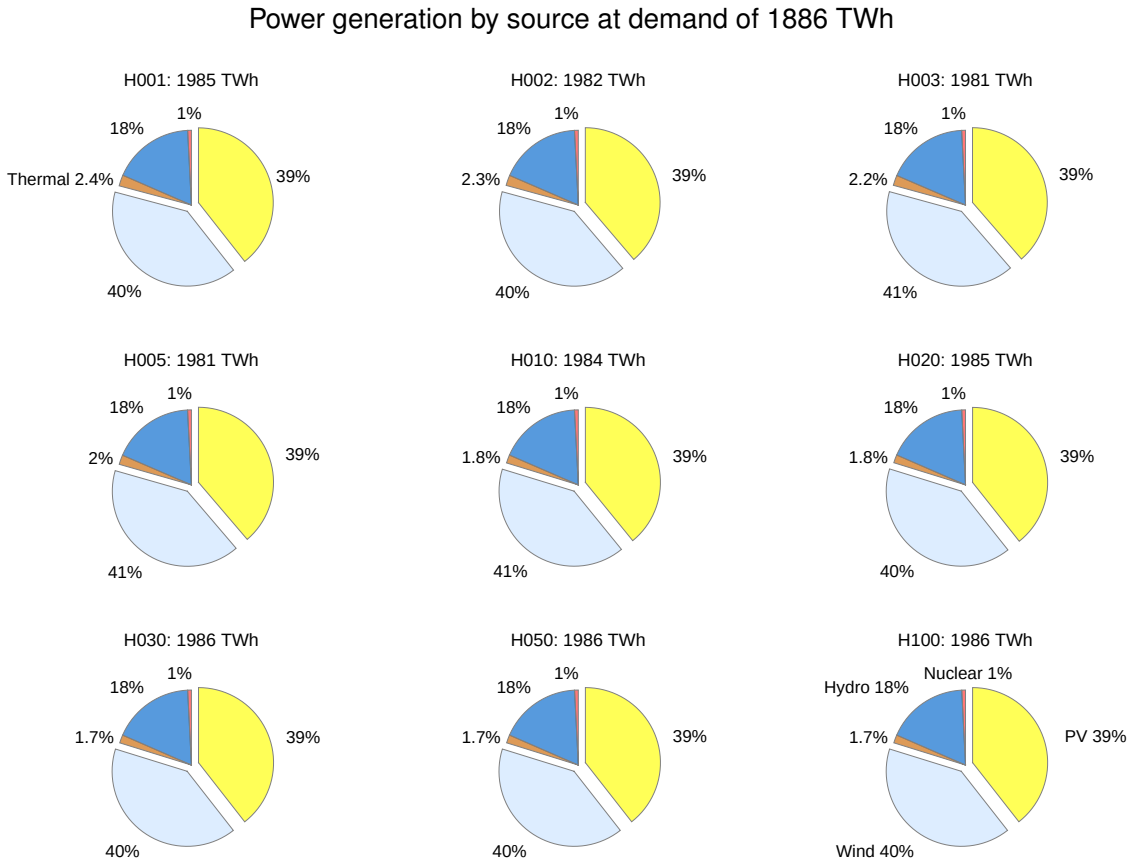

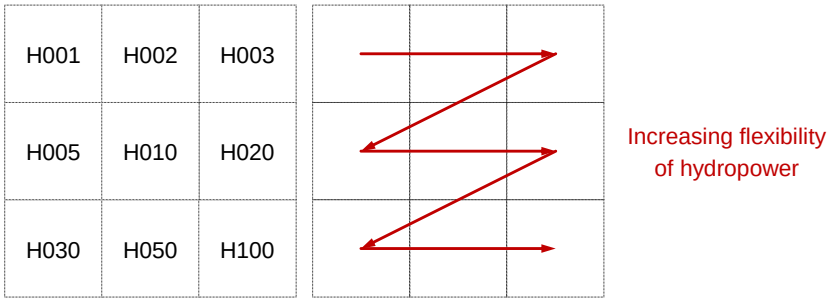

Figure A.26: Scenario 3b "Green hydrogen", scheme H100

A4.3 Installed generation capacity

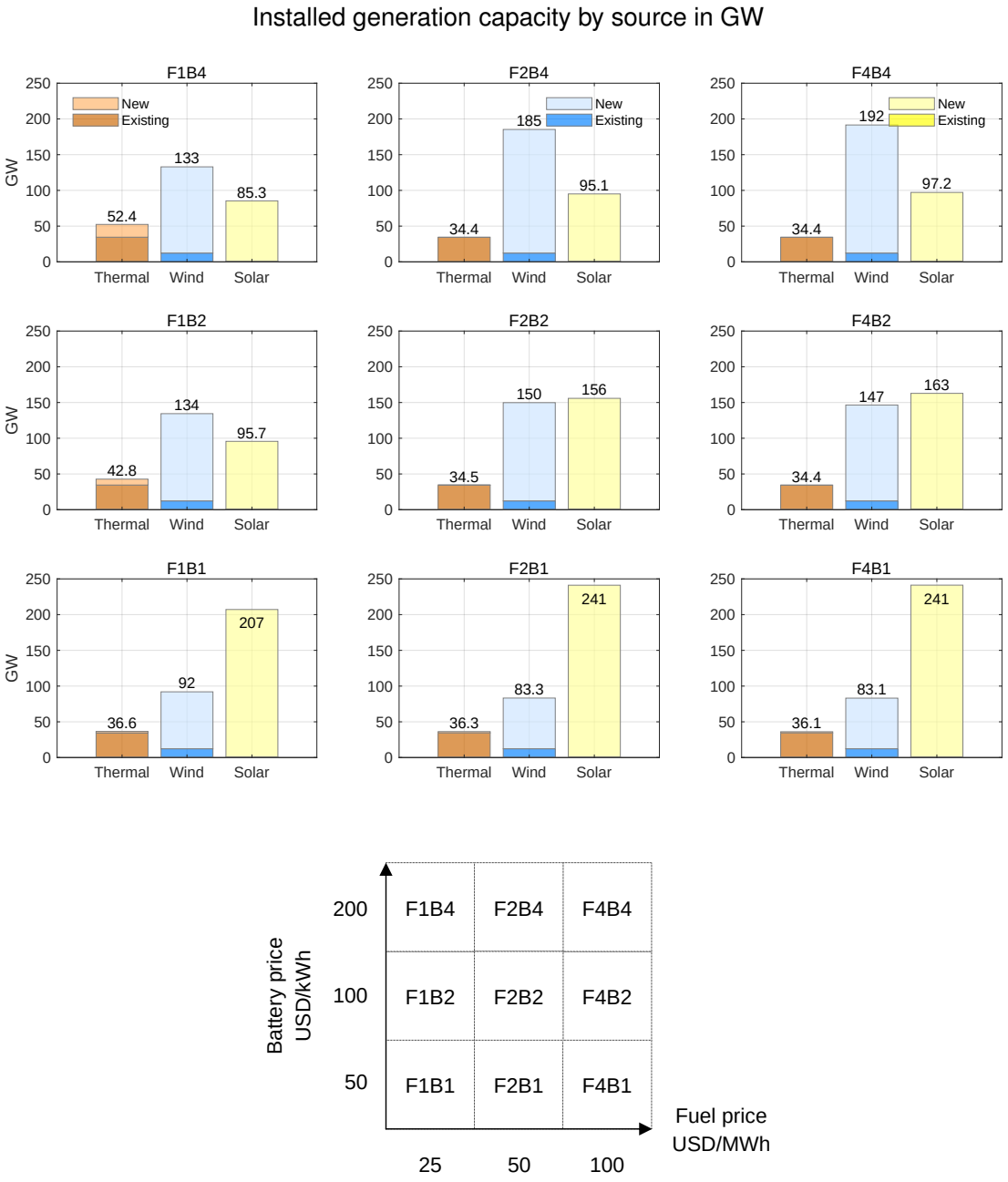

Figure A.27: Scenario 1a "Base", scheme FxB

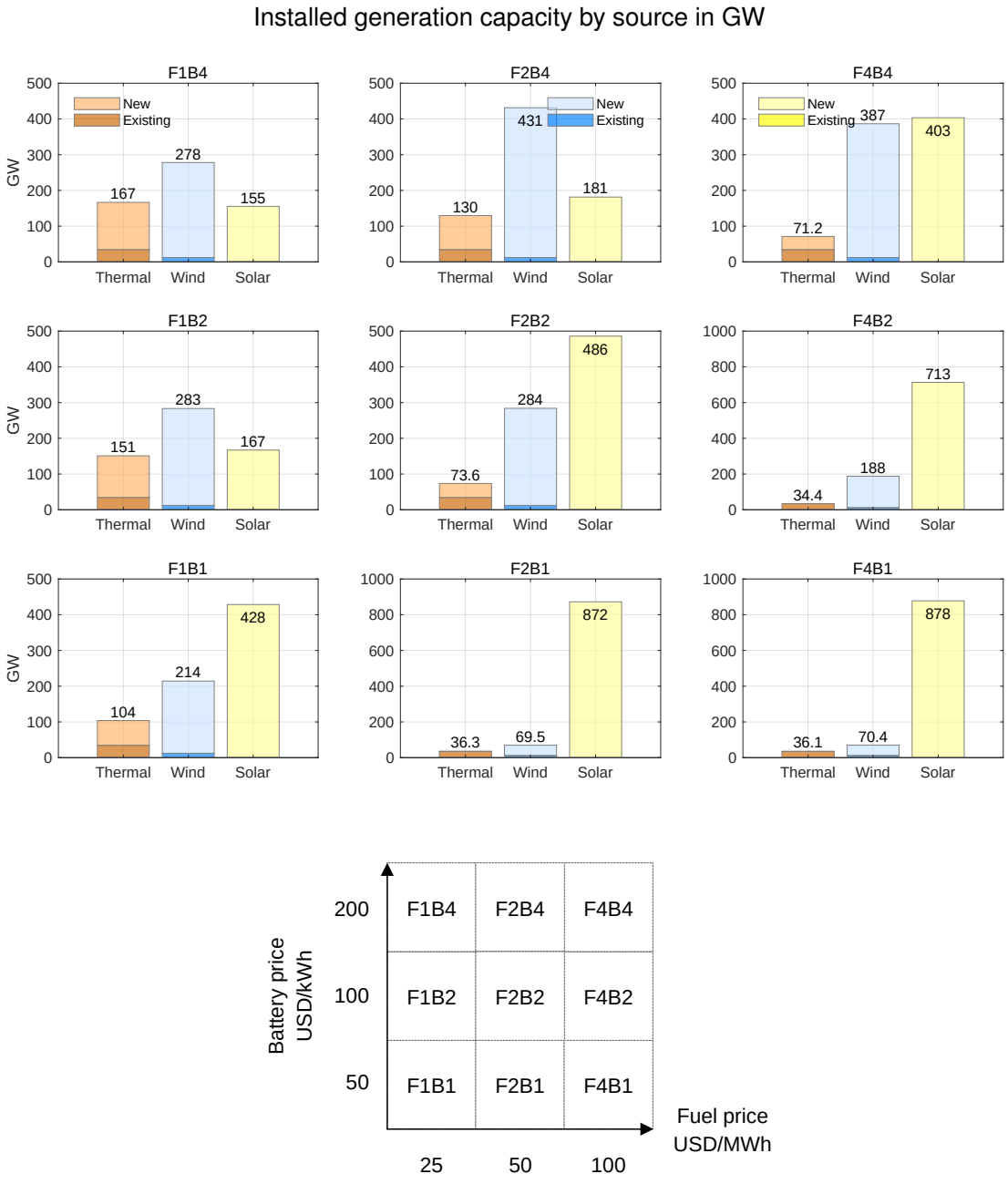

Figure A.28: Scenario 2a "Hydrogen", scheme FxB

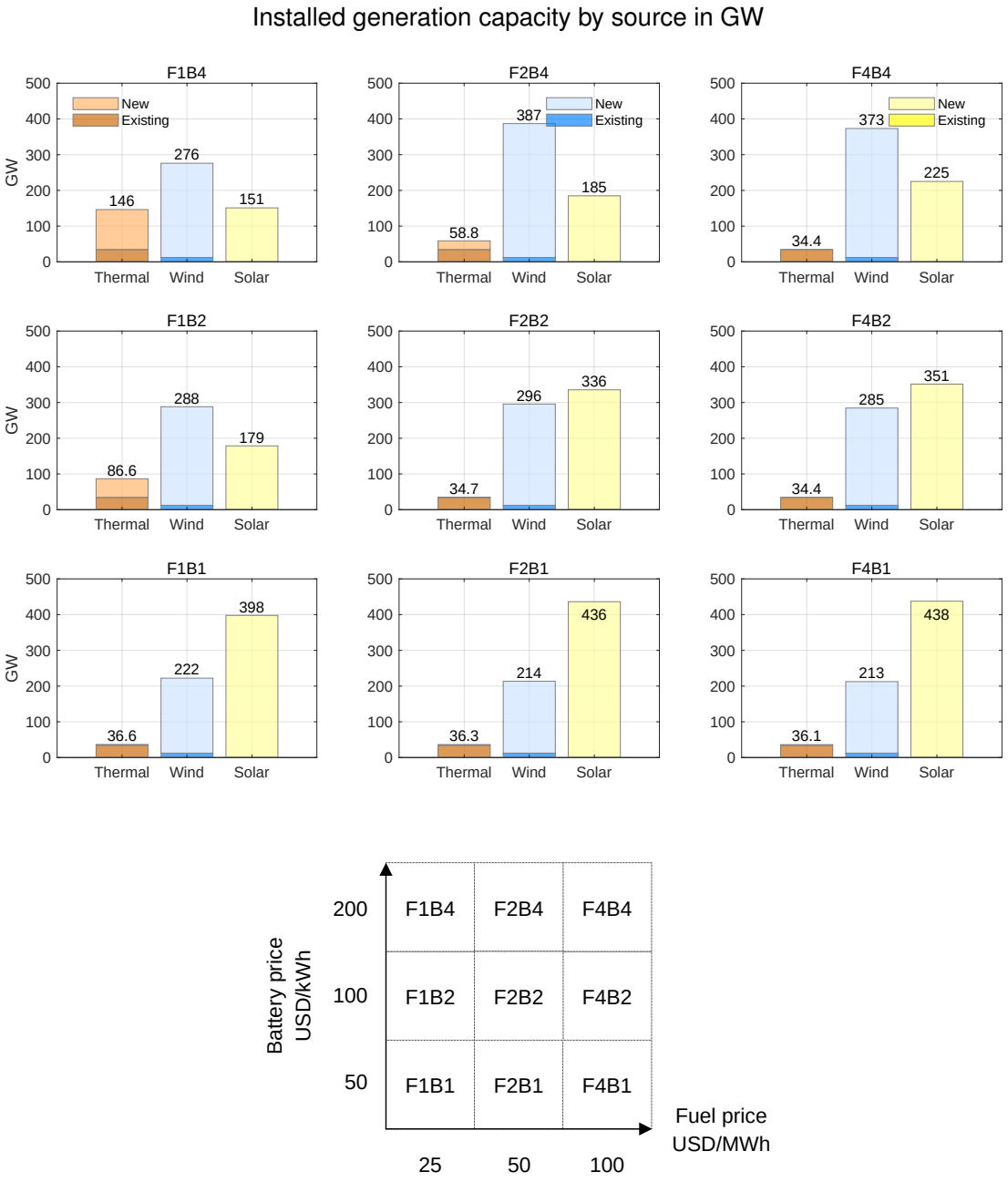

Figure A.29: Scenario 3a "Green hydrogen", scheme FxB

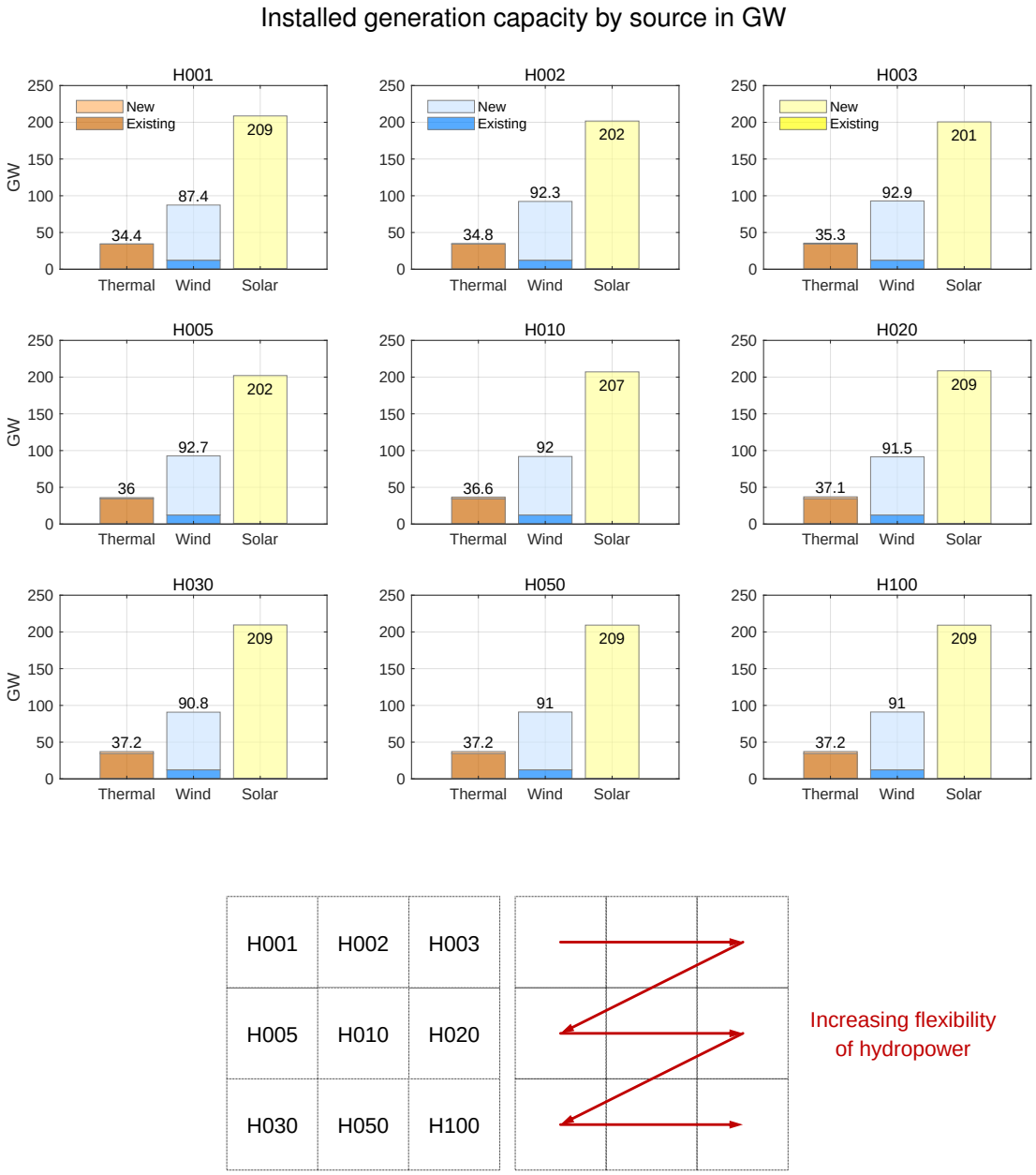

Figure A.30: Scenario 1b, scheme H100

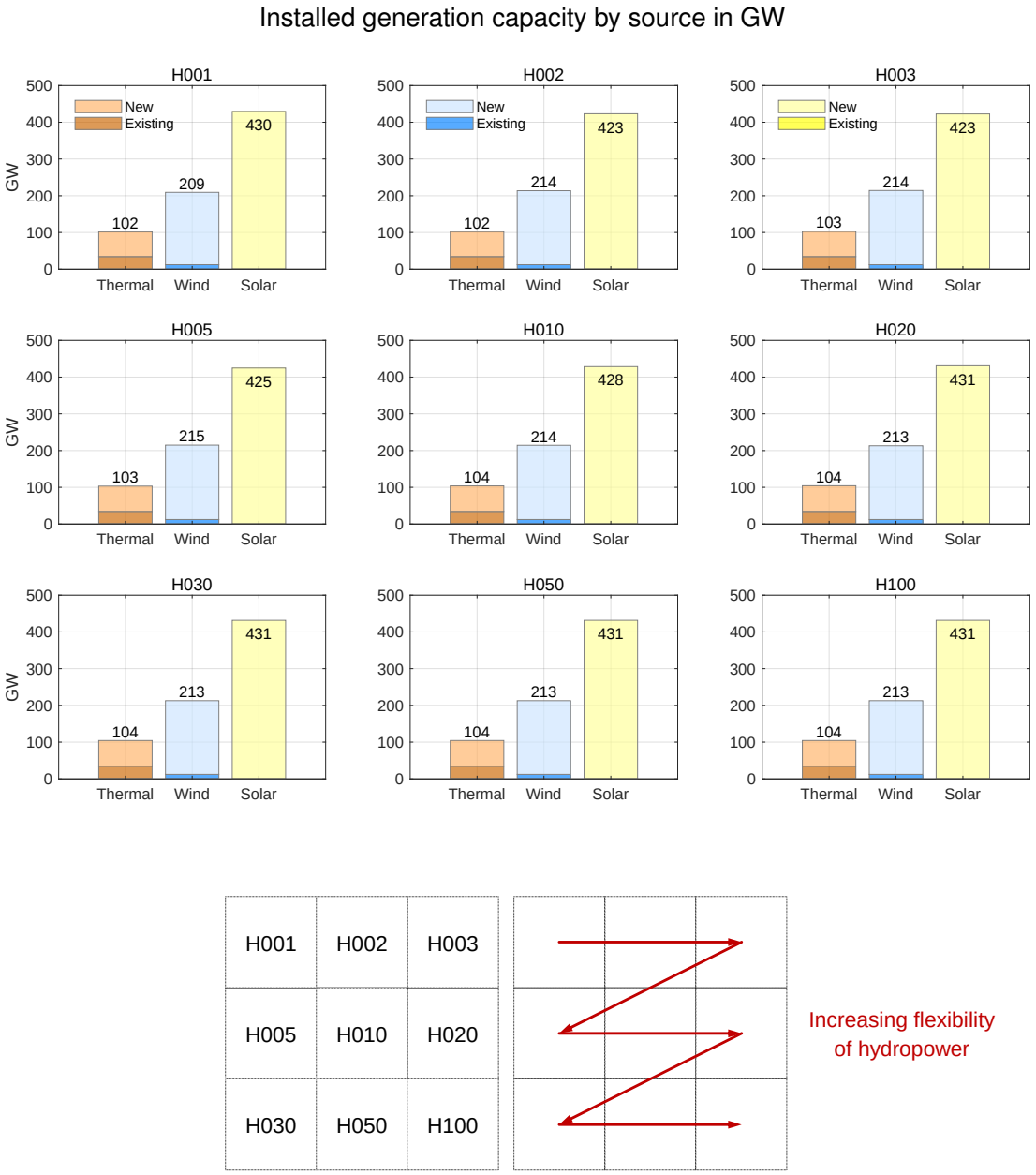

Figure A.31: Scenario 2b "Hydrogen", scheme H100

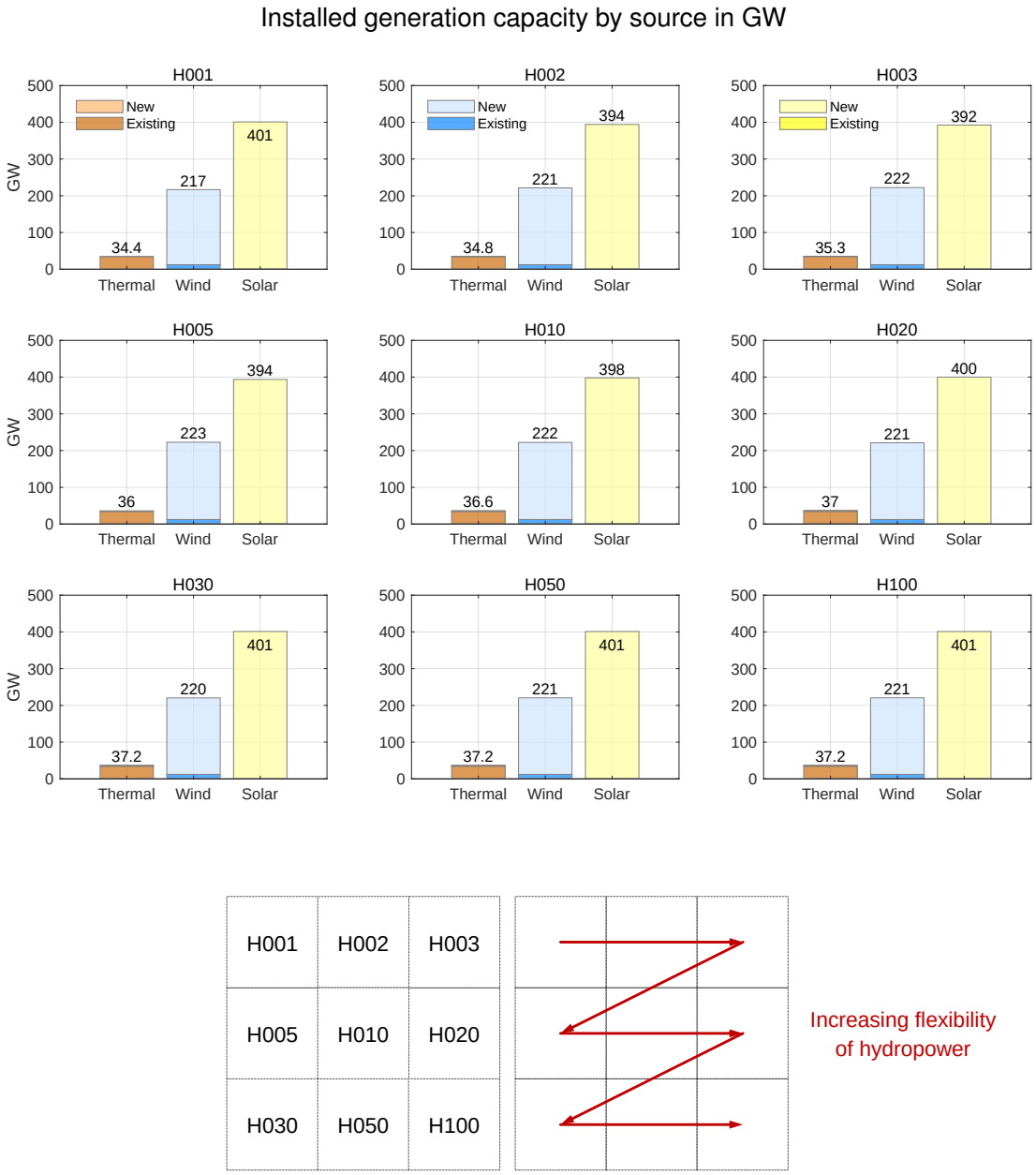

Figure A.32: Scenario 3b "Green hydrogen", scheme H100

A4.4 Installed battery storage capacity

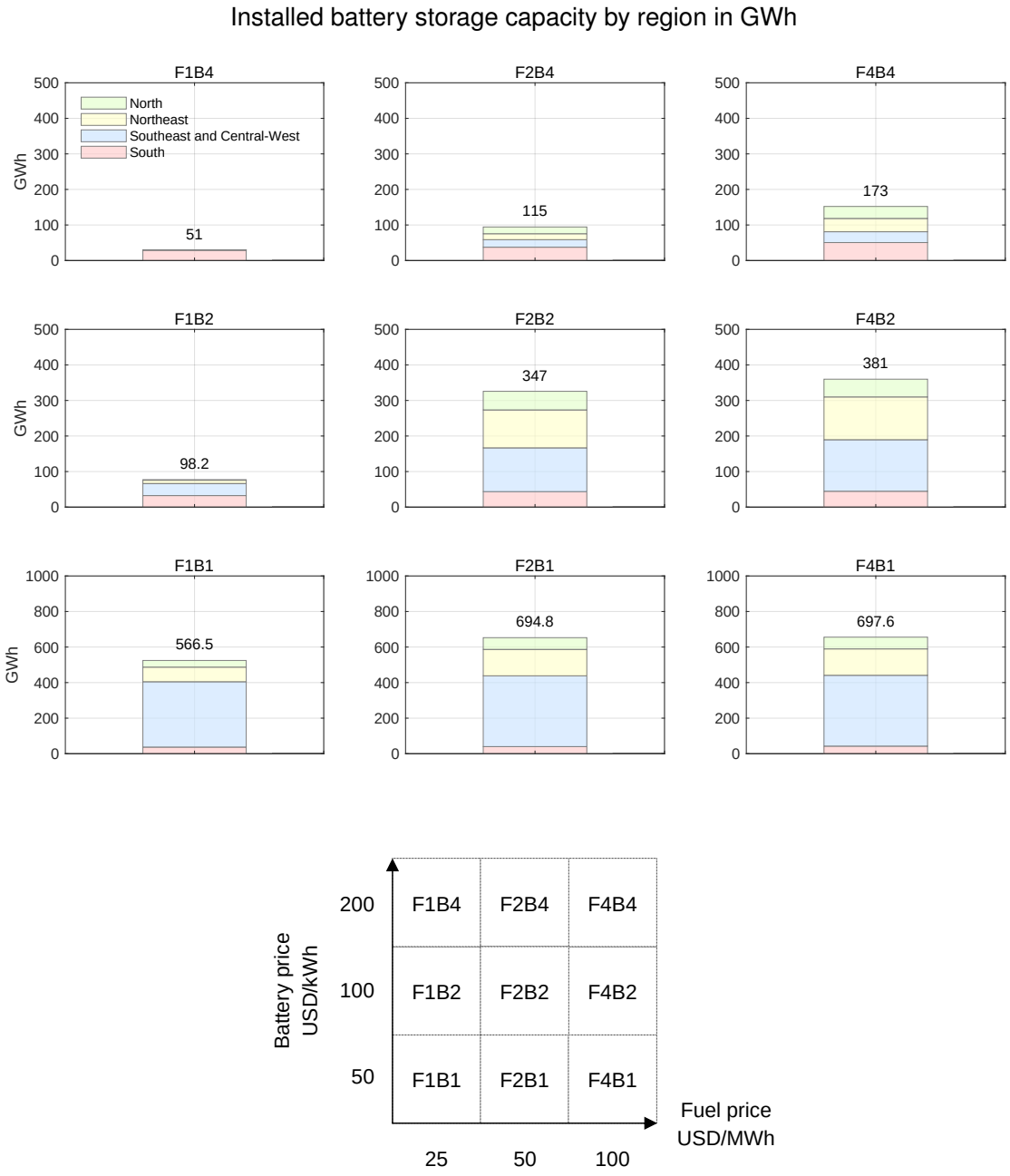

Figure A.33: Scenario 1a "Base", scheme FxB

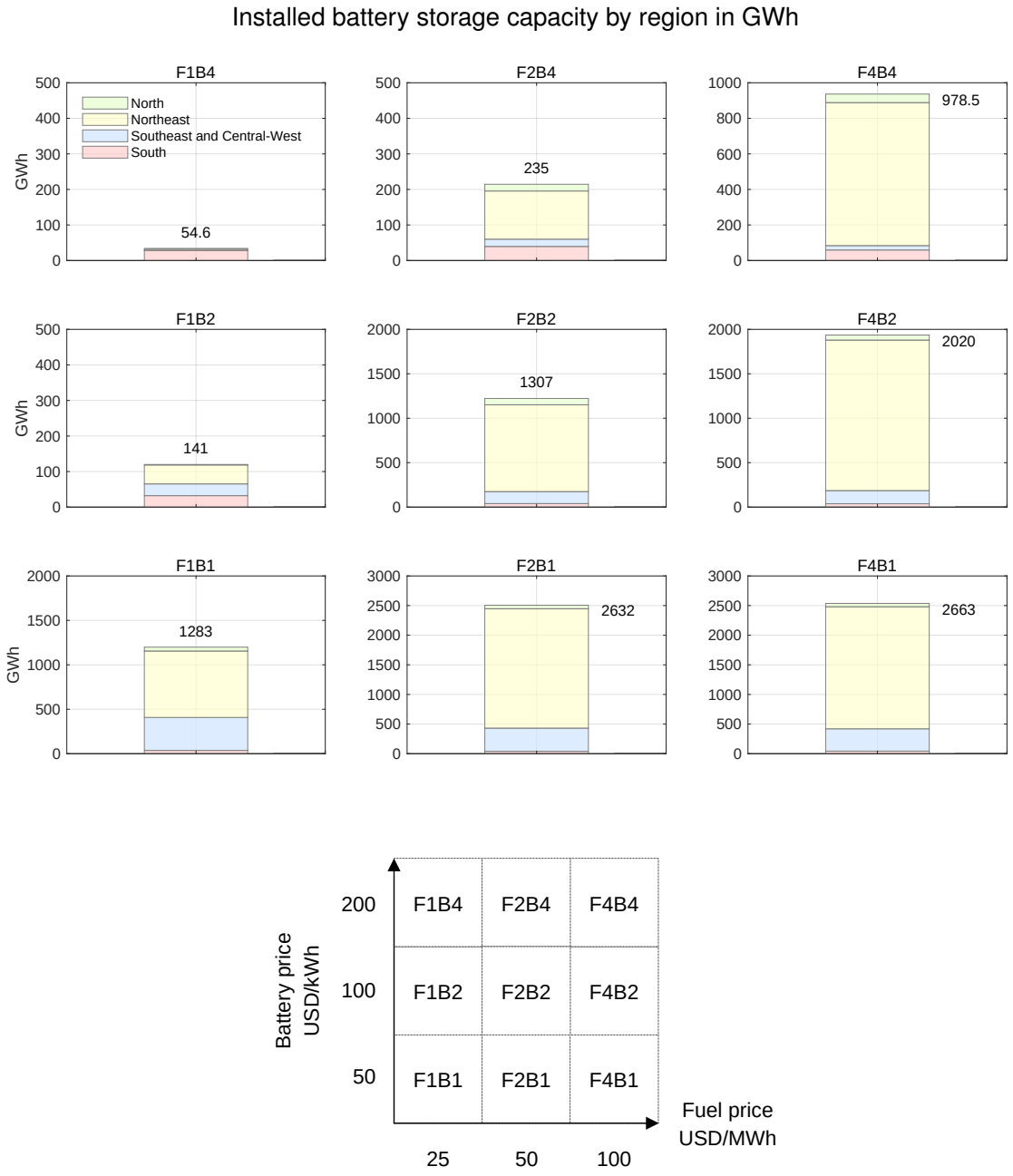

Figure A.34: Scenario 2a "Hydrogen", scheme FxB

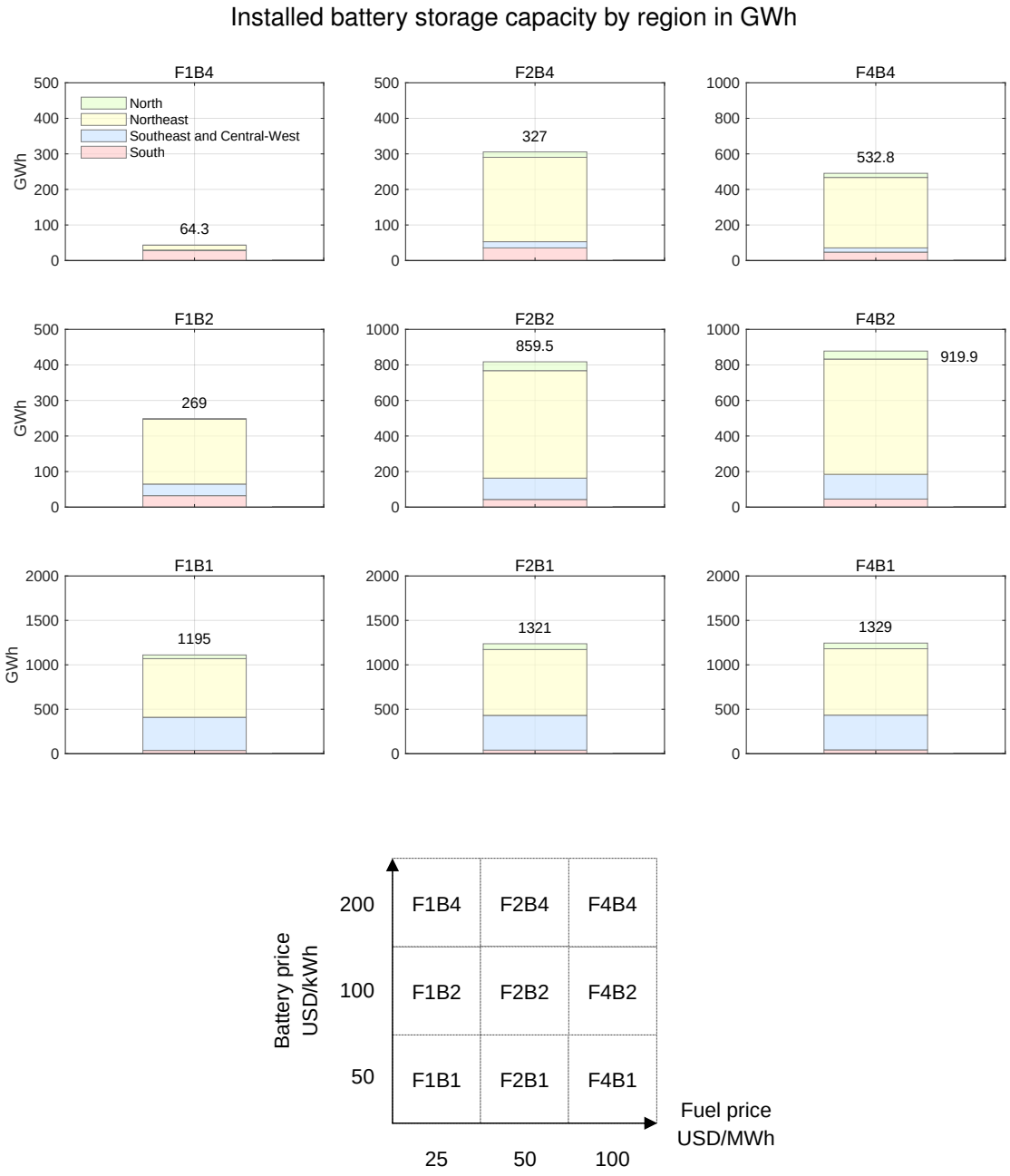

Figure A.35: Scenario 3a "Green hydrogen", scheme FxB

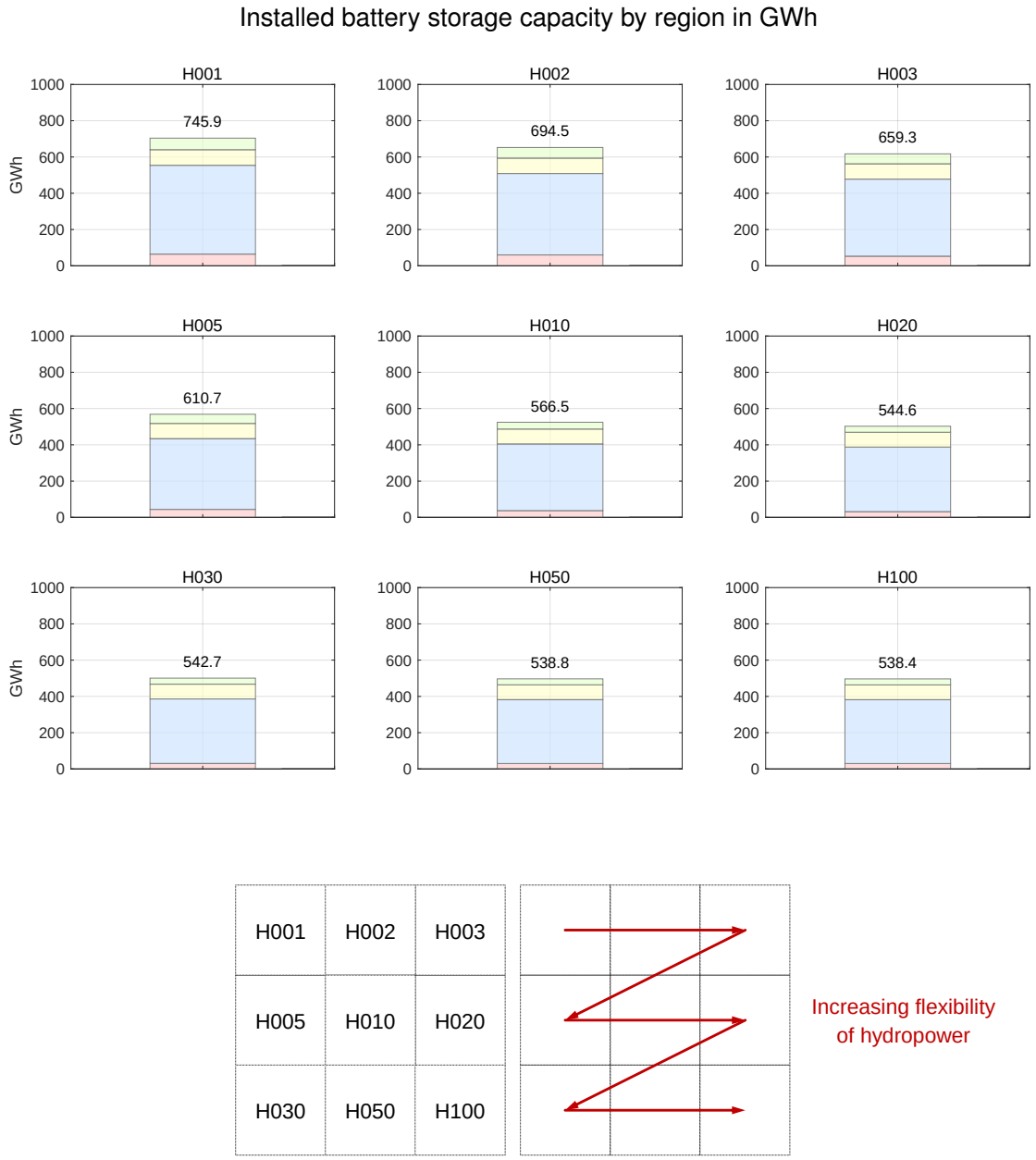

Figure A.36: Scenario 1b "Base", scheme H100

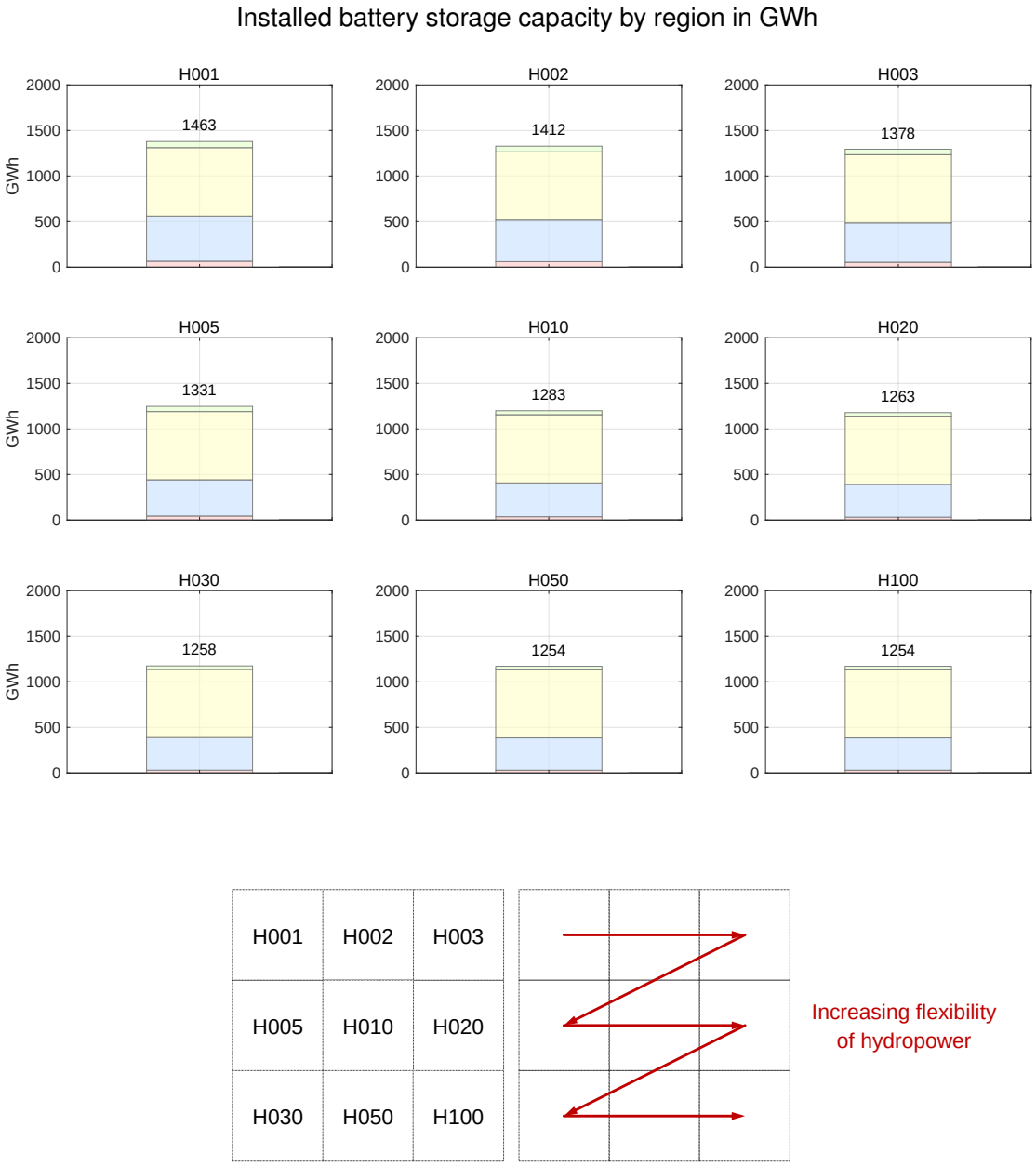

Figure A.37: Scenario 2b "Hydrogen", scheme H100

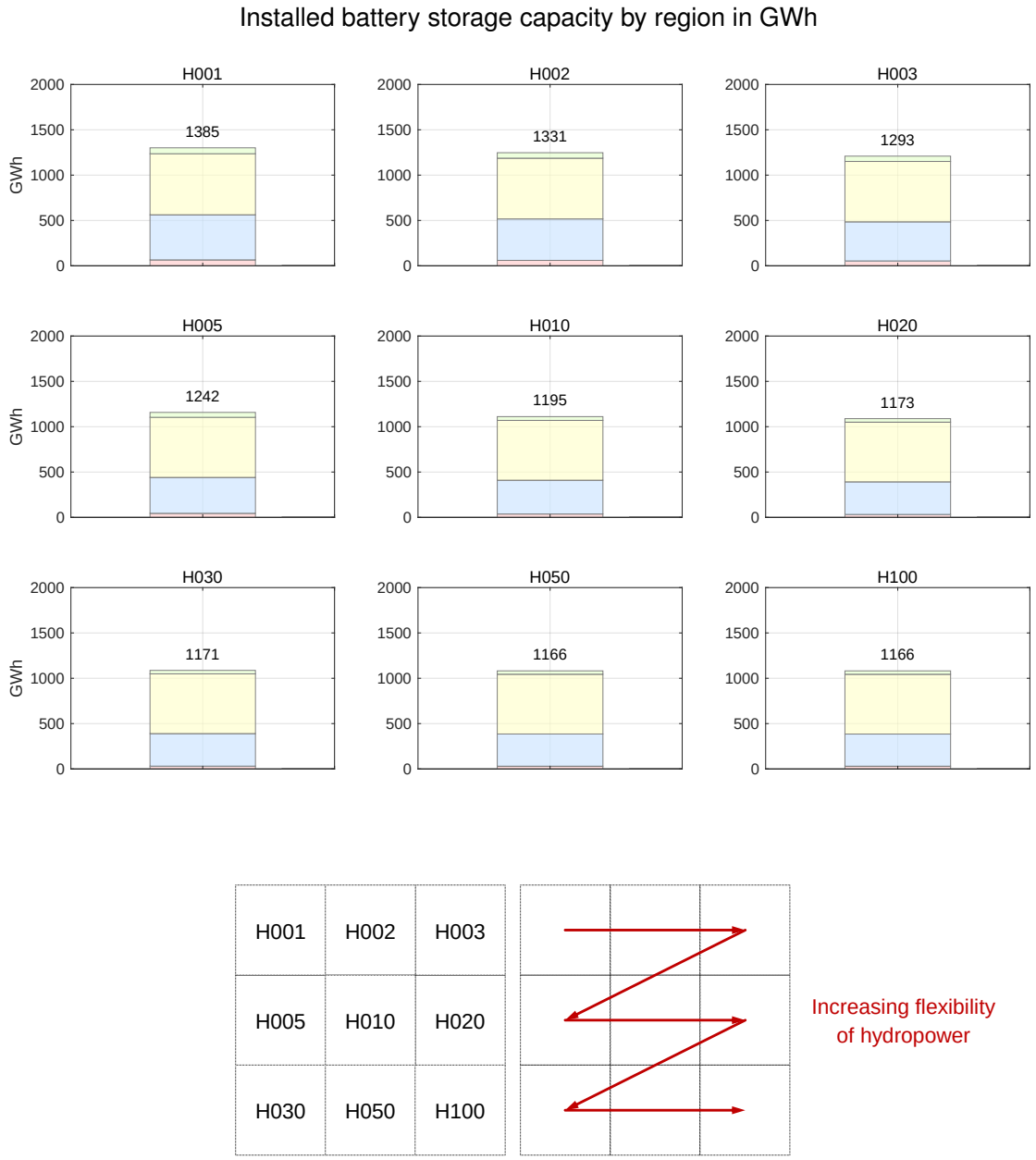

Figure A.38: Scenario 3b "Green hydrogen", scheme H100

A4.5 Generation and load

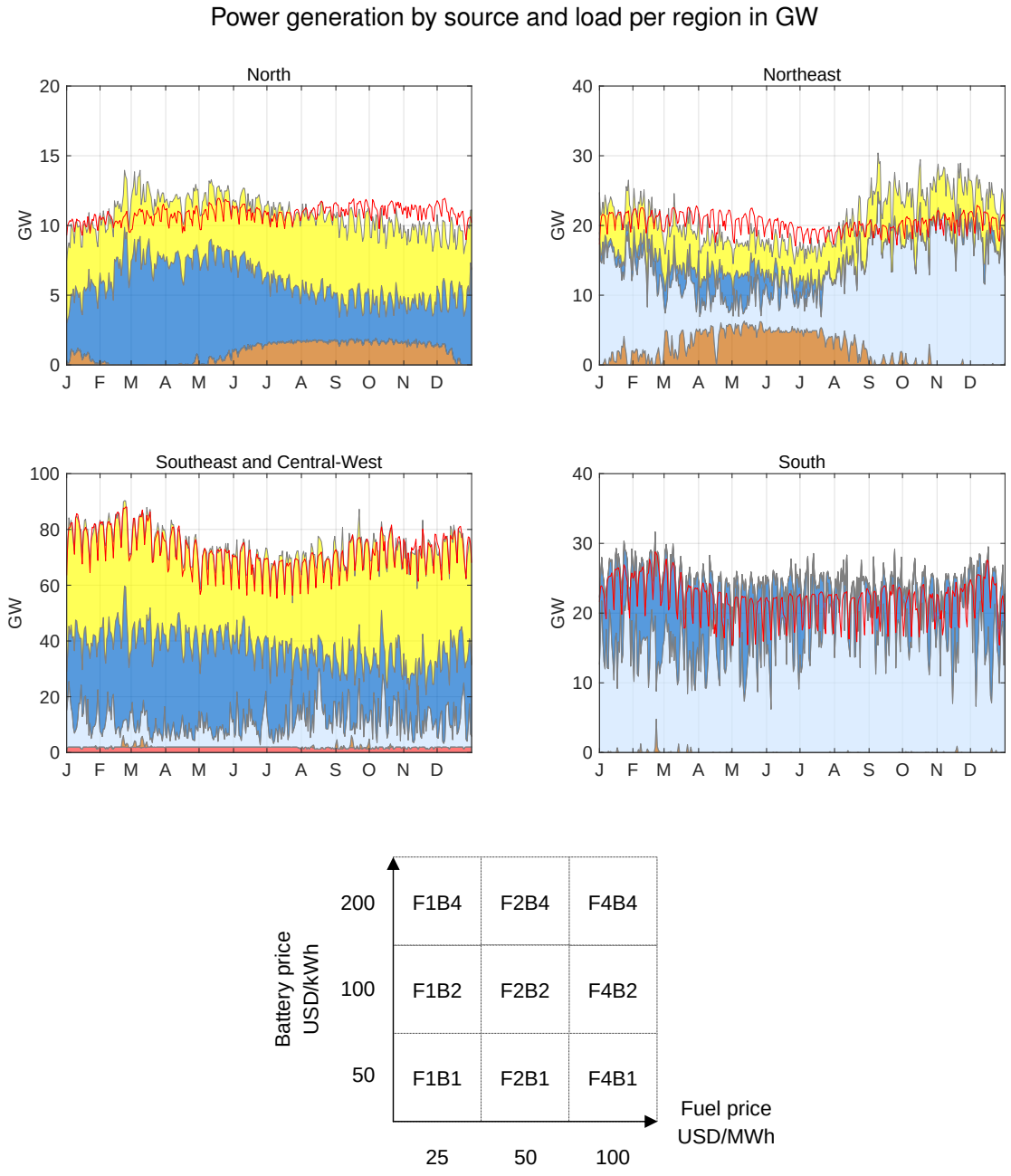

Figure A.39: Scenario 1a "Base", sub-scenario F1B1

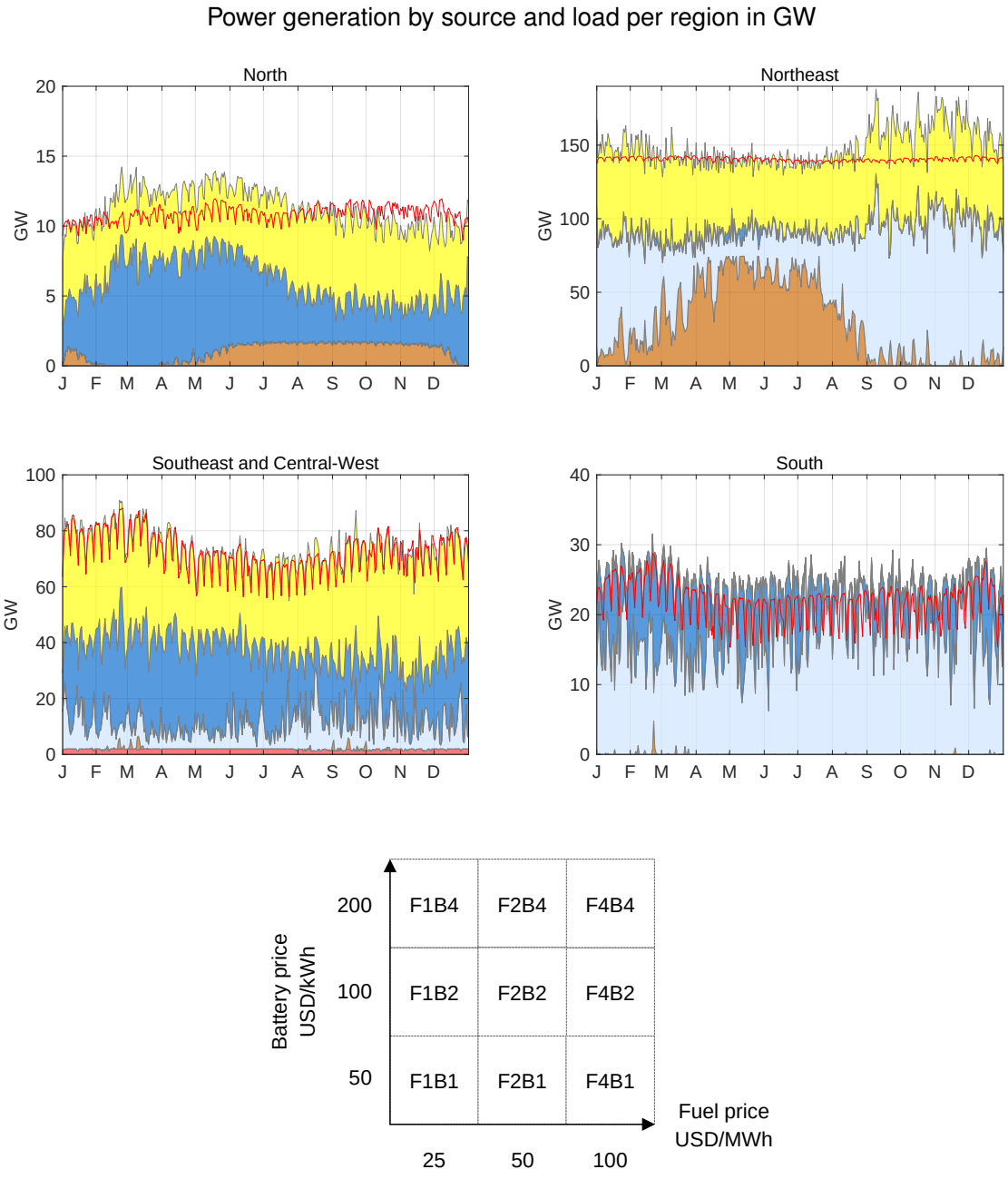

Figure A.40: Scenario 2a "Hydrogen", sub-scenario F1B1

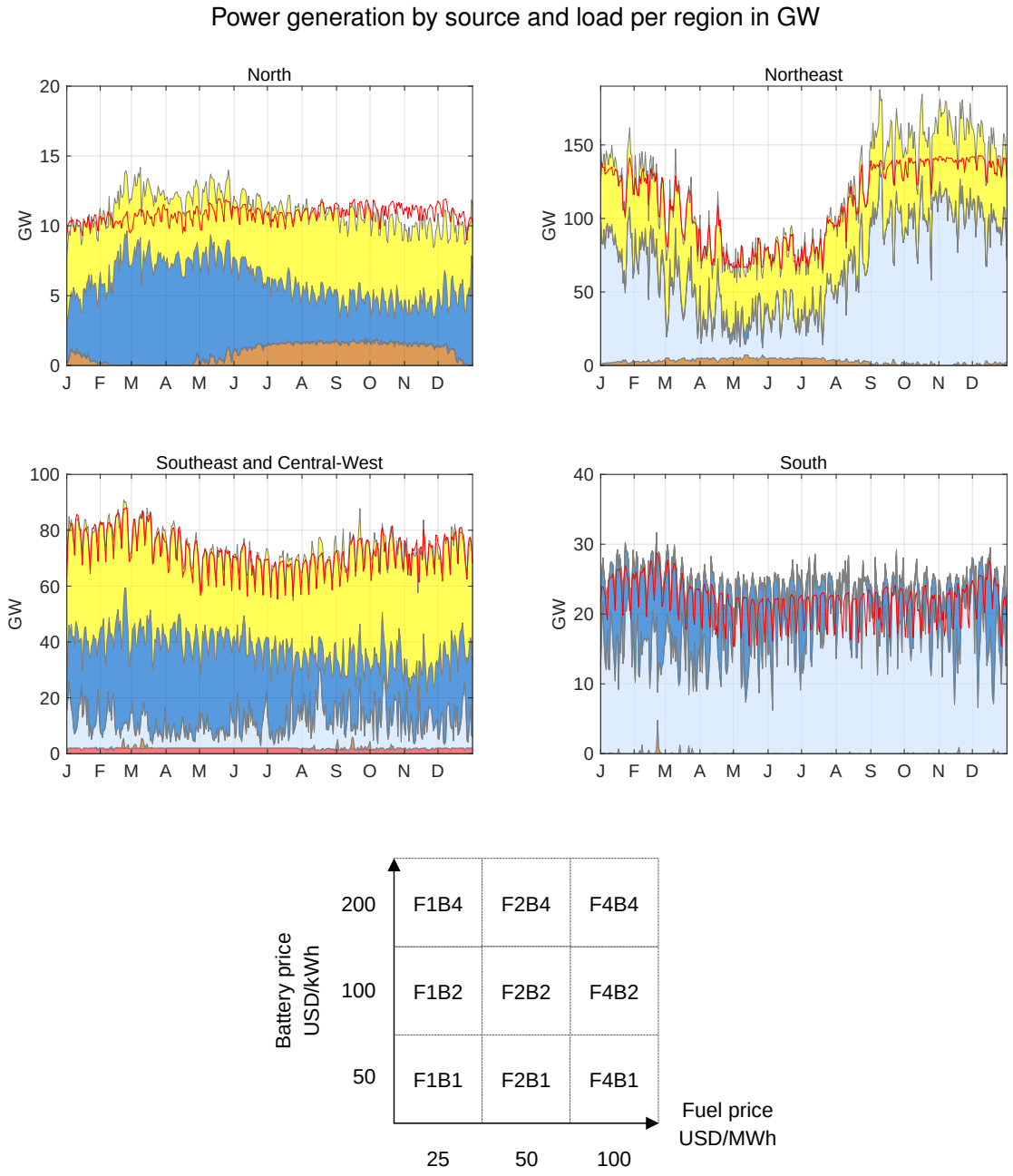

Figure A.41: Scenario 3a "Green hydrogen", sub-scenario F1B1

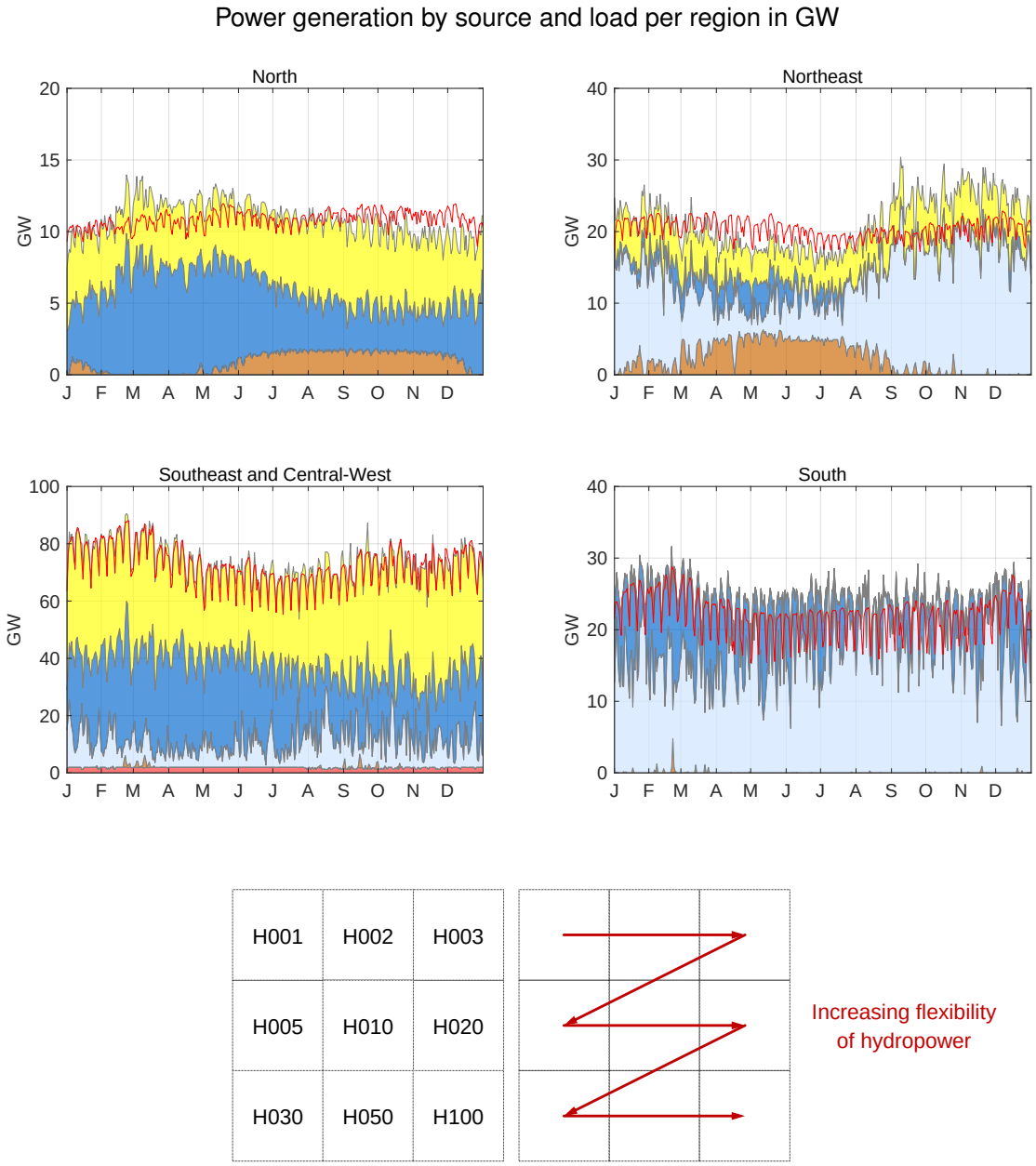

Figure A.42: Scenario 1b "Base", sub-scenario H010

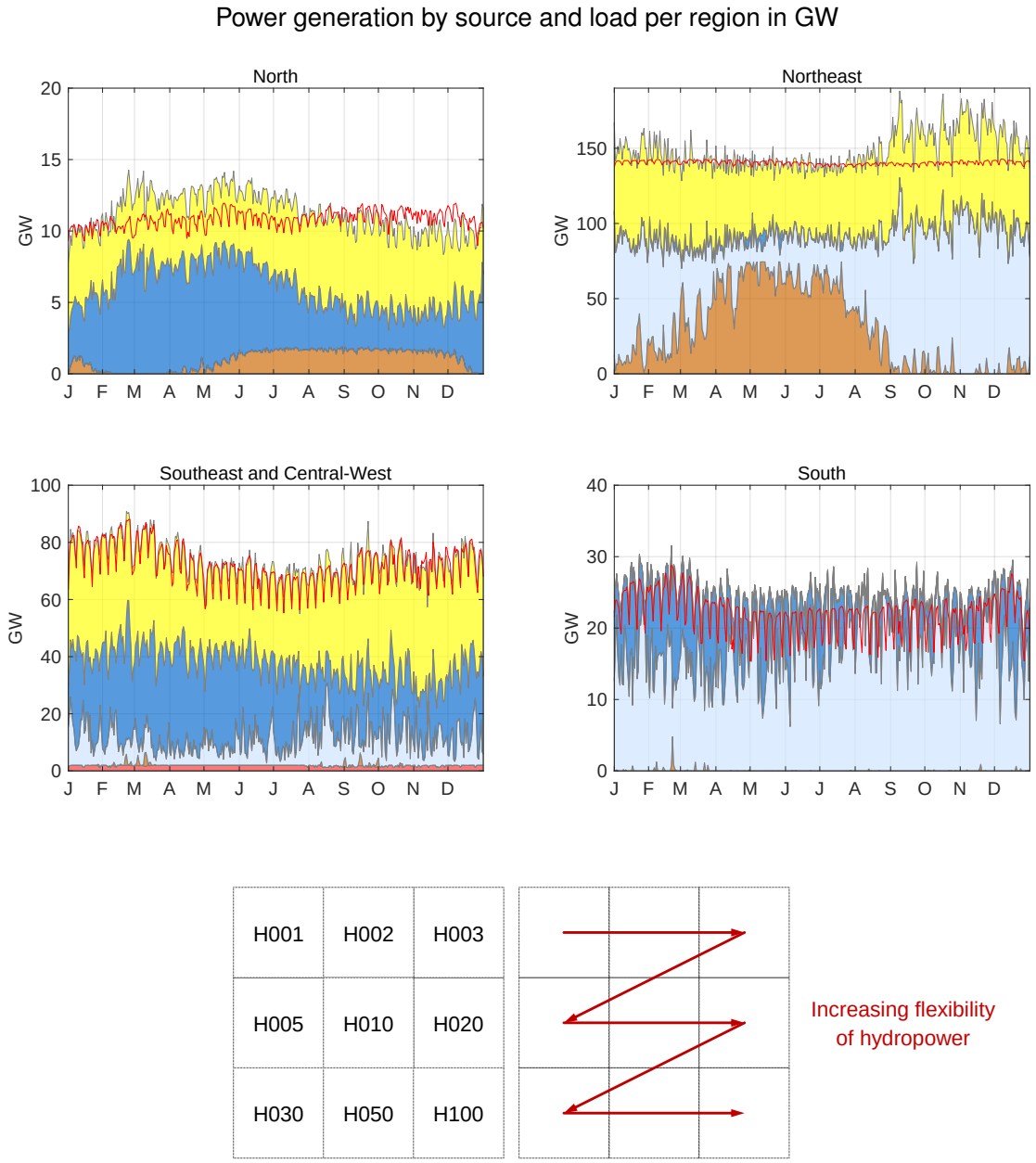

Figure A.43: Scenario 2b "Hydrogen", sub-scenario H010

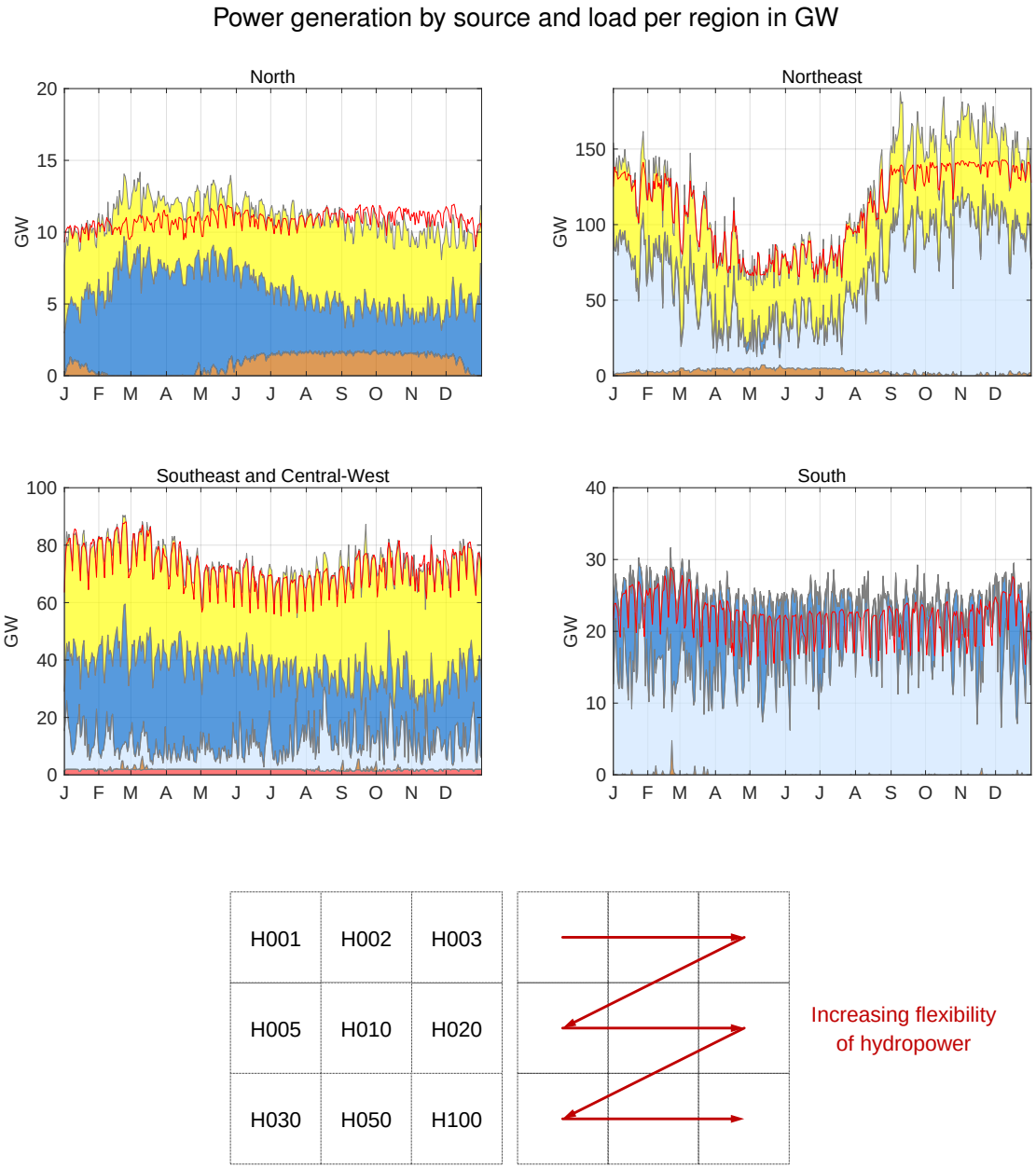

Figure A.44: Scenario 3b "Green hydrogen", sub-scenario H010

A4.6 Hydropower gradients and ramps

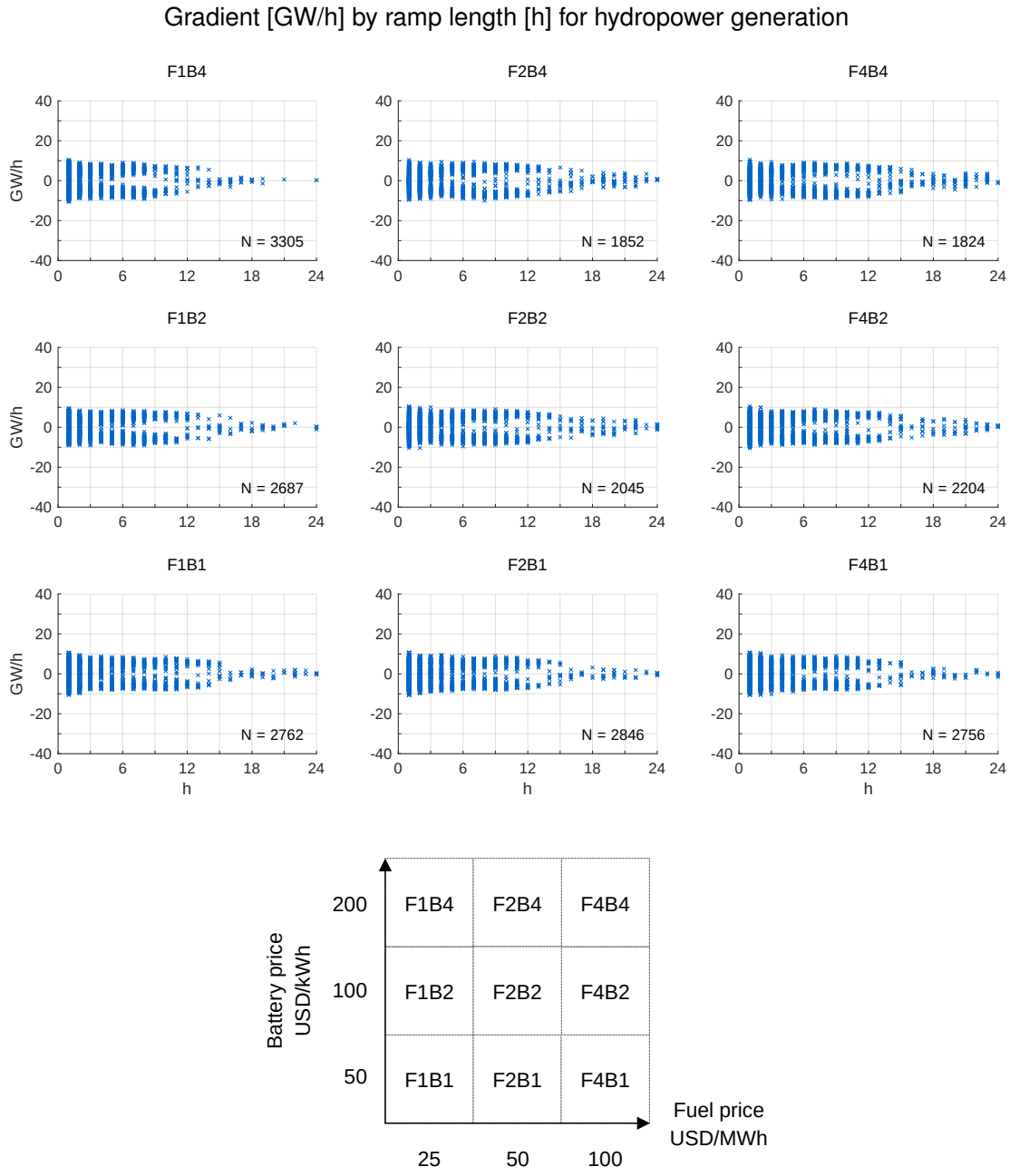

Figure A.45: Scenario 1a "Base", scheme FxB

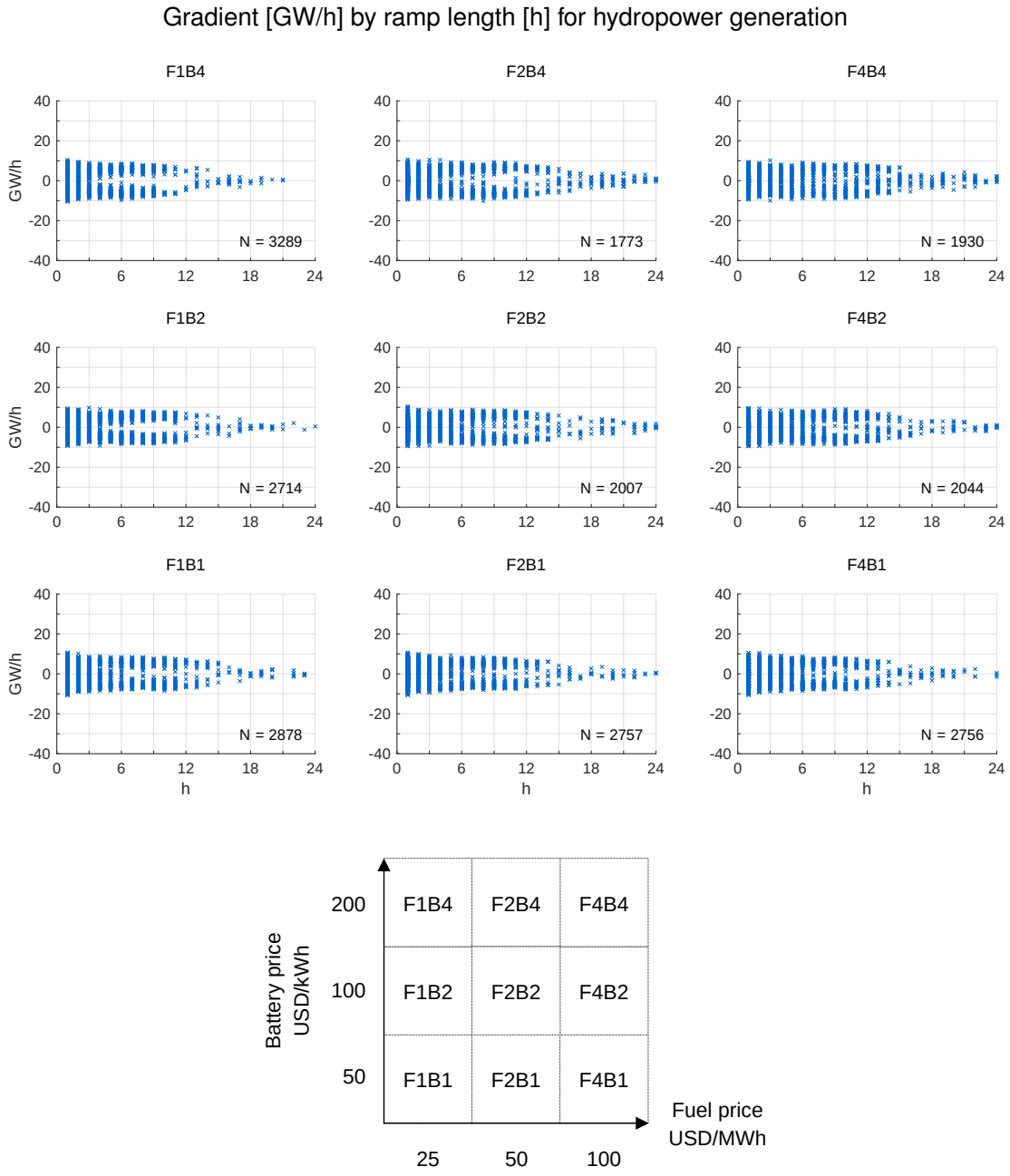

Figure A.46: Scenario 2a "Hydrogen", scheme FxB

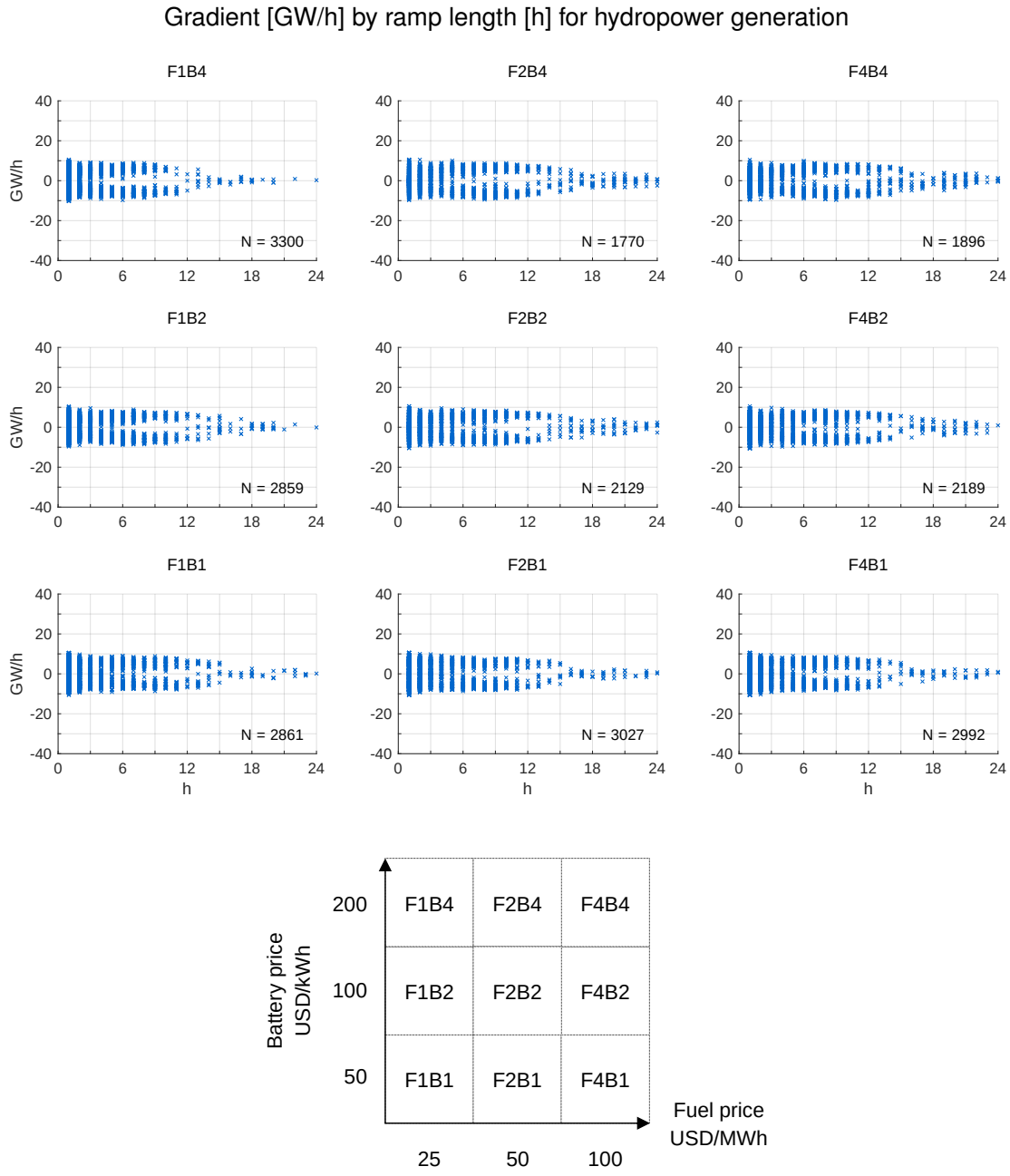

Figure A.47: Scenario 3a "Green hydrogen", scheme FxB

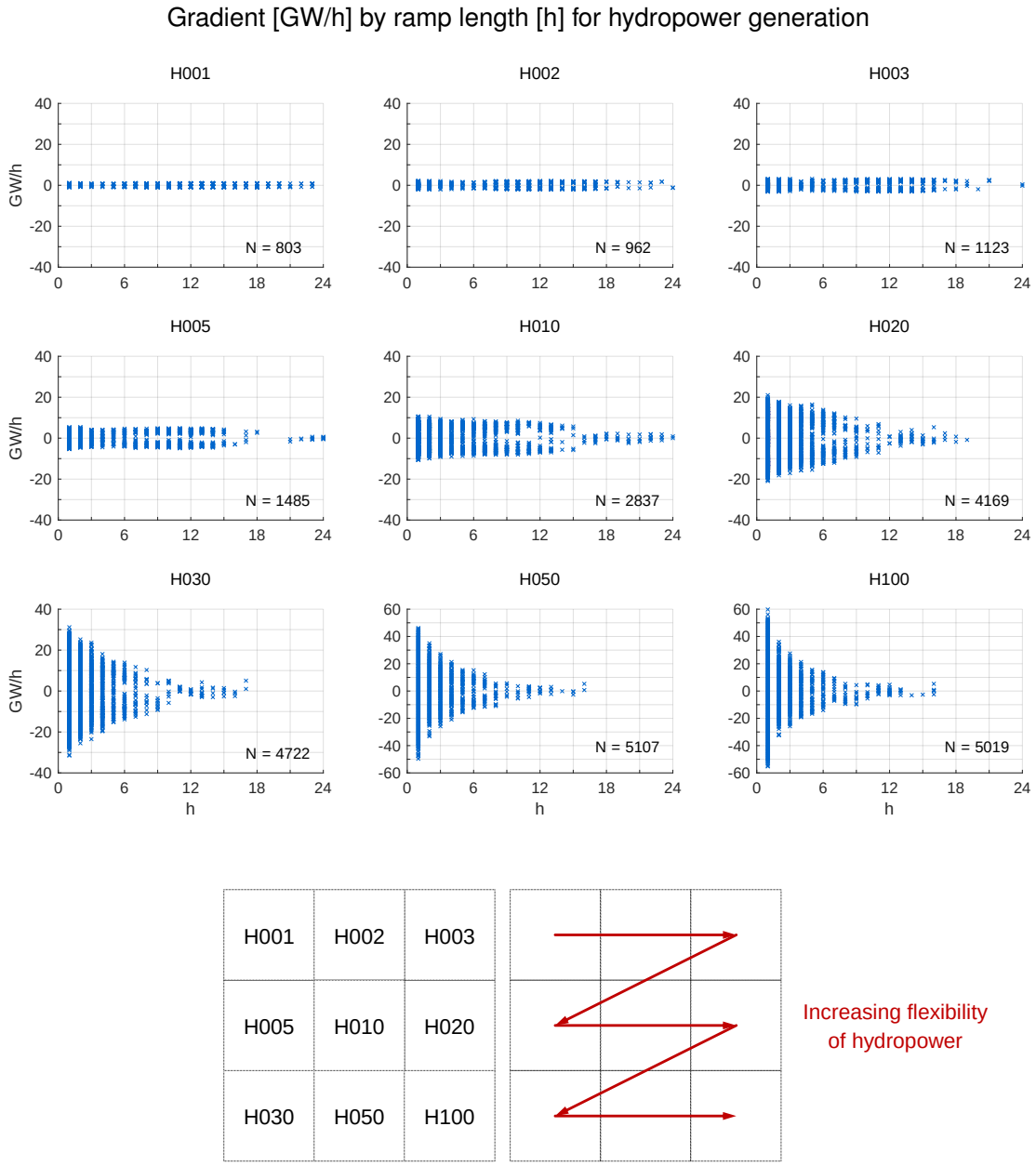

Figure A.48: Scenario 1b "Base", scheme H100

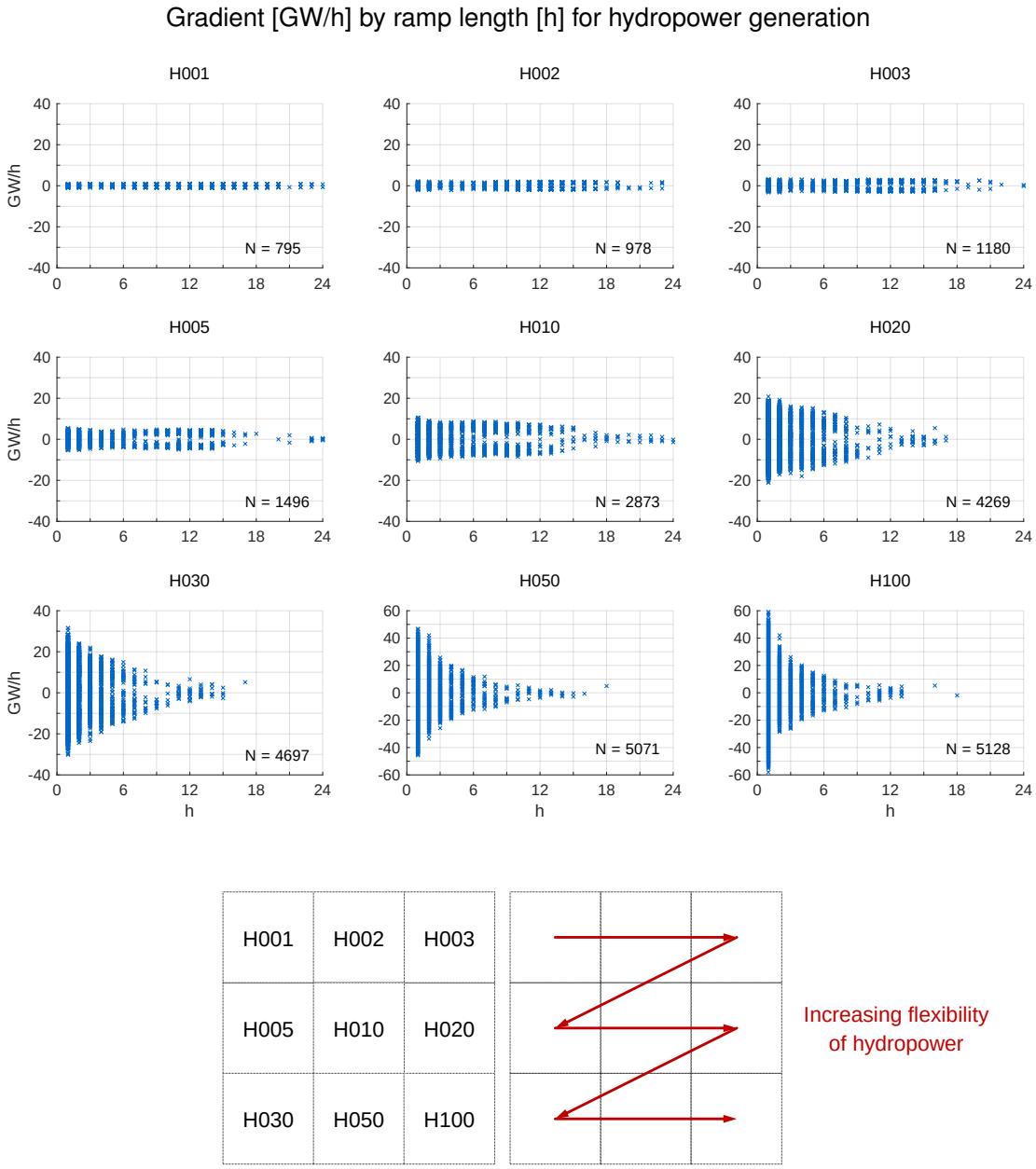

Figure A.49: Scenario 2b "Hydrogen", scheme H100

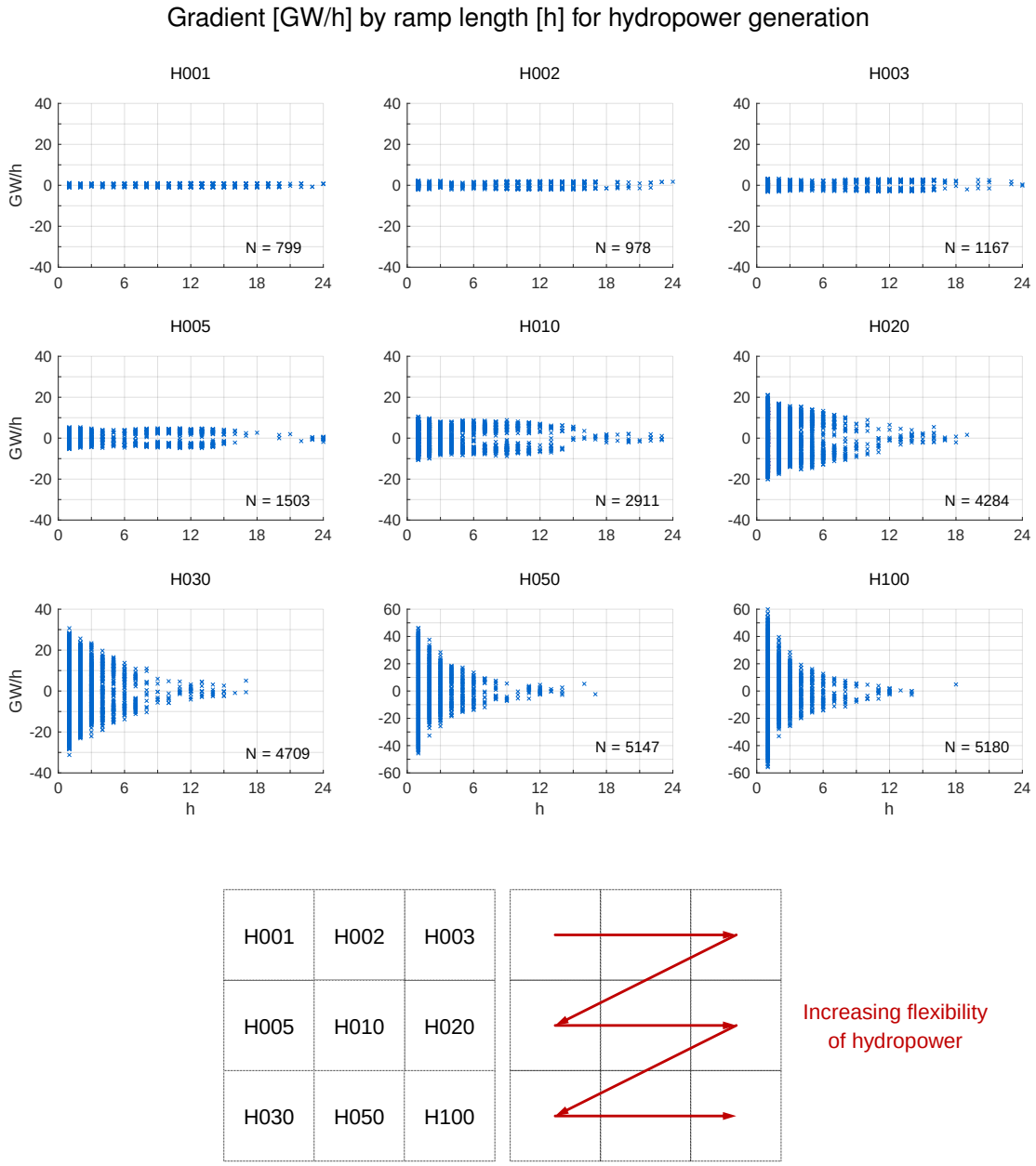

Figure A.50: Scenario 3b "Green hydrogen", scheme H100

A4.7 Transmission capacity between regions

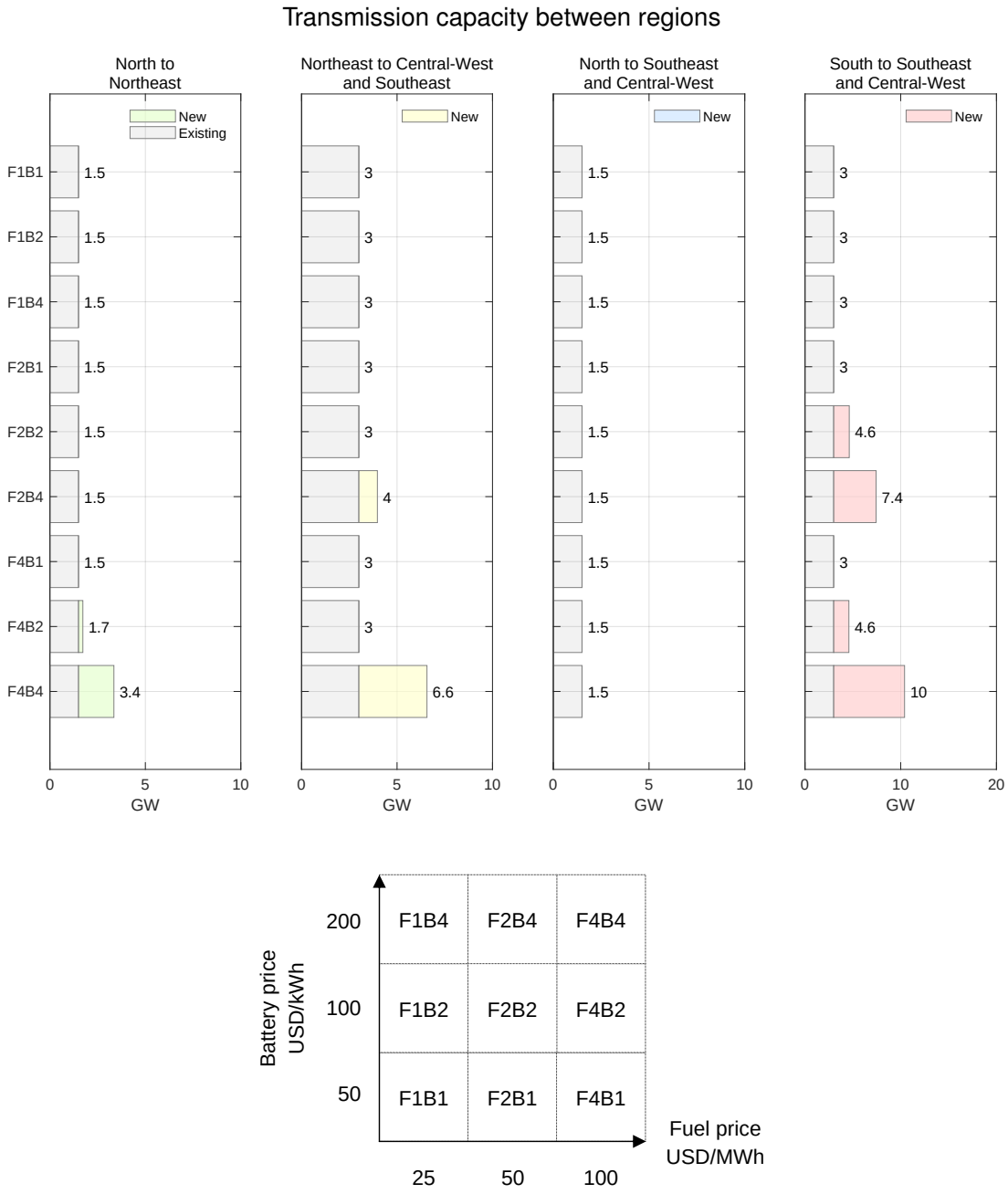

Figure A.51: Scenario 1a "Base", scheme FxB

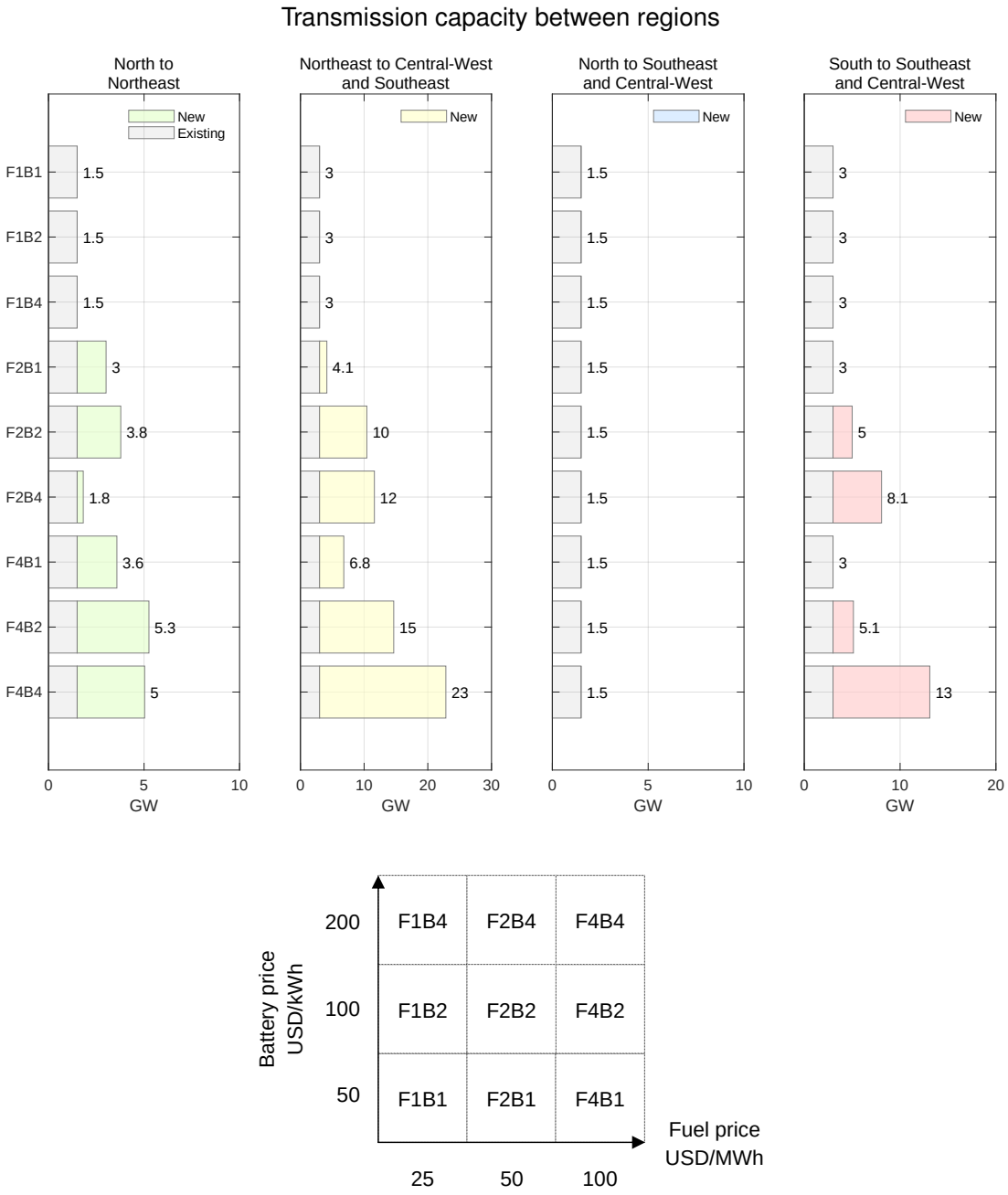

Figure A.52: Scenario 2a "Hydrogen", scheme FxB

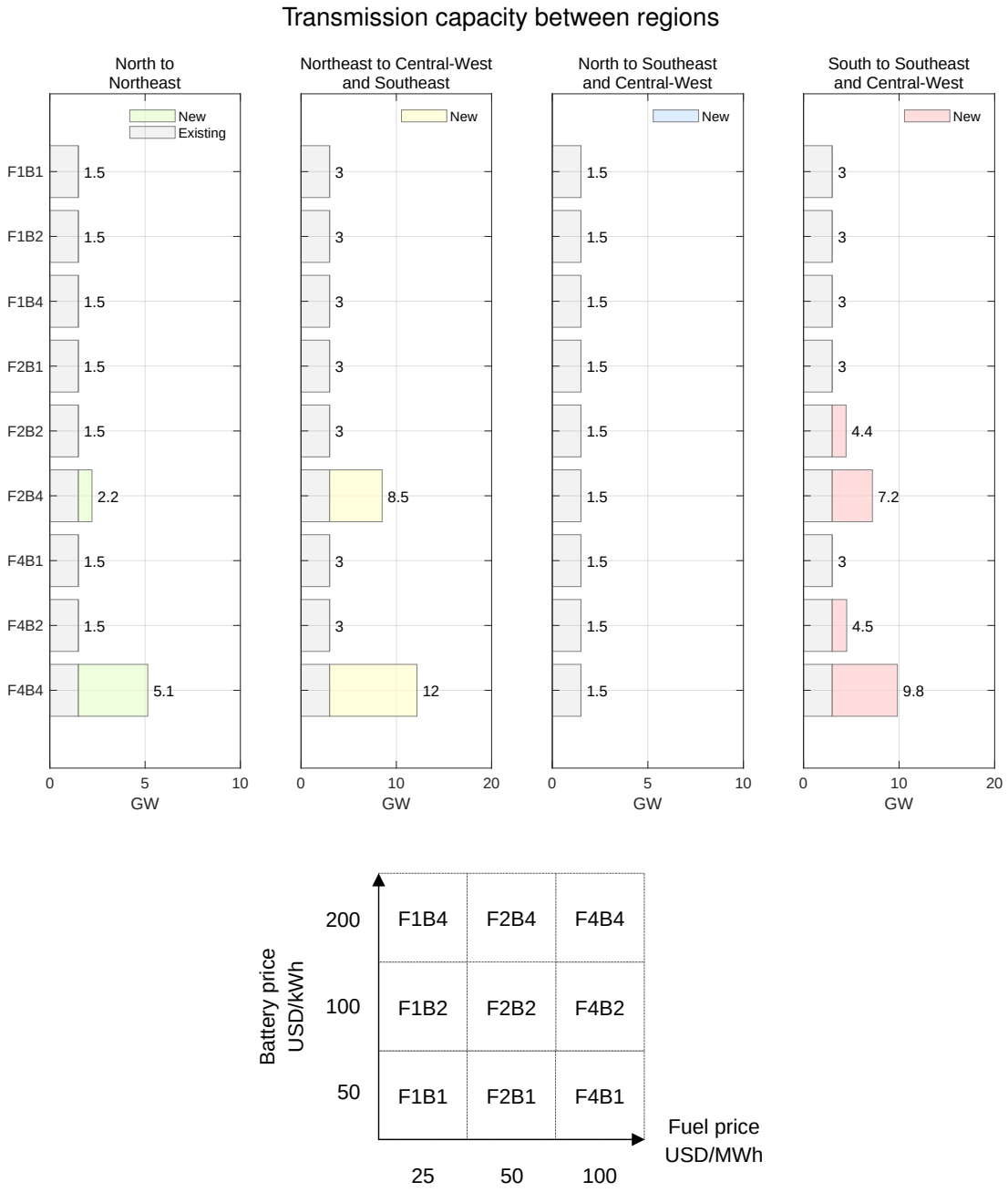

Figure A.53: Scenario 3a "Green hydrogen", scheme FxB

References

[1] M. C. Peel, B. L. Finlayson, and T. A. McMahon, “Updated world map of the Köppen-Geiger climate classification,” *Hydrology and Earth System Sciences*, vol. 11, no. 5, pp. 1633–1644, 2007.

[2] ESRI, “World Imagery,” 2009. [Online]. Available: https://services.arcgisonline.com/ArcGIS/rest/services/World_Imagery/MapServer

[3] IBGE, “Estimativas de População,” Rio de Janeiro, 2018. [Online]. Available: https://www.ibge.gov.br/estatisticas-novoportal/sociais/populacao/9103-estimativas-de-populacao.html

[4] The World Bank, “The World Bank Data,” Washington, D.C., 2017. [Online]. Available: https://data.worldbank.org/country/brazil

[5] Eurostat, “Gini-Koeffizient des verfügbaren Äquivalenzeinkommens,” Luxemburg, 2018. [Online]. Available: http://appsso.eurostat.ec.europa.eu/nui/show.do?dataset=ilc_di12

[6] Federal Reserve Bank of St. Louis, “Economic Research: Economic Data,” 2018. [Online]. Available: https://fred.stlouisfed.org/series

[7] Banco Central do Brasil, “Interest rates: Review Of COPOM Meetings and Short-Term Interest Rates.” 2018. [Online]. Available: http://www.bcb.gov.br/en/#!/c/INTEREST/

[8] Empresa de Pesquisa Energética, “BALANÇO ENERGÉTICO NACIONAL (Séries Completas - Tabelas): 1970-2016: ano base 2016,” Rio de Janeiro. [Online]. Available: https://ben.epe.gov.br/BENSeriesCompletas.aspx

[9] AGÊNCIA NACIONAL DE ENERGIA ELÉTRICA, “Ranking das Tarifas,” Brasília, 2018. [Online]. Available: http://www.aneel.gov.br/ranking-das-tarifas

[10] Empresa de Pesquisa Energética, “Anuário Estatístico de Energia Elétrica 2017: ano base 2016,” Rio de Janeiro.

[11] AGÊNCIA NACIONAL DE ENERGIA ELÉTRICA, “Fornecimento de energia elétrica no país melhora em 2017,” 2018. [Online]. Available: http://www.aneel.gov.br/sala-de-imprensa-exibicao/-/asset_publisher/XGPXSqdMFHrE/content/fornecimento-de-energia-eletrica-no-pais-melhora-em-2017/656877

[12] Empresa de Pesquisa Energética, “Anuário Estatístico de Energia Elétrica 2016: ano base 2015,” Rio de Janeiro.

[13] Food and Agriculture Organization, “FAOSTAT: Crops,” Rome, 2018. [Online]. Available: http://www.fao.org/faostat/en/?#data/QC

[14] Lima, Antônio Carlos de Oliveira, C. J. Caldas, and F. H. Saraiva, “Anuário Estatístico da Agroenergia 2014: Statistical Yearbook of Agrienergy 2014,” Brasília. [Online]. Available: http://www.agricultura.gov.br/assuntos/sustentabilidade/agroenergia/pasta-anuario-estatistico-da-agroenergia/anuario-estatistico-da-agroenergia-2014.pdf

[15] PROCEL and Eletrobrás, “Pesquisas de Posse e Hábitos de Consumo de Energia (PPHs): Classe Residencial Relatório Brasil: ano base 2005,” Rio de Janeiro. [Online]. Available: http://www.procelinfo.com.br

[16] INMET, “Arquivos climáticos INMET 2016,” Santa Catarina, 2016. [Online]. Available: http://www.labeee.ufsc.br/downloads/arquivos-climaticos/inmet2016

[17] ONS, “Histórico da Operação,” Brasília, 2018. [Online]. Available: http://ons.org.br/pt/paginas/resultados-da-operacao/historico-da-operacao

[18] W. Baer, “The Brazilian boom 1968–72: an explanation and interpretation,” *World Development*, vol. 1, no. 8, pp. 1–15, 1973.

[19] AGÊNCIA NACIONAL DE ENERGIA ELÉTRICA, “Relatórios de Consumo e Receita de Distribuição: Tarifa Média por Classe de Consumo e por Região,” Brasília, 2018. [Online]. Available: http://www.aneel.gov.br/relatorios-de-consumo-e-receita

[20] Empresa de Pesquisa Energética, “Demanda de energia no setor de transportes: Consolidação de bases de dados do setor transporte: 1970-2010,” Rio de Janeiro. [Online]. Available: http://www.epe.gov.br

[21] Umweltbundesamt, “Endenergieverbrauch und Energieeffizienz des Verkehrs,” Dessau-Roßlau, 2018. [Online]. Available: https://www.umweltbundesamt.de/daten/verkehr/endenergieverbrauch-energieeffizienz-des-verkehrs

[22] CIA, “The World Factbook 2018,” Washington, D.C., 2018. [Online]. Available: https://www.cia.gov/library/publications/the-world-factbook/geos/br.html

[23] IBGE, *Brasil - 500 anos de povoamento*. Rio de Janeiro: Instituto Brasileiro de Geografia e Estatística, 2007. [Online]. Available: https://biblioteca.ibge.gov.br/visualizacao/livros/liv6687.pdf

[24] ——, “Pesquisa de Orçamentos Familiares 2008-2009 - Perfil das Despesas no Brasil Indicadores selecionados: Proporção de domicílios particulares permanentes com água encanada, por fonte de aquecimento, segundo a situação do domicílio, as Grandes Regiões e as Unidades da Federação - período 2008-2009,” Rio de Janeiro. [Online]. Available: ftp://ftp.ibge.gov.br/Orcamentos_Familiares/Pesquisa_de_Orcamentos_Familiares_2008_2009/Perfil_das_Despesas_no_Brasil/tabelas_pdf/tab_1_02.pdf

[25] ——, “Contas Regionais do Brasil: Produto Interno Bruto das Grandes Regiões e Unidades da Federação,” Rio de Janeiro, 2012. [Online]. Available: https://ww2.ibge.gov.br/home/estatistica/economia/contasregionais/2012/default_xls_2002_2012.shtm

[26] C. A. Alvares, J. L. Stape, P. C. Sentelhas, J. L. de Moraes Gonçalves, and G. Sparovek, “Köppen’s climate classification map for Brazil,” *Meteorologische Zeitschrift*, vol. 22, no. 6, pp. 711–728, 2014.

[27] W. Köppen and R. Geiger, Eds., *Das geographische System der Klimate*, ser. Handbuch der Klimatologie. Berlin: Gebrüder Bornträger, 1936, vol. 1.

[28] B. P. Marques and R. C. Fernandes, “A Desflorestação da Amazónia: do "inferno verde" ao "deserto vermelho"?” *GeoINova*, no. 9, pp. 81–100, 2004. [Online]. Available: https://run.unl.pt/handle/10362/11486

[29] G. Eiten, “The Cerrado Vegetation of Brazil,” *Botanical Review*, no. 38, pp. 201–341, 1972. [Online]. Available: www.jstor.org/stable/4353829

[30] X.-P. Song, M. C. Hansen, S. V. Stehman, P. V. Potapov, A. Tyukavina, E. F. Vermote, and J. R. Townshend, “Global land change from 1982 to 2016,” *Nature*, vol. 560, no. 7720, pp. 639–643, 2018.

[31] N. Gorelick, M. Hancher, M. Dixon, S. Ilyushchenko, D. Thau, and R. Moore, “Google Earth Engine: Planetary-scale geospatial analysis for everyone,” *Remote Sensing of Environment*, vol. 202, pp. 18–27, 2017.

[32] E. Haddad, “Trade Liberalization, Space, and Regional Development,” in *Economic Development in Latin America*, H. S. Esfahani, G. Facchini, and G. J. D. Hewings, Eds. London: Palgrave Macmillan UK, 2010, pp. 201–2016.

[33] International Monetary Fund, “World Economic Outlook Database,” Washington, D.C., 2018. [Online]. Available: http://www.imf.org/external/pubs/ft/weo/2018/01/weodata/index.aspx

[34] The World Bank and Statista, “Brazil: Unemployment rate from 2007 to 2017,” Hamburg, 2018. [Online]. Available: https://www.statista.com/statistics/263711/unemployment-rate-in-brazil/

[35] ——, “Brazil: Distribution of employment by economic sector from 2007 to 2017,” Hamburg, 2018. [Online]. Available: https://www.statista.com/statistics/271042/employment-by-economic-sector-in-brazil/

[36] ——, “Brazil: Share of economic sectors in the GDP from 2007 to 2017,” Hamburg, 2018. [Online]. Available: https://www.statista.com/statistics/254407/share-of-economic-sectors-in-the-gdp-in-brazil/

[37] W. Baer, *The Brazilian Economy: Growth and Development*, 7th ed. Boulder, Colorado: Rienner, 2014.

[38] P. T. Kilborn, “Brazil’s economic ’miracle’ and its collapse,” *The New York Times*, vol. 1983, no. 26.11.1983, 26.11.1983. [Online]. Available: https://www.nytimes.com/1983/11/26/business/brazil-s-economic-miracle-and-its-collapse.html

[39] World Nuclear Association, "Nuclear Power in Brazil," London, 2018. [Online]. Available: http://www.world-nuclear.org/information-library/country-profiles/countries-a-f/brazil.aspx

[40] D. Budny, "The Global Dynamics of Biofuels: Potential Supply and Demand for Ethanol and Biodiesel in the Coming Decade," Washington, D.C. [Online]. Available: https://www.wilsoncenter.org/sites/default/files/Brazil_SR_e3.pdf

[41] W. Baer, *A Economia brasileira*, 2nd ed. São Paulo: Nobel, 2003.

[42] J. L. Love and W. Baer, Eds., *Brazil under Lula: Economy, politics, and society under the worker-president*. Basingstoke: Palgrave Macmillan, 2009.

[43] T. Fischermann, "Lulas letzter Kampf," *Die Zeit*, vol. 2016, pp. 1–3, 2016. [Online]. Available: https://www.zeit.de/politik/ausland/2016-03/brasilien-dilma-rousseff-lula-da-silva

[44] C. R. Azzoni, "Social Policies, Personal and Regional Income Inequality in Brazil: An I-O Analysis," in *Brazil under Lula*, J. L. Love and W. Baer, Eds. Basingstoke: Palgrave Macmillan, 2009, pp. 253–261.

[45] M. A. Haddad, "A Spatial Analysis of Bolsa Família: Is Allocation Targeting the Needy?" in *Brazil under Lula*, J. L. Love and W. Baer, Eds. Basingstoke: Palgrave Macmillan, 2009, pp. 187–203.

[46] J. Haughton and S. R. Khandker, *Handbook on Poverty and Inequality*. Washington, DC: World Bank, 2012.

[47] K. Storchmann, "Long-Run Gasoline demand for passenger cars: the role of income distribution," *Energy Economics*, vol. 27, no. 1, pp. 25–58, 2005.

[48] J. Watts, "Operation Car Wash: Is this the biggest corruption scandal in history?" *The Guardian*, vol. 2017, 01.06.2017. [Online]. Available: https://www.theguardian.com/world/2017/jun/01/brazil-operation-car-wash-is-this-the-biggest-corruption-scandal-in-history

[49] D. Biller, "Brazil's Highs and Lows," *Bloomberg*, vol. 2018, 06.04.2018. [Online]. Available: https://www.bloomberg.com/quicktake/brazils-highs-lows

[50] Transparency International, "Corruption Perceptions Index (CPI) 2017," Berlin, 2017. [Online]. Available: https://www.transparency.org/news/feature/corruption_perceptions_index_2017#table

[51] J. Shao, P. C. Ivanov, B. Podobnik, and H. E. Stanley, "Quantitative relations between corruption and economic factors," *The European Physical Journal B*, vol. 56, no. 2, pp. 157–166, 2007.

[52] The World Bank, "Doing Business 2018: Reforming to Create Jobs," Washington, D.C. [Online]. Available: http://www.doingbusiness.org/reports/global-reports/doing-business-2018

[53] ——, “Doing Business: Trading Across Borders,” Washington, D.C., 2018. [Online]. Available: http://www.doingbusiness.org/data/exploretopics/trading-across-borders

[54] The World Bank and Statista, “Where Global Tariffs Are Highest And Lowest,” Hamburg, 2018. [Online]. Available: https://www.statista.com/chart/13335/where-global-tariffs-are-highest-and-lowest/

[55] R. d. O. Batista, “Results and Perspectives of the Brazilian Electrical Sector Privatization Program,” Paper, The George Washington University, Washington, D.C., 1998.

[56] Queiroz, Leonardo Mendonça Oliveira de, “Assessing the overall performance of Brazilian electric distribution companies,” Paper, The George Washington University, Washington, D.C., 2010.

[57] T. J. Hammons, L. A. Barroso, and H. Rudnick, “Latin America: market mechanisms and supply adequacy in power sector reforms,” *Energy Systems*, vol. 2, no. 1, pp. 83–111, 2011.

[58] P. Mastropietro, C. Batlle, L. A. Barroso, and P. Rodilla, “Electricity auctions in South America: Towards convergence of system adequacy and RES-E support,” *Renewable and Sustainable Energy Reviews*, vol. 40, pp. 375–385, 2014.

[59] D. d. C. D. Melo, B. R. Scanlon, Z. Zhang, E. Wendland, and L. Yin, “Reservoir storage and hydrologic responses to droughts in the Paraná River basin, south-eastern Brazil,” *Hydrology and Earth System Sciences*, vol. 20, no. 11, pp. 4673–4688, 2016.

[60] FEDERATIVE REPUBLIC OF BRAZIL, “Intended Nationally Determined Contribution: Towards Achieving the Objective of the United Nations Framework Convention on Climate Change,” 2017. [Online]. Available: http://www4.unfccc.int/ndcregistry/PublishedDocuments/BrazilFirst/BRAZILiNDCenglishFINAL.pdf

[61] AGÊNCIA NACIONAL DE ENERGIA ELÉTRICA, “A Estrutura Tarifária para o Serviços de Distribuição de Energia Elétrica: Sumário Executivo,” Brasília.

[62] PKF, “Brazil Tax Guide 2016/17,” London. [Online]. Available: https://www.pkf.com/media/10028395/brazil-tax-guide-2016-17.pdf

[63] Rödl & Partner, “Besteuerung von Unternehmen in Brasilien,” São Paulo. [Online]. Available: https://www.roedl.de:10006/de-de/de/unternehmen/standorte/brasilien/Documents/besteuerung-unternehmen-brasilien.pdf

[64] AGÊNCIA NACIONAL DE ENERGIA ELÉTRICA, “Entendendo a Tarifa,” Brasília, 2017. [Online]. Available: http://www.aneel.gov.br/entendendo-a-tarifa

[65] Associação Brasileira de Distribuidores de Energia El(étrica, “Comparação Internacional de Tarifas de Energia Elétrica: Resumo Executivo,” Brasília. [Online]. Available: http://www.abradee.com.br/escolha-abradee-para-voce/material-de-divulgacao

[66] AGÊNCIA NACIONAL DE ENERGIA ELÉTRICA, "Procedimentos de Regulação Tarifária: Bandeiras Tarifárias," Brasília, 2015. [Online]. Available: http://www2.aneel.gov.br/aplicacoes/audiencia/arquivo/2015/067/documento/anexo_nt_267_-_minuta_proret_6_8.pdf

[67] ——, "Bandeiras Tarifárias," Brasília, 2018. [Online]. Available: http://www.aneel.gov.br/bandeiras-tarifarias

[68] ——, "RESOLUÇÃO NORMATIVA Nº 482: 482/2012," 17.04.2012. [Online]. Available: http://www2.aneel.gov.br/cedoc/ren2012482.pdf

[69] ——, "Micro e Minigeração Distribuída: Sistema de Compensação de Energia Elétrica," Brasília, 2014. [Online]. Available: http://www2.aneel.gov.br/biblioteca/downloads/livros/caderno-tematico-microeminigeracao.pdf

[70] ——, "Perguntas e Respostas sobre a aplicação da Resolução Normativa nº 482/2012 – atualizado em 25/05/2017," Brasília, 2017. [Online]. Available: http://www.aneel.gov.br/documents/656827/15234696/FAQ+-V3_20170524/ab9ec474-7dfd-c98c-6753-267852784d86

[71] ——, "RESOLUÇÃO NORMATIVA Nº 733: 733/2016," 06.09.2016. [Online]. Available: http://www2.aneel.gov.br/cedoc/ren2016733.pdf

[72] Associação Brasileira de Distribuidores de Energia El(étrica, "Tarifa Branca," Brasília. [Online]. Available: http://www.abradee.com.br/escolha-abradee-para-voce/material-de-divulgacao

[73] AGÊNCIA NACIONAL DE ENERGIA ELÉTRICA, "Tarifa Branca," Brasília, 17.02.2017. [Online]. Available: http://www.aneel.gov.br/tarifa-branca

[74] ——, "Qualidade do Serviço," Brasília, 2018. [Online]. Available: http://www.aneel.gov.br/qualidade-do-servico2

[75] N. Shah, M. Wei, V. Letschert, and A. Phadke, "Benefits of Leapfrogging to Superefficiency and Low Global Warming Potential Refrigerants in Room Air Conditioning," 2015. [Online]. Available: https://ies.lbl.gov/sites/all/files/lbnl-1003671.pdf

[76] Empresa de Planejamento e Logística, "Transporte inter-regional de carga no Brasil: Carregamento com a matriz origem-destino," Brasília, 2016. [Online]. Available: https://www.epl.gov.br/transporte-inter-regional-de-carga-no-brasil-panorama-2015

[77] Agência Nacional de Transportes Terrestres, "Evolução do Transporte Ferroviário," Brasília. [Online]. Available: http://www.antt.gov.br/ferrovias/arquivos/Evolucao_do_Transporte_Ferroviario.html

[78] ——, "Mapa do Subsistema Ferroviário Federal," Brasília. [Online]. Available: http://www.antt.gov.br/ferrovias/arquivos/Evolucao_do_Transporte_Ferroviario.html

[79] T. Dallmann and C. Façanha, “International Comparison of Brazilian Regulatory Standards for Light-Duty Vehicle Emissions,” Washington, D.C. [Online]. Available: www.theicct.org

[80] USDA, “Brazil’s Agricultural Land Use and Trade: Effects of Changes in Oil Prices and Ethanol Demand,” Washington, D.C. [Online]. Available: https://ageconsearch.umn.edu/bitstream/242449/2/err210.pdf

[81] J. Goldemberg, “The Brazilian biofuels industry,” *Biotechnology for biofuels*, vol. 1, no. 1, p. 6, 2008.

[82] P. J. P. Zuurbier and J. van de Vooren, *Sugarcane ethanol: Contributions to climate change mitigation and the environment*. Wageningen: Wageningen Academic Publication, 2008.

[83] IEA, “Global EV Outlook 2018: Towards cross-modal electrification,” Paris.

[84] P. Stephan and K. Stephan, “Thermodynamik: Anhang D: Diagramme und Tabellen,” in *Dubbel*, K.-H. Grote and J. Feldhusen, Eds. Berlin, Heidelberg: Springer Berlin Heidelberg, 2014, pp. 192–207.

[85] R. Baar, H. Baumgarten, and M. Beck, “Antriebe: Kapitel 5.9: Konventionelle und alternative Kraftstoffe und Energieträger,” in *Vieweg Handbuch Kraftfahrzeugtechnik*, ser. ATZ / MTZ-Fachbuch, S. Pischinger and U. Seiffert, Eds. Wiesbaden: Springer Vieweg, 2016, pp. 524–540.

[86] F. Posada and C. Façanha, “Brazil Passenger Vehicle Market Statistics: International comparative assessment of technology adoption and energy consumption,” Washington, DC. [Online]. Available: www.theicct.org

[87] BMW, “BMW i3: Technische Daten,” München, 2017. [Online]. Available: https://www.press.bmwgroup.com/deutschland/article/attachment/T0273661DE/392973

[88] Renault, “Renault ZOE: Technische Daten,” Boulogne-Billancourt, 2017. [Online]. Available: https://www.cdn.renault.com/content/dam/Renault/AT/downloadcenter/zoe/PL_ZOE.pdf

[89] Volkswagen, “e-Golf: Technische Daten,” Wolfsburg, 2018. [Online]. Available: https://www.volkswagen.de/de/models/e-golf.html

[90] Nissan, “Nissan LEAF,” Brühl, 2018. [Online]. Available: https://www.nissan.de/fahrzeuge/neuwagen/leaf/reichweite-aufladen.html

[91] Tesla, “Tesla Model S: Premium Electric Sedan,” Palo Alto, 2018. [Online]. Available: https://www.tesla.com/sites/default/files/tesla-model-s.pdf

[92] V. Wesselak and S. Voswinckel, *Photovoltaik - wie Sonne zu Strom wird: Wie Sonne zu Strom wird*, 2nd ed., ser. Technik im Fokus. Berlin, Heidelberg: Springer, 2016, vol. 2.

[93] AGÊNCIA NACIONAL DE ENERGIA ELÉTRICA, “Perdas Totais - ano civil,” Brasília, 2017. [Online]. Available: http://www.aneel.gov.br

[94] J. Sears, D. Roberts, and K. Glitman, “A comparison of electric vehicle Level 1 and Level 2 charging efficiency,” *2014 IEEE Conference on Technologies for Sustainability (SusTech)*, pp. 255–258, 2014. [Online]. Available: https://ieeexplore.ieee.org/document/7046253

[95] Denatran, “Frota de veículos, por tipo e com placa, segundo as Grandes Regiões e Unidades da Federação,” 2018. [Online]. Available: https://www.denatran.gov.br/frota.htm

[96] Halcrow-Sinergia Consortium, “Brazil TAV Project: Alignment Studies: Final Report,” Rio de Janeiro and London, 2009. [Online]. Available: http://portal.antt.gov.br/index.php/content/view/5448/Trem_de_Alta_Velocidade___TAV.html

[97] M. Chester and A. Horvath, “Life-cycle assessment of high-speed rail: the case of California,” *Environmental Research Letters*, vol. 5, no. 1, p. 014003, 2010.

[98] Verband der Elektrizitätswirtschaft e. V., “Repräsentative VDEW-Lastprofile,” Frankfurt am Main.

[99] N. M. Haegel, R. Margolis, T. Buonassisi, D. Feldman, A. Froitzheim, R. Garabedian, M. Green, S. Glunz, H.-M. Henning, B. Holder, I. Kaizuka, B. Kroposki, K. Matsubara, S. Niki, K. Sakurai, R. A. Schindler, W. Tumas, E. R. Weber, G. Wilson, M. Woodhouse, and S. Kurtz, “Terawatt-scale photovoltaics: Trajectories and challenges,” *Science (New York, N.Y.)*, vol. 356, no. 6334, pp. 141–143, 2017.

[100] T. Gobmaier, “Entwicklung und Anwendung einer Methodik zur Synthese zukünftiger Verbraucherlastgänge,” Ph.D. dissertation, Technische Universität München, München, 2013. [Online]. Available: https://d-nb.info/1047440725/34

[101] F. McLoughlin, A. Duffy, and M. Conlon, “The Generation of Domestic Electricity Load Profiles through Markov Chain Modelling,” *Euro-Asian Journal of Sustainable Energy Development Policy*, 2012. [Online]. Available: https://arrow.dit.ie/cgi/viewcontent.cgi?article=1060&context=dubenart

[102] ——, “A Parametric Analysis of Domestic Electricity Consumption Patterns in Ireland,” *Conference Proceedings of Tenth International Conference on Environment and Electrical Engineering (EEIC), Rome*, 2011. [Online]. Available: https://arrow.dit.ie/cgi/viewcontent.cgi?article=1065&context=dubencon2

[103] W. Labeeuw and G. Deconinck, “Residential Electrical Load Model Based on Mixture Model Clustering and Markov Models,” *IEEE Transactions on Industrial Informatics*, vol. 9, no. 3, pp. 1561–1569, 2013.

[104] A. Ozawa, R. Furusato, and Y. Yoshida, “Determining the relationship between a household’s lifestyle and its electricity consumption in Japan by analyzing measured electric load profiles,” *Energy and Buildings*, vol. 119, pp. 200–210, 2016.

[105] S. Pinnau and C. Breitkopf, “Determination of Thermal Energy Storage (TES) characteristics by Fourier analysis of heat load profiles,” *Energy Conversion and Management*, vol. 101, pp. 343–351, 2015.

[106] M. d. C. Tomé, “Análise do impacto do chuveiro elétrico em redes de distribuição no contexto da tarifa horossazonal: Impact analysis of the electric shower in distribution networks,” Master’s thesis, Unicamp, Campinas, 2014. [Online]. Available: http://repositorio.unicamp.br/bitstream/REPOSIP/259504/1/Tome_MauriciodeCastro_M.pdf

[107] J. Hoppmann, J. Volland, T. S. Schmidt, and V. H. Hoffmann, “The economic viability of battery storage for residential solar photovoltaic systems – A review and a simulation model,” *Renewable and Sustainable Energy Reviews*, vol. 39, pp. 1101–1118, 2014.

[108] Umweltbundesamt, “Batterien und Akkus,” Dessau-Roßlau, 2012. [Online]. Available: https://www.umweltbundesamt.de/sites/default/files/medien/publikation/long/4414.pdf

[109] Fraunhofer ISE, “Levelized cost of electricity renewable energy technologies,” Freiburg, 2018. [Online]. Available: https://www.ise.fraunhofer.de/content/dam/ise/en/documents/publications/studies/EN2018_Fraunhofer-ISE_LCOE_Renewable_Energy_Technologies.pdf

[110] J. D. Hunt, M. A. V. Freitas, and A. O. Pereira Junior, “Enhanced-Pumped-Storage: Combining pumped-storage in a yearly storage cycle with dams in cascade in Brazil,” *Energy*, vol. 78, no. 78, pp. 513–523, 2014.

[111] J. D. Hunt and M. A. V. d. Freitas, “Standardizing the selection of seasonal-pumped storage projects,” *Revista Interdisciplinar de Pesquisa em Engenharia (RIPE)*, no. 4, pp. 95–109, 2016. [Online]. Available: http://periodicos.unb.br/index.php/ripe/article/view/23439/0

[112] J. D. Hunt, M. A. V. d. Freitas, and A. O. Pereira Junior, “A review of seasonal pumped-storage combined with dams in cascade in Brazil,” *Renewable and Sustainable Energy Reviews*, vol. 70, pp. 385–398, 2017.

[113] P. P. B. Machado, D. S. Ramos, G. C. Tenaglia, and J. D. Hunt, “Reducing Intermittence of Renewable Energy Sources with Seasonal-Pumped-Storage Plants,” *Energy and Power Engineering*, vol. 09, no. 04, pp. 273–292, 2017.

[114] J. L. d. S. Soito and M. A. V. Freitas, “Amazon and the expansion of hydropower in Brazil: Vulnerability, impacts and possibilities for adaptation to global climate change,” *Renewable and Sustainable Energy Reviews*, vol. 15, no. 6, pp. 3165–3177, 2011.

[115] C. M. Stickler, M. T. Coe, M. H. Costa, D. C. Nepstad, D. G. McGrath, L. C. P. Dias, H. O. Rodrigues, and B. S. Soares-Filho, “Dependence of hydropower energy generation on forests in the Amazon Basin at local and regional scales,” *Proceedings of the National Academy of Sciences of the United States of America*, vol. 110, no. 23, pp. 9601–9606, 2013.

[116] J. Schmidt, R. Cancella, and A. O. Pereira, “An optimal mix of solar PV, wind and hydro power for a low-carbon electricity supply in Brazil,” *Renewable Energy*, vol. 85, pp. 137–147, 2016.

[117] L. d. S. N. S. Barbosa, J. F. Orozco, D. Bogdanov, P. Vainikka, and C. Breyer, Eds., *Hydropower and Power-to-gas Storage Options: The Brazilian Energy System Case*, vol. 99, 2016.

[118] Deutsches Institut für Normung, “DIN 4048-2: Wasserbau, Begriffe, Wasserkraftanlagen (Water engineering, terms, waterpower plants),” Berlin, 1994.

[119] N. H. Crawford and S. M. Thurin, *Hydrologic Estimates for Small Hydroelectric Projects*. Mountain View: Small Decentralized Hydropower Program, International Programs Division, National Rural Electric Cooperative Association, 1981. [Online]. Available: https://searchworks.stanford.edu/view/10328584

[120] S. Herzog, D. Atabay, J. Jungwirth, and V. Mikulovic, “Self-adapting building models for model predictive control,” *Proceedings of BS2013*, pp. 2489–2493, 2013.

[121] L. Ljung, “System Identification Toolbox: User’s Guide,” Natick.

[122] A. Kohli and K. Frenken, “Evaporation from artificial lakes and reservoirs.” [Online]. Available: http://www.fao.org/3/a-bc814e.pdf

[123] SIGEL and ANEEL, “Sistema de Informações Georreferenciadas do Setor Elétrico,” 2017. [Online]. Available: https://sigel.aneel.gov.br/Down/

[124] L. Zotarelli, Dukes, Michael D., Romero, Consuelo C., K. W. Migliaccio, and K. T. Morgan, “Step by Step Calculation of the Penman-Monteith Evapotranspiration (FAO-56 Method),” 2016. [Online]. Available: http://edis.ifas.ufl.edu/pdffiles/AE/AE45900.pdf

[125] T. H. Bakken, Å. Killingtveit, K. Engeland, K. Alfredsen, and A. Harby, “Water consumption from hydropower plants – review of published estimates and an assessment of the concept,” *Hydrology and Earth System Sciences*, vol. 17, no. 10, pp. 3983–4000, 2013.

[126] U.S. Department of Energy, “Wind Technologies Market Report 2016,” Washington, D.C. [Online]. Available: https://www.energy.gov/sites/prod/files/2017/08/f35/2016_Wind_Technologies_Market_Report_0.pdf

[127] BMWi, “Erneuerbare Energien in Zahlen: Nationale und internationale Entwicklung im Jahr 2019,” Berlin, 2020. [Online]. Available: https://www.bmwi.de/Redaktion/DE/Publikationen/Energie/erneuerbare-energien-in-zahlen-2019.pdf

[128] DWD, “Global Radiation in Germany: Based on satellite derived values and ground measurements at DWD stations,” Hamburg, 2020. [Online]. Available: https://www.dwd.de/EN/ourservices/solarenergy/solarenergy.html

[129] M. M. El-Halwagi, *Sustainable design through process integration: Fundamentals and applications to industrial pollution prevention, resource conservation, and profitability enhancement*. Boston, MA: Butterworth-Heinemann, 2012.

[130] S. Richter, *Entwicklung einer Methode zur integralen Beschreibung und Optimierung urbaner Energiesysteme. Erste Anwendung am Beispiel Augsburg.* Garching: Max-Planck-Institut fur ¨ Plasmaphysik, 2004. [Online]. Available: https://d-nb.info/973199415/34

[131] J. Dorfner, "Open Source Modelling and Optimisation of Energy Infrastructure at Urban Scale," Doctoral thesis, Technische Universität München, Munich, 2016. [Online]. Available: https://mediatum.ub.tum.de/1285570

[132] G. Berckmans, M. Messagie, J. Smekens, N. Omar, L. Vanhaverbeke, and J. van Mierlo, "Cost Projection of State of the Art Lithium-Ion Batteries for Electric Vehicles Up to 2030," *Energies*, vol. 10, no. 9, p. 1314, 2017.

[133] Fraunhofer ISI, "Opportunities and challenges when importing green hydrogen and synthesis products," Karlsruhe. [Online]. Available: https://www.isi.fraunhofer.de/content/dam/isi/dokumente/cce/2020/policy_brief_hydrogen.pdf

[134] B. Reuter, "Assessment of sustainability issues for the selection of materials and technologies during product design: A case study of lithium-ion batteries for electric vehicles," *International Journal on Interactive Design and Manufacturing (IJIDeM)*, vol. 10, no. 3, pp. 217–227, 2016.

[135] Umweltbundesamt, "Potenzial der Windenergie an Land: Studie zur Ermittlung des bundesweiten Flächen- und Leistungspotenzials der Windenergienutzung an Land," Dessau-Roßlau. [Online]. Available: https://www.umweltbundesamt.de/sites/default/files/medien/378/publikationen/potenzial_der_windenergie.pdf

[136] O. A. Alduchov and R. E. Eskridge, "Improved Magnus Form Approximation of Saturation Vapor Pressure," *Journal of Applied Meteorology*, vol. 35, no. 4, pp. 601–609, 1996.

[137] D. Sonntag, "Fortschritte in der Hygrometrie," *Meteorologische Zeitschrift*, vol. 3, no. 2, pp. 51–66, 1994.

[138] K. Lucas, *Thermodynamik: Die Grundgesetze der Energie- und Stoffumwandlungen*, 7th ed., ser. Springer-Lehrbuch. Berlin, Heidelberg: Springer-Verlag, 2008.

[139] L. Perridon, M. Steiner, and A. W. Rathgeber, *Finanzwirtschaft der Unternehmung*, 16th ed., ser. Vahlens Handbücher der Wirtschafts- und Sozialwissenschaften. München: Vahlen, 2012.

[140] E. Hau, *Windkraftanlagen*. Berlin, Heidelberg: Springer Berlin Heidelberg, 2016.

[141] Enercon, "Enercon product overview," Aurich. [Online]. Available: https://www.enercon.de/fileadmin/Redakteur/Medien-Portal/broschueren/pdf/EC_Produkt_en_042017.pdf

[142] ANA, “Sistema Nacional de Informações sobre Recursos Hídricos: Quantidade de água,” Brasília, 2018. [Online]. Available: http://www.snirh.gov.br/snirh/snirh-1/acesso-tematico/quantidade-de-agua